

**Structural and dynamical studies on human  
epidermal-type fatty acid binding protein using  
high-resolution NMR spectroscopy**

**Dissertation**

zur Erlangung des Doktorgrades  
der Naturwissenschaften

**vorgelegt beim  
Fachbereich Chemie und Pharmazeutische Wissenschaften  
der Johann Wolfgang Goethe-Universität  
in Frankfurt am Main**

von

**Luis Horacio  
Gutiérrez González**

aus Saltillo, Mexiko

Frankfurt am Main, 2002  
(DF1)

vom Fachbereich Chemische und Pharmazeutische Wissenschaften der  
Johann Wolfgang Goethe-Universität als Dissertation angenommen.

Dekan: Prof. Dr. W. Müller

1. Gutachter: Prof. Dr. H. Rüterjans
2. Gutachter: Prof. Dr. B. Ludwig

Tag der Disputation: 5. März 2002

Für Wiebke und Nicolás

## Danksagung

Die vorliegende Arbeit wurde am Institut für Biophysikalische Chemie der Johann Wolfgang Goethe-Universität Frankfurt am Main unter der Anleitung von Herrn Prof. Dr. Heinz Rüterjans im Zeitraum von April 1997 bis November 2001 angefertigt.

Herrn Prof. Dr. Heinz Rüterjans gilt mein besonderer Dank für die interessante Themenstellung sowie für seine Unterstützung und die Schaffung hervorragender Arbeitsbedingungen.

Weiterhin möchte ich danken:

Herrn Dr. Christian Lücke für die konkrete Hilfestellung und für die vielen anregenden Diskussionen bei NMR-Fragen aller Art,

Herrn Dr. Christian Ludwig für die Aufnahme von NMR-Spektren und die anregenden fachlichen Diskussionen.

Herrn Prof. Dr. Carlos Pérez für die vielen fachlichen Gespräche,

Herrn Dr. Helmut Hanssum für die vielen Gespräche über NMR, Gerätetechnik und physikalische Themen;

den Herren Dipl.-Chem. Marco Betz, Dipl.-Biochem. Alex Koglin, Dipl.-Chem. Ulrich Schieborr, Dr. Michael Weimer und Dipl.-Chem. Bernd Weyrauch für die stete Hilfsbereitschaft bei Computerproblemen aller Art,

Herrn Dipl. Chem. Martin Rademacher für seine Unterstützung bei dem präparativen Teil dieser Arbeit,

allen nicht namentlich genannten Mitgliedern des Arbeitskreises für die freundliche Aufnahme und das ausgezeichnete Arbeitsklima,

dem Deutschen Akademischen Austauschdienst für die finanzielle Unterstützung durch ein Stipendium.

## Abbreviations

A-FABP	Adipocyte-type Fatty Acid Binding Protein
B-FABP	Brain-type Fatty Acid Binding Protein
COSY	Correlation Spectroscopy
CSA	Chemical Shift Anisotropy
DD	Dipole-Dipole Interaction
DEPT	Distorsionless Enhancement by Polarization Transfer
E-FABP	Epidermal-type Fatty Acid Binding Protein
FABP	Fatty Acid Binding Protein
H-FABP	Heart-type Fatty Acid Binding Protein
HSQC	Heteronuclear Single-Quantum Coherence
HTQC	Heteronuclear Triple-Quantum Coherence
I-FABP	Intestinal-type Fatty Acid Binding Protein
ILBP	Ileal Lipid Binding Protein
INEPT	Insensitive Nuclei Enhancement by Polarization Transfer
L-FABP	Liver-type Fatty Acid Binding Protein
LBP	Lipid Binding Protein
M-FABP	Myelin-type Fatty Acid Binding Protein
NMR	Nuclear Magnetic Resonance
NOE	Nuclear Overhauser Effect
NOESY	Nuclear Overhauser Effect and Exchange Spectroscopy
ppm	Parts per million
RMSD	Root-Mean-Square Deviation
TOCSY	Total Correlation Spectroscopy
TPPI	Time Proportional Phase Incrementation

---

# Index

## 1 Introduction

- 1.1 The lipid binding protein family 1
- 1.2 The epidermal-type fatty acid binding protein 5

## 2 Theoretical aspects

- 2.1 Structure determination 10
  - 2.1.1 Resonance assignments 10
  - 2.1.2 The nuclear Overhauser effect 11
  - 2.1.3 NMR experiments 15
    - 2.1.3.1 COSY 15
    - 2.1.3.2 TOCSY 16
    - 2.1.3.3 NOESY 16
    - 2.1.3.4 INEPT 17
    - 2.1.3.5 DEPT 18
    - 2.1.3.6  $^1\text{H}, ^{15}\text{N}$ -HSQC 18
    - 2.1.3.7  $^1\text{H}, ^{15}\text{N}$ -HTQC 19
    - 2.1.3.8 3D TOCSY-( $^1\text{H}, ^{15}\text{N}$ )-HSQC 20
    - 2.1.3.9 3D NOESY-( $^1\text{H}, ^{15}\text{N}$ )-HSQC 21
  - 2.1.4 Torsion-angle dynamics calculations 21
  - 2.1.5 Energy minimization 26
- 2.2 Backbone dynamics 28
  - 2.2.1 Relaxation 28
  - 2.2.2 The dipole-dipole interaction 31
  - 2.2.3 The chemical shift anisotropy 33
  - 2.2.4 The spectral density function of Lipari and Szabo 34
  - 2.2.5 The Clore-Gronenborn model 36
  - 2.2.6 The exchange parameter 37

## 3 Materials and methods

- 3.1 Protein preparation 38
- 3.2 NMR data collection and processing 38
- 3.3 Constraint generation and structure calculation 40
- 3.4 Relaxation measurements 42

---

<b>4</b>	<b>Results and discussion</b>	
4.1	Resonance assignments of human E-FABP	46
4.2	Solution structure of human E-FABP	59
4.3	Backbone dynamics of human E-FABP	64
<b>5</b>	<b>Summary</b>	75
<b>6</b>	<b>References</b>	77
<b>7</b>	<b>Appendixes</b>	
	Appendix A.1	88
	Appendix A.2	98
	Appendix A.3	103
	Appendix A.4	104

---

# 1 Introduction

## 1.1 The lipid binding protein family

The multigene family of intracellular lipid binding proteins (LBPs) comprises a group of homologous 14-15 kDa proteins that specifically bind and facilitate the transport of fatty acids, bile acids, retinoids or eicosanoids. Members of this family include several types of fatty acid binding proteins (FABPs), ileal lipid binding protein and cellular retinoid binding proteins (Table 1.1). Fatty acid binding proteins are cytosolic non-enzymatic proteins that display tissue-specific expression and may play a role in the metabolism of long-chain, unsaturated free fatty acids [Veerkamp and Maatman, 1995]. Members of this protein family have a high affinity for amphiphiles. It has been proposed that these proteins are involved in the cellular uptake of lipids, their transport to metabolic pathways [Kaikaus *et al.*, 1990], and in the regulation of lipid transport and metabolizing proteins [Wolfrum *et al.*, 1999]. It has furthermore been proposed that several proteins within the FABP family are important during cellular growth and differentiation [Ross, 1993; Yang *et al.*, 1994]. Moreover, liver-type FABP for example may be involved in the transport of fatty acids and peroxisome proliferators from the cytosol into the nucleus for interactions with peroxisome proliferator-activated receptors (PPARs) [Wolfrum *et al.*, 1999]. These proteins have been isolated from a number of mammalian tissues as well as fatty acid-metabolizing tissues of chicken, fish and insects [Bass, 1988; Borchers and Spener, 1994].

At least thirteen types of LBPs have been identified to the present: liver (L-FABP), intestinal (I-FABP), heart (H-FABP), adipocyte (A-FABP), myelin (M-FABP), brain (B-FABP) and epidermal (E-FABP) fatty acid binding proteins and ileal lipid binding protein (ILBP), as well as cellular retinol binding proteins (CRBP I, II and very recently III) and cellular retinoic acid binding proteins (CRABP I and II). They contain 127-135 amino acid residues and are named after the tissue of first isolation or identification. These proteins have been originally identified using FABP-specific antibodies in enzyme-linked immunosorbent assays (ELISA), Western blotting, or immuno-histochemistry; corresponding mRNA was detected by hybridization with respective cDNAs or oligonucleotides in Northern blotting or *in situ* hybridization. Most FABPs are rather tissue specific, whereas H-FABP has a widespread distribution. The presence of more than one LBP type in a particular tissue is



**Table 1.1** Family of intracellular lipid binding proteins [Börchers and Spener, 1994; Storch and Thumser, 2000; Vogel *et al.*, 2001].

Protein	Previous/other names	Ligand	Tissue localization
E-FABP	K-FABP, Mal-1, KLBP, skin FABP, psoriasis-associated FABP	fatty acid	epidermis, adipose and mammary tissue, tongue epithelia, testis
L-FABP	Z-protein, heme binding protein, hepatic FABP	fatty acids, others	liver, small intestine
I-FABP	gut FABP	fatty acid	small intestine (proximal)
H-FABP	muscle FABP, M-FABP	fatty acid	cardial and skeletal muscle, brain, mammary gland, kidney, adrenals, ovaries, testis, aorta
A-FABP	aP2, ALBP	fatty acid	adipose, monocytes
B-FABP	BLBP, O-FABP	fatty acid	brain, central nervous system
M-FABP	myelin P2	fatty acid	peripheral nervous system
ILBP	gastrotropin; ileal FABP, II-FABP, I-BABP	bile acid, fatty acid	small intestine (distal)
CRBP I		retinol	liver, kidney, testis, lung
CRBP II		retinol, retinal	small intestine
CRBP III		Retinol	heart, muscle, adipose tissue
CRABP I		retinoic acid	brain, skin, testis
CRABP II		retinoic acid	epidermis, adrenals

generally regarded as a functional diversification of this protein family [Börchers and Spener, 1994]. The sequence similarity among the various LBPs ranges between 38 and 70 %. Generally, the similarity is high for sequences of the same tissue type isolated from different host organisms, while the similarity is low for different LBP types of the same host organism [Veerkamp and Maatman, 1995].

The sequence homologies among the different types of LBPs constitute an important classification principle within this protein family. Some of the most conserved amino acids are glycines, asparagines, and aspartates that are necessary for the formation of narrow  $\beta$ -turns, as well as aromatic residues located in several regions and with different functions that correspond to positions 11, 19, 22, 67 and 73 of E-FABP. Also highly conserved is a triad of protein side-chains consisting of two arginines and one tyrosine (E-FABP numbering R109, R129 and Y131).

The aligned amino acid sequences of the FABP family show the large similarity between the heart, myelin, adipocyte, brain and epidermal types, while CRBPs and CRABPs show only 20-45% similarity with the FABPs. The FABP types differ considerably in their surface charge. The heart-type FABP has an isoelectric point of about 5, the liver and

	1	10	20	30	40	
E-FABP	MATVQQLEGR		WRLVDSKGF	EYMKELGVGI	ALRKMGA .	.KPCIIITCD 100%
M-FABP	...SNKFLGT		WKLVSSENF	DYMKALGVGL	ATRKLGNLA .	.KPTVIISK 56%
A-FABP	...CDAFVGT		WKLVSSENF	DYMKELGVGF	ATRKVAGMA .	.KPNMIISVN 52%
H-FABP	...VDAFLGT		WKLVDKSNF	DYMKSLGVGF	ATRQVASMT .	.KPTTIEKN 49%
B-FABP	...VEAFCAT		WKLTVSQNF	EYMKALGVGF	ATRQVGNVT .	.KPTVIISQE 45%
I-FABP	.....AFDST		WKVDRSENYD	KFMEKMGVNI	VKRKLAHD .	.NLKLTITQE 25%
L-FABP	.....MSFSGK		YQLQSQENFE	AFMKAIGLPE	ELIQKGKDI .	.KGVSEIVQN 23%
ILBP	.....AFTGK		YEIESEKNYD	EFMKRLALPS	DAIDKARNL .	.KIISEVKQD 22%
CRBP I	...PVDFTGY		WKMLVNENFE	EYLRALDVNV	ALRKIANLL .	.KPDKEIVQD 28%
CRBP II	...TKDQNGT		WEMESNENFE	GYMKALDIDF	ATRKIAVRL .	.TQTKIIVQD 27%
CRBP III	..MPPNLTGY		YRFVSQKNME	DYLQALNISL	AVRKIALLL .	.KPDKEIEHQ 28%
CRABP I	...PN.FAGT		WKMRSENF	ELLKALGVNA	MLRKVAVAAA	SKPHVEIRQD 36%
CRABP II	...PN.FSGN		WKIIRSENF	ELLKVLGVNV	MLRKIAVAAA	SKPAVEIKQE 34%
	50	60	70	80	90	
E-FABP	GKNLTIKTES	.TLKTTQFSC	TLGKFEETT	..ADGRKTQT	VCNFTD.GAL	
M-FABP	GDIITIRTES	.TFKNTAISF	KLQGFEEET	..ADNRKTKS	IVTLQR.GSL	
A-FABP	GDVITIKSES	.TFKNTAISF	ILQGFDEVT	..ADDRKVK	TITLDG.GVL	
H-FABP	GDILTLLKTHS	.TFKNTAISF	KLQGFDEET	..ADDRKVK	IVTLDG.GKL	
B-FABP	GDKVVIRTLS	.TFKNTAISF	QLGEEFDEET	..ADDRNCK	VVSLDG.DKL	
I-FABP	GNKFTVKES	.AFRNIEVVF	ELGVTFNYNL	..ADGTELRG	TWSLEG.NKL	
L-FABP	GKHFKFTITA	.GSKVIQNEF	TVGEECELET	..MTGEKVK	VVQLEGDKL	
ILBP	GQNFTWSQQY	PGGHSITNTF	TIGKECIET	..IGGKKFKA	TVQMEG.GKV	
CRBP I	GDHMIIRTLS	.TFRNYIMDF	QVGKEFEEDL	TGIDDRKCM	TVSWDG.DKL	
CRBP II	GDNFKTKTNS	.TFRNYDLDF	TVGVEFDEHT	KGLDGRNVK	LVTWEG.NTL	
CRBP III	GNHMTVRTLS	.TFRNYTVQF	DVGVEFEEDL	RSVDGRKCQ	IVTWEE.EHL	
CRABP I	GDQFYIKTST	.TVRTTEINF	KVGEGFEEET	..VDGRKCR	LATWENENK	
CRABP II	GDTFYIKTST	.TVRTTEINF	KVGEEFEEQ	..VDGRPKS	LVKWESENKM	
	100		110	120	130	
E-FABP	VQHQE...W.	.DGKESTITR	KLK.DGKLVV	ECVMNNVTCT	RIYEKVE	135
M-FABP	NQVQR...W.	.NGKETTIKR	KLK.DGKMVA	ECKMKGVCCT	RIYEKV	131
A-FABP	VHVQK...W.	.DGKSTTIKR	KRE.DDKLVV	ECVMKGVST	RVYERA	131
H-FABP	VHLQK...W.	.DGQETTLVR	ELI.DGKLIL	TLTHGTAVCT	RTYEKEA	132
B-FABP	VHIQK...W.	.DGKETNFVR	EIK.DGKMVM	TLTFGDVVAV	RHYEKA	131
I-FABP	IGKFK...RT	DNGNELNTR	EII.GDELVQ	TYVYEGVEAK	RIFKKD	131
L-FABP	VTTFK.....	.NIK...SVT	ELN.GDIITN	TMTLGDIVFK	RISKRI	127
ILBP	VVNSP.....	.NYH...HTA	EIV.DGKLVE	VSTVGGVSYE	RVSKKLA	127
CRBP I	QCVQK...G.	.EKEGRGWTQ	WIE.GDELHL	EMRVEGVVCK	QVFKKVQ	134
CRBP II	VCVQK...G.	.EKENRGWKQ	WVE.GDKLYL	ELTCGDQVCR	QVFKKK	133
CRBP III	VCVQK...G.	.EVPNRGWRH	WLE.GEMLYL	ELTARDAVCE	QVFRKVR	135
CRABP I	HCTQTLLG.	.DGPPTYWTR	ELAND.ELIL	TFGADDVCT	RIYVRE	136
CRABP II	VCEQKLLKG.	.EGPKTSWTR	ELTNDGELIL	TMTADDVCT	RVYVRE	137

**Table 1.2** Alignment of the amino acid sequences of the members of the LBP family. The percentage of identity and the total number of amino acids are indicated. All sequences are for human proteins, except for ILBP (pig) and CRBP II (rat), and were taken from the following references: E-FABP [Madsen *et al.*, 1992]; H-FABP [Peeters *et al.*, 1991]; M-FABP [Hayasaka *et al.*, 1991]; B-FABP [Shimizu *et al.*, 1997]; A-FABP [Baxa *et al.*, 1989]; ILBP [Walz *et al.*, 1988]; L-FABP [Lowe *et al.*, 1985]; I-FABP [Sweetser *et al.*, 1987]; CRBP-I [Nilsson *et al.*, 1988]; CRBP-II [Schaefer *et al.*, 1989]; CRBP-III [Folli *et al.*, 2001]; CRABP-I and CRABP-II [Åstrom *et al.*, 1991].

epidermal FABP types of about 6 and the adipocyte and myelin FABP types are basic proteins (with pI values of 7.6-9.0) [Veerkamp and Maatman, 1995].

Lipid binding proteins can be grouped according to sequence homology, which is consistent with the ligand binding characteristics [Hohoff and Spener, 1998]. The proteins are classified into four categories: (I) the intracellular retinoid binding proteins; (II) the ileal lipid binding protein (ILBP, binds bile acid) and L-FABP (binds two fatty acids); (III) I-FABP (binds a single fatty acid in a linear conformation); and (IV) FABPs with the fatty acid bound in a highly bent or U-shaped conformation. To the last group belongs the E-FABP examined here, as well as adipocyte- (A-), brain- (B-), heart- (H-) and myelin- (M-) type FABPs, where the carboxylate end of the fatty acid is buried within the binding cavity and forms hydrogen bonds to highly conserved tyrosine and arginine residues, either directly or through an ordered water molecule. The hydrocarbon tail of the fatty acid forms van der Waals interactions with hydrophobic residues in the binding cavity and with ordered water molecules that are in contact with polar residues in the binding pocket [Scapin *et al.*, 1993].

Lbps have been detected in vertebrates (including fish) [Di Pietro *et al.*, 1996; Londraville and Sidell, 1995 and 1996] as well as in invertebrates [Becker *et al.*, 1994; Moser *et al.*, 1991]. Evolutionary studies have been performed on LBP sequences, and phylogenetic trees were constructed [Börchers and Spener, 1994; Matarese *et al.*, 1989; Medzihradsky *et al.*, 1996; Schleicher *et al.*, 1995]. These analyses showed that cellular retinoid binding proteins and the subfamily comprising A-FABP, M-FABP, H-FABP, B-FABP and E-FABP have a common progenitor that diverged early from I-FABP and from the L-FABP/ILBP subfamily. Thus, the specialized function of retinoid binding has evolved separately from fatty acid binding. The L-FABP/ILBP subfamily has the longest evolutionary distance from the other members, as reflected by their binding characteristics. A calculation made by Matarese *et al.* [1989] indicated that the different subfamilies diverged from the common ancestral gene about 700 million years ago, *i.e.*, before the invertebrate-vertebrate divergence.

## 1.2 The epidermal-type fatty acid binding protein

The human epidermal-type fatty acid binding protein (E-FABP) was originally detected in patients suffering from psoriasis, a hyperproliferative skin disease characterized by abnormal differentiation and disordered lipid metabolism [Madsen *et al.*, 1992; Rasmussen *et al.*, 1992].

In this pathological situation, E-FABP was immuno-histochemically localized in differentiated keratinocytes [Siegenthaler *et al.*, 1994]. It has also been called skin-FABP (S-FABP) [Krieg *et al.*, 1993], keratinocyte FABP (K-FABP) and psoriasis-associated-FABP (PA-FABP) [Madsen *et al.*, 1992]. Its cDNA showed similarity to human H-FABP (48%), A-FABP (52%) and M-FABP (58%). The protein is identical to a melanogenic inhibitor isolated from grafted human skin, that inhibits tyrosinase activity in normal melanocytes as well as in a melanoma cell line, and that reduces cellular proliferation of these cells when added exogenously, while normal skin fibroblasts remain unaffected [Farooqui *et al.*, 1995].

E-FABP, which consists of 135 amino acids (15.2 kDa), shows a high binding affinity to stearic acid, which decreases on reduction of the number of carbon atoms or the introduction of double bonds into the fatty acid chain [Siegenthaler *et al.*, 1994]. Moreover, it displays a different electrophoretic mobility compared to FABPs from other human tissues or cellular retinoic acid- and retinol binding proteins. The FABP5 gene of human E-FABP is located in chromosome 8, with a possible duplication in chromosome 11. Expression levels of this FABP are low in normal epidermis, higher in cultured keratinocytes and still higher in psoriatic skin [Madsen *et al.*, 1992; Siegenthaler *et al.*, 1993]. Krieg *et al.* [1993] described

Human	MATVQQLEGR	WRLVDSKGF	EYMKELGVGI	ALRKMAMAK	PDCIITCDGK
Bovine	MATVQQLVGR	WRLVESKGF	EYMKEVGVGM	ALRKVGAMAK	PDCIITSDGK
Rat	MASLKDLEGK	WRLVESHGFE	DYMKELGVGL	ALRKMAMAK	PDCIITLDGN
Murine	MASLKDLEGK	WRLMESHGFE	EYMKELGVGL	ALRKMAAMAK	PDCIITCDGN
Human	NLTIKTESTL	KTTQFSCTLG	EKFEETTADG	RKTQTVCNFT	DGALVQHQEW
Bovine	NLSIKTESTL	KTTQFSCKLG	EKFEETTADG	RKTQTVCNFT	DGALVQHQEW
Rat	NLTVKTESTV	KTTVFSCCTLG	EKFDETTADG	RKTETVCTFT	DGALVQHQQW
Murine	NITVKTESTV	KTTVFSCNLG	EKFDETTADG	RKTETVCTFQ	DGALVQHQQW
Human	DGKESTITRK	LKDGKLVVEC	VMNNVTCTRI	YEKVE	100%
Bovine	DGKESTITRK	LEDGKLVVVC	VMNNVTCTRV	YEKVE	91%
Rat	EGKESTITRK	LKDGKLVVEC	VMNNAICTRV	YEKVQ	81%
Murine	DGKESTITRK	LKDGKMIVEC	VMNNAICTRV	YEKVQ	80%

**Table 1.3** Amino acid alignment of E-FABP homologues: mouse (*Mus musculus*) [Krieg *et al.*, 1993; Bleck *et al.*, 1998; Hertz and Bernlohr, 1998], rat (*Rattus norvegicus*) [Wen *et al.*, 1995; Watanabe *et al.*, 1994; de León *et al.*, 1996] and cattle (*Bos taurus*) [Jaworski and Wistow, 1996; Kingma *et al.*, 1998].

the cDNA for keratinocyte lipid binding protein named mal-1, which is up-regulated in both benign papilloma and malignant squamous cell carcinoma stages during tumor development and that has been shown to be identical with E-FABP. The derived amino acid sequence is closely related to the mouse myelin- and adipocyte-type FABPs [Veerkamp and Maatman, 1995]. E-FABP has also been localized in other organisms: mouse (*Mus musculus*) [Krieg *et al.*, 1993; Bleck *et al.*, 1998; Hertzler and Bernlohr, 1998], rat (*Rattus norvegicus*) [Wen *et al.*, 1995; Watanabe *et al.*, 1994; de León *et al.*, 1996] and cattle (*Bos taurus*) [Jaworski and Wistow, 1996; Kingma *et al.*, 1998].

Additionally, it is known that E-FABP forms a complex with psoriasin (S100A7) [Hagens *et al.*, 1999], a protein of the S100 gene family that has been associated with psoriasiform epidermal hyperplasia and is secreted by neoplastic keratinocytes in bladder and breast carcinoma [Celis *et al.*, 1996; Watson *et al.*, 1998]. Thus, an investigation of the E-FABP:psoriasin complex in solution may eventually be useful to understand the coordinated up-regulation of E-FABP and S100A7 in psoriasis.

Most members of the FABP family display amino acid motifs aimed at high-affinity long-chain fatty acid binding. Tertiary structures of this protein family show a highly conserved fold, *i.e.*, a  $\beta$ -barrel (or  $\beta$ -clam) consisting of two orthogonal  $\beta$ -sheets with five antiparallel  $\beta$ -strands each and a helix-turn-helix domain partially covering the internal cavity [Sacchettini *et al.*, 1989]. Strands  $\beta$ A through  $\beta$ E and the first half of strand  $\beta$ F form one  $\beta$ -sheet, while the second half of strand  $\beta$ F together with strands  $\beta$ G through  $\beta$ J form the second  $\beta$ -sheet. The center of strand  $\beta$ F is shared by both sheets. There is no network of hydrogen bridges between  $\beta$ D and  $\beta$ E, because of the large distance between the backbone atoms. However, there is a hydrogen-bonding network between the first and the tenth strand ( $\beta$ A and  $\beta$ J), thus forming an *up/down*  $\beta$ -cylinder. The cylinder is closed at one end by a cluster of hydrophobic side-chains and at the other end by the helix-turn-helix domain that connects the strands  $\beta$ A and  $\beta$ B.

The helices are designated as  $\alpha$ I and  $\alpha$ II. The inner surface of the cavity is limited by polar and non-polar amino acids, with the non-polar amino acids occupying a deeper position in the cavity. For the different FABP types, the volume of the binding cavity that is available to other atoms is of the order of  $500 \text{ \AA}^3$ , while the volume defined by the van der Waals surface of all the component atoms comprises approximately  $1000 \text{ \AA}^3$  [Banaszak *et al.*, 1994]. The fatty acid is non-covalently bound inside the cavity, almost inaccessible to the external

solvent, and occupies between one third to one half of the cavity volume. FABPs bind only one ligand, with exception of L-FABP, that can bind two fatty acid molecules [Glatz and van der Vusse, 1996; Thompson *et al.*, 1997]. In most cases, the carboxyl group of the fatty acid is located inside the  $\beta$ -barrel and non-covalently bound to arginine and tyrosine residues. Crystallographic analyses have shown that there are several water molecules in the binding cavity, some of which show van der Waals interactions with the fatty acid [Banaszak *et al.*, 1994].

The crystallographic structure of E-FABP has been recently resolved to 2.05 Å and refined to an *R* factor of 20.7% [Hohoff *et al.*, 1999]. E-FABP is a typical member of the 10-stranded  $\beta$ -clam structure group. Its backbone structure is virtually identical to that of H-FABP [Scapin *et al.*, 1993] and I-FABP [Sacchetini and Gordon, 1993]. Root-mean-square deviations (RMSD) of the  $C\alpha$  atoms after superposition of the structure with H-FABP (for 115 residues) and with I-FABP (for 93 residues) are 0.62 Å and 1.03 Å, respectively. The electron density map shows that the ligand is bound within a central cavity of 252 Å<sup>3</sup> in a U-shaped conformation [Hohoff *et al.*, 1999]. The carboxyl group of the ligand interacts with Y131, R129 and R109, in the latter case via an ordered water molecule. The loop between strands  $\beta$ C and  $\beta$ D probably adopts two or more conformations in the crystal, which may be related to the partial occupancy of the bound fatty acid. In all FABPs, this region interacts with the aliphatic end of bound fatty acids and is called the portal region, since it is believed that the fatty acid enters and exits the cavity at this site [Herr *et al.*, 1996]. In E-FABP this loop includes L60, which is a phenylalanine in most other FABP sequences, and which is thought to affect the dynamics of lipid exchange with the exterior [Xu *et al.*, 1993]. The homologues of human E-FABP detected in rat, mouse and cattle have also a hydrophobic residue at this position (Table 1.3).

Epidermal-type FABPs are unique because of the presence of 5-6 conserved cysteines, a number unusually high for members of this protein family. Four of these cysteines are unique to E-FABP: C43, C47, C67 and C87. The crystallographic structure of human E-FABP [Hohoff *et al.*, 1999] has shown the existence of a disulfide bridge between cysteines 120 and 127, the only reported case in the entire LBP family. Cysteines 67 and 87 are also in close vicinity. Some FABPs have one or two cysteines homologous to C120 or C127 in E-FABP, but only M-FABP has both (at respective positions 117 and 124). Biochemical results suggested that these cysteines in M-FABP form a disulfide bridge [Kitamura *et al.*, 1980], but the crystallographic structure determination did not confirm this observation.

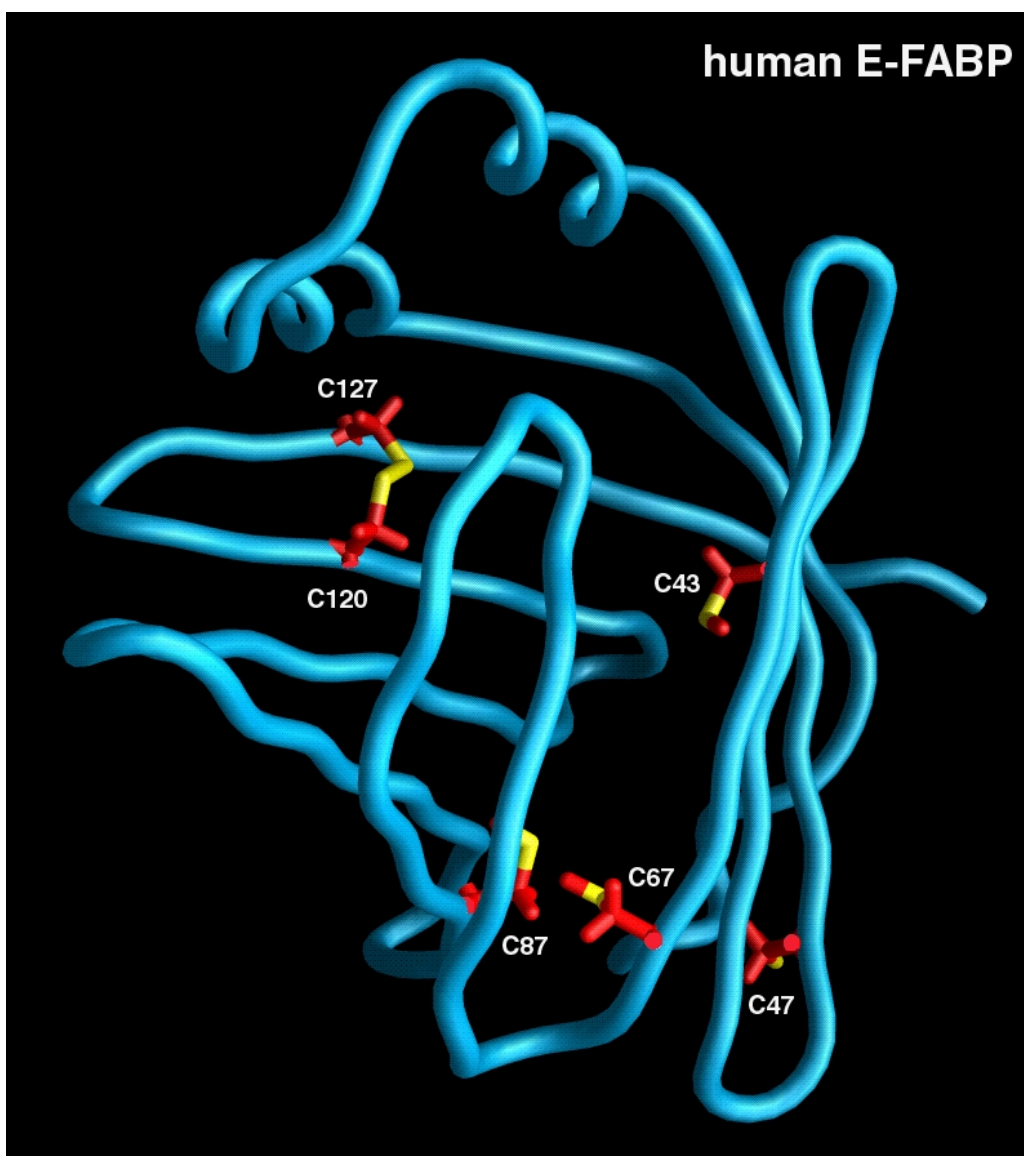


**Figure 1.1** Crystallographic structure of human E-FABP [Hohoff *et al.*, 1999]. The six cysteines and the disulfide bridge between C120 and C127 are highlighted.

In addition to the solution structure, the present study describes the backbone dynamics of human E-FABP determined by means of  $^{15}\text{N}$ -edited NMR relaxation ( $T_1$  and  $T_2$ ) and steady-state heteronuclear  $^{15}\text{N}\{^1\text{H}\}$  NOE measurements. Protein dynamics is an important aspect of the relationship between structure and function for most biochemical processes.

---

Differences previously observed in the hydrogen exchange rates of backbone amide protons have indicated that protein stability and dynamics are distinct for several LBPs [Lücke *et al.*, 1996]. Therefore,  $^{15}\text{N}$ -NMR backbone relaxation experiments may shed more light on the dynamic differences between the various members of this protein family. Consequently, backbone relaxation and hydrogen exchange in human E-FABP are compared with other LBPs, in order to obtain a better understanding of the relationship between their structure, dynamics and function.



## 2 Theoretical aspects

### 2.1 Structure determination in solution

#### 2.1.1 Resonance assignments

The various protons of a molecule can be distinguished in a NMR spectrum by means of the resonance frequencies. This distinction based on chemical shift differences depends on the electron distributions, anisotropy and steric effects. However, in the case of chemically equivalent protons, degenerate resonance frequencies can occur. The standard chemical shift values for the proton resonances of the 20 L-amino acids were collected by Bundi and Wüthrich [1979]. In proteins, however, these values may be shifted because of shielding and deshielding effects due to different molecular environments. Furthermore, in the case of larger molecules such as proteins, signal overlap may become quite unfavourable for the assignment of resonance frequencies.

The scalar-coupled protons of a molecule form so-called spin-systems, which are limited by heteroatoms that carry no protons. Thus, the amino acids in proteins are characterized by specific proton spin-systems, that are separated within the polypeptide chain by the carbonyl groups of the peptide linkage. The protons of aromatic ring structures or side-chain amides form additional spin-systems, which show no scalar coupling to the backbone spin-systems.

In order to identify the proton resonances in a protein, it is possible to use the classical assignment strategy of Wüthrich in a modified form [Wüthrich, 1986; Bax, 1989; Bax and Grzesiek, 1993]. TOCSY and COSY spectra are analyzed to detect spin-systems that are either characterized as specific amino acid residues or classified into amino acid categories. Scalar coupling relations are found in the TOCSY spectrum of a protein, displaying couplings from the backbone amide proton to possibly all other proton resonances of a particular spin-system. Geminal ( $^2J$ ) or vicinal ( $^3J$ ) couplings of directly neighbouring protons can be assigned with a COSY spectrum. Thus, the combination of TOCSY and COSY spectra allows the complete characterization of the proton resonances into amino acid spin-systems. Furthermore, experimental evidence about hydrogen bonds can be obtained from hydrogen/deuterium exchange in perdeuterated buffer, where labile protons, such as those of hydroxyl, thiol, amide and imino groups, are substituted by the deuterium atoms of the solvent over time. Depending on the presence of hydrogen bonds, the signals of slow-exchanging protons remain visible for longer periods of time.

The sequential assignment of the amino acid spin-systems is achieved using NOESY spectra. Dipolar couplings between the HN resonance of amino acid  $i$  and the  $C_\alpha$  and  $C_\beta$  protons of the preceding amino acid  $i - 1$  are usually observed. The sequence of spin-systems obtained with this method is subsequently compared with the primary structure of the polypeptide chain, until all residues are identified and the assignment of all proton resonances is completed.

### 2.1.2 The nuclear Overhauser effect

The nuclear Overhauser effect (NOE) describes a change in the signal intensity of a NMR resonance belonging to nucleus  $i$  after perturbation of the resonance of a second nucleus  $s$  through irradiation of the corresponding frequency. This effect is caused by dipole-dipole cross-relaxation. Its intensity is a function of the distance between the dipole-coupled nuclei  $i$  and  $s$  [Neuhaus and Williamson, 1989].

The resonance belonging to nucleus  $s$  normally undergoes a process of saturation, *i.e.*, the population differences across certain transitions will be eliminated by means of a weak radio-frequency pulse. The NOE effect corresponds to the tendency of the system to remain in thermal equilibrium. The change of the population in one part of the system is balanced through a change in other parts. In general:

$$\eta_i(s) = (I - I_0) / I_0 \quad (2.1.2.1)$$

where  $I_0$  is the reference intensity of one resonance,  $I$  the intensity during saturation of another resonance and  $\eta_i(s)$  the NOE in nucleus  $i$  after saturation of nucleus  $s$ .

For a system of two spin- $1/2$  nuclei  $i$  and  $s$  with the same gyromagnetic ratio  $\gamma$ , different chemical shifts and no J-coupling to each other, four energy levels exist, corresponding to the nuclei in the states  $\alpha\alpha$ ,  $\alpha\beta$ ,  $\beta\alpha$  and  $\beta\beta$  (Figure 2.1, left side). The total number of nuclei in the system is  $4N$ . Since chemical shifts are generally very small in comparison with Larmor frequencies, the transitions of each nucleus are almost equal in energy, making the states  $\alpha\beta$  and  $\beta\alpha$  nearly degenerate with equal populations. The lower energy state  $\alpha\alpha$  will contain an excess of  $\delta$  nuclei, while  $\beta\beta$  will be deficient by an equal amount, *i.e.*, the population difference for a transition  $\Delta m = 1$ , with a transition probability  $W_1$ , will be  $\delta$ . For a transition of  $\Delta m = 0$ , with a transition probability  $W_0$ , the population difference will be 0; for a transition  $\Delta m = 2$ , with a transition probability  $W_2$ , the population difference will be  $2\delta$ .

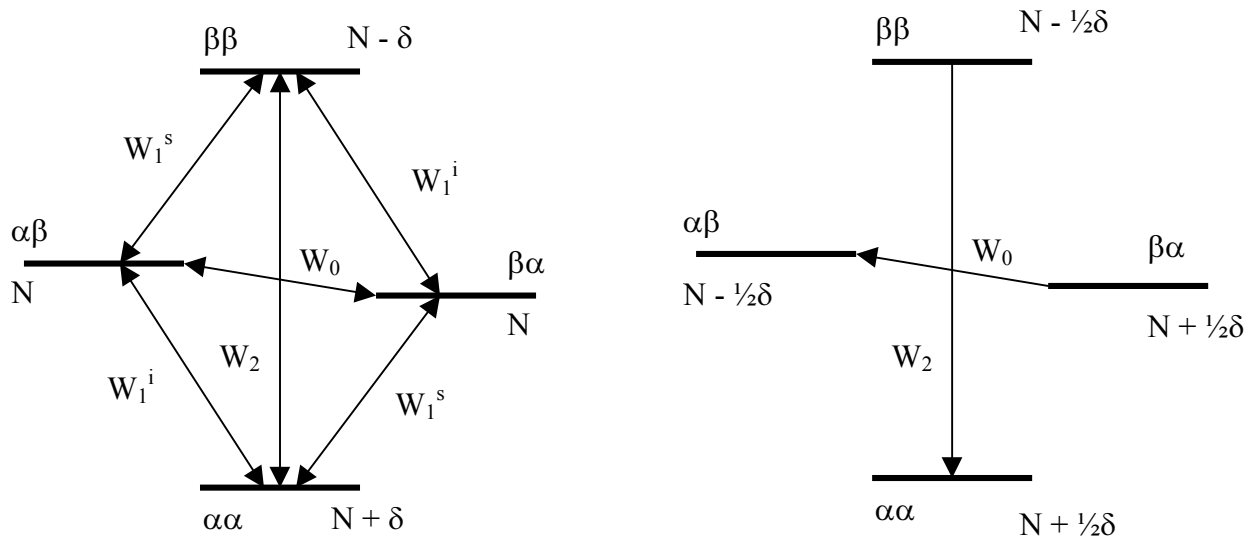


**Figure 2.1** Energy levels and populations of a two spin- $\frac{1}{2}$  homonuclear system. Left: in thermal equilibrium. Right: after saturation of the system  $s$ , the thermal equilibrium can be reestablished only through the forbidden zero- and double-quantum transitions.

In a NOE experiment, the population differences across certain transitions are forced to change. This induces a change in other transitions, whose signals are observed. After the saturation of  $s$ , the new populations are  $N - \frac{1}{2}\delta$  for  $\alpha\alpha$  and  $\alpha\beta$  and  $N + \frac{1}{2}\delta$  for  $\beta\alpha$  and  $\beta\beta$ . The populations after the perturbation are represented on the right side of Figure 2.1. The system as a whole is no longer in equilibrium and the population difference between  $\alpha\beta$  and  $\beta\alpha$  is equal to  $\delta$ . Since the population differences along the  $i$  transitions correspond to the equilibrium state, they cannot contribute to reestablish the equilibrium. If only single-quantum transitions are active as relaxation pathways, saturating  $s$  does not affect the intensity of  $i$ , that is, there is no NOE at nucleus  $i$  due to the saturation of nucleus  $s$ .

For the transition probabilities  $W_2$  and  $W_0$ , the population difference between  $\alpha\beta$  and  $\beta\alpha$  is equal to  $\delta$ , while at equilibrium it is zero. Thus,  $W_0$  acts so as to transfer population from the state  $\beta\alpha$  to the state  $\alpha\beta$ , trying to restore a population difference of 0. This increases the population at the top level of one  $i$  transition and decreases the population at the bottom of the other one, thereby decreasing the total intensity of signals due to transitions of nucleus  $i$ . If the zero-quantum transition  $W_0$  is the dominant relaxation process, the saturation of the  $s$

transitions causes a decrease in the intensity of the absorption signals of  $i$ , that is, there is a negative NOE at nucleus  $i$  due to the saturation of nucleus  $s$ .

For a double-quantum transition  $W_2$ , the population difference  $\alpha\alpha - \beta\beta$  is equal to  $\delta$ , while at equilibrium it is  $2\delta$ . Thus,  $W_2$  acts so as to transfer population from the state  $\beta\beta$  to the state  $\alpha\alpha$ , in order to restore the population difference of  $2\delta$ . Thereby, the population at the top level of one of the  $i$  transitions decreases and the population at the bottom of the other one increases, increasing the intensity of the signals originating from transitions of nucleus  $i$ . If  $W_2$  is the dominant relaxation process, then saturating  $s$  increases the intensity of signals due to  $i$ , that is, there is a positive NOE at nucleus  $i$  due to the saturation of nucleus  $s$ .

The new equilibrium in the system is given by:

$$\eta_i(s) = (W_2 - W_0) / (2W_1^i + W_2 + W_0) \quad (2.1.2.2)$$

The NOEs are positive for small molecules in non-viscous solutions ( $W_2$  dominance) and negative in very viscous solutions or for macromolecules ( $W_0$  dominance). Between these two cases exists a region where  $W_0$  and  $W_2$  are in balance and the NOE disappears.

The interaction that gives rise to the NOE is the dipolar coupling between two nuclei. The rapid reorientation of the dipolar interactions is a suitable source of fluctuating fields to stimulate longitudinal relaxation. The intensity of the dipolar interaction, *i.e.*, of the NOE cross-peaks, will depend on the internuclear distance. To connect the dipolar coupling with both longitudinal relaxation and NOE requires an explanation of the motion of molecules in solution. The random motions can be summarized by a single parameter, the molecular correlation time  $\tau_c$ . The variation in  $\tau_c$  will then affect relaxation times and the relative importance of the different relaxation pathways. The rate of relaxation will be determined by the intensities of the fluctuating fields that carry the right frequencies to stimulate the transitions of interest.

In a system of two spins separated by a distance  $r$ , the relaxation rates via dipolar coupling are:

$$W_1^i \propto 3 \tau_c / r^6 (1 + \omega_i^2 \tau_c^2) \quad (2.1.2.3)$$

$$W_0 \propto 2 \tau_c / r^6 (1 + (\omega_i - \omega_s)^2 \tau_c^2) \quad (2.1.2.4)$$

$$W_2 \propto 12 \tau_c / r^6 (1 + (\omega_i + \omega_s)^2 \tau_c^2) \quad (2.1.2.5)$$

where the constant of proportionality is the same in each case, and  $\omega_i$  and  $\omega_s$  are the Larmor frequencies of the two nuclei  $i$  and  $s$ .

The condition  $1/\tau_c \gg \omega_0$  may be expressed as  $\omega^2 \tau_c^2 \ll 1$  (known as the extreme narrowing limit), in which case all the frequency dependent terms in the denominators of the above expressions become negligible, such that:

$$\begin{aligned} W_1 &\propto 3 \tau_c / r^6 \\ W_0 &\propto 2 \tau_c / r^6 \\ W_2 &\propto 12 \tau_c / r^6 \end{aligned} \quad (2.1.2.6)$$

The net cross-relaxation is represented by the numerator in equation (2.1.2.2):

$$\sigma_{is} = W_2 - W_0 \quad (2.1.2.7)$$

while the denominator represents the total relaxation for nucleus  $i$ :

$$\rho_i = 2W_1^i + W_2 + W_0 \quad (2.1.2.8)$$

For a pure homonuclear dipolar relaxation between spin- $1/2$  nuclei:

$$\eta_i(s) = \sigma_{is} / \rho_i = 1/2 \quad (2.1.2.9)$$

*i.e.*,

$$\rho_i = 2 \sigma_{is} \quad (2.1.2.10)$$

If there are other relaxation mechanisms operating without cross-relaxation, they will be included as an extra contribution  $\rho^*$ :

$$\eta_i(s) = \sigma_{is} / (\rho_i + \rho^*) = \rho_i / 2 (\rho_i + \rho^*) \quad (2.1.2.11)$$

### 2.1.3 NMR experiments

In homonuclear protein NMR spectroscopy, there are three essential 2D experiments: COSY, TOCSY and NOESY. These spectra contain the information required to assign the different proton resonances in a spectrum to the corresponding protons in a protein. With larger molecular masses, it may be necessary to use  $^{13}\text{C}$ - or  $^{15}\text{N}$ -labeled proteins for less spectral overlap in the resonance assignment. Pulse sequence elements can be combined to produce more complex sequences designed to perform specific tasks. In this case, the basic NMR techniques used for coherence transfer are the INEPT and DEPT pulse sequences.

Three- and four-dimensional heteronuclear-edited NMR experiments resolve cross-peaks between  $^1\text{H}$  spins according to the chemical shift of the heteronuclei bonded directly to the  $^1\text{H}$  spins. A 3D heteronuclear-edited experiment consists of a homonuclear pulse sequence, usually a TOCSY or NOESY experiment, and a HSQC pulse sequence [Cavanagh *et al.*, 1996].

#### 2.1.3.1 COSY

In a  $^1\text{H}, ^1\text{H}$ -COSY experiment (Correlated Spectroscopy [Aue *et al.*, 1976]; Figure 2.2), the magnetization transfer occurs via scalar couplings. Since the aliphatic bonds have  $^4\text{J}$  coupling constants almost equal to zero, the COSY experiment provides correlations between pairs of protons separated by two or three bonds, *i.e.*, that have  $^2\text{J}$  or  $^3\text{J}$  connectivities. Assigning entire spin systems in the COSY spectrum is rarely possible because of chemical shift degeneracy in the upfield region of the spectrum. Instead, the COSY spectrum is best used to identify correlations in the fingerprint regions, which are well separated from each other and usually contain well-resolved cross-peaks, whose number reflect the size of the protein.

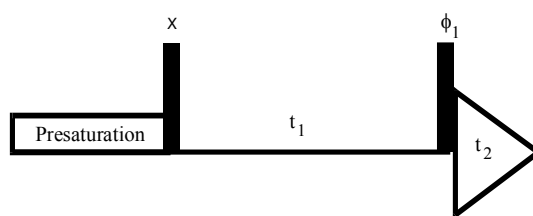


**Figure 2.2** Pulse sequence for a COSY experiment. The phase cycle is  $\phi_1 = x, -x, y, -y$ ; receiver =  $x, -x, y, -y$ .

### 2.1.3.2 TOCSY

A  $^1\text{H},^1\text{H}$ -TOCSY experiment (Total Correlation Spectroscopy [Braunschweiler and Ernst, 1983]; Figure 2.3) utilizes isotropic mixing to transfer in-phase magnetization between spins by means of the strong scalar coupling Hamiltonian. Magnetization can be transferred through several couplings during the course of the mixing, which occurs while a spinlock field is applied. In the absence of relaxation, cross-peaks are generated between all resonances within a spin system. A frequently used pulse sequence for the mixing is the MLEV-17 pulse sequence [Bax and Davies, 1985]. The extent of the magnetization exchange can be regulated via the duration of the applied spinlock field. The magnitude of a given cross-peak will depend on the topology of the spin system, the coupling constants between pairs of spins, the efficiency of the isotropic mixing sequence employed, and the rate of relaxation during the isotropic mixing pulse.

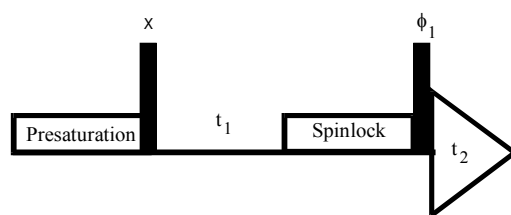


**Figure 2.3** Pulse sequence for a TOCSY experiment. The phase cycle depends on the spinlock field (SL).

### 2.1.3.3 NOESY

The sequential assignment process can be completed using the NOE information to correlate protons that are close in space. Distance constraints for structure determination of proteins are derived primarily from NOE interactions. The pulse sequence for the  $^1\text{H},^1\text{H}$ -NOESY experiment (Nuclear Overhauser and exchange spectroscopy [Jeener *et al.*, 1979]) is shown in Figure 2.4. Initially, a  $90^\circ$ - $t_1$ - $90^\circ$  period labels the spins according to the frequency and returns the magnetization to the  $z$  axis. Magnetization transfer occurs via dipolar coupling during the mixing for a period  $\tau_m$  before observable transverse magnetization is created by the final  $90^\circ$  pulse. The NOE interaction between two protons is usually observable up to a distance of 5 Å.

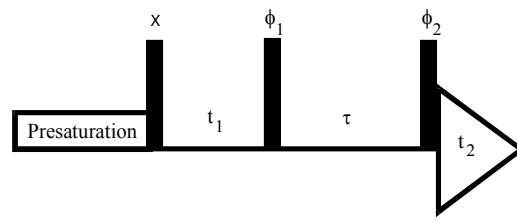


**Figure 2.4** Pulse sequence for the NOESY experiment. The basic phase cycle is  $\phi_1 = x, -x, \phi_2 = 2(x), 2(-x); 2(y), 2(-y);$  receiver =  $x, -x, -x, x, y, -y, -y, y.$

### 2.1.3.4 INEPT

The INEPT sequence (Insensitive Nuclei Enhanced by Polarization Transfer [Morris and Freeman, 1979]; Figure 2.5) is a crucial component in many multidimensional NMR experiments. The aim of the INEPT sequence is to transfer magnetization from a sensitive nucleus with a high gyromagnetic ratio (usually protons) to a less sensitive nucleus with a lower gyromagnetic ratio (*e.g.*, nitrogen or carbon) by means of scalar coupling. By doing this, the detected signal of the heteronucleus will be increased. Applying a spin echo sequence,  $t-180^\circ-t$ , to the spin I causes the decoupling of the S and I spins. Heteronuclear scalar coupling interaction evolves over the duration of a spin echo sequence if  $180^\circ$  pulses are applied to both the I and S spins simultaneously. The INEPT sequence can be written as

$$\begin{array}{l} \text{I spin:} \quad 90^\circ_x \quad -t- \quad 180^\circ_x \quad -t- \quad 90^\circ_y \\ \text{S spin:} \quad \quad \quad \quad \quad \quad \quad 180^\circ_x \quad \quad \quad 90^\circ_x \quad \quad \quad -\text{detect} \end{array}$$

Up to the final pair of  $90^\circ$  pulses, the sequence is a spin-echo in which both spins have been affected by  $180^\circ_x$  pulses, with the chemical shift components refocused during the echo, but scalar coupling fully evolved.

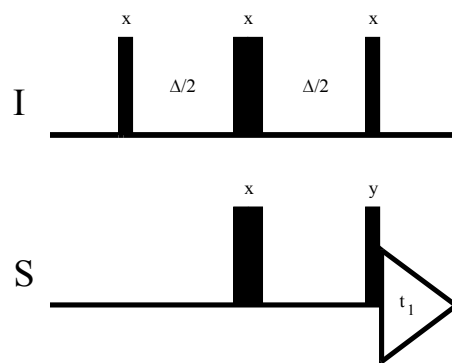


**Figure 2.5** Pulse sequence for the INEPT experiment. The delay  $\Delta/2$  is  $(4J_{IS})^{-1}$  to refocus the scalar coupling between both spins.



### 2.1.3.5 DEPT

The DEPT sequence (Distorsionless Enhancement Polarization Transfer [Bendall *et al.*, 1981]; Figure 2.6) is an improved version of the INEPT experiment. It is based on coherence transfer and depends on the multiplicity of the spin S. The initial pulses for I and S are used to refocus the chemical shift, so that I and S are in resonance. In contrast to the INEPT experiment, the  $90^\circ$  pulse on the S spin precedes the last pulse of flip angle  $\beta$  on the I spins. This sequence can be used for experiments designed to separate signals from the spin systems IS,  $I_2S$  and  $I_3S$  by linear combinations of spectra obtained with different values of the flip angle  $\beta$ , for example  $45^\circ$ ,  $90^\circ$  and  $135^\circ$  (which correspond, *e.g.*, to CH, CH<sub>2</sub> and CH<sub>3</sub> groups). Usually, a value of  $\Delta = (2J_{IS})^{-1}$  is chosen to maximize the antiphase component of the magnetization.

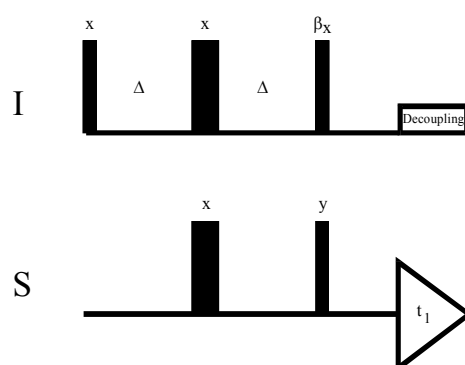


**Figure 2.6** Pulse sequence for the DEPT experiment. The proton pulse  $\beta x$  with a flip angle of  $\beta^\circ$  is used to optimize the pulse sequence to IS,  $I_2S$ - or  $I_3S$ -spin systems. The delay  $\Delta$  is  $(2J_{IS})^{-1}$  to refocus the scalar coupling between both spin types.

### 2.1.3.6 $^1\text{H}$ , $^{15}\text{N}$ -HSQC

The HSQC experiment (heteronuclear single-quantum coherence [Bodenhausen and Ruben, 1980]; Figure 2.7) includes two INEPT sequences. The first one is used as the preparation stage to create antiphase heteronuclear coherence, and the second one converts this coherence back to observable magnetization. The frequency labeling of the I nucleus is done by systematically incrementing the duration  $t_1$ . In the center of the  $t_1$  period a selective  $180^\circ$  pulse is applied to refocus the effect of J modulation. The sensitivity of the experiment can be increased by applying gradients [Kay *et al.*, 1992].

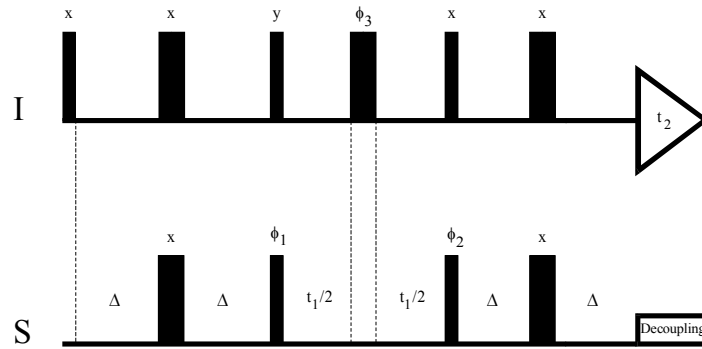


**Figure 2.7** Pulse sequence for the HSQC experiment. The phase cycling is  $\phi_1 = x, -x$ ;  $\phi_2 = 2(x), 2(-x)$ ;  $\phi_3 = (4y), 4(-y)$ ; and receiver =  $2(x, -x, -x, x)$ . It is essential that the first and second  $90^\circ$  pulse on spin I are mutually  $90^\circ$  out of phase.

### 2.1.3.7 $^1\text{H}, ^{15}\text{N}$ -HTQC

Filtering methods offer the possibility of selectively extracting spectral information from isotope-labeled compounds. The HTQC experiment (heteronuclear triple-quantum coherence [Schmidt and Rüterjans, 1990]; Figure 2.8) is based on the application of polarization transfer in conjunction with proton detection. It allows to exclusively detect heteronuclear spin systems of the type  $I_2S$ , I and S representing protons and a heteronucleus, respectively. Hence, a 2D spectrum is obtained showing only signals of the  $^{15}\text{NH}_2$  groups. This type of selection is extremely useful in discriminating asparagine and glutamine side-chain amide protons from those located in the backbone of the polypeptide chain.

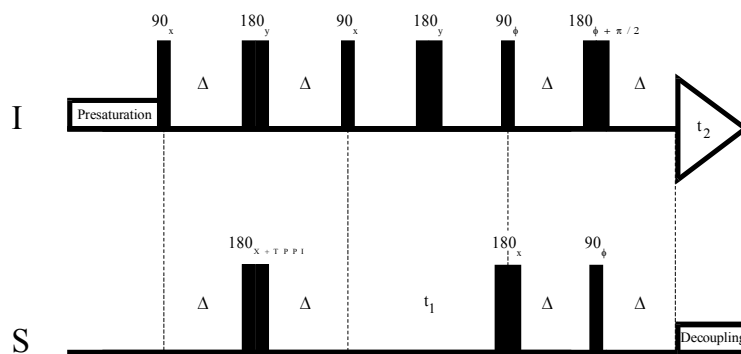


**Figure 2.8** Pulse scheme for heteronuclear shift correlation via  $I_2S$  three-quantum coherences in the HTQC experiment. The delay  $\Delta$  should match  $1/(2J_{SI})$ . The phases are cycled as follows:  $\phi = x, -x$ ;  $\psi = x, x, -x, -x, y, y, -y, -y$ ; ref =  $x, -x, -x, x, -y, y, y, -y$ .

### 2.1.3.8 3D TOCSY-( $^1\text{H}$ , $^{15}\text{N}$ )-HSQC

The information obtained from a 3D TOCSY-( $^1\text{H}$ ,  $^{15}\text{N}$ )-HSQC spectrum is the same as that obtained from the  $F_1(^1\text{H})$ - $F_2(^{15}\text{N})$  region of a 2D  $^1\text{H}$ - $^{15}\text{N}$  TOCSY spectrum, but it is edited according to the  $^{15}\text{N}$  chemical shift associated with the amide  $^1\text{H}^{\text{N}}$ . Since this 3D version shows less spectral overlap, it may provide intraresidue correlations that are important for the sequential assignment process or may be used to obtain qualitative estimates of  $^3J_{\text{H}\alpha\text{H}\beta}$  coupling constants from the relative intensities of well-resolved  $^1\text{H}^{\text{N}}$ - $^1\text{H}^{\beta}$  cross-peaks.

Following the initial  $t_1$  evolution period, a  $90^\circ(^1\text{H})$  pulse returns the frequency-labeled magnetization to the  $\pm z$  axis for the isotropic mixing period. The DIPSI isotropic mixing sequence [Cavanagh and Rance, 1992] transfers  $^1\text{H}$  magnetization from aliphatic spins to the corresponding intraresidual amide protons, while minimizing rotating-frame NOE effects. The  $90^\circ(^1\text{H})$  pulse following the mixing sequence rotates the resulting  $z$ -magnetization back into the transverse plane, and is therefore analogous to the first pulse in an HSQC experiment. The remainder of the sequence is equivalent to a  $^1\text{H}$ - $^{15}\text{N}$  HSQC experiment (Figure 2.9). Following the Fourier transform,  $^{15}\text{N}$ -edited homonuclear TOCSY spectra are obtained.

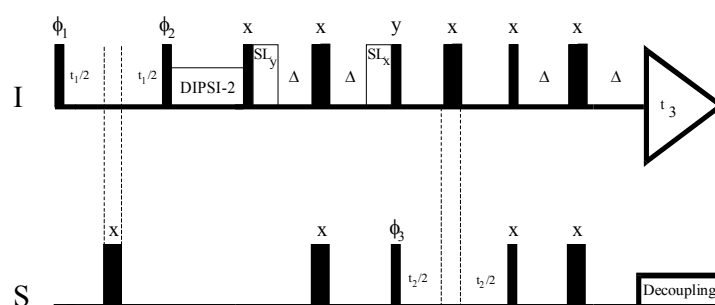


**Figure 2.9** Pulse sequence for the 3D  $^1\text{H}$ - $^{15}\text{N}$  TOCSY-HSQC experiment. The phase cycling is  $\phi_1 = 2(x), 2(-x)$ ;  $\phi_2 = 4(x), 4(-x)$ ;  $\phi_3 = x, -x$ ; receiver =  $x, -x, -x, x, -x, x, x, -x$ . The spinlock purge pulses (SL) are applied for 1-2 ms. ( $I = ^1\text{H}$ ,  $S = ^{13}\text{C}$  or  $^{15}\text{N}$ .)

### 2.1.3.9 3D NOESY-( $^1\text{H}$ , $^{15}\text{N}$ )-HSQC

The 3D NOESY-( $^1\text{H}$ ,  $^{15}\text{N}$ )-HSQC combines a NOESY experiment and a HSQC pulse sequence [Cavanagh *et al.*, 1996]. At the beginning, the sequence is a homonuclear NOESY experiment with  $^{15}\text{N}$  spin decoupling during the  $t_1$  evolution period. Decoupling of the  $J^{\text{H}^{15}\text{N}}$  coupling interaction is achieved by replication of a composite decoupling pulse scheme throughout  $t_1$ . The  $90^\circ(^1\text{H})$  pulse immediately following the mixing time  $t_m$  is equivalent to the first  $90^\circ(^1\text{H})$  pulse in the HSQC experiment, and the remainder of the pulse sequence is identical to the HSQC experiment (Figure 2.10). In the final 3D spectrum, the  $F_1(^1\text{H}) - F_3(^1\text{H})$  projection corresponds to the  $F_1(^1\text{H}) - F_2(^1\text{H}^{\text{N}})$  region of a conventional 2D  $^1\text{H}-^1\text{H}$  NOESY spectrum, and the  $F_2(^{15}\text{N}) - F_3(^1\text{H})$  corresponds to the  $F_1(^{15}\text{N}) - F_2(^1\text{H})$  of a 2D HSQC spectrum.

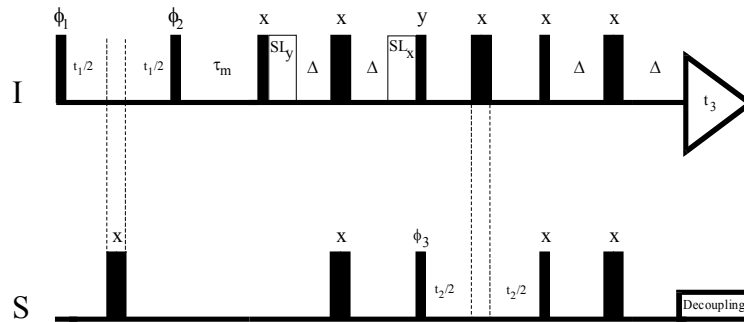


**Figure 2.10** Pulse sequence for the 3D  $^1\text{H}-^{15}\text{N}$  NOESY-HSQC experiment. The phase cycling is  $\phi_1 = 2(x), 2(-x)$ ;  $\phi_2 = 4(x), 4(-x)$ ;  $\phi_3 = x, -x$ ; receiver =  $x, -x, -x, x, -x, x, x, -x$ . The spinlock purge pulses (SL) are applied for 1-2 ms. (I= $^1\text{H}$ , S= $^{13}\text{C}$  or  $^{15}\text{N}$ .)

### 2.1.4 DYANA

During the DYANA calculations, the molecule is represented as a rigid structure with  $n$  bodies fixed by rotating bonds [Abe *et al.*, 1983]. The degrees of freedom consist exclusively of dihedral angles. The target function  $T$  is proportional to the potential energy  $E_{\text{pot}} = \omega_0 T$ , with a constant of proportionality  $\omega_0 = 10 \text{ kJ / mol} \cdot \text{\AA}^2$  :

$$T = \sum_{c=u,l,v} \omega_c \sum_{(\alpha,\beta) \in \mathcal{C}} f_c(d_{\alpha\beta}, b_{\alpha\beta}) + \omega_d \sum_{j \in \mathcal{D}} (1 - 1/2 (\Delta_j / \Gamma_j)^2) \Delta_j^2 \quad (2.1.4.1)$$

Upper and lower bounds,  $b_{\alpha\beta}$ , on distances between two atoms  $\alpha$  and  $\beta$ ,  $d_{\alpha\beta}$ , as well as constraints on individual torsion angles,  $\theta_k$ , in the form of allowed intervals,  $[\theta_k^{\min}, \theta_k^{\max}]$ , are considered.  $I_u$ ,  $I_l$  and  $I_v$  are the sets of atom pairs ( $\alpha, \beta$ ) with upper, lower or van der Waals distance bounds, respectively, and  $I_d$  is the set of restrained torsion angles.  $w_u$ ,  $w_l$ ,  $w_v$  and  $w_d$  are weighting factors for the different types of constraints.  $\Gamma_k = \pi - (\theta_k^{\max} - \theta_k^{\min})/2$  denotes the half-width of the forbidden range of torsion angle values, and  $\Delta_k$  is the size of the torsion angle constraint violation.

For equation (2.1.4.1),  $T \geq 0$ .  $T$  equals 0 only when all the distance and angle constraints are satisfied and when the non-bonding atom pairs show no overlap. The function  $f_c$  indicates the distance constraint violations and can be represented as:

$$f_c(d,b) = ((d^2 - b^2) / 2b)^2 \quad (2.1.4.2a)$$

$$f_c(d,b) = (d - b)^2 \quad (2.1.4.2b)$$

$$f_c(d,b) = \beta^2 [ \sqrt{1 + (d^2 - b^2) / \beta b^2} - 1 ] / 2 \quad (2.1.4.2c)$$

or

$$f_c(d,b) = 2 \beta^2 b^2 [ \sqrt{1 + (d - b)^2 / \beta^2 b^2} - 1 ] \quad (2.1.4.2d)$$

where  $d$  is the experimental distance,  $b$  the distance constraint and  $\beta$  a dimensionless parameter that weighs large violations. The functions (2.1.4.2a), (2.1.4.2b) and (2.1.4.2d) have  $\text{\AA}^2$  units; (2.1.4.2c) is dimensionless. For small distance constraint violations, equations (2.1.4.2a) and (2.1.4.2d) approach equation (2.1.4.2b), and equation (2.1.4.2c) becomes  $((d - b) / b)^2$ . Equation (2.1.4.2a) is used in this work.

For all rigid bodies with  $k = 1, 2, \dots, n$ , the angular velocity vector  $\boldsymbol{\omega}_k$  and the linear velocity vector at the reference point  $\mathbf{v}_k = \mathbf{r}_k$  are calculated recursively [Jain *et al.*, 1993]:

$$\boldsymbol{\omega}_k = \boldsymbol{\omega}_{p(k)} + \mathbf{e}_k d\theta/dt \quad (2.1.4.3)$$

$$\mathbf{v}_k = \mathbf{v}_{p(k)} - (\mathbf{r}_k - \mathbf{r}_{p(k)}) \wedge \boldsymbol{\omega}_{p(k)} \quad (2.1.4.4)$$

The inertia tensor  $\mathbf{I}_k$  of the rigid body  $k$  with respect to its reference point is expressed as a symmetric  $3 \times 3$  matrix with elements given by [Arnold, 1978]:

$$(\mathbf{I}_k)_{ij} = \sum_{\alpha} m_{\alpha} (y_{\alpha}^2 \delta_{ij} - y_{\alpha i} y_{\alpha j}) \quad (2.1.4.5)$$

where  $\mathbf{y}_\alpha$  represents the vector of the reference point of atom  $\alpha$  with mass  $m_\alpha$ . The center of mass and the center of inertia are calculated only once by summation of all atoms with every rigid body in a standard orientation. The obtained values are included in  $\mathbf{Y}_k^{(0)}$  and  $\mathbf{I}_k^{(0)}$ , which may be calculated with the help of the rotation vector  $\mathbf{R}_k$ , where a superscript T denotes the transposed matrix:

$$\mathbf{Y}_k = \mathbf{R}_k \mathbf{Y}_k^{(0)} \quad (2.1.4.6)$$

$$\mathbf{I}_k = \mathbf{R}_k \mathbf{I}_k^{(0)} \mathbf{R}_k^T \quad (2.1.4.7)$$

The kinetic energy is then calculated as

$$E_{\text{kin}} = \frac{1}{2} \sum_{k=1}^n [m_k \mathbf{v}_k^2 + \boldsymbol{\omega} \cdot \mathbf{I}_k \boldsymbol{\omega} + 2 \mathbf{v}_k \cdot (\boldsymbol{\omega}_k \wedge m_k \mathbf{Y}_k)] \quad (2.1.4.8)$$

In order to improve the algorithm efficiency, the molecules are considered as spheres of mass  $m_k$  and radius  $\rho$  centered at the reference point  $\mathbf{r}_k$ . The equations (2.1.4.6) and (2.1.4.7) are then transformed into

$$\mathbf{Y}_k = \mathbf{0} \quad (2.1.4.9)$$

and

$$\mathbf{I}_k = 2 m_k \rho^2 \mathbf{1}_3 \quad (2.1.4.10)$$

where  $\mathbf{1}_3$  is the  $3 \times 3$  unit matrix.

The angular movement in a classical system can be described by the Lagrange equation [Arnold, 1978]:

$$d(\partial L / \partial (d^2 \theta_k / dt^2)) / dt - \partial L / \partial \theta_k = 0 \quad (k = 1, 2, \dots, n) \quad (2.1.4.11)$$

where  $L = E_{\text{kin}} - E_{\text{pot}}$ . For the calculation of the Lagrange operator, the algorithm of Jain *et al.* [1993] is used. The six-dimensional initial vectors  $a_k$ ,  $e_k$  and  $z_k$  are then calculated for all rigid bodies:

$$a_k = \begin{vmatrix} (\boldsymbol{\omega}_k \wedge \mathbf{e}_k) d\theta_k / dt \\ \boldsymbol{\omega}_{p(k)} \wedge (\mathbf{v}_k - \mathbf{v}_{p(k)}) \end{vmatrix} \quad (2.1.4.12)$$

$$e_k = \begin{vmatrix} \mathbf{e}_k \\ \mathbf{0} \end{vmatrix} \quad (2.1.4.13)$$

$$z_k = \begin{vmatrix} \boldsymbol{\omega}_k \wedge \mathbf{I}_k \boldsymbol{\omega}_k \\ (\boldsymbol{\omega}_k \cdot m_k \mathbf{Y}_k) \boldsymbol{\omega}_k - \omega_k^2 m_k \mathbf{Y}_k \end{vmatrix} \quad (2.1.4.14)$$

$$P_k = \begin{vmatrix} \mathbf{I}_k & m_k \mathbf{A}(\mathbf{Y}_k) \\ -m_k \mathbf{A}(\mathbf{Y}_k) & m_k \mathbf{1}_3 \end{vmatrix} \quad (2.1.4.15)$$

$$\varphi_k = \begin{vmatrix} \mathbf{1}_3 & \mathbf{A}(\mathbf{r}_k - \mathbf{r}_{p(k)}) \\ \mathbf{0}_3 & \mathbf{1}_3 \end{vmatrix} \quad (2.1.4.16)$$

where  $\mathbf{0}_3$  is the  $3 \times 3$  zero matrix and  $\mathbf{A}(\mathbf{x})$  is the antisymmetric  $3 \times 3$  matrix associated with the cross product, *i.e.*,  $\mathbf{A}(\mathbf{x}) \mathbf{y} = \mathbf{x} \wedge \mathbf{y}$  for all vectors  $\mathbf{y}$ .

The additional magnitudes

$$D_k = \mathbf{e}_k \cdot P_k \mathbf{e}_k$$

$$G_k = P_k \mathbf{e}_k / D_k$$

$$\varepsilon_k = -\varepsilon_k \cdot (z_k + P_k \mathbf{a}_k) - \partial V / \partial \theta_k$$

$$P_{p(k)} \leftarrow P_{p(k)} + \varphi_k (P_k - G_k \mathbf{e}_k^T P_k) \varphi_k^T$$

$$z_{p(k)} \leftarrow z_{p(k)} + \varphi_k (z_k + P_k \mathbf{a}_k + G_k \mathbf{e}_k) \quad (2.1.4.17)$$

are calculated by executing a recursive loop over all rigid bodies in the backward direction ( $k = n, n - 1, \dots, 1$ ).  $D_k$  and  $\varepsilon_k$  are scalars and  $G_k$  is a six-dimensional vector. The angular acceleration is calculated by recursive iteration ( $k = 1, \dots, n$ ):

$$\alpha_k = \varphi_k^T \alpha_{p(k)}$$

$$d^2 \theta_k / dt^2 = \varepsilon_k / D_k - G_k \cdot \alpha_k \quad (2.1.4.18)$$

$$\alpha_k \leftarrow \alpha_k + \varepsilon_k d^2 \theta_k / dt^2 + \alpha_k$$

The integration of the equations of motion in torsion angle dynamics [Mathiowetz *et al.*, 1994] follows a variant of the leap-frog algorithm used in Cartesian dynamics [Allen and Tildesley, 1987]. The temperature is regulated by weak coupling to an external bath [Berendsen *et al.*, 1984]. A time step,  $t \rightarrow t + \Delta t$ , that follows a preceding time step,  $t - \Delta t' \rightarrow t$ , consists of the following parts:

1. The Cartesian coordinates of all atoms are calculated on the basis of the torsional positions  $\theta(t)$  [Güntert, 1993].
2. The potential energy  $E_{\text{pot}}(t) = E_{\text{pot}}(\theta(t))$  and its gradient  $\nabla E_{\text{pot}}(t)$  are calculated using the Cartesian coordinates from equation (2.1.4.1).
3. The time step  $\Delta t = \lambda_{\epsilon} \Delta t'$  is calculated using the time step scaling factor:

$$\lambda_{\epsilon} = \min(\lambda_{\epsilon}^{\text{max}}, \sqrt{[1 + (\epsilon^{\text{ref}} - \epsilon(t))/\tau \epsilon(t)]}) \quad (2.1.4.19)$$

where  $\lambda_{\epsilon}$  is based on the reference value for the relative accuracy of energy conservation,  $\epsilon^{\text{ref}}$ , and on the relative change  $\epsilon(t)$  of the total energy  $E = E_{\text{kin}} + E_{\text{pot}}$  in the preceding time-step,  $\epsilon(t)$ , as given by:

$$\epsilon(t) = | (E(t) - E(t - \Delta t')) / E(t) | \quad (2.1.4.20)$$

$\lambda_{\epsilon}^{\text{max}}$  is the maximal value of the scaling factor. The time constant,  $\tau \gg 1$ , is a user-defined parameter that is measured in units of the time step. During the calculation of  $\epsilon(t)$ ,  $E(t)$  is used before scaling velocity is applied (step 4); whereas for  $E(t - \Delta t')$  the value after velocity scaling in the preceding time step is used. The measurement of the accuracy of energy conservation (equation 2.1.4.20) is not affected by the scaling of velocities.

4. The temperature is modified by means of a scaling factor  $\lambda_T$  for the torsional velocities [Berendsen *et al.*, 1984]:

$$\lambda_T = \sqrt{[1 + (T^{\text{ref}} - T(t)) / \tau T(t)]} \quad (2.1.4.21)$$

where

$$T(t) = 2 E_{\text{kin}}(t) / nk_B \quad (2.1.4.22)$$

and  $T^{\text{ref}}$  is the reference temperature,  $n$  the number of torsion angles and  $k_B$  the Boltzmann constant ( $1.3806568 \times 10^{-23} \text{ JK}^{-1}$ ).

5. The torsional accelerations  $d^2\theta(t)/dt^2 = d^2\theta[(\theta(t), d\theta_e(t)/dt)]/dt^2$  are calculated using equations (2.1.4.12) - (2.1.4.18).



6. The new velocities at half time step are determined by:

$$d\theta(t + \Delta t/2)/dt = d\theta(t - \Delta t'/2)/dt + \frac{1}{2}(\Delta t + \Delta t') d^2\theta(t)/dt^2 \quad (2.1.4.23)$$

7. The new estimated velocities at full time step are obtained by means of

$$d\theta_e(t + \Delta t)/dt = (1 + \Delta t/(\Delta t + \Delta t'))d\theta(t + \Delta t/2)/dt - \\ (\Delta t/(\Delta t + \Delta t')) d\theta(t - \Delta t'/2)/dt \quad (2.1.4.24)$$

8. The new torsional positions are:

$$\theta(t + \Delta t) = \theta(t) + \Delta t d\theta(t + \Delta t'/2) / dt \quad (2.1.4.25)$$

The algorithm is initialized by setting  $t = 0$ ,  $\Delta t' = \Delta t$ , and  $d\theta_e(0)/dt = d\theta(-\Delta t/2)/dt$  with torsional velocities  $d\theta(-\Delta t/2)/dt$ , which are chosen randomly from a normal distribution with zero mean value and a standard deviation that ensures that the initial temperature has a predefined value,  $T(0)$ . Once the time step  $t \rightarrow t + \Delta t$  is completed by going through the operations (1) to (8),  $t$  is replaced by  $t + \Delta t$  and  $\Delta t'$  by  $\Delta t$ .

Calculating steps with total energy changes ( $\Delta E$ ) of more than 10% are eliminated and substituted by two calculating steps with halved duration. With this procedure it is possible to avoid large energy violations.

### 2.1.5 Energy minimization

The conformers obtained from a distance geometry calculation do not necessarily correspond to a minimal energy structure. Therefore, it is necessary to energy minimize the resulting structures. There are two energy minimization algorithms that are widely used: *steepest descent* and *conjugate gradient*.

The *steepest descent* algorithm looks for the energy minimum along the gradient  $-\nabla E(\mathbf{r})$  on the energy hypersurface. Each line search produces a new direction that is perpendicular to the previous gradient; however, the directions oscillate along the way to the minimum. The algorithm is repeated either for a preestablished number of calculation steps or until the gradient is smaller than a certain  $\varepsilon$ :

$$\varepsilon = 2 \pi \nu \sqrt{2 m k T} \quad (2.1.5.1)$$

where  $\nu$  is the oscillation frequency,  $m$  the reduced mass and  $k$  the Boltzmann constant.

Convergence is slow near the minimum because the gradient approaches zero, where each segment of the path tends to partially reverse progress made in an earlier iteration (since this algorithm does not preserve the results of the previous search, it may be under certain circumstances very inefficient), but it is the method most likely to generate a lower-energy structure regardless of what the function is or where it begins. Therefore, steepest descent is often used when the gradients are large and the structures are far from the minimum.

The conjugate gradient algorithm produces a complete basis set of mutually conjugate directions such that each successive step continually refines the direction toward the minimum. This prevents the next direction vector from undoing earlier progress.

In conjugate gradient,  $\mathbf{h}_{i+1}$ , the new direction vector leading from point  $i+1$ , is computed by adding the gradient at point  $i+1$ ,  $\mathbf{g}_{i+1}$ , to the previous direction  $\mathbf{h}_i$  scaled by a constant  $\gamma_i$ :

$$\mathbf{h}_{i+1} = \mathbf{g}_{i+1} + \gamma_i \mathbf{h}_i \quad (2.1.5.2)$$

where  $\gamma_i$  is a scalar that can be defined in two ways. In the Polak-Ribiere method,  $\gamma_i$  is defined as:

$$\gamma_i = \mathbf{g}_{i+1} \cdot \mathbf{g}_{i+1} / \mathbf{g}_i \cdot \mathbf{g}_i \quad (2.1.5.3)$$

In the Fletcher-Reeves [Fletcher, 1980] method,  $\gamma_i$  is defined as:

$$\gamma_i = (\mathbf{g}_{i+1} - \mathbf{g}_i) \cdot \mathbf{g}_{i+1} / \mathbf{g}_i \cdot \mathbf{g}_i \quad (2.1.5.4)$$

The  $\mathbf{h}_{i+1}$  direction is then used in place of the gradient, and a new line search is conducted. This construction has the characteristic that the next gradient,  $\mathbf{g}_{i+1}$ , is orthogonal to all previous gradients,  $\mathbf{g}_0, \mathbf{g}_1, \mathbf{g}_2, \dots, \mathbf{g}_i$ , and that the next direction,  $\mathbf{h}_{i+1}$ , is conjugate to all previous directions,  $\mathbf{h}_0, \mathbf{h}_1, \mathbf{h}_2, \dots, \mathbf{h}_i$ . Thus, the algorithm produces a set of mutually orthogonal gradients and a set of mutually conjugate directions.

The conjugate gradient method is used for large systems, because only the previous  $3N$  gradients and directions have to be stored. This algorithm is especially effective on flat hypersurfaces. However, to ensure that the directions are mutually conjugate, more complete line search minimizations must be performed along each direction. Since these line searches consume several function evaluations per search, the time per iteration is longer for conjugate gradient than for steepest descent. In practice, both algorithms are used, first the steepest descent and then the *conjugate gradient*.

## 2.2 Backbone dynamics

In recent years, many three-dimensional structures of proteins have been determined by X-ray diffraction and multidimensional NMR. There have been great advances in the knowledge of protein architecture, chemical structure of active sites and biomolecular interfaces, but it has been recognized that knowledge of the static structure is not always sufficient to explain biomolecular function. In order to understand how a biomolecule works, it is necessary to analyze both the slow (on the milli- to microsecond time scale) as well as the fast (on the nano- to picosecond time scale) dynamics in relation to molecular function.

### 2.2.1 Relaxation

For a single spin with quantum number  $I = \frac{1}{2}$  in a magnetic field  $\mathbf{B}_0$ , there are two possible states:  $|\alpha\rangle$  with energy  $E_\alpha = -\frac{1}{2} \gamma \hbar B_0$ , and  $|\beta\rangle$  with energy  $E_\beta = \frac{1}{2} \gamma \hbar B_0$ . In the lower-energy state  $|\alpha\rangle$ , the component of the magnetic moment  $\boldsymbol{\mu}$  along the  $B_0$  axis is  $\mu_z = \frac{1}{2} \gamma \hbar$ , and in the higher-energy state  $|\beta\rangle$  it is  $\mu_z = -\frac{1}{2} \gamma \hbar$ . The total length of the vector  $\boldsymbol{\mu}$  is given by  $|\boldsymbol{\mu}|^2 / \gamma^2 \hbar^2 = I(I+1) = \frac{3}{4}$ . In the plane perpendicular to  $\mathbf{B}_0$ , the  $xy$  plane, there is no preferred orientation. The  $\boldsymbol{\mu}$  vectors of the spins in the  $|\alpha\rangle$  state form a cone pointing along  $\mathbf{B}_0$ , and those in the  $|\beta\rangle$  state form a cone in the opposite direction. Due to the Larmor precession of the spins, the cones as a whole precess around  $\mathbf{B}_0$ . The ratio of the two populations is given by the Boltzmann distribution

$$N_\alpha / N_\beta = \exp(E_\beta - E_\alpha) / kT = \exp(\gamma \hbar B_0 / kT) \quad (2.2.1.1)$$

The population difference generates a net magnetization vector  $\mathbf{M}$  pointing along  $\mathbf{B}_0$ . In the transverse plane, all orientations of the vectors  $\boldsymbol{\mu}$  of the individual spins are equally populated ( $M_x = M_y = 0$ ). If a  $90^\circ$  pulse is applied to this spin system, the  $M_z$  component of  $\mathbf{M}$  will become zero, and  $\mathbf{M}$  will be in the  $xy$  plane. The excess of  $|\alpha\rangle$  disappears and there is no longer a random distribution of the vectors  $\boldsymbol{\mu}$  in the  $xy$  plane, but a favoured orientation. The original situation may be restored by two processes: (a) transitions from the  $|\beta\rangle$  to the  $|\alpha\rangle$  state in order to restore  $M_z$ , *i.e.*, longitudinal relaxation, and (b) dephasing in the  $xy$  plane, *i.e.*, transverse relaxation.

The surroundings of the spins are called the lattice, which provides random fields fluctuating both in direction and magnitude. The mechanisms underlying these fields are

anisotropic interactions between the spins and the  $\mathbf{B}_0$  field, as well as between the spins mutually. Anisotropic means that the strength of the interaction depends on the orientation of the molecule relative to the static  $\mathbf{B}_0$  field. In general, the shielding or deshielding that gives rise to the chemical shift of a nucleus is anisotropic.

Rapid fluctuations are associated with high frequencies and slow ones with low frequencies, making it necessary to determine the characteristic time scale of a random function; furthermore, it is necessary to average over all the spins of the ensemble. The correlation function  $C(\tau)$  is therefore defined as:

$$C(\tau) = \overline{H(t) H(t + \tau)} \quad (2.2.1.2)$$

where the bar indicates that the ensemble average must be taken. The correlation function  $C(\tau)$  is a decaying function of  $\tau$  and is independent of  $t$ . For  $\tau = 0$ ,

$$C(0) = \overline{H(t) H(t)} = \overline{H(0)^2} \quad (2.2.1.3)$$

Averaging over the ensemble of  $H(t)$  is equivalent to averaging over time  $t$ . The quantity  $\overline{H(0)^2}$  is called the power of the interaction represented by  $H(t)$ . If  $\tau$  is very long, then

$$\lim_{\tau \rightarrow \infty} C(\tau) = 0 \quad (2.2.1.4)$$

*i.e.*, if  $\tau$  is long enough, then  $H(t)$  and  $H(t + \tau)$  are no longer correlated.

Correlation functions involved in NMR relaxation are exponentially decaying with one or more characteristic time constant, called correlation time. For a single correlation time  $\tau_c$ ,

$$C(\tau) = \overline{H(0)^2} \exp(-|\tau| / \tau_c) \quad (2.2.1.5)$$

The correlation function  $C(\tau)$  provides the time scale, characterized by the correlation times of the interaction  $H(t)$ . The spectral density function  $J(\omega)$ , *i.e.*, the cosine Fourier transform of  $C(\tau)$ , gives the frequency characteristics:

$$J(\omega) = \int_0^\infty \cos(\omega t) C(\tau) d\tau \quad (2.2.1.6)$$

Substitution of  $C(\tau)$  given by equation (2.2.1.5) yields the Lorentzian

$$J(\omega) = \tau_c / (1 + \omega^2 \tau_c^2) \quad (2.2.1.7)$$

The power of the interaction,  $\overline{H(0)^2}$ , is usually excluded from the definition of the spectral density function  $J(\omega)$ .

The time change of a spin system is defined by its Hamiltonian, which can be divided into two parts:

$$H = H_0 + H_1(t) \quad (2.2.1.8)$$

where  $H_0$  represents the time-independent part of the Hamiltonian (e.g. chemical shift or scalar coupling) and  $H_1(t)$  the randomly fluctuating part, *i.e.*, the coupling between the spin system and the environment, which is assumed to have an average value of zero for dipolar interaction and chemical shift anisotropy. The spin system can exchange energy with the environment through  $H_1(t)$ , which is then responsible for the relaxation. If the Hamiltonian is defined as in equation (2.2.1.8), the Liouville equation of motion of the density operator is

$$d\sigma(t)/dt = -i [H(t), \sigma(t)] = -i [H_0 + H_1(t), \sigma(t)] \quad (2.2.1.9)$$

For dissipative processes, only the time-independent or stochastic part of the Hamiltonian is important. The density operator and stochastic Hamiltonian are defined as

$$\sigma^T(t) = \exp\{iH_0t\} \sigma(t) \exp\{-iH_0t\} \quad (2.2.1.10)$$

$$H_1^T(t) = \exp\{iH_0t\} H_1(t) \exp\{-iH_0t\} \quad (2.2.1.11)$$

from which the form of the transformed Liouville equation can be determined. The final result is

$$d\sigma(t)/dt = -i [H_1^T(t), \sigma^T(t)] \quad (2.2.1.12)$$

A very large number of physical interactions give rise to stochastic Hamiltonians capable of mediating spin relaxation. The most common are the intramolecular magnetic dipole-dipole (DD), chemical shift anisotropy (CSA), quadrupolar, and scalar coupling interactions. Intramolecular paramagnetic relaxation has the same Hamiltonian as for nuclear dipolar relaxation, except that the interaction occurs between a nucleus and an unpaired electron. For spin  $\frac{1}{2}$  nuclei in diamagnetic biological macromolecules, the dominant relaxation mechanisms are the magnetic DD and CSA interactions. For nuclei with spin  $> \frac{1}{2}$ , specially  $^{14}\text{N}$  and  $^2\text{H}$  in proteins, the dominant relaxation mechanism is based on quadrupolar interactions. The cross-relaxation mechanism between the DD and the CSA interactions

becomes important for large proteins in strong magnetic fields. In this case, the Hamiltonian equals

$$H_1(t) = H^{\text{DD}}(t) + H^{\text{CSA}}(t) + H^{\text{CSA/DD}}(t) \quad (2.2.1.13)$$

where  $H^{\text{DD}}$  is the Hamiltonian for the dipole-dipole interaction,  $H^{\text{CSA}}$  for the interaction of the chemical shift with the external magnetic field and  $H^{\text{CSA/DD}}$  for cross-relaxation between the DD and the CSA interactions. In two-spin systems, a cross-relaxation produces a differentiated relaxation of lines, *i.e.*, the doublet components show a different line width.

Relaxation rate constants for nuclei in proteins depend on a large number of factors, including overall rotational correlation times, internal motions, the geometric arrangement of nuclei, and the relative strengths of the applicable relaxation mechanisms. In general,  $^1\text{H}$  relaxation in proteins is dominated by dipolar interactions with other protons (within approximately  $5\text{\AA}$ ) and by interactions with directly bonded heteronuclei, which arise from dipolar interactions with  $^{13}\text{C}$  and  $^{15}\text{N}$  in isotopically enriched proteins or from scalar relaxation between the quadrupolar  $^{14}\text{N}$  nuclei and amide protons. Relaxation of protonated  $^{13}\text{C}$  and  $^{15}\text{N}$  heteronuclei, in turn, is dominated by dipolar interactions with the directly bonded protons, and secondly by CSA (for  $^{15}\text{N}$  spins and aromatic  $^{13}\text{C}$  spins). At 500 MHz magnetic field strength, the  $^{15}\text{N}$  nucleus relaxes 80% by dipolar interaction with the attached amide proton and 20% by CSA. On the other hand, relaxation of unprotonated heteronuclei, notably carbonyl  $^{13}\text{C}$  and unprotonated aromatic  $^{13}\text{C}$  spins, is dominated by CSA interactions [Cavanagh *et al.*, 1996].

## 2.2.2 The dipole-dipole interaction

The most important relaxation mechanism is that caused by the dipole-dipole interaction. Classically, the interaction energy of two magnetic moments,  $\boldsymbol{\mu}_1$  and  $\boldsymbol{\mu}_2$ , is

$$E_{1,2} = \{ \boldsymbol{\mu}_1 \cdot \boldsymbol{\mu}_2 - 3(\boldsymbol{\mu}_1 \cdot \mathbf{n}_{1,2})(\boldsymbol{\mu}_2 \cdot \mathbf{n}_{1,2}) \} / r_{1,2}^3 \quad (2.2.2.1)$$

where  $\mathbf{r}_{1,2}$  is the distance between  $\boldsymbol{\mu}_1$  and  $\boldsymbol{\mu}_2$  (assumed to be point dipoles as a good approximation for NMR), and  $\mathbf{n}_{1,2}$  is the unit vector along the line connecting them, *i.e.*,  $\mathbf{n}_{1,2} = \mathbf{r}_{1,2} / |\mathbf{r}_{1,2}|$ . In a quantum mechanical formalism [Fischer *et al.*, 1998]:

$$H_{1,2} = \gamma_1 \gamma_2 \hbar \{ \mathbf{I}_1 \cdot \mathbf{I}_2 - 3 (\mathbf{I}_1 \cdot \mathbf{n}_{1,2})(\mathbf{I}_2 \cdot \mathbf{n}_{1,2}) \} / r_{1,2}^3 \quad (2.2.2.2)$$

In the Euclidian coordinate system with the z-axis parallel to  $\mathbf{n}_{1,2}$ ,  $H_{1,2}$  becomes

$$H_{1,2} = \gamma_1 \gamma_2 \hbar \{ \mathbf{I}_1 \cdot \mathbf{I}_2 - 3 I_Z^{(1)} I_Z^{(2)} \} / r_{1,2}^3 \quad (2.2.2.3)$$

The relaxation due to dipole-dipole interaction between two nuclei can be described by the correlation function [Wallach, 1967; Wittebort and Szabo, 1978]:

$$C(\tau) = \langle D_{qo}^{(2)*}(\Omega_{LF}(0)) D_{qo}^{(2)}(\Omega_{LF}(\tau)) \rangle \quad (2.2.2.4)$$

where  $D_{mn}^{(2)}(\Omega)$  is a Wigner rotation matrix element [Brink and Satchler, 1968] and the Euler angles,  $\Omega_{LF}$ , specify the orientation of the unit vector,  $\boldsymbol{\mu}_{LF}$ , connecting the two nuclei in the laboratory coordinate system. This correlation function also describes quadrupolar and chemical shift anisotropy relaxation in the special case where the involved tensors are axially symmetric. For a system in solution, the correlation function does not depend on the index  $q$  and can be rewritten by using the addition theorem for spherical harmonics [Brink and Satchler, 1968] as a correlation function that can be factored as [Lipari and Szabo, 1982a,b]:

$$C(\tau) = C_0(\tau)C_i(\tau) \quad (2.2.2.5)$$

where, in the case of overall isotropic motion,

$$C_0(\tau) = (1/5) \exp(-6D_M\tau) = (1/5) \exp(-\tau/\tau_M) \quad (2.2.2.6)$$

with  $D_M$  and  $\tau_M$  as the rotational diffusion constant and correlation time of the macromolecule, respectively, and where the correlation function for internal motions is

$$C_i(\tau) = \langle P_2(\boldsymbol{\mu}(0) \cdot \boldsymbol{\mu}(\tau)) \rangle \quad (2.2.2.7)$$

The  $P_2(x)$  element is the second Legendre polynomial

$$P_2(x) = (1/2) (3x^2 - 1) \quad (2.2.2.8)$$

The correlation function therefore equals:

$$C(\tau) = (1/5) \langle P_2(\boldsymbol{\mu}_{\text{LF}}(0) \cdot \boldsymbol{\mu}_{\text{LF}}(\tau)) \rangle \quad (2.2.2.9)$$

For  $^{15}\text{N}$  NMR of protonated nitrogens, where at currently available fields the relaxation is primarily dipolar, the relaxation times and the nuclear Overhauser effect (NOE) are given by [Abragam, 1961; Farrow *et al.*, 1994]:

$$T_1^{-1} = d^2 [J(\omega_{\text{H}} - \omega_{\text{N}}) + 3J(\omega_{\text{N}}) + 6J(\omega_{\text{H}} + \omega_{\text{N}})] + c^2 J(\omega_{\text{N}}) \quad (2.2.2.10)$$

$$T_2^{-1} = 0.5 d^2 [4J(0) + J(\omega_{\text{H}} - \omega_{\text{N}}) + 3J(\omega_{\text{N}}) + 6J(\omega_{\text{H}}) + 6J(\omega_{\text{H}} + \omega_{\text{N}})] + (1/6) c^2 [3J(\omega_{\text{N}}) + 4J(0)] \quad (2.2.2.11)$$

$$\text{NOE} = 1 + (\gamma_{\text{H}}/\gamma_{\text{N}}) d^2 [6J(\omega_{\text{H}} + \omega_{\text{N}}) - J(\omega_{\text{H}} - \omega_{\text{N}})] T_1 \quad (2.2.2.12)$$

The constants  $d^2$  and  $c^2$  are defined as

$$d^2 = 0.1 \gamma_{\text{H}}^2 \gamma_{\text{N}}^2 h^2 / (4\pi^2) \langle 1/r_{\text{NH}}^3 \rangle^2 \quad (2.2.2.13)$$

$$c^2 = (2/15) \gamma_{\text{N}}^2 H_0^2 (\sigma_{\parallel} - \sigma_{\perp})^2 \quad (2.2.2.14)$$

where  $\gamma_{\text{H}}$  and  $\gamma_{\text{N}}$  are the gyromagnetic ratios of the  $^1\text{H}$  and  $^{15}\text{N}$  nuclei, respectively,  $\omega_{\text{H}}$  and  $\omega_{\text{N}}$  are their Larmor precessional frequencies, respectively,  $r_{\text{NH}}$  is their internuclear distance (1.02 Å), and  $H_0$  is the magnetic field strength. The parallel and perpendicular components of the axially symmetrical  $^{15}\text{N}$  chemical shift tensor are represented by  $\sigma_{\parallel}$  and  $\sigma_{\perp}$ , respectively. The assumption of an axially symmetric chemical shift tensor has been shown to be valid for backbone amides in proteins with a value of  $-160$  ppm for  $\sigma_{\parallel} - \sigma_{\perp}$  [Hiyama *et al.*, 1988].

### 2.2.3 The chemical shift anisotropy relaxation

The interaction energy of the magnetic dipole of a nuclear spin,  $I$ , and the external field,  $B_0$ , modulated by the chemical shift tensor,  $\sigma$ , is denoted by the chemical shift Hamiltonian

$$H^{\text{CS}} = \gamma \sum_{ij} B_i \sigma_{ij} I_j \quad (2.2.3.1)$$



where  $i$  and  $j$  correspond to the components  $x'$ ,  $y'$  and  $z'$  of a coordinate system attached to the molecule. Since  $\sigma$  is a hermitian operator, it has real eigenvalues and orthogonal eigenvectors. As a consequence, the unitary transformation that diagonalizes  $\sigma$  is equivalent to a rotation or change of coordinate axes to the principle axes,  $xyz$ , where the Hamiltonian is defined as [Fischer *et al.*, 1998]:

$$H^{\text{CS}} = \gamma \{ \sigma_{\text{XX}} B_X I_X + \sigma_{\text{YY}} B_Y I_Y + \sigma_{\text{ZZ}} B_Z I_Z \} \quad (2.2.3.2)$$

Since any arbitrary tensor can be written as the sum of two axially symmetric tensors, it can be assumed that the chemical shift tensor is axially symmetric, *i.e.*, that  $\sigma_{\text{XX}} = \sigma_{\text{YY}} = \sigma_{\perp}$  and  $\sigma_{\text{ZZ}} = \sigma_{\parallel}$ , making the calculations much simpler. The chemical shift Hamiltonian may thus be written as

$$\begin{aligned} H^{\text{CS}} &= \gamma \{ \sigma_{\parallel} B_Z I_Z + \sigma_{\perp} (B_X I_X + B_Y I_Y) \} \\ &= \gamma \{ (1/3)(\sigma_{\parallel} + 2\sigma_{\perp}) \mathbf{B} \cdot \mathbf{I} + (1/3)(\sigma_{\parallel} - \sigma_{\perp}) (2 B_Z I_Z - B_X I_X - B_Y I_Y) \} \end{aligned} \quad (2.2.3.3)$$

The first term is invariant under rotation and does not contribute to relaxation as the molecule tumbles. This term is the ordinary, isotropic chemical shift  $\sigma_{\text{iso}} = (1/3)(\sigma_{\parallel} + 2\sigma_{\perp})$ . The second term is the chemical shift anisotropy interaction,  $H^{\text{CSA}}$ , which may be written in a form identical to that of the dipolar interaction:

$$H^{\text{CSA}} = -(1/3) \gamma (\sigma_{\parallel} - \sigma_{\perp}) (\mathbf{B} \cdot \mathbf{I} - 3 B_Z I_Z) \quad (2.2.3.4)$$

## 2.2.4 The spectral density function of Lipari and Szabo

In order to obtain useful information about protein dynamics from the  $^{15}\text{N}$  relaxation parameters, it is necessary to use a functional form for the spectral density. Two separate descriptions of the spectral density are often used, each expressing a different dependence on the molecular motions responsible for relaxation: the model-free formalism of Lipari and Szabo and the model-free formalism of Clore and Gronenborn.

The information on fast internal motions that is contained in an NMR relaxation experiment can be described completely by (a) a generalized order parameter,  $S$ , which is the measure of the degree of spatial restriction of the motion and satisfies the inequalities  $0 \leq S^2 \leq 1$ , and (b) an effective correlation time,  $\tau_e$ , which is a measure of the rate of the motion. The relaxation of nuclei in proteins is determined by their global movement and by local dynamical effects. Therefore, it is necessary to use a model that also takes into account these local effects. In the model-free approach of Lipari and Szabo [1982a,b], the global and the local motions do not have an influence on each other, *i.e.*, there is no coupling between them. This can be expressed by means of a correlation function that can be factored as described in the section 2.2.2.

For the formulation of local dynamics in the protein backbone, Lipari and Szabo [1982a,b] made the following assumptions:

1.  $C_i(0) = \langle P_2(\boldsymbol{\mu}(0) \cdot \boldsymbol{\mu}(0)) \rangle = 1$
2. The correlation function must be monotonously decreasing.
3. Because of steric restrictions, a NH vector set will not be uniformly distributed over a spherical surface, but will cover only a fraction of the surface. For the correlation function, this implies that  $C(\infty) = S^2$ .
4. The correlation function for the overall tumbling is assumed to be isotropic and mono-exponential. The simplest approximation of  $C_i(t)$  which is exact at  $t=0$  and at  $t=\infty$  has the form

$$C_i(\tau) = S^2 + (1 - S^2) \exp(-\tau/\tau_e) \quad (2.2.4.3)$$

where  $\tau_e$  is the effective correlation time.

The overall tumbling of the macromolecule and its internal motions are described by the expression

$$J(\omega) = S^2 \tau_m / (1 + \omega^2 \tau_m^2) + (1 - S^2) \tau / (1 + \omega^2 \tau^2) \quad (2.2.4.4)$$

The dynamics of each backbone amide is characterized by a time-correlation function factorizable into two independent components: the overall tumbling of the macromolecule and the internal motion of the NH vector.  $S^2$  is known as the generalized order parameter, a model-independent measure of the degree of spatial restriction of the motion (within the

limits  $0 \leq S^2 \leq 1$ ). If the internal motion is isotropic,  $S^2$  vanishes; if the amide is completely restricted in its motion,  $S^2$  equals unity. The effective correlation time resulting from internal motions is  $\tau_e$ , where

$$1 / \tau = 1 / \tau_m + 1 / \tau_e \quad (2.2.4.5)$$

## 2.2.5 The Clore-Gronenborn model

An extended form of the model-free formalism has been developed [Clore *et al.*, 1990a,b] to describe internal motions that take place on two distinct time scales, differing by at least one order of magnitude and affecting all three NMR relaxation parameters:  $T_1$ ,  $T_2$  and NOE.

In the Clore-Gronenborn model, the order parameter is divided into two components: a fast order parameter ( $S_f$ ) and a slow one ( $S_s$ ). For each order parameter there is a corresponding local correlation time. The generalized order parameter then becomes a product of the individual fast and slow order parameters:

$$S^2 = S_f^2 S_s^2 \quad (2.2.5.1)$$

Consequently, the correlation function is expressed in a four-parameter equation

$$\begin{aligned} C_i(\tau) &= \{S_f^2 + (1 - S_f^2) \exp(-\tau/\tau_f)\} \{S_s^2 + (1 - S_s^2) \exp(-\tau/\tau_s)\} \\ &= S_f^2 S_s^2 + S_f^2 (1 - S_s^2) \exp(-\tau/\tau_s) + S_s^2 (1 - S_f^2) \exp(-\tau/\tau_f) + \dots \\ &\dots + (1 - S_f^2) (1 - S_s^2) \exp(-\tau/\tau_f) \exp(-\tau/\tau_s) \end{aligned} \quad (2.2.5.2)$$

Assuming slower global motions within the observation range ( $\tau \approx \tau_s \gg \tau_f$ ) and faster thermal motions, the double exponential term in equation (2.2.5.2) may be neglected. As a result, a four-parameter bi-exponential model is obtained:

$$C_i(\tau) = S_f^2 S_s^2 + S_f^2 (1 - S_s^2) \exp(-\tau/\tau_s) + S_s^2 (1 - S_f^2) \exp(-\tau/\tau_f) \quad (2.2.5.3)$$

Assuming that the correlation time describing the faster of the two time scales,  $\tau_f$ , is sufficiently small to make only a negligible contribution to the relaxation, the extended spectral density can be described as

$$J(\omega) = S^2 t_m / (1 + \omega^2 \tau_m^2) + (S_f^2 - S^2) \tau / (1 + \omega^2 \tau^2) \quad (2.2.5.4)$$

where the effective correlation time for slow internal motions,  $\tau_s$ , is derived from the relationship

$$1 / \tau = 1 / \tau_m + 1 / \tau_s \quad (2.2.5.5)$$

## 2.2.6 The exchange parameter

An additional term, the exchange parameter  $R_{ex}$ , can be used to account for contributions to the transverse relaxation rate from processes other than the dipole-dipole interaction and chemical shift anisotropy. In most cases, these contributions are the result of conformational exchange averaging. The additional  $R_{ex}$  term is included by a modification of the transverse relaxation rate:

$$1 / T_2 = 1 / T_{2(DD)} + 1 / T_{2(CSA)} + R_{ex} \quad (2.2.6.1)$$

where DD and CSA refer to the contributions of the dipole-dipole interaction and the chemical shift anisotropy to the relaxation, respectively. While the generalized order parameter and internal correlation time are sensitive to motions faster than the overall correlation time ( $\tau_e$  is generally in the range of nanoseconds to picoseconds), chemical exchange processes contributing to the  $R_{ex}$  term occur on a time scale several orders of magnitude slower (milliseconds to microseconds).

## 3 Materials and methods

### 3.1 Protein preparation

The recombinant human E-FABP samples were kindly provided by Carsten Hohoff and Thorsten Hanhoff from the University of Münster. The protein was heterologously expressed in *Escherichia coli* and purified according to the procedure reported by Hohoff *et al.* [1999].

To obtain  $^{15}\text{N}$ -enriched E-FABP, the protein was expressed in M9 minimal medium with  $^{15}\text{NH}_4\text{Cl}$  (Cambridge Isotope Laboratories, Andover, USA) as the sole nitrogen source. All protein samples were delipidated with Lipidex-1000 according to the method of Glatz and Veerkamp [1983] and subsequently relipidated using a threefold excess of stearic acid (C18:0), for which E-FABP shows the highest binding affinity [Siegenthaler *et al.*, 1994].

Recombinant bovine H-FABP was prepared and delipidated as reported elsewhere [Lassen *et al.*, 1995]. The hydrogen/deuterium exchange of H-FABP in the apo-form (1.2 mM) was performed as previously described for holo H-FABP [Lücke *et al.*, 1992]. A series of homonuclear 1D and 2D NMR experiments were collected at a temperature of 310 K and a  $^1\text{H}$  resonance frequency of 600.13 MHz to follow the amide proton exchange over time.

### 3.2 NMR data collection and processing

The NMR data collection was performed at pH 5.6 and 298 K. The E-FABP samples were prepared at 3-4 mM concentration in 20 mM potassium phosphate buffer ( $\text{H}_2\text{O}:\text{D}_2\text{O} = 90:10$ , v/v) with 0.05%  $\text{NaN}_3$ .

Homonuclear TOCSY and NOESY as well as  $^{15}\text{N}$ -edited HTQC, HSQC, TOCSY-HSQC and NOESY-HSQC experiments were carried out on a Bruker DMX spectrometer operating at a  $^1\text{H}$  resonance frequency of 600.13 MHz and using a 5 mm triple-resonance ( $^1\text{H}/^{13}\text{C}/^{15}\text{N}$ ) probe with XYZ-gradient capability (Table 3.1). The homonuclear TOCSY and NOESY spectra were recorded in a phase-sensitive mode with time-proportional phase incrementation (TPPI) of the initial pulse. Quadrature detection was used in both dimensions with the carrier placed in the center of the spectrum on the water resonance. The water signal was suppressed by selective presaturation during the relaxation delay. In the NOESY experiments water saturation was applied also during the mixing time. The TOCSY experiments were performed with the Bruker program mlevprtp (homonuclear Hartman-Hahn

**Table 3.1** Acquisition parameters for homonuclear TOCSY and NOESY as well as  $^{15}\text{N}$ -edited HTQC, HSQC, TOCSY-HSQC and NOESY-HSQC experiments.

### Homonuclear TOCSY and NOESY experiments

Experiment		TOCSY	TOCSY	NOESY
Spinlock or mixing time (ms)		80	4.8	200
Data points	F <sub>1</sub>	512	512	512
	F <sub>2</sub>	2048	2048	2048
Spectral width (Hz)	F <sub>1</sub>	7374.63	7374.63	7374.63
	F <sub>2</sub>	7374.63	7374.63	7374.63
Spectral width (ppm)	F <sub>1</sub>	12.29	12.29	12.29
	F <sub>2</sub>	12.29	12.29	12.29
Resonance frequencies (MHz)	F <sub>1</sub>	600.130	600.130	600.130
	F <sub>2</sub>	600.130	600.130	600.130

### $^{15}\text{N}$ -edited HTQC and HSQC

Experiment		HTQC	HSQC	HSQC
Data points	F <sub>1</sub>	256	512	512
	F <sub>2</sub>	512	1024	1024
Spectral width (Hz)	F <sub>1</sub>	608.18	4257.18	2219.81
	F <sub>2</sub>	2097.32	4194.63	4194.63
Spectral width (ppm)	F <sub>1</sub>	10.00	70.00	36.50
	F <sub>2</sub>	3.49	6.99	6.99
Resonance frequencies (MHz)	F <sub>1</sub>	60.810	60.810	60.810
	F <sub>2</sub>	600.130	600.130	600.130

### $^{15}\text{N}$ -edited TOCSY-HSQC and NOESY-HSQC

Experiment		TOCSY-HSQC	NOESY-HSQC
Data points	F <sub>1</sub>	80	80
	F <sub>2</sub>	256	256
	F <sub>3</sub>	1024	1024
Spectral width (Hz)	F <sub>1</sub>	2219.85	2219.85
	F <sub>2</sub>	7788.16	7788.16
	F <sub>3</sub>	7788.16	7788.16
Spectral width (ppm)	F <sub>1</sub>	36.500	36.50
	F <sub>2</sub>	12.98	12.98
	F <sub>3</sub>	12.98	12.98
Resonance frequencies (MHz)	F <sub>1</sub>	60.810	60.810
	F <sub>2</sub>	600.130	600.130
	F <sub>3</sub>	600.130	600.130

transfer using the MLEV17 sequence for mixing and two different power levels for excitation and spinlock [Bax and Davis, 1985]). The spinlock times were set to either 80 or 4.8 ms (to obtain COSY-type information with less spectral overlap). For the NOESY experiments, a modified version of the Bruker program noesyprtp (2D homonuclear correlation via dipolar coupling with presaturation during relaxation delay and mixing time) was used with mixing times ranging between 150 and 200 ms.

All three-dimensional experiments made use of pulsed-field gradients for coherence selection and artifact suppression, while gradient-sensitivity-enhancement schemes were utilized when appropriate [Kay *et al.*, 1992; Schleucher *et al.*, 1993]. Quadrature detection in the indirectly-detected dimensions was achieved by either the States/TPPI or the echo-antiecho method. Baseline corrections were applied wherever necessary. All spectra were calibrated with respect to 2,2-dimethyl-2-silapentane-5-sulfonate (Cambridge Isotope Laboratories, Andover, USA) as an external reference [Wishart *et al.*, 1995].

The spectral data were processed on a Silicon Graphics workstation using the Bruker XWIN-NMR 1.3 software package. Peak-picking and data analysis of the transformed spectra were performed with the AURELIA 2.5.9 program (Bruker, Karlsruhe, Germany).

### 3.3 Constraint generation and structure calculation

The complete  $^1\text{H}$  and  $^{15}\text{N}$  resonance assignments were obtained via the classical NOE-based assignment strategy of Wüthrich in a modified form [Wüthrich, 1986; Bax, 1989; Bax and Grzesiek, 1993], as described in section 2.1.1. of this work. The assignments for the  $\text{NH}_2$  groups of the asparagine and glutamine side-chains were derived from a  $^1\text{H}/^{15}\text{N}$ -HTQC spectrum. The side-chain amide resonances of the arginine residues were obtained using a  $^1\text{H}/^{15}\text{N}$ -HSQC spectrum with a large spectral width of 70 ppm (Table 3.1).

The NOE-derived distance constraints were determined from 2D homonuclear NOESY and 3D  $^{15}\text{N}$ -edited NOESY-HSQC spectra. Automated assignments of the NOEs were made on the basis of only chemical shifts using a self-written MATLAB 5.0 routine. The upper distance limits were set by an internal calibration based on the intensities of sequential and medium-range NOE values from residues within well-defined secondary structure elements. For the distance calibration of the sequential  $\text{H}\alpha$ -HN sequential NOE connectivities in the  $\beta$ -sheet structures were set to an atom distance of 2.5 Å, based on the following residue pairs: L13-V14, C43-I44, T76-T77, Q84-T85, G92-A93, Q96-H97, K115-L116 and V118-

E119. For the interstrand HN-HN and H $\alpha$ -HN NOE connectivities, corresponding to a distance limit of 3.5 Å, the following pairs were used: V134-W11, E132-L13, V121-C127, L13-D42, C43-W11, N51-D48, I54-F65, L116-Y131, V95-F89 and G9-I45. Finally, for the HN-HN( $i, i + 2$ ) connectivities in an  $\alpha$ -helix, representing a distance of 4.5 Å, the NOEs between residues K17-F19, M23-E25, G29-A31 and M35-A37 served as calibration references. The cross-peak intensities were subsequently grouped into four different distance categories: 2.5, 3.5, 4.5 and 6.0 Å.

Experimental evidence about hydrogen bonds was obtained from hydrogen/deuterium exchange. First, the NMR sample buffer, 20 mM potassium phosphate buffer (H<sub>2</sub>O:D<sub>2</sub>O = 90:10, v/v) with 0.05% NaN<sub>3</sub> and pH 5.6, was lyophilized and subsequently D<sub>2</sub>O was added. This was repeated twice in order to obtain a perdeuterated buffer. Approximately 6 mg of E-FABP in protonated solution were concentrated to 100  $\mu$ l and then 1.9 ml of perdeuterated buffer were added. The solution was centrifugated at 277 K until it reached again a volume of 100  $\mu$ l. This procedure was repeated 6 times in 6 hours until the protein sample had a 1.5-2.0 mM concentration in perdeuterated 20 mM potassium phosphate buffer with 0.05% NaN<sub>3</sub> and pH 7.6 (uncorrected reading). The protein sample was then put into a Bruker DMX spectrometer operating at a <sup>1</sup>H resonance frequency of 600.13 MHz and the temperature was set to 298 K. An alternating series of 1D and homonuclear TOCSY experiments was then started immediately. The TOCSY experiments (with a spinlock time of 80 ms) were carried out 19 min and 1, 2, 5, 15, 24, 33 and 43 hours after the sample was set to 298 K. Slow-exchanging backbone amide protons were then identified to be part of the hydrogen-bonding network in the  $\beta$ -sheet and subsequently converted into additional distance constraints. The distance between N and O atoms in the hydrogen bridges was fixed at 3.2 Å; the distance between H<sup>N</sup> and O atoms at 2.2 Å.

The structure calculations were performed with the DYANA 1.5 program package [Güntert *et al.*, 1997], which uses simulated annealing combined with molecular dynamics in torsion angle space. The distance constraints used for the structure calculations are listed in Appendix A.1. Assignments of ambiguous NOE cross-peaks were made by applying a structure-aided filtering strategy in repeated rounds of structure calculations. Starting *ab initio*, 300 conformers were calculated in 8000 annealing steps each. A total of 126 stereospecific assignments of the prochiral methylene and isopropyl groups were obtained with the program GLOMSA [Güntert *et al.*, 1991]. Pseudoatom correction for unassigned stereo partners and magnetically equivalent protons (Table 3.2) was applied as proposed by Wüthrich and co-workers [Wüthrich *et al.*, 1983]. Subsequent energy minimization in the



**Table 3.2** Amino acid pseudoatoms used for the interpretation of NOE distance constraints in proteins. The indices A, B, G, D, E and H are used instead of the more common Greek letters to identify the side-chain atom positions [Wüthrich *et al.*, 1983].

Chemically equivalent protons	Pseudoatom	Correction value (Å)
Methylene group	QA, QB, QG, QD, QE, QH	0.9
Methyl group	QB, QG, QD	1.1
Isopropyl group	QQG, QQD	2.3
Phenyl ring (H $\delta$ or H $\epsilon$ )	QD, QE	2.2
Phenyl ring (all protons)	QR	2.5

presence of the NMR restraints was performed on the 20 best DYANA conformers using the DISCOVER module of the INSIGHT 97 software package (Molecular Simulations Inc., San Diego, USA). The consistent valence force field (CVFF) [Dauber-Ogusthorpe *et al.*, 1988] was used with a dielectric constant equal to  $r$  (distance in Å). A force constant of 20 kcal mol<sup>-1</sup> Å<sup>-2</sup> was used in the NOE restraint term. The resulting structures were analyzed with PROCHECK-NMR [Laskowski *et al.*, 1993].

### 3.4 Relaxation measurements

$T_1$ ,  $T_2$  and steady-state heteronuclear  $^{15}\text{N}\{^1\text{H}\}$  NOE measurements were performed according to known pulse schemes with a gradient-selected echo/antiecho sensitivity enhancement technique [Stone *et al.*, 1992; Akke *et al.*, 1994]. For the longitudinal ( $R_1$ ) and transverse ( $R_2$ ) relaxation rate constants, a series of 8 - 12 spectra with relaxation periods between 16 - 960 msec for  $T_1$  and 25 - 282 msec for  $T_2$  were collected on Bruker DMX spectrometers operating at  $^1\text{H}$  resonance frequencies of 499.87, 600.13 and 800.13 MHz (Table 3.3).  $R_1$  and  $R_2$  rates were determined by non-linear least square fitting of the integrated peak intensities versus time, using mono-exponential functions provided in the RMX software package developed in our laboratory by Jürgen Schmidt (presently at the National Institute for Medical Research, London). The steady-state heteronuclear  $^{15}\text{N}\{^1\text{H}\}$  NOEs were obtained from the ratio of the

**Table 3.3** Relaxation periods for the longitudinal ( $T_1$ ) and transverse ( $T_2$ ) relaxation. $T_1$  at 499 MHz

Loop counter	Spectrum number	Relaxation period (ms)
2	1	16
80	2	640
10	3	80
28	4	224
38	5	304
14	6	112
6	7	48
64	8	512
20	9	160
4	10	32
50	11	400

 $T_2$  at 499 MHz

Loop counter	Spectrum number	Relaxation period (ms)
3	1	23.24
27	2	209.17
6	3	46.48
24	4	185.93
15	5	116.21
21	6	162.69
9	7	69.72
12	8	92.97
18	9	139.45

 $T_1$  at 600 MHz

Loop counter	Spectrum number	Relaxation period (ms)
96	1	768
2	2	16
24	3	192
12	4	96
64	5	512
4	6	32
16	7	128
48	8	384
6	9	48

 $T_2$  at 600 MHz

Loop counter	Spectrum number	Relaxation period (ms)
18	1	153.85
21	2	179.49
33	3	282.06
6	4	51.28
30	5	256.42
9	6	76.92
24	7	205.13
15	8	128.21
3	9	25.64

 $T_1$  at 800 MHz

Loop counter	Spectrum number	Relaxation period (ms)
24	1	240
10	2	100
48	3	480
6	4	60
96	5	960
2	6	20
32	7	320
8	8	80
64	9	640
4	10	40
16	11	160
12	12	120

 $T_2$  at 800 MHz

Loop counter	Spectrum number	Relaxation period (ms)
12	1	112.13
21	2	196.22
3	3	28.03
24	4	224.26
6	5	56.06
18	6	168.19
9	7	84.10
15	8	140.16

peak intensities observed with and without  $^1\text{H}$  saturation. In order to suppress time- or temperature-dependent effects, the spectra were acquired in an interleaved mode with incremented relaxation delays. All experiments were recorded with 256  $t_1$  increments of 2048 data points in  $t_2$ . The spectral widths were set to 6010 Hz ( $^1\text{H}$ ) / 1773 Hz ( $^{15}\text{N}$ ) at 500 MHz, 7184 Hz ( $^1\text{H}$ ) / 2131 Hz ( $^{15}\text{N}$ ) at 600 MHz and 9766 Hz ( $^1\text{H}$ ) / 2841 Hz ( $^{15}\text{N}$ ) at 800 MHz. Acquisition and processing parameters for the relaxation experiments of human E-FABP complexed with stearic acid are listed in Appendix A.2.

The overall molecular shape of the members of the FABP family is not spherical, but rather resembles an oblate ellipsoid. The ratio of the principal components of the rotational diffusion tensor obtained from hydrodynamic calculations using the bead method [García de la Torre and Bloomfield, 1981] is 1.00 : 0.92 : 0.83 for E-FABP. This suggests a small degree of anisotropy of the overall rotation for E-FABP, which can in principle be detected by NMR relaxation measurements [Tjandra *et al.*, 1995]. However, since the anisotropy of the rotational diffusion tensor is rather small, anisotropic modelling of the global motion did not result in a statistically significant improvement of the fit. Therefore, the dynamics calculations were performed by assuming an isotropic model in solution, as previously reported for bovine H-FABP and porcine ILBP [Lücke *et al.*, 1999]. Consequently, an estimate of the overall rotational correlation time  $\tau_c$  was derived for  $T_1(\text{N})/T_2(\text{N})$  ratios that fell within one standard deviation of the mean  $T_1(\text{N})/T_2(\text{N})$  ratio [Kay *et al.*, 1989].

The microdynamic parameters of the backbone HN vectors (the generalized order parameter  $S^2$  and the effective correlation time  $\tau_e$ ) as well as the conformational exchange contribution to the transverse relaxation rate (the exchange parameter  $R_{ex}$ ) were calculated and fitted with the Modelfree4 program of Palmer and co-workers [Mandel *et al.*, 1995; Palmer *et al.*, 1991]. The order parameter  $S^2$  represents the amplitude of the nanosecond-to-picosecond backbone mobility ( $S^2 = 1$  corresponds to a completely restricted orientation of the HN vector, while  $S^2 = 0$  indicates unrestricted motion). Non-zero values of the transverse relaxation rate  $R_{ex}$  are expected to appear when processes of conformational or chemical exchange occur within the millisecond-to-microsecond time range. Three models for the spectral density function were applied to derive backbone dynamics information from the experimentally determined relaxation rates  $R_1$ ,  $R_2$  and NOE. The first model was based on the single time scale model-free formalism proposed by Lipari and Szabo [1982], with fitting of both  $S^2$  and  $\tau_e$ . The second model added an  $R_{ex}$  term to the model-free formalism, providing fits to  $S^2$  and  $R_{ex}$ . Finally, the extended form of the model-free formalism [Clore *et al.*, 1990], where the

---

generalized order parameter becomes a product of the individual fast and slow time scale order parameters,  $S^2 = S_f^2 S_s^2$ , was used as another model of the spectral density function, fitting the parameters  $S_s^2$ ,  $S_f^2$  and  $\tau_e$ . The model-free formalism was used for 72 of 120 amino acids; the second model was used for 47 amino acids; the model of Clore was used only for the C-terminal residue.

## 4 Results and discussion

### 4.1 Resonance assignments of human E-FABP

Using homonuclear and heteronuclear NMR experiments, the  $^1\text{H}$  and  $^{15}\text{N}$  resonance assignments were completed for recombinant human E-FABP and are reported in Table 4.1. They are also available at the BioMagResBank (<http://www.bmrb.wisc.edu>) under the accession number BMRB-5083. The proton resonance assignments were carried out mainly with 2D homonuclear TOCSY (Figure 4.1) and NOESY (Figure 4.2) spectra.  $^1\text{H}/^{15}\text{N}$ -correlated 3D TOCSY-HSQC and 3D NOESY-HSQC spectra were used to identify the  $^{15}\text{N}$  resonances of backbone amides and to verify the obtained proton resonance assignments. A 2D homonuclear TOCSY spectrum with a short spinlock time of 4.8 ms helped to characterize directly neighbouring protons in the side-chains (Figure 4.3). Reported in Appendix A.3 are the 126 stereospecific assignments of the prochiral methylene and isopropyl groups obtained with the program GLOMSA [Güntert *et al.*, 1991]. Side-chain  $\text{NH}_2$  groups were identified using a  $^1\text{H}/^{15}\text{N}$ -HTQC spectrum (Figure 4.4). The sequential resonance assignments of the amide groups are indicated in the 2D  $^1\text{H}/^{15}\text{N}$ -HSQC spectrum (Figure 4.5).

Resonance assignments of FABPs are often hindered by the occurrence of multiple spin-systems. For bovine H-FABP, such spin-system heterogeneities within the so-called 'portal region' indicated up to four separate conformational states due to a mixture of different fatty acid ligands [Lücke *et al.*, 2001]. The portal region is located between helix  $\alpha\text{II}$  (see Figure 4.9 for secondary structure denotation) and the turns connecting  $\beta$ -strands  $\beta\text{C}$  and  $\beta\text{D}$  as well as  $\beta\text{E}$  and  $\beta\text{F}$ , apparently representing the only opening in the protein surface through which the fatty acid ligand can enter and exit the internal binding cavity [Sacchettini *et al.*, 1992]. In the case of human E-FABP, however, just nine out of 22 residues that exhibit spin-system heterogeneities are part of this portal region, which encompasses residues 27-39, 57-62 and 76-82. Two separate proton spin-systems were observed for each of the following amino acid residues: R12 ( $\beta\text{A}$ ), V28 ( $\alpha\text{I}$ - $\alpha\text{II}$  turn), M35, A37 (both  $\alpha\text{II}$ ), A39 ( $\alpha\text{II}$ - $\beta\text{B}$  linker), I44, T46 (both  $\beta\text{B}$ ), K55 ( $\beta\text{C}$ ), Q64 ( $\beta\text{D}$ ), G70, E71 (both  $\beta\text{D}$ - $\beta\text{E}$  turn), T76 ( $\beta\text{E}$ ), A78, D79 (both  $\beta\text{E}$ - $\beta\text{F}$  turn), F89 ( $\beta\text{F}$ ), T90 ( $\beta\text{F}$ - $\beta\text{G}$  turn), V95 ( $\beta\text{G}$ ), K110 ( $\beta\text{H}$ ), V121 ( $\beta\text{I}$ ) and E135 (C-terminus). Three different proton spin-systems were observed for G36 ( $\alpha\text{II}$ ) and T77 ( $\beta\text{E}$ - $\beta\text{F}$  turn). Remarkably, the  $\text{O}^\gamma\text{H}$  resonance of T77 shows three distinct signals around 5.84 ppm, analogous to the corresponding residue T74 in bovine H-FABP [Lücke *et al.*, 2001]. Moreover, G36 in  $\alpha$ -helix II belongs to a number of sequentially neighbouring residues (M35, G36, A37 and A39) that display multiple spin-systems also in bovine H-FABP (V32, G33,

N34 and T36). The same applies to A78 and D79 in the  $\beta$ E- $\beta$ F turn, which correspond to A75 and D76 in H-FABP. In contrast to bovine H-FABP, where all these residues showed multiple spin-systems of almost the same intensity (representing separate, equally-populated conformational states due to different bound fatty acids), one major form is always observed in the spectra of human E-FABP, since the protein had been complexed with only a single type of ligand molecule, *i.e.*, stearic acid. Consequently, the spin-system heterogeneities observed around the portal region in human E-FABP may be due to the presence of a minor, ligand-free protein form. All other cases of multiple spin-systems, however, are distributed randomly throughout the amino acid sequence, suggesting a different origin.

In the X-ray structure of human E-FABP, the turn between  $\beta$ -strands  $\beta$ C and  $\beta$ D, which comprises residues 58-61 and is assumed to be part of the portal region, displayed a less well-defined structure due to weak electron density. This has been interpreted as an indication that two or more conformational states may occur in the crystal at that position

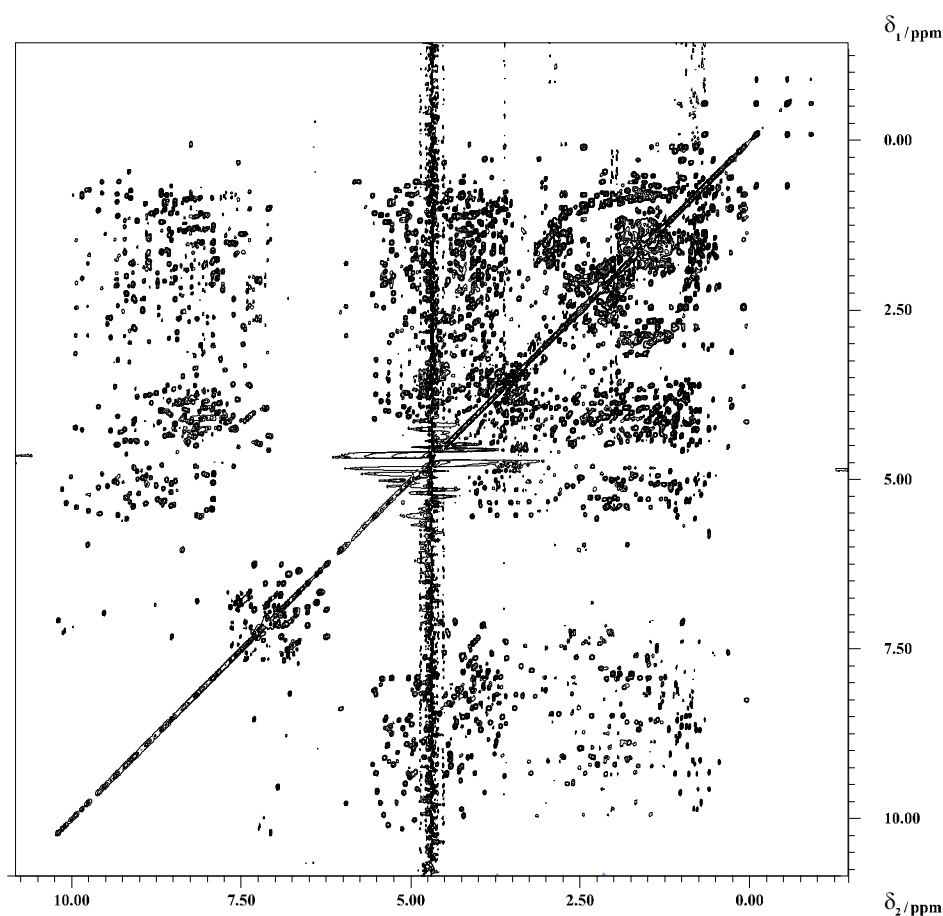


**Figure 4.1** 2D homonuclear TOCSY spectrum of human E-FABP at pH 5.6 and 298 K ( $^1\text{H}$  resonance frequency of 600.13 MHz). The spinlock time was set to 80 ms.

[Hohoff *et al.*, 1999]. In the solution structure, on the other hand, no spin-system heterogeneities were observed for these particular residues, thus excluding separate long-lived conformational states as reported for H-FABP [Lücke *et al.*, 2001]. However, a less well-defined structure in the  $\beta$ C- $\beta$ D turn together with a lack of the otherwise highly conserved F57 portal lid might explain why E-FABP shows a relatively low oleic acid binding affinity compared to other FABPs in the LBP subfamily *IV* [Zimmerman *et al.*, 2001].

The E-FABP chemical shift data show several values that fall outside five standard deviations of the mean chemical shift for the atom indicated according to the BMRB statistics. Precisely, these are:  $H^{\gamma 2}$  of E75 (1.16 ppm, compared to a mean chemical shift of  $2.33 \pm 5 \times 0.21$  ppm in the BMRB),  $H^{\delta 2}$  of R81 (0.38 ppm, compared to  $3.13 \pm 5 \times 0.19$  ppm),  $H^{\beta 2}$  and  $H^{\beta 3}$  of K103 (both 0.11 ppm, compared to  $1.77 \pm 5 \times 0.25$  ppm and  $1.80 \pm 5 \times 0.24$  ppm, respectively) and  $H^{\beta 2}$  of L116 (-0.85 ppm, compared to  $1.62 \pm 5 \times 0.32$  ppm). In all of these cases, an aromatic ring in the neighbourhood of the protons involved can explain these

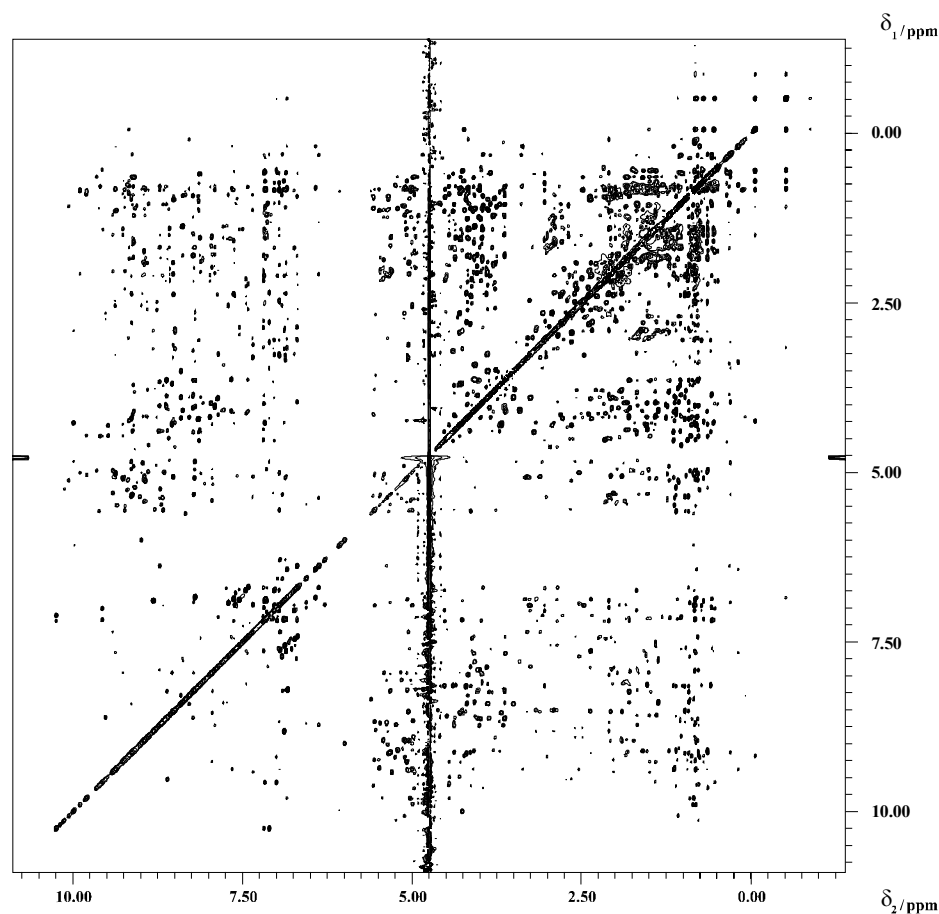


**Figure 4.2** 2D homonuclear NOESY spectrum of human E-FABP at pH 5.6 and 298 K ( $^1\text{H}$  resonance frequency of 600.13 MHz).

extreme values of the chemical shift. According to the model originally developed by Johnson and Bovey [1958], an aromatic ring may induce a shielding effect that modifies the chemical shift of any proton located up to 4 Å perpendicularly from the plane of the ring. All the above-mentioned amino acids with extreme chemical shift are less than 3.5 Å away from the plane of a neighbouring aromatic ring: F65 (for E75), W100 (for R81 and K103) and W11 (for L116), which can explain a difference of up to 2 ppm with respect to the mean chemical shift.

The presence of six cysteines in the amino acid sequence of human E-FABP is highly unusual in the LBP family. Four cysteines are unique to E-FABP: C43, C47, C67 and C87. The cysteine residues C120 and C127 of E-FABP are partially conserved in some LBPs, but only the M-FABP sequence includes both (at the respective positions 117 and 124). In the three-dimensional structure of E-FABP, two cysteine pairs (C67/C87 and C120/C127) were identified by X-ray analysis to be close enough to allow disulfide bridge formation, but a S-S bond was actually found only between C120 and C127 [Hohoff *et al.*, 1999].

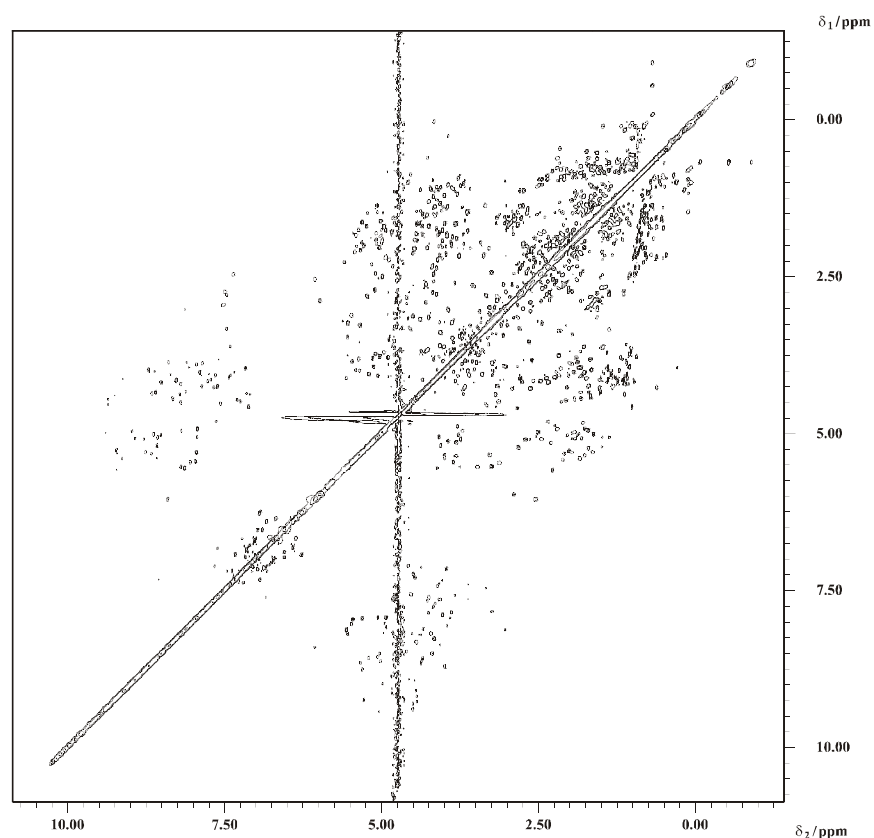


**Figure 4.3** 2D homonuclear TOCSY spectrum of human E-FABP at pH 5.6 and 298 K ( $^1\text{H}$  resonance frequency of 600.13 MHz). The spinlock time was set to 4.8 ms to characterize directly neighbouring protons in the side-chains.



**Table 4.1** Chemical shift values of  $^1\text{H}$  and  $^{15}\text{N}$  resonances for recombinant human E-FABP at pH 5.6 and 298 K. Sequence numbers marked with prime and double-prime correspond to multiple spin-systems. Stereospecific assignments are written with italics; tentative assignments are marked with asterisk (\*).

Residue	Amino acid	N	NH	C $^{\alpha}$ H	C $^{\beta}$ H	Other H	Other N
1	Met						
2	Ala						
3	Thr	115,3	8,23	4,55	4,42	1,17 $\gamma^2$	
4	Val	123,0	8,16	3,07	1,04	0,61;0,75 $\gamma$	
5	Gln	119,0	8,12	3,91	1,92;2,05	2,62;2,26 $\gamma$ 7,42;6,69 $\epsilon$	111,2 $\epsilon$
6	Gln	116,7	7,47	4,15	2,27;2,17	2,42;2,52 $\gamma$ 7,62;6,95 $\epsilon$	112,4 $\epsilon$
7	Leu	116,1	7,65	4,28	1,61;1,73	1,48 $\gamma$ 0,85;0,58 $\delta$	
8	Glu	115,3	7,20	4,01	2,18;2,08	2,01;2,78 $\gamma$	
9	Gly	109,8	8,66	3,66;4,04			
10	Arg	119,8	8,20	4,86	1,72;1,58	1,30;1,17 $\gamma$ 3,37;2,84 $\delta$	
11	Trp	128,4	9,21	5,26	3,20;2,87	7,50 $\epsilon$ 7,02 $\delta^1$ 9,58 $\epsilon^1$ 7,07 $\epsilon^3$ 7,19 $\zeta^2$ 7,01 $\zeta^3$ 6,91 $\eta^2$	82,6 $\epsilon$ 127,5 $\epsilon^1$
12	Arg	126,2	10,14	5,40	1,80;1,58	1,72 $\gamma$ 3,04;3,24 $\delta$ 9,18 $\epsilon$	86,5 $\epsilon$
12'	Arg	126,2	10,14	5,40	1,80;1,58	1,72 $\gamma$ 3,04;3,24 $\delta$ 9,13 $\epsilon$	86,4 $\epsilon$
13	Leu	129,2	7,99	3,41	1,43;1,03	1,17 $\gamma$ 0,22;0,78 $\delta$	
14	Val	119,8	9,39	4,54	2,18	0,96;0,85 $\gamma$	
15	Asp	119,8	7,65	4,86	2,39;2,62		
16	Ser	116,4	8,22	5,00	3,75;3,40		
17	Lys	129,2	8,92	4,89	1,91;1,84	1,52;1,48 $\gamma$ 1,75;1,69 $\delta$ 3,03 $\epsilon$	
18	Gly	111,6	8,99	4,18;4,39			
19	Phe	121,0	8,35	4,54	2,88;3,17	7,20 $\delta$ 7,10 $\epsilon$ 7,15 $\zeta$	
20	Asp	119,0	8,77	4,20	2,61;2,51		
21	Glu	119,3	8,91	3,81	2,22;2,32	2,59;1,94 $\gamma$	
22	Tyr	121,8	7,98	3,99	2,91;3,08	6,72 $\delta$ 6,40 $\epsilon$	
23	Met	116,7	8,25	3,84	1,45;1,19	2,20;1,86 $\gamma$ 2,09 $\epsilon$	

Residue	Amino acid	N	NH	C <sup>α</sup> H	C <sup>β</sup> H	Other H	Other N
24	Lys	119,3	8,26	3,84	1,71;1,93	1,44 $\gamma$ 1,62 $\delta$ 2,91 $\epsilon$	
25	Glu	124,1	7,92	3,93	2,10;2,03	2,39;2,20 $\gamma$	
26	Leu	115,8	7,63	3,86	1,57;1,74	1,05 $\gamma$ 0,34;0,61 $\delta$	
27	Gly	106,4	7,68	4,10;3,64			
28	Val	120,4	7,44	3,64	1,51	1,07;0,81 $\gamma$	
28'	Val	120,4	7,45	3,68	1,53	1,06;0,80 $\gamma$	
29	Gly	114,1	8,64	4,06;3,89			
30	Ile	119,3	8,24	3,66	1,82	1,26;1,51 $\gamma^1$ 0,94 $\gamma^2$ 0,89 $\delta$	
31	Ala	122,7	8,39	4,09	1,39		
32	Leu	119,3	7,78	4,21	1,56;1,46	1,06 $\gamma$ 0,91;0,82 $\delta$	
33	Arg	120,4	8,41	4,13	1,77;1,40	1,69 $\gamma$ 3,06;2,79 $\delta$ 7,53 $\epsilon$	82,4 $\epsilon$
34	Lys	119,5	8,10	3,99	1,91;1,86	1,59;1,39 $\gamma$ 1,65 $\delta$ 2,99 $\epsilon$	
35	Met	117,3	7,38	4,07	2,07;2,26	2,70;2,43 $\gamma$ 2,03 $\epsilon$	
35'	Met	117,0	7,44	4,12	2,06;2,21	2,74;2,48 $\gamma$ 2,04 $\epsilon$	
36	Gly	107,6	9,21	3,76;3,62			
36'	Gly	107,0	9,11	3,76;3,62			
36''	Gly	106,1	9,02	3,77;3,59			
37	Ala	121,8	8,14	4,37	1,55		
37'	Ala	121,8	8,19	4,36	1,54		
38	Met	113,8	7,33	4,51	2,10	2,65;2,71 $\gamma$ 1,99 $\epsilon$	
39	Ala	121,8	7,57	4,18	1,43		
39'	Ala	121,8	7,51	4,20	1,43		
40	Lys	123,5	8,93	4,76	1,85	1,47;1,27 $\gamma$ 1,70 $\delta$ 3,01 $\epsilon$	
41	Pro			4,82	2,07	1,81;1,98 $\gamma$ 4,09;3,80 $\delta$	
42	Asp	116,7	8,43	6,08	2,57;2,49		
43	Cys	121,5	9,99	5,46	2,52;2,14	1,53 $\gamma$	
44	Ile	129,0	9,80	5,27	1,74	1,32;1,16 $\gamma^1$ 0,78 $\gamma^2$ 0,88 $\delta$	
44'	Ile	129,1	9,83	5,24	1,74	1,32;1,16 $\gamma^1$ 0,78 $\gamma^2$ 0,85 $\delta$	
45	Ile	129,5	9,22	4,77	2,20	0,74;1,77 $\gamma^1$ 0,51 $\gamma^2$ 0,55 $\delta$	
46	Thr	123,0	8,89	4,76	3,91	1,13 $\gamma^2$	
46'	Thr	121,8	8,91	4,80	3,97	1,12 $\gamma^2$	

Residue	Amino acid	N	NH	C <sup>α</sup> H	C <sup>β</sup> H	Other H	Other N
47	Cys	125,8	10,20	5,19	2,85;2,35		
48	Asp	126,7	7,95	4,80	2,66;3,08		
49	Gly	110,1	8,24	4,40;3,23			
50	Lys	122,7	8,63	4,39	1,87	1,45;1,36 γ 1,69 δ 2,97 ε	
51	Asn	120,1	9,54	5,14	2,75;2,68	8,21;6,84 δ	116,2 δ
52	Leu	127,0	8,95	5,12	1,20;1,86	1,42 γ 0,83 δ	
53	Thr	122,1	8,97	5,06	3,81	0,98 γ <sup>2</sup>	
54	Ile	121,8	7,60	4,57	0,92	0,77 γ <sup>1</sup> 0,38 γ <sup>2</sup> 0,60 δ	
55	Lys	131,8	9,10	5,04	1,89;1,65	1,16 γ 1,43 δ 2,80 ε	
55'	Lys	132,1	9,23	5,03	1,97;1,68	1,15 γ 1,40 δ 2,84 ε	
56	Thr	124,1	9,38	5,12	4,12	1,16 γ <sup>2</sup>	
57	Glu	126,7	9,40	5,03	1,81;2,02	2,10;2,19 γ	
58	Ser	118,1	8,12	4,97	4,20;3,74		
59	Thr	113,6	8,38	4,02	4,21	1,28 γ <sup>2</sup>	
60	Leu	118,7	7,69	4,31	1,57	1,36 γ 0,89;0,84 δ	
61	Lys	117,0	7,13	4,41	1,72;1,85	1,52 γ 1,30 δ 2,84 ε	
62	Thr	124,1	8,74	5,39	4,04	1,26 γ <sup>2</sup>	
63	Thr	118,7	8,91	4,80	4,25	1,16 γ <sup>2</sup>	
64	Gln	118,4	8,60	5,44	1,87;1,98	2,16;2,07 γ 7,46;6,73 ε	111,7 ε
64'	Gln	118,4	8,56	5,43	1,93;1,96	2,16;2,07 γ 7,46;6,73 ε	111,7 ε
65	Phe	117,0	7,96	5,09	3,28;3,36	6,87 δ 7,17 ε 6,87 ζ	
66	Ser	114,7	8,22	5,57	3,50;3,79		
67	Cys	116,7	9,25	4,68	1,59;2,58	1,12 *γ	
68	Thr	118,1	9,10	4,93	3,83	1,24 γ <sup>2</sup>	
69	Leu	127,8	9,12	4,14	1,63;1,82	1,20 γ 0,68;0,80 δ	
70	Gly	109,8	9,10	4,27;3,67			
70'	Gly	109,0	9,16	4,30;3,70			
71	Glu	120,1	7,83	4,80	2,02;1,87	2,19;2,06 γ	
71'	Glu	120,1	7,94	4,80	2,02;1,87	2,19;2,06 γ	
72	Lys	130,1	8,96	4,99	1,76	1,41 γ 1,65 δ 2,94 ε	
73	Phe	123,0	9,43	5,08	3,31;3,12	7,37 δ 6,98 ε 6,31 ζ	
74	Glu	119,5	8,53	5,07	2,09	1,93 γ	
75	Glu	133,8	8,96	4,51	1,95	1,16;1,52 γ	
76	Thr	121,5	8,59	5,23	4,10	1,13 γ <sup>2</sup>	
76'	Thr	121,5	8,52	5,23	4,10	1,13 γ <sup>2</sup>	

Residue	Amino acid	N	NH	C <sup>α</sup> H	C <sup>β</sup> H	Other H	Other N
77	Thr	120,1	9,10	4,49	4,30	0,66 $\gamma^2$ 5,84 $\gamma^1$	
77'	Thr	120,1	9,10	4,49	4,30	0,66 $\gamma^2$ 5,89 $\gamma^1$	
77''	Thr	120,1	9,10	4,49	4,30	0,66 $\gamma^2$ 5,81 $\gamma^1$	
78	Ala	124,1	9,56	3,97	1,41		
78'	Ala	124,1	9,65	3,97	1,41		
79	Asp	108,1	9,28	4,31	2,25;2,67		
79'	Asp	107,6	9,35	4,34	2,20;2,73		
80	Gly	108,1	7,80	3,44;4,10			
81	Arg	118,7	7,18	4,00	1,46;0,57	0,93;1,11 $\gamma$ 0,38;2,63 $\delta$ 9,30 $\epsilon$ 7,37 $\eta^1$	90,5 $\epsilon$ 73,2 $\eta^1$
82	Lys	121,0	7,98	5,35	1,67;1,56	1,31;1,37 $\gamma$ 1,58 $\delta$ 2,94 $\epsilon$	
83	Thr	115,0	9,14	4,87	3,97	0,33 $\gamma^2$	
84	Gln	119,5	8,98	4,76	1,93;2,11	2,13;2,38 $\gamma$ 7,62;6,87 $\epsilon$	112,7 $\epsilon$
85	Thr	127,2	9,25	5,63	2,32	0,87 $\gamma^2$	
86	Val	121,0	8,36	4,48	1,97	0,93 $\gamma$	
87	Cys	126,1	9,83	6,02	2,50;2,94	1,87 $\gamma$	
88	Asn	120,4	9,02	5,02	2,58;2,54	7,72;6,92 $\delta$	114,1 $\delta$
89	Phe	125,2	9,37	5,57	2,50;3,27	6,98 $\delta$ 7,05 $\epsilon$ 6,76 $\zeta$	
89'	Phe	125,2	9,32	5,66	2,52;3,25	6,98 $\delta$ 7,05 $\epsilon$ 6,76 $\zeta$	
90	Thr	123,5	8,69	4,40	3,74	1,07 $\gamma^2$	
90'	Thr	123,0	8,57	4,40	3,73	1,07 $\gamma^2$	
91	Asp	127,8	9,15	4,17	2,40;2,82		
92	Gly	101,9	7,85	3,27;3,92			
93	Ala	121,8	7,15	4,62	1,07		
94	Leu	120,4	8,90	5,02	1,50;1,94	1,41 $\gamma$ 0,84;0,73 $\delta$	
95	Val	133,8	9,91	4,31	2,08	0,84;0,89 $\gamma$	
95'	Val	134,1	10,05	4,29	2,02	0,84;0,88 $\gamma$	
96	Gln	129,8	8,95	5,12	2,49	2,14;1,73 $\gamma$ 6,75;6,05 $\epsilon$	113,7 $\epsilon$
97	His	127,0	9,20	5,38	3,04;3,32	7,37 $\delta^2$ 8,58 $\epsilon^1$	
98	Gln	124,7	9,03	4,93	1,53;1,81	2,28;2,45 $\gamma$ 7,79;6,28 $\epsilon$	114,7 $\epsilon$
99	Glu	118,7	8,80	5,35	2,01;2,12	2,20;2,15 $\gamma$	
100	Trp	126,7	8,24	4,85	3,48;3,09	7,13 $\delta^1$ 10,26 $\epsilon^1$ 6,93 $\epsilon^3$ 7,20 $\zeta^2$ 6,58 $\zeta^3$ 7,01 $\eta^2$	129,5 $\epsilon^1$
101	Asp	121,8	9,15	4,22	2,38;2,81		
102	Gly	104,1	8,42	3,92;3,53			

Residue	Amino acid	N	NH	C <sup>α</sup> H	C <sup>β</sup> H	Other H	Other N
103	Lys	122,4	8,31	4,20	0,11	1,05;0,86 γ 1,43;1,18 δ 2,84;2,78 ε	
104	Glu	115,0	7,99	5,48	1,85;2,01	2,11;2,08 γ	
105	Ser	112,4	8,71	5,18	4,40;3,85	5,39 γ	
106	Thr	120,7	8,08	5,50	3,89	1,15 γ <sup>2</sup>	
107	Ile	127,2	9,36	5,00	1,75	1,43 γ <sup>1</sup> 0,66 γ <sup>2</sup> 0,75 δ	
108	Thr	127,8	9,66	5,17	3,97	1,09 γ <sup>2</sup>	
109	Arg	124,7	9,07	5,26	1,27;1,53	1,85;1,76 *γ 2,52;2,72 *δ 8,33 *ε 6,70 *η <sup>1</sup>	84,3 *ε 70,2 *η <sup>1</sup>
110	Lys	121,3	8,71	4,80	1,38;1,67	1,08 γ 1,48 δ 2,68 ε	
110'	Lys	121,3	8,73	4,83	1,39;1,70	1,11 γ 1,49 δ 2,72 ε	
111	Leu	122,1	8,59	5,11	1,42;1,52	1,42 γ 0,85;0,73 δ	
112	Lys	125,8	9,28	4,47	1,51;1,71	1,33;1,24 γ 1,59;1,65 δ 2,94 ε	
113	Asp	128,4	9,48	4,33	2,95;2,67		
114	Gly	102,7	8,55	4,31;3,71			
115	Lys	121,3	7,96	4,96	1,81;2,00	1,54 γ 1,68;1,59 δ 3,08 ε	
116	Leu	123,8	8,23	4,27	-0,85;1,10	0,72 γ -0,03;-0,49 δ	
117	Val	128,7	9,19	4,49	1,87	0,82;0,90 γ	
118	Val	130,4	9,61	4,97	2,23	0,66;0,83 γ	
119	Glu	125,8	9,15	5,45	1,86;2,00	2,19;2,17 γ	
120	Cys	123,0	8,93	5,41	2,09;2,26		
121	Val	120,7	8,69	5,36	2,14	1,00;0,95 γ	
121'	Val	120,4	8,64	5,31	2,07	0,99;0,95 γ	
122	Met	130,1	9,15	4,87	1,83;2,04	2,91;2,36 γ 2,12 ε	
123	Asn	127,2	10,01	4,28	3,19;2,93	8,83;6,89 δ	115,4 δ
124	Asn	115,8	8,50	4,64	2,87;2,99	7,55;6,88 δ	113,0 δ
125	Val	123,5	8,54	4,22	2,39	0,94;1,00 γ	
126	Thr	118,4	8,16	5,59	4,15	1,13 γ <sup>2</sup>	
127	Cys	120,4	9,64	5,56	3,58;2,69		
128	Thr	117,3	8,81	5,14	3,77	1,10 γ <sup>2</sup>	
129	Arg	131,2	10,07	5,01	1,80;1,54	1,95;1,37* γ 2,67;2,53 *δ 8,40 *ε	85,0 *ε
130	Ile	122,7	8,66	5,05	1,67	1,56;1,19 γ <sup>1</sup> 0,86 γ <sup>2</sup> 0,82 δ	

Residue	Amino acid	N	NH	C <sup>α</sup> H	C <sup>β</sup> H	Other H	Other N
131	Tyr	127,2	9,82	5,51	3,05;3,17	6,87 δ 6,45 ε	
132	Glu	119,5	9,25	5,32	2,05	2,41;2,31 γ	
133	Lys	127,0	9,42	3,68	1,21;1,52	0,85;0,14 γ 1,00 ;1,08 δ 2,54;2,50 ε	
134	Val	127,5	8,74	4,03	1,70	0,85;0,80 γ	
135	Glu	129,0	7,92	4,07	1,97;1,81	2,08 γ	
135'	Glu	129,5	7,99	4,13	2,00;1,86	2,17 γ	

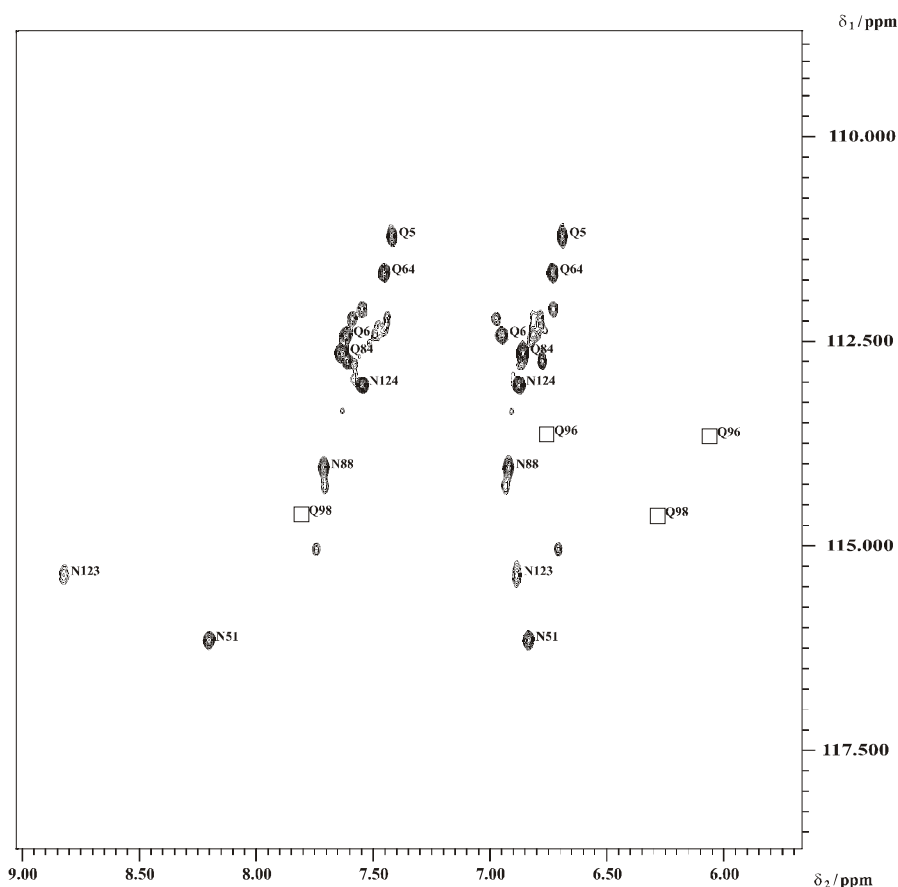


**Figure 4.4**  $^1\text{H}/^{15}\text{N}$ -HTQC spectrum of human E-FABP at pH 5.6 and 298 K ( $^1\text{H}$  resonance frequency of 600.13 MHz). The peak assignments for the  $\text{NH}_2$  groups of the Asn and Gln residues are indicated. Due to spin-system heterogeneities, several residues displayed multiple amide signals, which are not additionally labeled. Peaks observed below the plot level are indicated by squares.

Since the exclusion of a disulfide bridge between C67 and C87 improved the  $R_{\text{free}}$  factor of the crystallographic model, the existence of a covalent bond between these two side-chains was considered unlikely. The NMR data now provide a definite answer to this question: the possibility of a second disulfide bridge in solution could be ruled out, since  $S^{\gamma}\text{H}$  resonances were detected for the cysteine residues C43, C67 (tentative assignment) and C87.

Because of the high structural homology, the disulfide bridge between C120 and C127 in E-FABP strongly suggests the presence of a cystine bond in M-FABP as well. Even though

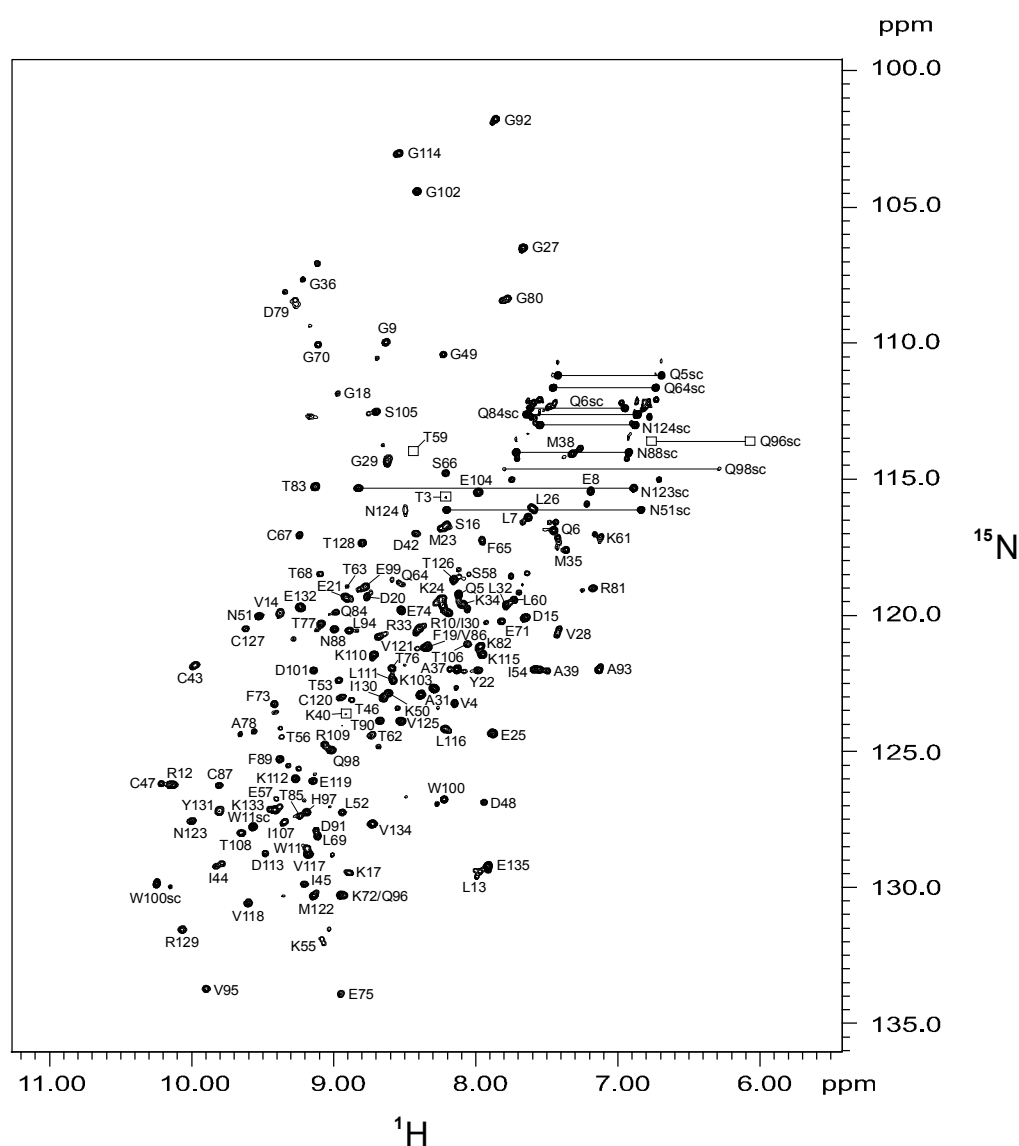


**Figure 4.5**  $^1\text{H}/^{15}\text{N}$ -HSQC spectrum of human E-FABP at pH 5.6 and 298 K ( $^1\text{H}$  resonance frequency of 600.13 MHz). Backbone and side-chain (sc) amide assignments are shown for each residue. Due to spin-system heterogeneities, several residues displayed multiple backbone amide signals (not additionally labeled). Peaks observed below the plot level are indicated by squares. Signals from side-chain  $\text{NH}_2$  groups are connected by solid lines.

biochemical studies have actually indicated that the respective residues C117 and C124 are S-S linked in M-FABP [Kitamura *et al.*, 1980], the  $S^{\gamma}$  positions are too far apart (4.5 Å) in the crystal structure for the presence of a disulfide bridge [Cowan *et al.*, 1993]. A comparison with the E-FABP structure provides no obvious explanation for this structural discrepancy observed between the two proteins, except maybe for the lower atomic resolution (2.7 Å) of the M-FABP data.

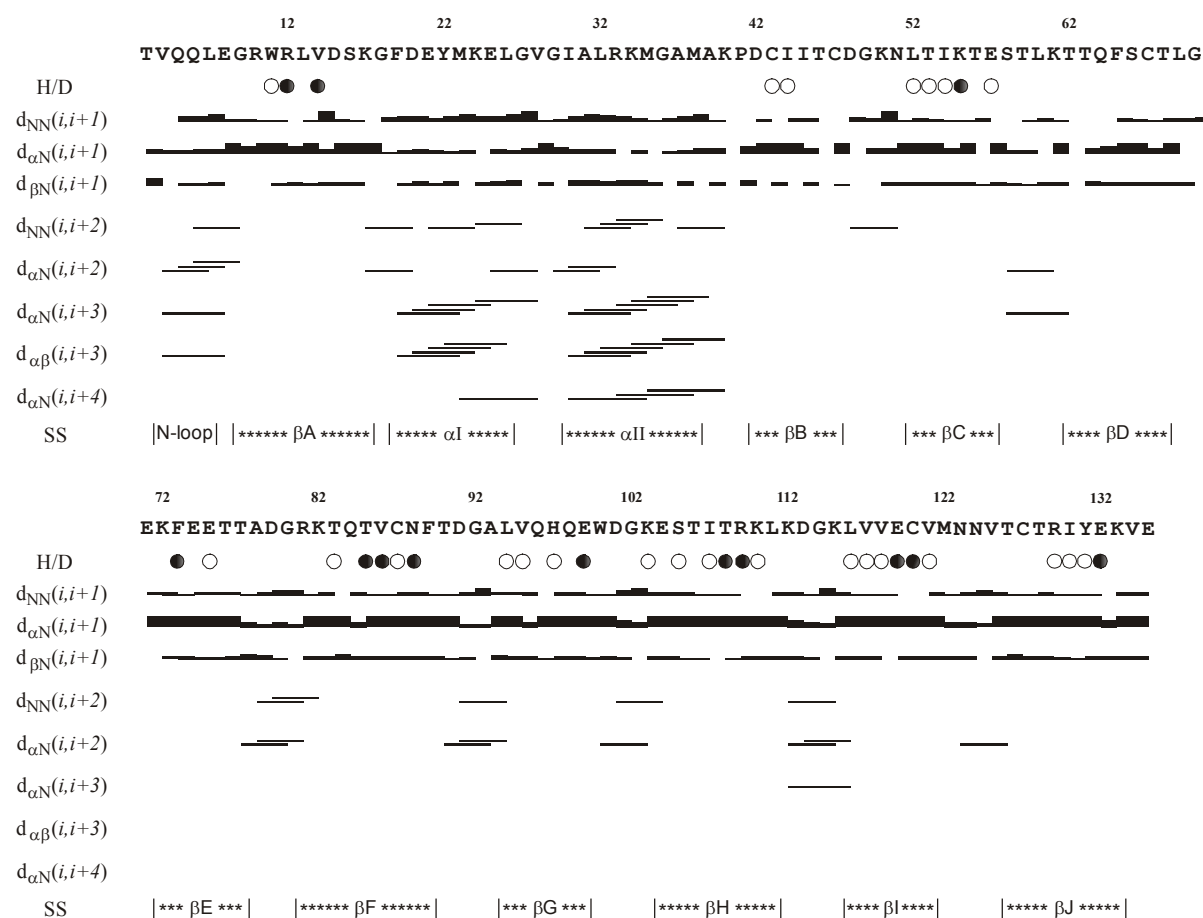


**Figure 4.6** Amino acid sequence of human E-FABP with a survey of the short-range and medium-range NOE connectivities, which were used to establish the sequence-specific  $^1\text{H}$  NMR assignment and to identify elements of regular secondary structure (SS). H/D indicates residues with slow-exchanging backbone amide protons that remained visible in  $\text{D}_2\text{O}$  solution after 80 min (open circles) or 2 days (full circles) at 298 K.



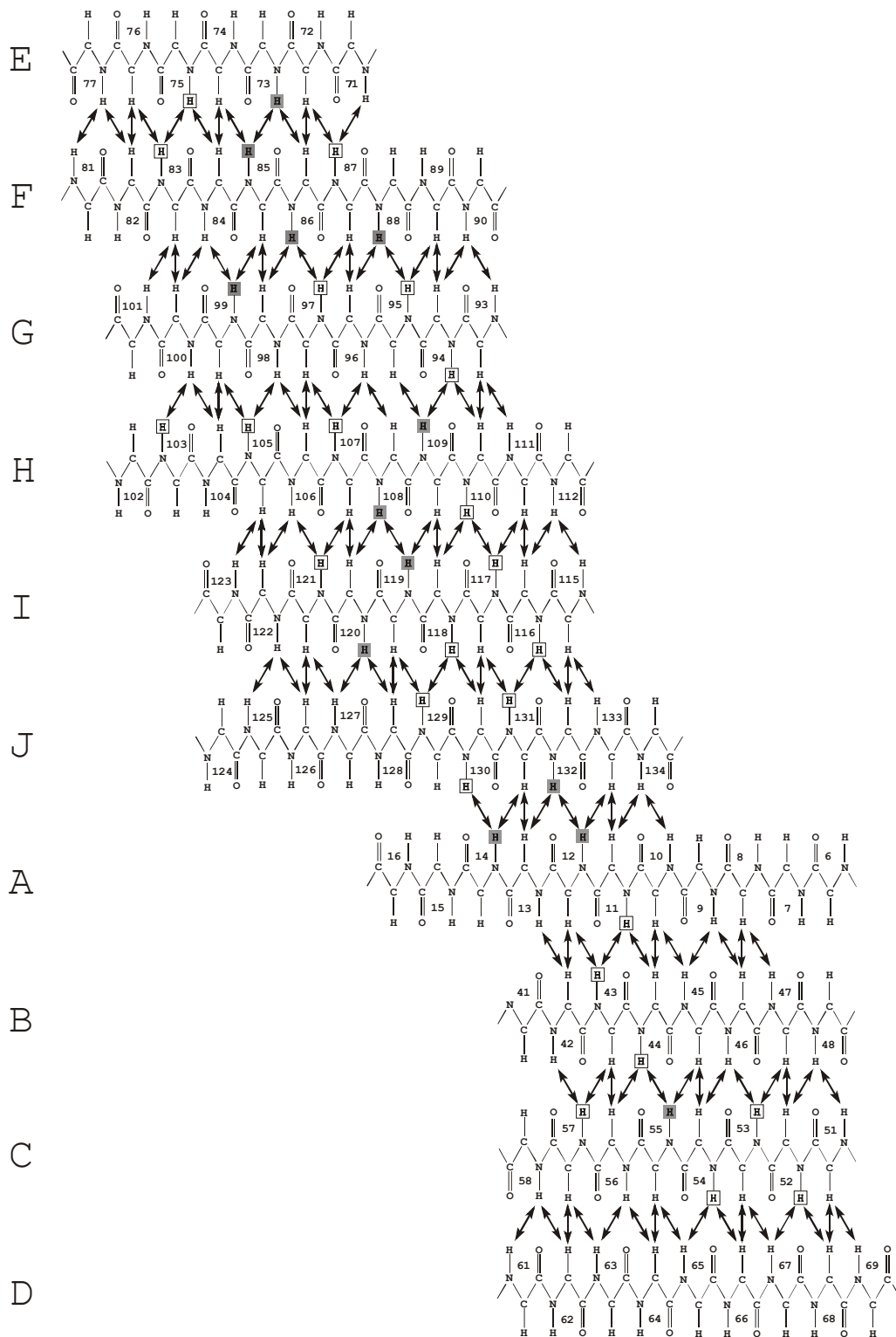


**Figure 4.7** Schematic representation of the  $\beta$ -sheet structure of E-FABP with the corresponding hydrogen bonding network. Residues with slow-exchanging backbone amide protons that remained visible in  $D_2O$  solution after 80 min (white boxes) or 2 days (shaded boxes) at 298 K are indicated.

## 4.2 Solution structure of human E-FABP

To determine the three-dimensional conformation of E-FABP by NMR spectroscopy, the intensity of the NOE signals obtained from NOESY spectra were translated into pairwise interatomic distances. Figure 4.6 shows the short- and medium-range NOE connectivities assigned to the backbone protons. Helical structures, characterized by strong sequential HN-HN and medium-range HN-HN( $i, i+2$ ), H $\alpha$ -HN( $i, i+2$ ), H $\alpha$ -HN( $i, i+3$ ), H $\alpha$ -H $\beta$  ( $i, i+3$ ) and H $\alpha$ -HN( $i, i+4$ ) connectivities, are present in segments V4-L7, F19-L26 and I30-M38. NOE connectivity patterns common to antiparallel  $\beta$ -sheet structures were detected between the backbone protons of  $\beta$ -strands  $\beta$ A,  $\beta$ B,  $\beta$ C and  $\beta$ D, as well as between  $\beta$ -strands  $\beta$ E,  $\beta$ F,  $\beta$ G,  $\beta$ H,  $\beta$ I and  $\beta$ J, and also between the N-terminal  $\beta$ -strand  $\beta$ A and the C-terminal  $\beta$ -strand  $\beta$ J. Backbone amide protons that exchange slowly in D<sub>2</sub>O solution due to hydrogen-bonding network between the  $\beta$ -strands are also indicated in Figure 4.6. The  $\beta$ -sheet structure of E-FABP with the corresponding hydrogen bonding network is represented schematically in Figure 4.7. Only between  $\beta$ -strands  $\beta$ D and  $\beta$ E, neither backbone NOE connectivities nor slow-exchanging backbone amide protons were observed. This interruption of the  $\beta$ -sheet structure has been referred to as the ‘gap’ region [Sacchettini *et al.*, 1989].

Based on the NOE and hydrogen exchange data, an ensemble of 20 energy-minimized conformers representing the solution structure of human E-FABP complexed with stearic acid has been obtained. The analysis of homonuclear 2D and <sup>15</sup>N-edited 3D NOESY spectra led to a total of 2926 NOE-derived distance constraints. Furthermore, 37 slow-exchanging backbone amide protons were identified to be part of the hydrogen-bonding network in the  $\beta$ -sheet and subsequently converted into 74 additional distance constraints. Finally, the disulfide bridge between C120 and C127 was defined by 3 upper and 3 lower distance bounds. The structure calculation program DYANA regarded 998 of these constraints as irrelevant, *i.e.*, they did not restrict the distance between two protons. Out of the remaining 2008 non-trivial distance constraints, 371 were intraresidual ( $i = j$ ), 508 sequential ( $j = |i + 1|$ ), 233 medium-range ( $|i - 5| < j < |i + 5|$ ), and 896 long-range ( $j > |i + 4|$ ). The resulting ensemble of 20 conformers as well as the ribbon diagram of the best DYANA structure after energy minimization are shown in Figures 4.8 and 4.9, respectively. The structure coordinates have been deposited at the RCSB data bank under PDB ID code 1JJJ. Experimental distance restraints and structural statistics of the calculated conformers are described in Table 4.2.

**Table 4.2 Structural statistics of the 20 selected conformers of human E-FABP after energy minimization**

Structural statistics	
Total number of residues	133
Total number of distance restraints	2008
Intraresidual	371
Sequential ( $ i - j  = 1$ )	508
Medium range ( $1 <  i - j  < 5$ )	233
Long range ( $ i - j  > 4$ )	896
Hydrogen bond distance restraints	$2 \times 37$
Disulfide bridge distance restraints	$2 \times 3$
Total number of restraint violations $>0.3 \text{ \AA}$	0
Total number of restraint violations $>0.2 \text{ \AA}$	23
Maximal restraint violation ( $\text{\AA}$ )	0.28
Ramachandran plot statistics (%)	
Residues in most favoured regions	85.1
Residues in additionally allowed regions	13.6
Residues in generously allowed regions	0.6
Residues in disallowed regions	0.7
Structural precision ( $\text{\AA}$ )	
Backbone atom <sup>a</sup> RMSD (residues 4-134)	$0.92 \pm 0.11$
Heavy atom RMSD (residues 4-134)	$1.46 \pm 0.10$
Backbone atom <sup>a</sup> RMSD (residues 4-26, 40-56, 63-75, 83-134)	$0.85 \pm 0.10$
Heavy atom RMSD (residues 4-26, 40-56, 63-75, 83-134)	$1.46 \pm 0.11$

<sup>a</sup> N, C<sup>α</sup>, C' and O.

The solution structure of human E-FABP consists of 10 antiparallel  $\beta$ -strands, defining two nearly orthogonal  $\beta$ -sheets of five  $\beta$ -strands each, and two short  $\alpha$ -helices that form a helix-turn-helix domain. The center of  $\beta$ -strand  $\beta$ F (K82-F89) is shared by both  $\beta$ -sheets. The N-terminal residues V4-L7 form a helical loop (presumably  $3_{10}$  conformation), which leads to  $\beta$ -strand  $\beta$ A (G9-K17). Residues V14 and D15 create a  $\beta$ -bulge inside  $\beta$ -strand  $\beta$ A. The residue G18 connects the first  $\beta$ -strand  $\beta$ A with helix  $\alpha$ I, which consists of residues F19-L26. Residues G27-G29 form a turn that leads into helix  $\alpha$ II, spanning residues I30-M38. The connection between helix  $\alpha$ II and the second  $\beta$ -strand  $\beta$ B (D42-C47) is made up of residues A39-P41. The rest of the structure consists of a series of  $\beta$ -strands:  $\beta$ C (L52-E57),  $\beta$ D (T62-T68),  $\beta$ E (K72-T77),  $\beta$ F (R81-F89),  $\beta$ G (L94-E99),  $\beta$ H (E104-L111),  $\beta$ I (L116-V121), and  $\beta$ J (T126-K133), which are connected mostly by hairpin turns.

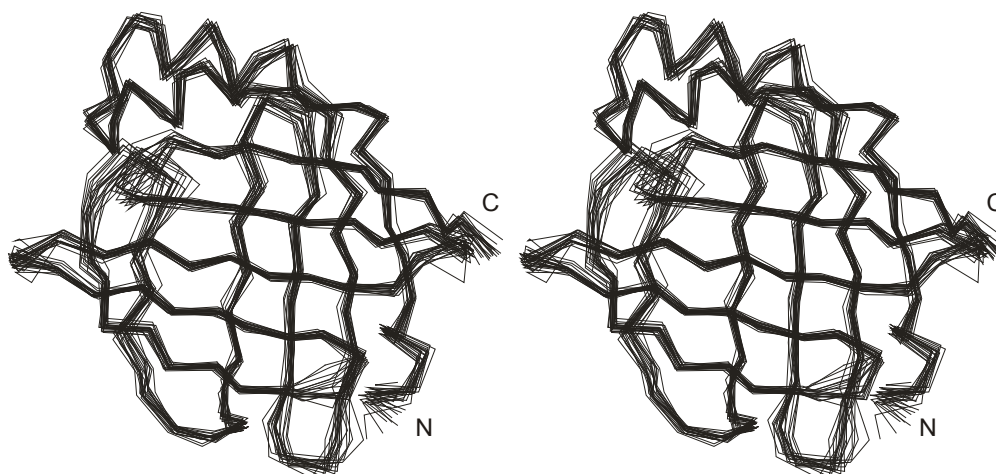


**Figure 4.8** Stereoview of the ensemble showing the  $C\alpha$  traces of the 20 selected conformers that represent human holo E-FABP in solution, derived from torsion angle dynamics and restrained energy-minimization calculations.

The helical loop at the N-terminal segment between V4 and L7 has been deduced from the presence of medium-range NOE connectivities. An  $\alpha$ - and  $3_{10}$ -helical fold can be distinguished on the basis of the  $H\alpha$ -HN( $i,i+2$ ) distances. For an  $\alpha$ -helix, the average  $H\alpha$ -HN( $i,i+2$ ) distance corresponds to 4.4 Å, while in a  $3_{10}$ -helix it corresponds to 3.8 Å. In the 20 energy-minimized conformers of human E-FABP, the  $H\alpha$ -HN( $i,i+2$ ) distances between residues V4 and Q6 as well as Q5 and L7 were  $3.96 \pm 0.32$  Å and  $3.95 \pm 0.32$  Å, respectively. Therefore, the N-terminal loop structure may represent a  $3_{10}$ -helix. The presence of an N-terminal helical-loop, however, is a unique attribute of the LBP subfamily *IV* that binds fatty acids in U-shaped conformation. The loop usually consists of 4 residues, starting with a hydrophobic amino acid followed by one or two hydrophilic residues and a highly conserved phenylalanine (substituted by a leucine residue only in the case of E-FABP) in the last position. The nonpolar residues in the first and last position are part of the hydrophobic cluster at the bottom of the protein cavity, while the hydrophilic residues are accessible to the external solvent. This additional structural feature might therefore contribute to the overall stability of the  $\beta$ -barrel fold.

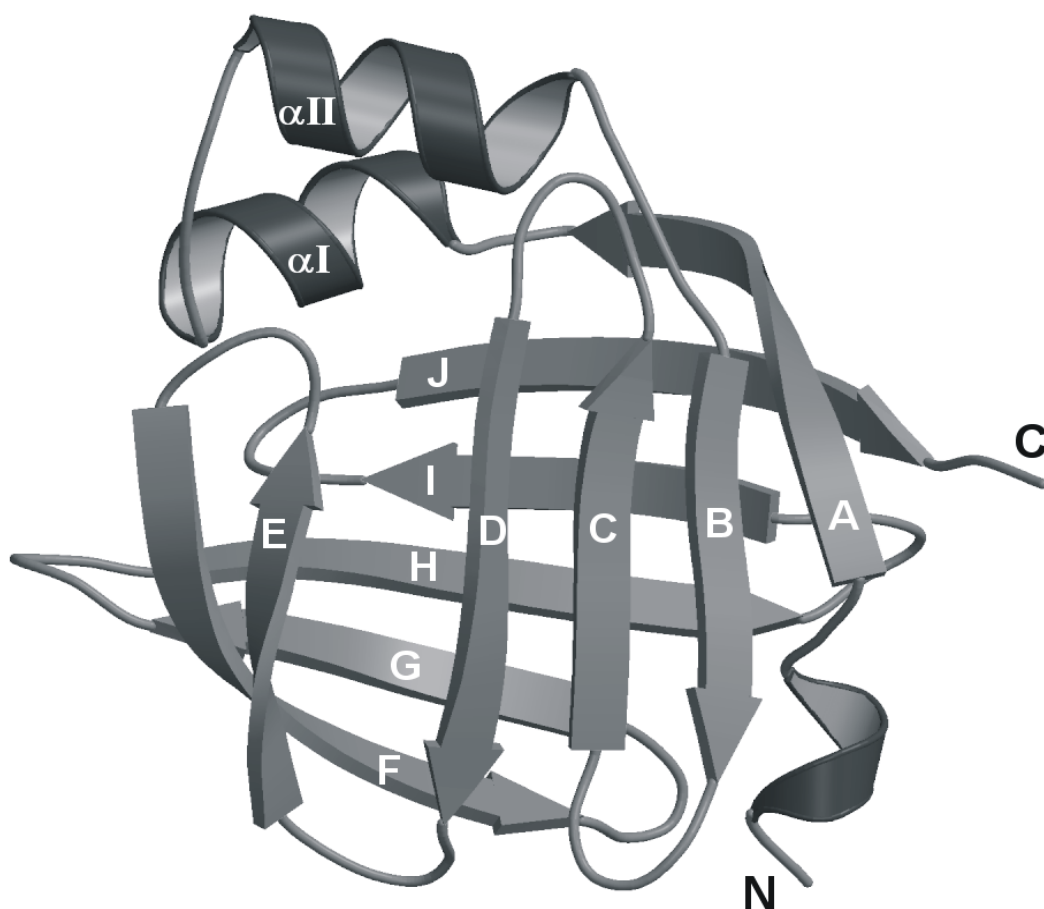


**Figure 4.9** Ribbon drawing of the best solution structure of human E-FABP showing ten antiparallel  $\beta$ -strands ( $\beta$ A- $\beta$ J), which are arranged in two almost orthogonal  $\beta$ -sheets forming a  $\beta$ -barrel, and two short  $\alpha$ -helices that close the  $\beta$ -barrel structure on one side. The hydrogen-bonding network within the  $\beta$ -sheets is continuous, except for a gap between  $\beta$ -strands  $\beta$ D and  $\beta$ E. The N-terminal residues form an additional helical loop. (Produced with MOLSCRIPT [Kraulis, 1991] and Raster3D [Merrit and Bacon, 1997]).

The overall structural fold of human E-FABP in solution is similar to the solution structures of other members of the LBP family, such as H-FABP [Lassen *et al.*, 1995; Lücke *et al.*, 2001], ILBP [Lücke *et al.*, 1996], I-FABP [Hodsdon *et al.*, 1996; Zhang *et al.*, 1997], B-FABP [Rademacher and Lücke, unpublished results], as well as cellular retinoic acid binding protein type II [Wang *et al.*, 1998] and cellular retinol binding protein type II [Lu *et al.*, 2000]. For the 20 best E-FABP conformers, average root-mean-square deviations (RMSD) of  $0.92 \pm 0.11$  Å and  $1.46 \pm 0.10$  Å were determined for the backbone and heavy

atoms, respectively, excluding the terminal residues. Without the portal region (*i.e.*, for residues 4-26, 40-56, 63-75 and 83-134), an average backbone RMSD of  $0.85 \pm 0.10$  was obtained, thus reflecting the higher conformational dispersion in the portal region. Superposition with the X-ray structure of human E-FABP (excluding the terminal residues) yielded average backbone RMSD values of  $1.00 \pm 0.07$  Å for the entire residue range and  $0.98 \pm 0.06$  Å without the portal region. This indicates a close similarity of the crystallographic and the solution structures. According to the Ramachandran plot, the backbone dihedral angles of residues within the major secondary structure elements show well-defined values with low deviation. A total of 99.3 % of the non-glycine/non-proline residues are found in the allowed regions of conformational space. Most of the cases found in the disallowed regions belong to either V4 (N-terminus), D91 ( $\beta$ F- $\beta$ G turn) or N123 ( $\beta$ I- $\beta$ J turn), *i.e.*, residues that might not be well-defined in the structure calculation due to rather exposed positions either in turns or at terminal ends.

Marked differences in conformational stability and binding affinity for fatty acids have been reported for paralogous FABPs of LBP subfamily *IV* [Veerkamp and Zimmerman, 2001; Zimmerman *et al.*, 2001]. In all types of this subgroup, the fatty acid inside the cavity is bound in an U-shaped conformation with hydrogen-bond formation between the carboxylate group and a triad of protein side-chains consisting of two arginines (one via an ordered water molecule) and one tyrosine (E-FABP numbering R109, R129 and Y131). Among these FABP types, E-FABP displays the lowest conformational stability in the presence of urea, in spite of the presence of a unique disulfide bridge. Furthermore, E-FABP shows the second lowest binding affinity for oleic acid, after A-FABP. In contrast, H-FABP exhibits a very stable conformation and strong ligand binding.

A cluster of hydrophobic side-chains, which closes the end of the  $\beta$ -barrel structure that is located opposite to the helix-turn-helix domain, might play a significant role in both ligand binding and protein stability. Several members of this hydrophobic cluster are substituted in E-FABP (relative to H-FABP) by residues with different hydrophobicities: L7 (F4), F65 (I62), C67 (F64), C87 (V84) and F89 (L86). This might in part explain the decreased conformational stability of E-FABP, whereas other substitutions, like L60 (F57) and V118 (L115), could be responsible for the weaker stability of the E-FABP:fatty acid complex.

The determination of the solution structure of human E-FABP will now permit further studies on intermolecular interactions, in particular with S100A7 in regard to psoriasis, as alluded to in the introduction.

### 4.3 Backbone dynamics of human E-FABP

In spite of the high degree of structural similarity, most members of the fatty acid binding protein family show marked functional differences. Since ligand binding may also be influenced by intrinsic dynamical properties of the protein, it is important to characterize the backbone dynamics of E-FABP.  $^{15}\text{N}$  longitudinal and transverse relaxation rates as well as heteronuclear NOE values of human holo E-FABP were measured at three different fields (500, 600 and 800 MHz). The numerical values of  $R_1$ ,  $R_2$  and NOE are listed in Appendix A.4, with the error of the NOE set to a constant value (0.03) for all residues. The experimental values of the relaxation rates  $R_1$  and  $R_2$ , plotted against residue number, are displayed graphically in Figures 4.10a and 4.10b, respectively; the experimental NOE values are shown in Figure 4.11. These data were subsequently combined and analyzed for 120 of 132 backbone amide groups to yield the microdynamic parameters  $S^2$ ,  $\tau_e$  and  $R_{ex}$  (Table 4.3), which provide information about the mobility of the backbone HN vectors, the correlation time of local motion and the conformational exchange contribution the transverse relaxation, respectively.

Backbone amide order parameters ( $S^2$ ) combined for all 3 fields were determined, with a resulting molecular tumbling correlation time of the protein of  $\tau_c = 8.6$  ns for E-FABP, which may be compared to values of 8.70 ns for A-FABP, 9.05 ns for H-FABP (both calculated with a modified method [Constantine *et al.*, 1998]), 5.8 ns for both ILBP and H-FABP ([Lücke *et al.*, 1999], or 6.7 ns and 6.2 ns for apo and holo I-FABP, respectively [Hodsdon and Cistola, 1997]). The  $\tau_c$  values for other members of the LBP family are 8.2 ns and 7.9 ns for apo and holo CRBP II, respectively [Lu *et al.*, 1999; Lu *et al.*, 2000], and 7.6 ns and 7.1 ns for apo and holo CRABP I [Krishnan *et al.*, 2000]. Such  $\tau_c$  values are not unusual for proteins of this molecular size. Nearly all non-terminal backbone amide groups show  $S^2$  values  $> 0.8$ , with an average value of  $0.88 \pm 0.04$ ; the same average  $S^2$  value holds for the residues belonging to the secondary structure elements. As can be seen in Figure 4.12, the order parameters (representing backbone mobility within the nanosecond-to-picosecond time scale) show little correlation with secondary structure. Interestingly, the N-terminal helical loop and  $\alpha$ -helix I both exhibit above-average  $S^2$  values, indicating reduced backbone mobility, while  $\alpha$ -helix II as part of the portal region displays a higher flexibility. Overall, however, the structure of human E-FABP shows a rather uniform dynamic behaviour throughout the entire amino acid sequence. Therefore, these data for E-FABP suggest an overall protein backbone structure of low flexibility ( $S^2$  values  $> 0.8$  imply a cone semiangle of  $< 21^\circ$  assuming the wobbling-in-a-cone model for the NH-vector motion).

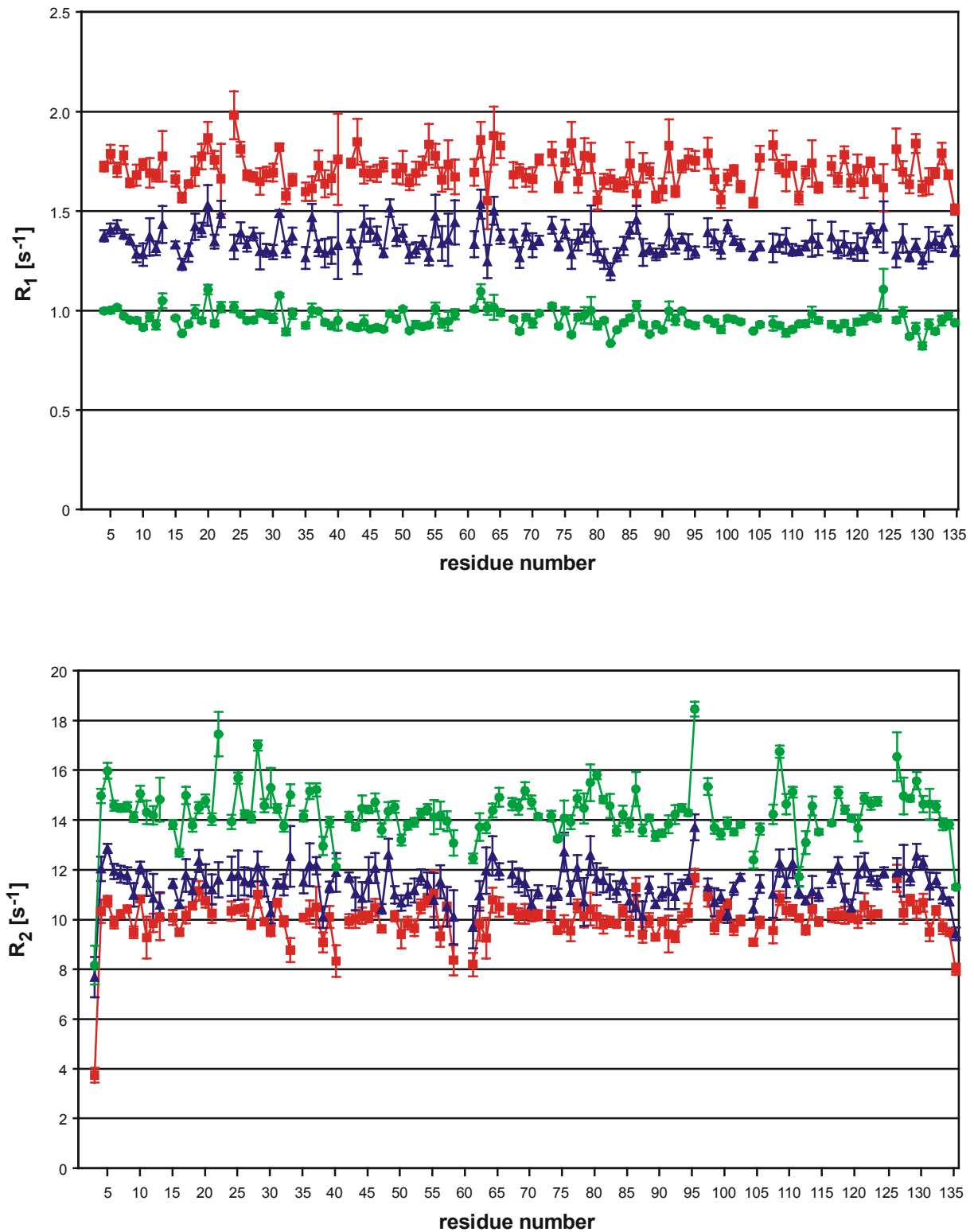


**Figure 4.10** Experimental longitudinal ( $R_1$ ) and transverse ( $R_2$ )  $^{15}\text{N}$  relaxation rates obtained for human E-FABP at 500 (■), 600 (▲) and 800 (●) MHz. Error bars represent standard deviations.



The dynamic behaviour of E-FABP contrasts, for example, that of ILBP [Lücke *et al.*, 1999], which shows a larger spread in the order parameter values and several non-terminal residues with  $S^2$  well below 0.7. Yet other members of the LBP family also exhibit distinct patterns of backbone mobility. It has been observed that A-FABP has a greater backbone mobility than H-FABP, especially in the portal region [Constantine *et al.*, 1998]. This is due to the fact that A-FABP has lower order parameters in the portal region, while H-FABP shows higher  $S^2$  values uniformly distributed throughout the amino acid sequence. For I-FABP, on the other hand, a very high mobility in the portal region has been described [Hodsdon and Cistola, 1997], even though the  $S^2$  values for some residues in this region were abnormally low.

Based on hydrogen/deuterium exchange [Lassen *et al.*, 1995; Lücke *et al.*, 1996] and  $^{15}\text{N}$  relaxation experiments [Lücke *et al.*, 1999], significant differences in the backbone dynamics between bovine H-FABP and porcine ILBP have been previously reported. The extremely slow amide proton exchange behaviour observed for H-FABP indicated a clear distinction in the stability of the hydrogen-bonding network between these two  $\beta$ -barrel structures. Hence, both the hydrogen/deuterium exchange behaviour and the microdynamic

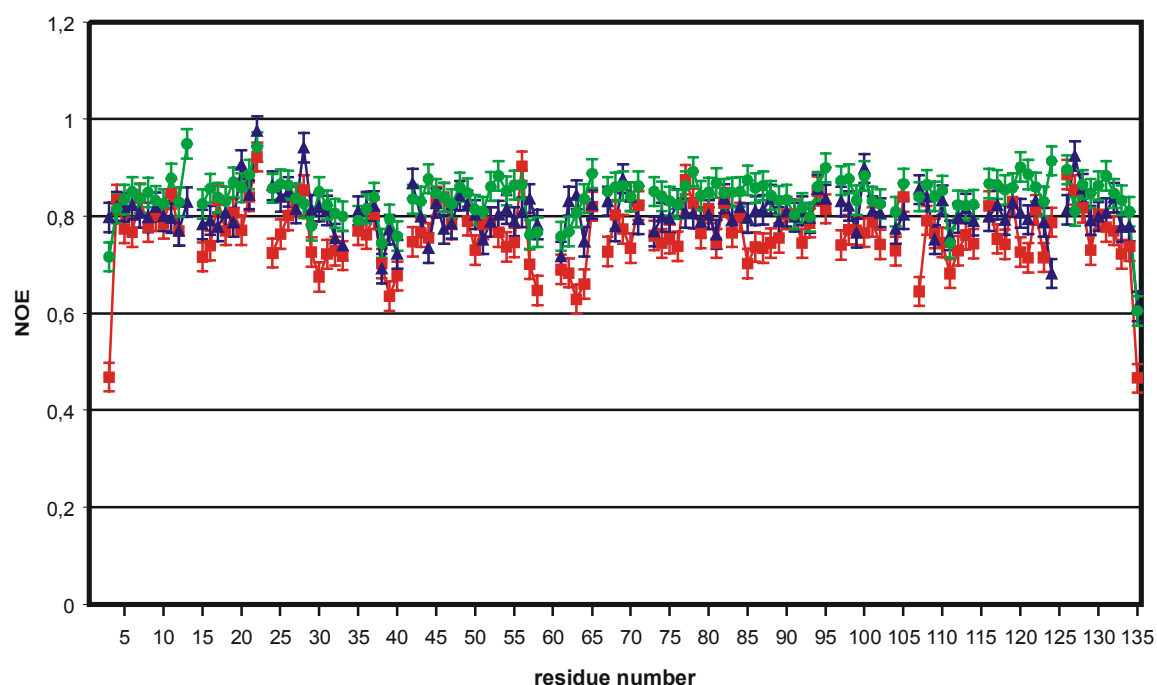


**Figure 4.11** Experimental NOE values obtained for human E-FABP at 500 (■), 600 (▲) and 800 (●) MHz. Error bars represent standard deviations.

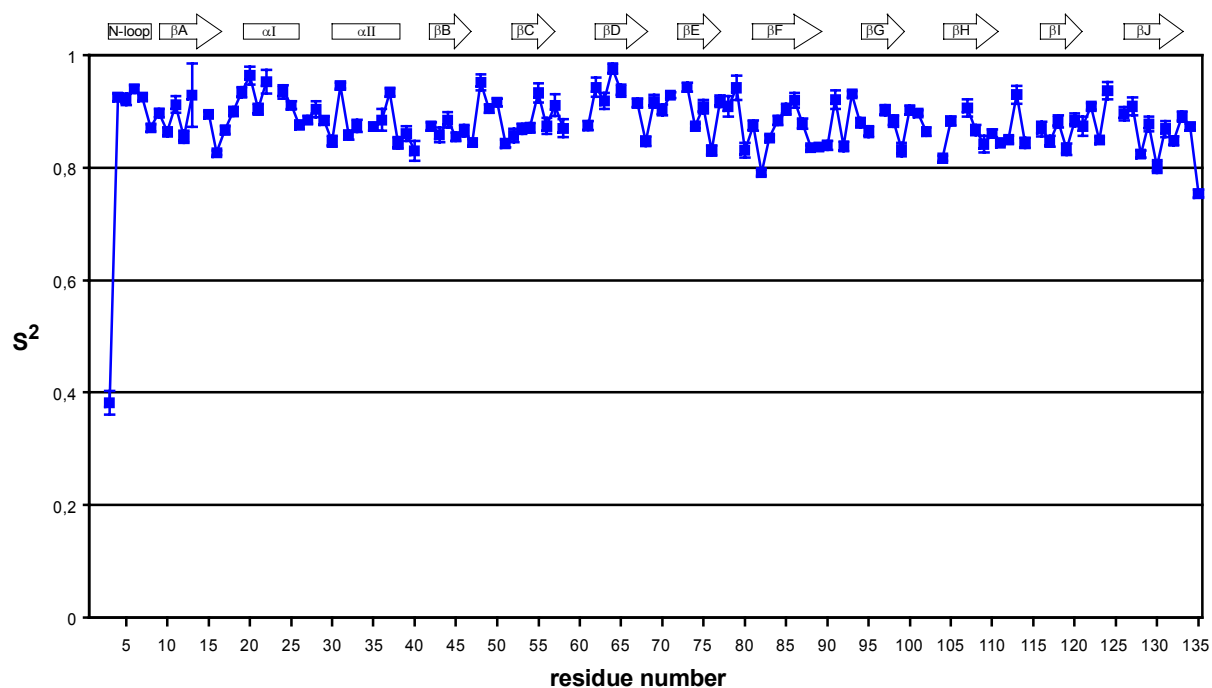


**Figure 4.12** Backbone amide order parameters ( $S^2$ ) determined for human holo E-FABP. The error bars represent standard deviations. All non-terminal residues exhibit a rather uniform dynamic behaviour, suggesting a low backbone mobility for the entire protein structure. The secondary structure elements are indicated schematically above the graph.

parameters can provide valuable information about the influence of dynamic molecular processes on the functional properties of different LBPs. The backbone dynamics data of human E-FABP are therefore compared below with those from other previously studied members of the LBP family [Lücke *et al.*, 1999], *i.e.*, bovine H-FABP and porcine ILBP.

Since the  $^{15}\text{N}$  relaxation data of both H-FABP and ILBP have been previously obtained for the apo-forms [Lücke *et al.*, 1999], we decided to perform an additional proton/deuterium exchange experiment with apo H-FABP for better compatibility. Lassen *et al.* [1995] have reported that 70 backbone amide protons displayed very slow exchange in bovine holo H-FABP over a period of several days at 310 K. For the apo-form, we now observed 39 such amide resonances after 4 days under identical conditions. This indicates a lower stability in the hydrogen-bonding network of the  $\beta$ -sheet structure for the apo-form compared to H-FABP complexed with a fatty acid. Such a stabilizing effect due to ligand binding has been reported before in the case of porcine ILBP [Lücke *et al.*, 1996]. Still, the amide proton exchange behaviour within the  $\beta$ -sheet is unusually slow also for apo H-FABP compared to other LBP types.

**Table 4.3** Microdynamic parameters obtained for human holo E-FABP. Only non-zero values of  $\tau_e$  and  $R_{ex}$  are shown in the table. Residues for which no value could be calculated are marked “n.v.” The spectral density models are defined as described in Materials and Methods.

AA	S <sup>2</sup>	$\tau_e$ [ps]	$R_{ex}$ [s <sup>-1</sup> ]	Model
M1	n.v.	n.v.	n.v.	
A2	n.v.	n.v.	n.v.	
T3	0.382 ± 0.021	5.200 ± 0.793		1
V4	0.925 ± 0.007	5.285 ± 11.370		1
Q5	0.922 ± 0.010		0.746 ± 0.111	2
Q6	0.940 ± 0.007	14.909 ± 13.768		1
L7	0.925 ± 0.006			1
E8	0.871 ± 0.006		0.575 ± 0.073	2
G9	0.897 ± 0.007	2.142 ± 8.065		1
R10	0.864 ± 0.008		0.748 ± 0.107	2
W11	0.912 ± 0.015			1
R12	0.855 ± 0.011		0.511 ± 0.150	2
L13	0.929 ± 0.056			1
V14	n.v.	n.v.	n.v.	
D15	0.895 ± 0.005	16.283 ± 7.323		1
S16	0.827 ± 0.004	6.216 ± 4.010		1
K17	0.867 ± 0.007	3.133 ± 6.060		1
G18	0.900 ± 0.008	11.558 ± 8.721		1
F19	0.934 ± 0.009			1
D20	0.964 ± 0.016	400.000 ± 607.616		1
E21	0.904 ± 0.010			1
Y22	0.953 ± 0.021		0.814 ± 0.318	2
M23	n.v.	n.v.	n.v.	
K24	0.935 ± 0.012	4.147 ± 13.664		1
E25	0.911 ± 0.007		0.522 ± 0.089	2
L26	0.876 ± 0.007		0.544 ± 0.071	2
G27	0.885 ± 0.007	0.603 ± 7.154		1
V28	0.904 ± 0.014		1.421 ± 0.113	2
G29	0.884 ± 0.007	27.259 ± 6.935		1
I30	0.847 ± 0.010	11.991 ± 5.313		1
A31	0.946 ± 0.005	86.641 ± 18.747		1
L32	0.858 ± 0.008	14.709 ± 5.730		1
R33	0.874 ± 0.011	26.347 ± 6.999		1
K34	n.v.	n.v.	n.v.	
M35	0.873 ± 0.007	10.879 ± 6.427		1
G36	0.885 ± 0.019		0.793 ± 0.169	2
A37	0.934 ± 0.007		0.549 ± 0.105	2
M38	0.844 ± 0.010	36.798 ± 5.561		1
A39	0.861 ± 0.013		0.460 ± 0.109	2
K40	0.830 ± 0.018	28.825 ± 6.220		1
P41	n.v.	n.v.	n.v.	
D42	0.874 ± 0.007		0.456 ± 0.079	2
C43	0.858 ± 0.013		0.447 ± 0.094	2
I44	0.885 ± 0.014	10.874 ± 7.513		1
I45	0.855 ± 0.007		0.691 ± 0.073	2
T46	0.866 ± 0.010		0.720 ± 0.140	2

AA	S <sup>2</sup>	$\tau_e$ [ps]	$R_{ex}$ [s <sup>-1</sup> ]	Model
C47	0.845 ± 0.006	10.279 ± 4.851		1
D48	0.952 ± 0.014			1
G49	0.905 ± 0.008	0.248 ± 8.901		1
K50	0.916 ± 0.007	37.914 ± 9.876		1
N51	0.843 ± 0.007		0.504 ± 0.080	2
L52	0.857 ± 0.012		0.486 ± 0.098	2
T53	0.869 ± 0.009		0.573 ± 0.087	2
I54	0.871 ± 0.009		0.628 ± 0.090	2
K55	0.933 ± 0.017	14.390 ± 13.568		1
T56	0.874 ± 0.014			1
E57	0.911 ± 0.019	32.786 ± 12.775		1
S58	0.870 ± 0.016	34.945 ± 8.004		1
T59	n.v.	n.v.	n.v.	
L60	n.v.	n.v.	n.v.	
K61	0.875 ± 0.008	52.769 ± 7.593		1
T62	0.943 ± 0.017	68.162 ± 30.110		1
T63	0.919 ± 0.014	34.047 ± 12.698		1
Q64	0.976 ± 0.009	215.923 ± 278.933		1
F65	0.937 ± 0.011			1
S66	n.v.	n.v.	n.v.	
C67	0.915 ± 0.008	2.207 ± 9.861		1
T68	0.847 ± 0.009		0.720 ± 0.120	2
L69	0.918 ± 0.011			1
G70	0.903 ± 0.010	4.214 ± 8.854		1
E71	0.929 ± 0.005			1
K72	n.v.	n.v.	n.v.	
F73	0.943 ± 0.008	33.527 ± 15.137		1
E74	0.874 ± 0.004	3.052 ± 6.068		1
E75	0.908 ± 0.012	19.284 ± 9.400		1
T76	0.831 ± 0.009		0.607 ± 0.115	2
T77	0.918 ± 0.010			1
A78	0.909 ± 0.018			1
D79	0.942 ± 0.022	19.671 ± 17.567		1
G80	0.831 ± 0.013		1.393 ± 0.102	2
R81	0.875 ± 0.009		0.751 ± 0.076	2
K82	0.791 ± 0.005		0.863 ± 0.135	2
T83	0.853 ± 0.005	3.311 ± 5.113		1
Q84	0.884 ± 0.008			1
T85	0.904 ± 0.010	11.737 ± 8.693		1
V86	0.920 ± 0.013	12.108 ± 10.961		1
C87	0.878 ± 0.009	4.420 ± 6.704		1
N88	0.836 ± 0.004		0.701 ± 0.055	2
F89	0.837 ± 0.005	13.134 ± 4.631		1
T90	0.84 ± 0.008		0.385 ± 0.072	2
D91	0.921 ± 0.017	18.261 ± 12.010		1
G92	0.838 ± 0.009	10.170 ± 4.951		1
A93	0.931 ± 0.005	22.093 ± 11.121		1
L94	0.88 ± 0.008		0.525 ± 0.063	2
V95	0.864 ± 0.010		2.160 ± 0.127	2
Q96	n.v.	n.v.	n.v.	
H97	0.902 ± 0.009		0.590 ± 0.127	2
Q98	0.883 ± 0.010			1

AA	S <sup>2</sup>	$\tau_e$ [ps]	$R_{ex}$ [s <sup>-1</sup> ]	Model
E99	0.832 ± 0.012		0.452 ± 0.105	2
W100	0.902 ± 0.008			1
D101	0.897 ± 0.005	5.397 ± 7.622		1
G102	0.864 ± 0.007		0.446 ± 0.066	2
K103	n.v.	n.v.	n.v.	
E104	0.817 ± 0.005	22.646 ± 3.745		1
S105	0.883 ± 0.008			1
T106	n.v.	n.v.	n.v.	
I107	0.906 ± 0.015	15.439 ± 9.543		1
T108	0.867 ± 0.009		1.454 ± 0.104	2
R109	0.842 ± 0.015		0.785 ± 0.171	2
K110	0.861 ± 0.007		0.873 ± 0.090	2
L111	0.844 ± 0.005	33.690 ± 4.649		1
K112	0.850 ± 0.007	14.900 ± 5.321		1
D113	0.930 ± 0.016	16.573 ± 13.394		1
G114	0.844 ± 0.009		0.411 ± 0.071	2
K115	n.v.	n.v.	n.v.	
L116	0.869 ± 0.013		0.449 ± 0.084	2
V117	0.847 ± 0.010		0.986 ± 0.101	2
V118	0.882 ± 0.011		0.546 ± 0.092	2
E119	0.833 ± 0.010		0.690 ± 0.080	2
C120	0.885 ± 0.011	0.780 ± 7.328		1
V121	0.874 ± 0.017		0.804 ± 0.130	2
M122	0.909 ± 0.006		0.405 ± 0.093	2
N123	0.849 ± 0.006		0.672 ± 0.075	2
N124	0.937 ± 0.015	14.704 ± 14.863		1
V125	n.v.	n.v.	n.v.	
T126	0.896 ± 0.012		0.910 ± 0.268	2
C127	0.909 ± 0.016			1
T128	0.824 ± 0.006		1.084 ± 0.060	2
R129	0.878 ± 0.013		0.939 ± 0.148	2
I130	0.802 ± 0.011		1.255 ± 0.125	2
Y131	0.869 ± 0.014			1
E132	0.848 ± 0.008		0.703 ± 0.092	2
K133	0.891 ± 0.009	17.646 ± 7.941		1
V134	0.873 ± 0.006	22.218 ± 6.459		1
E135	0.754 ± 0.007	400.000 ± 50.008		3

The conformational stabilities of various LBP types have been evaluated by examination of the fluorescence spectra of the proteins at different urea concentrations. It has been observed that oleic acid binding to H-FABP is less sensitive to urea than the binding to E-FABP. It has also been found that, for example, the oleic acid binding constants vary from 0.44  $\mu$ M for human H-FABP to 0.82  $\mu$ M for human E-FABP and  $\gg 1$   $\mu$ M for human ILBP

[Zimmerman *et al.*, 2001]. The transition curves of E-FABP and, to a lesser extent, ILBP are shifted to the left in comparison with H-FABP. Their midpoints of transition are markedly lower than for H-FABP. Therefore, in spite of the presence of a disulfide bridge, E-FABP has the lowest stability of binding and conformation.

Due to the rather low structural stability of E-FABP, and due to the fact that the LBP holo-forms usually are more stable than the apo-forms as mentioned above, we have chosen to investigate human E-FABP in complex with stearic acid at a decreased temperature of 298 K. The comparison with the apo-forms of H-FABP and ILBP [Lücke *et al.*, 1999] should nevertheless provide useful information about the relative conformational stabilities of these FABP types. First, human E-FABP is compared to bovine H-FABP. The order parameter ( $S^2$ ) distributions of apo H-FABP and holo E-FABP are rather similar, *i.e.*, they show a uniform distribution throughout the amino acid sequence, indicating a relatively low flexibility within the entire backbone structure (average  $S^2 = 0.89 \pm 0.06$  for apo H-FABP and  $0.88 \pm 0.06$  for holo E-FABP). However, E-FABP shows a much faster hydrogen exchange compared to H-FABP. For apo H-FABP, 49 slow-exchanging backbone amide protons involved in the hydrogen-bonding network within the  $\beta$ -sheet structure were observed after 6 h in perdeuterated buffer at 310 K (Figure 4.13A), of which 39 remained detectable after four days. In the case of holo E-FABP, on the other hand, only 37 amide proton resonance signals remained observable after 2 h in perdeuterated solution at 298 K (Figure 4.13C), and just 13 signals could be detected after two days. Thus it appears that, compared to apo H-FABP, the hydrogen-bonding network of the  $\beta$ -sheet structure of E-FABP is less stable even in the holo-form. These data agree with the conformational stabilities reported by Zimmerman *et al.* [2001]. Interestingly, in the case of holo E-FABP the analysis of the relaxation data produced exchange parameter terms ( $R_{ex}$ ) for 47 residues (Figure 4.13D), the majority of which are located in the center sections of the  $\beta$ -strands where also the slow-exchanging amide protons are concentrated. This suggests a direct correlation between the slow exchange of backbone amide protons in the  $\beta$ -sheets and the occurrence of  $R_{ex}$  terms (representing exchange processes on the millisecond-to-microsecond time scale). For apo H-FABP, on the other hand, the occurrence of  $R_{ex}$  terms is reduced to only 8 residues, which are distributed randomly throughout the amino acid sequence (Figure 4.13B). Since apo H-FABP had been investigated at a considerably higher temperature [Lassen *et al.*, 1995], these results indicate a strongly decreased hydrogen exchange within the  $\beta$ -sheet structure of apo H-FABP relative to holo E-FABP.

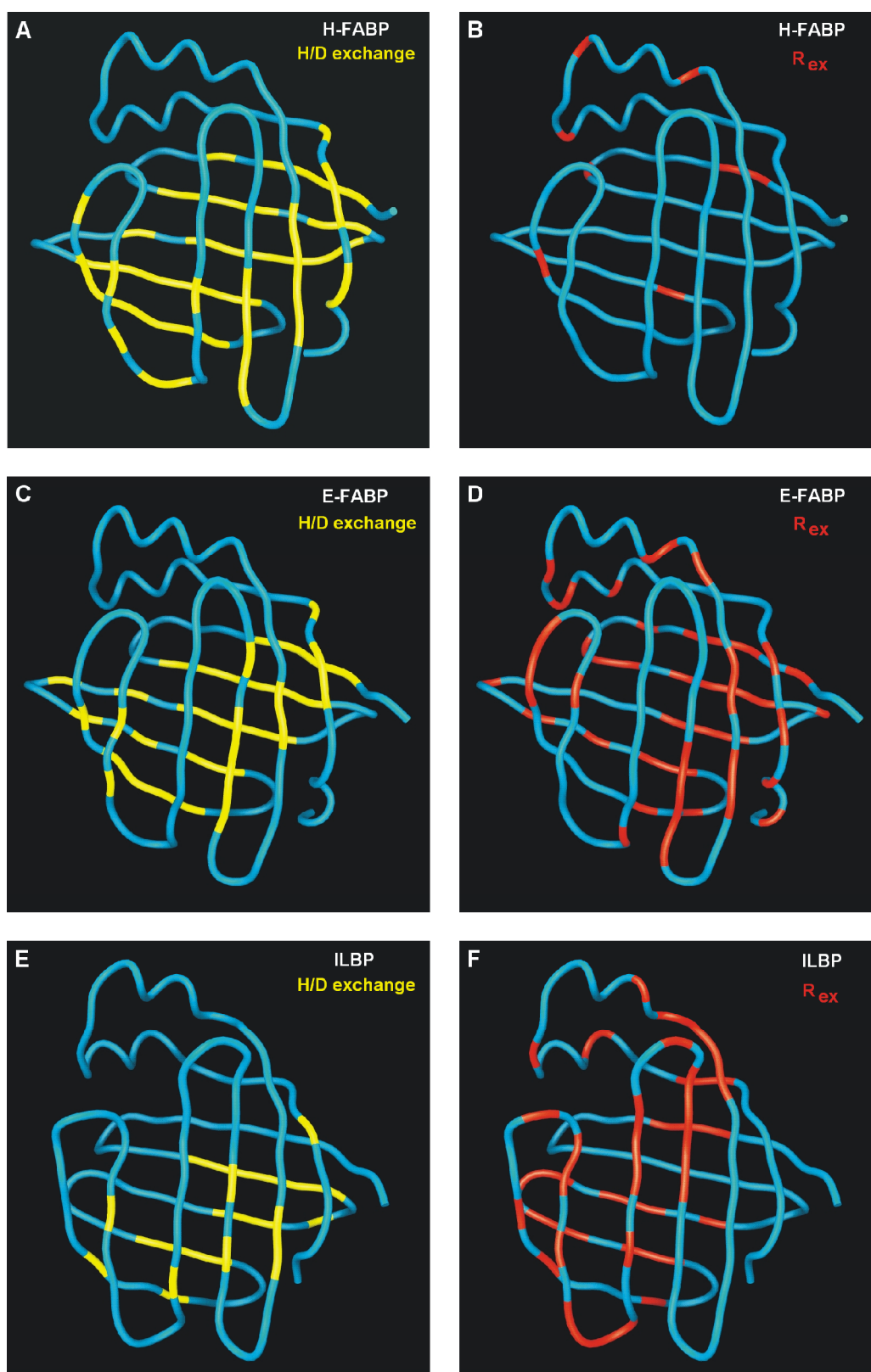


**Figure 4.13 (Previous page) Backbone worm representation indicating slow-exchanging amide protons (H/D in yellow) and non-zero conformational exchange parameter values ( $R_{ex}$  in red) in different LBP family members. Hydrogen/deuterium exchange experiments and the microdynamic parameters obtained from  $^{15}\text{N}$  relaxation analysis show significant differences in the chemical exchange with the solvent for the backbone amide protons. In bovine apo H-FABP (top panels), 49 slow-exchanging amide protons remain visible after 6 h at 310 K in  $\text{D}_2\text{O}$  solution (panel A), while only 8 residues show exchange parameters (panel B). For human holo E-FABP (center panels), 37 slow-exchanging amide protons are detected after 2 h at 298 K in  $\text{D}_2\text{O}$  solution (panel C) and 47 residues with  $R_{ex}$  terms occur in the central  $\beta$ -sheet (panel D). Porcine apo ILBP (bottom panels), finally, exhibits 20 slow-exchanging amide protons after 30 min at 310 K in  $\text{D}_2\text{O}$  solution (panel E) and 43 residues with exchange parameters (panel F). Human holo E-FABP appears to rank between apo H-FABP and apo ILBP in the hydrogen/deuterium exchange, with  $R_{ex}$  terms in the  $\beta$ -strands indicating exchange in the millisecond-to-microsecond time range. Clearly, the hydrogen-bonding network in the  $\beta$ -sheet structure of holo E-FABP is less stable relative to apo H-FABP. (Produced using GRASP [Nicholls *et al.*, 1991].)**

Comparing the backbone dynamics data of human E-FABP with the previously reported results for porcine ILBP [Lücke *et al.*, 1999], however, presents a quite different scenario. In the case of apo ILBP, several non-terminal residues displayed strongly decreased order parameter ( $S^2$ ) values, suggesting a relatively high flexibility within certain regions of the backbone structure. In addition, an even faster hydrogen exchange was reported for apo ILBP [Lücke *et al.*, 1996] compared to that of holo E-FABP presented here. For apo-ILBP, merely 20 amide proton resonance signals remained detectable after only 30 min in perdeuterated solution at 310 K (Figure 4.13E), all of which disappeared completely after 4 h. ILBP in complex with chenodeoxycholate showed a slower hydrogen exchange relative to apo ILBP, with complete exchange of all backbone amide protons after 18 h at 310 K, thus implying a stabilizing effect induced by the bound ligand. Nevertheless, the exchange of the backbone amide resonances within the  $\beta$ -sheet structure apparently proceeds faster for both apo and holo ILBP than in the cases of apo H-FABP or holo E-FABP, indicating a lower stability of the hydrogen-bonding network in ILBP. Moreover,  $R_{ex}$  terms occur in apo ILBP for a total of 43 residues that are located mainly within the  $\beta$ -strands (Figure 4.13F), suggesting that the exchange of backbone amide protons in this LBP may also be subjected to processes that take place within the millisecond-to-microsecond time range.



Summarizing the above results, it can be concluded that the different LBP family members E-FABP, H-FABP and ILBP are characterized by varying stabilities in the protein backbone structures. Hydrogen/deuterium exchange experiments showed significant differences in the chemical exchange with the solvent for the backbone amide protons belonging to the hydrogen-bonding network in the  $\beta$ -sheets. The  $\beta$ -barrel structure of bovine H-FABP appears to be the most rigid, with exchange processes presumably slower than the millisecond-to-microsecond time range. Porcine ILBP, on the other hand, shows the fastest hydrogen exchange as well as a significant number of exchange parameters ( $R_{ex}$ ), indicating a decreased stability in the  $\beta$ -sheet structure. Human E-FABP, finally, appears to rank between these two proteins based on the hydrogen/deuterium exchange, with  $R_{ex}$  terms in the  $\beta$ -strands indicating millisecond-to-microsecond exchange processes like in ILBP.

It has now become clear from this study that within the LBP family there are distinctions in protein stability. According to Zimmerman and co-workers [2001], the conformational stabilities of the human paralogs H-FABP, ILBP and E-FABP decrease in this order, which partially contrasts the results presented here. However, both studies agree that within LBP subfamily *IV* the H-FABP has a much more rigid structure than E-FABP. Responsible for this distinction may be differences in the arrangement of the hydrophobic cluster inside the protein cavity, in particular the replacement of F4 (H-FABP) by L7 (E-FABP). Moreover, the higher conformational stability of H-FABP could also be related to the tighter binding of fatty acid ligands to H-FABP relative to E-FABP [Zimmerman *et al.*, 2001]. Possibly, there is a correlation between protein stability and ligand binding affinity, if a more flexible structure allows the bound ligand to leave the binding cavity more easily. On the other hand, the lack of the highly conserved phenylalanine portal lid (F57 in H-FABP) in E-FABP could be the predominant factor for the lower fatty acid binding affinities of the latter. Future site-directed mutagenesis studies on human E-FABP may provide definite answers to these questions. Moreover, further NMR investigations on the dynamics of different LBPs will be needed for a more concise interpretation of the distinctions in binding affinity and specificity.

## 5 Summary

Human epidermal-type fatty acid binding protein (E-FABP) belongs to a family of intracellular non-enzymatic 14-15 kDa lipid binding proteins (LBP) that specifically bind and facilitate the transport of fatty acids, bile acids or retinoids. Their functions have also been associated with fatty acid signalling, cell growth, regulation and differentiation. As a contribution to better understand the structure-function relationship of this protein, the features of its solution structure determined by NMR spectroscopy are reported here. Both unlabeled and  $^{15}\text{N}$ -enriched samples of recombinant human E-FABP were used for multidimensional high-resolution NMR. The sequential backbone as well as side-chain resonance assignments have been completed. They are reported here and are also available at the BioMagResBank under the accession number BMRB-5083.

The presence of six cysteines in the amino acid sequence of human E-FABP is highly unusual for LBPs. Four of the six cysteines are unique to the E-FABPs: C43, C47, C67 and C87. In the three-dimensional structure of E-FABP, two cysteine pairs (C67/C87 and C120/C127) were identified by X-ray analysis to be close enough to allow disulfide bridge formation, but a S-S bond was actually found only between C120 and C127 [Hohoff *et al.*, 1999]. Since the exclusion of a disulfide bridge between C67 and C87 improved the  $R_{\text{free}}$  factor of the crystallographic model, the existence of a covalent bond between these two side-chains was considered unlikely. This agrees with the NMR data, where  $S^{\gamma}\text{H}$  resonances have been observed for the cysteine residues C43, C67 (tentative assignment) and C87, thus excluding the possibility of a second disulfide bridge in solution.

Based on the NOE and hydrogen exchange data, an ensemble of 20 energy-minimized conformers representing the solution structure of human E-FABP complexed with stearic acid has been obtained. The analysis of homonuclear 2D NOESY and  $^{15}\text{N}$ -edited 3D NOESY spectra led to a total of 2926 NOE-derived distance constraints. Furthermore, 37 slow-exchanging backbone amide protons were identified to be part of the hydrogen-bonding network in the  $\beta$ -sheet and subsequently converted into 74 additional distance constraints. Finally, the disulfide bridge between C120 and C127 was defined by 3 upper and 3 lower distance bounds. The structure calculation program DYANA regarded 998 of these constraints as irrelevant, *i.e.*, they did not restrict the distance between two protons. Out of the remaining 2008 non-trivial distance constraints, 371 were intraresidual ( $i = j$ ), 508 sequential ( $|i - j| = 1$ ), 233 medium-range ( $1 < |i - j| \leq 4$ ), and 896 long-range ( $|i - j| > 4$ ) NOEs. The protein mainly consists of 10 antiparallel  $\beta$ -strands forming a  $\beta$ -barrel structure with a large

---

internal cavity. The three-dimensional solution structure of human E-FABP has been determined with a root-mean-square deviation of  $0.92 \pm 0.11$  Å and  $1.46 \pm 0.10$  Å for the backbone and heavy atoms, respectively, excluding the terminal residues. Without the portal region (*i.e.*, for residues 4-26, 40-56, 63-75 and 83-134; the portal region apparently represents the only opening in the protein surface through which the fatty acid ligand can enter and exit the internal binding cavity), an average backbone RMSD of  $0.85 \pm 0.10$  Å was obtained, thus reflecting the higher conformational dispersion in the portal region. Superposition with the X-ray structure of human E-FABP (excluding the terminal residues) yielded average backbone RMSD values of  $1.00 \pm 0.07$  Å for the entire residue range and  $0.98 \pm 0.06$  Å without the portal region. This indicates a close similarity of the crystallographic and the solution structures. The structure coordinates have been deposited at the RCSB data bank under PDB ID code 1JJJ.

The measurement of  $^{15}\text{N}$  relaxation experiments ( $T_1$ ,  $T_2$  and heteronuclear NOE) at three different fields (500, 600 and 800 MHz) provided information on the internal dynamics of the protein backbone. Nearly all non-terminal backbone amide groups showed order parameters  $S^2 > 0.8$ , with an average value of  $0.88 \pm 0.04$ , suggesting a uniformly low backbone mobility in the nanosecond-to-picosecond time range throughout the entire protein sequence. Moreover, hydrogen/deuterium exchange experiments indicated a direct correlation between the stability of the hydrogen-bonding network in the  $\beta$ -sheet structure and the conformational exchange ( $R_{ex}$ ) in the millisecond-to-microsecond time range. The features of E-FABP backbone dynamics elaborated here differ from those of the phylogenetically closely related heart-type FABP and the more distantly related ileal lipid binding protein. The results on protein dynamics obtained in this work allow to conclude that the different LBP family members E-FABP, H-FABP and ILBP are characterized by varying stabilities in the protein backbone structures. Hydrogen/deuterium exchange experiments displayed significant differences in the chemical exchange with the solvent for the backbone amide protons belonging to the hydrogen-bonding network in the  $\beta$ -sheets. The  $\beta$ -barrel structure of H-FABP appears to be the most rigid, with exchange processes presumably slower than the millisecond-to-microsecond time range. ILBP, on the other hand, shows the fastest hydrogen exchange as well as a significant number of exchange parameters ( $R_{ex}$ ), implying a decreased stability in the  $\beta$ -sheet structure. E-FABP, finally, appears to rank between these two proteins based on the hydrogen/deuterium exchange, with  $R_{ex}$  terms in the  $\beta$ -strands indicating millisecond-to-microsecond exchange processes like in ILBP.

## 6 References

- Abe, H., Braun, W., Noguti, T. and Gö, N. (1983). Rapid calculation of first and second derivatives of conformational energy with respect to dihedral angles in proteins. General recurrent questions. *Comput. Chem.* **8**, 239-247
- Abraham, A. (1961). *Principles of Nuclear Magnetism*, Clarendon Press, Oxford
- Akke, M., Carr, P. A. and Palmer, A. G. (1994). Heteronuclear correlation NMR spectroscopy with simultaneous isotope filtration, quadrature detection, and sensitivity enhancement using z rotations. *J. Magn. Reson.* **B 104**, 298-302
- Allen, M. and Tildesley, D. (1987). *Computer Simulations of Liquids*, Clarendon Press, Oxford
- Åstrom, A., Tavakkol, A., Petterson, U., Cromie, M., Elder, J. T. and Voorhees, J. J. (1991). Molecular cloning of two human cellular retinoic acid-binding proteins (CRABP). *J. Biol. Chem.* **266**, 17662-17666
- Arnold, V. (1978). *Mathematical Methods of Classical Mechanics*, Springer, New York
- Aue, W. P., Bartholdi, E., Ernst, R. R. (1976). Two-dimensional spectroscopy. application to nuclear magnetic resonance. *J. Chem. Phys.* **64**, 2229-2246
- Banaszak, L., Winter, N., Xu, Z., Bernlohr, D., Cowan, S. and Jones, T. (1994). Lipid-binding proteins: A family of fatty acid and retinoid transport proteins. *Adv. Prot. Chem.* **45**, 89-151
- Bass, N. M. (1988). The cellular fatty acid binding proteins: aspects of structure, regulation, and function. *Int. Rev. Cytol.* **111**, 143-184
- Bax, A. and Davis, D. G. (1985). MLEV-17 based two-dimensional homonuclear magnetization transfer spectroscopy. *J. Magn. Reson.* **65**, 355-360
- Bax, A. (1989). Two-dimensional NMR and protein structure. *Annu. Rev. Biochem.* **58**, 223-256
- Bax, A. and Grzesiek, S. (1993). Methodological advances in protein NMR. *Acc. Chem. Res.* **26**, 131-138
- Baxa, C. A., Sha, R. S., Buelt, M. K., Smith, A. J., Matarese, V., Chinander, L. L., Boundy, K. L. and Bernlohr, D. A. (1989). Human adipocyte lipid-binding protein: purification of the protein and cloning of its complementary DNA. *Biochemistry* **28**, 8683-8690
- Becker, M. M., Kalinna, B. H., Waive, G. J. and McManus D. P. (1994). Gene cloning, overproduction and purification of a functionally active cytoplasmic fatty acid-binding

- protein (Sj-FABP<sub>C</sub>) from the human blood fluke *Schistosoma japonicum*. *Gene* **148**, 321-325
- Bendall, M. R., Doddrell, D. M. and Pegg, D. T. (1981). Editing of <sup>13</sup>C NMR spectra. A pulse sequence for the generation of subspectra. *J. Am. Chem. Soc.* **103**, 4603-4605
- Berendsen, H., Postma, J., Dinola, A. and Haak, J. (1984). Molecular dynamics with coupling to an external bath. *J. Chem. Phys.* **81**, 3684-3690
- Bleck, B., Hohoff, C., Binas, B., Rustow, B., Dixkens C., Hameister, H., Börchers, T. and Spener, F. (1998). Cloning and chromosomal localisation of the murine epidermal-type fatty acid-binding protein gene (Fabpe). *Gene* **215**, 123-130
- Bodenhausen, G. and Ruben, D. J. (1980). Natural abundance nitrogen-15 NMR by enhanced heteronuclear spectroscopy. *Chem. Phys. Lett.* **69**, 185-189
- Börchers, T. and Spener, F. (1994). Fatty acid binding proteins. *Curr. Top. Membr.* **40**, 261-294
- Braunschweiler, L. and Ernst, R. R. (1983) Coherence transfer by isotropic mixing: application to proton correlation spectroscopy. *J. Magn. Reson.* **53**, 521-528
- Brink, D. M. and Satchler, G. R. (1968). *Angular Momentum*, Clarendon Press, Oxford
- Bundi, A. and Wüthrich, K. (1979). <sup>1</sup>H-NMR parameters of the common amino acid residues measured in aqueous solutions of the linear tetrapeptides H-Gly-Gly-X-L-Ala-OH. *Biopolymers* **18**, 285-297
- Cavanagh, J. and Rance, M. (1992). Suppression of cross-relaxation effects in TOCSY spectra via a modified DIPSI-2 mixing sequence. *J. Magn. Reson.* **96**, 670-678
- Cavanagh, J., Fairbrother, W. J., Palmer III, A. G. and Skelton, N. J. (1996). *Protein NMR Spectroscopy: Principles and Practice*, Academic Press, San Diego
- Celis, J. E., Rasmussen, H. H., Vorum, H., Madsen, P., Wolf, B., Wolf, H., Orntoft, T. F. (1996). Bladder squamous cell carcinomas express psoriasin and externalise it to the urine. *J. Urol.* **155**, 2105-2112
- Clore, G. M., Driscoll, P. C., Wingfield, P. T. and Gronenborn, A. M. (1990a). Analysis of the backbone dynamics of interleukin-1 $\beta$  using two-dimensional inverse detected heteronuclear <sup>15</sup>N-<sup>1</sup>H NMR spectroscopy. *Biochemistry* **29**, 7387-7401
- Clore, G. M., Szabo, A., Bax, A., Kay, L. E., Driscoll, P. C. and Gronenborn, A. M. (1990b). Deviations from the two-parameter model-free approach to the interpretation of nitrogen-15 nuclear magnetic relaxation of proteins. *J. Am. Chem. Soc.* **112**, 4989-4991
- Constantine, K. L., Friedrichs, M. S., Wittekind, M., Jamil, H., Chu, C. H., Parker, R. A., Goldfarb, V., Mueller, L. and Farmer, B. T. II (1998). Backbone and side chain dynamics

- of uncomplexed human adipocyte and muscle fatty acid-binding proteins. *Biochemistry* **37**,7965-7980
- Cowan, S. W., Newcomer, M. E. and Jones, T. A. (1993). Crystallographic studies on a family of cellular lipophilic transport proteins. Refinement of P2 myelin protein and the structure determination and refinement of cellular retinol-binding protein in complex with all-trans-retinol. *J. Mol. Biol.* **230**, 1225-1246
- Dauber-Osguthorpe, P., Roberts, V. A., Osguthorpe, D. J., Wolff, D. J., Genest, M. and Hagler, A. T. (1988). Structure and energetics of ligand binding to proteins: *Escherichia coli* dihydrofolate reductase-trimethoprim, a drug receptor system. *Proteins Struct. Funct. Genet.* **4**, 31-47
- De León, M., Welcher, A. A., Nahin, R. H., Liu, Y., Ruda, M. A., Shooter, E. M. and Molina, C. A. (1996). Fatty acid binding protein is induced in neurons of the dorsal root ganglia after peripheral nerve injury. *J. Neurosci. Res.* **44**, 283-292
- Delva, L., Bastie, J. N., Rochette-Egly, C., Kraiba, R., Balitrand, N., Despouy, G., Chambon, P. and Chomienne, C. (1999). Physical and functional interactions between cellular retinoic acid binding protein II and the retinoic acid-dependent nuclear complex. *Mol. Cell Biol.* **19**, 7158-7167
- Di Pietro, S. M., Dell'Angelica, E. C., Schleicher, C. H. and Santomé, J. A. (1996). Purification and structural characterization of a fatty acid-binding protein from the liver of the catfish *Rhamdia sapo*. *Comp. Biochem. Physiol.* **B 113**, 503-509
- Dodrell, D. M., Pegg, D. T. and Bendall, M. R. (1982). Distortionless enhancement of NMR signals by polarization transfer. *J. Magn. Reson.* **48**, 323-327
- Eads, J., Sacchettini, J. C., Kromminga, A. and Gordon, J. I. (1993). *Escherichia coli*-derived rat intestinal fatty acid binding protein with bound myristate at 1.5 Å resolution and I-FABPArg106-->Gln with bound oleate at 1.74 Å resolution. *J. Biol. Chem.* **268**, 26375-26385
- Farooqui, J. Z., Robb, E., Boyce, S. T., Warden, G. D. and Nordlund, J. J. (1995). Isolation of a unique melanogenic inhibitor from human skin xenografts: initial *in vitro* and *in vivo* characterization. *J. Invest. Dermatol.* **104**, 739-743
- Farrow, N. A., Muhandiram, R., Singer, A. U., Pascal, S. M., Kay, C. M., Gish, G., Shoelson, S. E., Pawson, T., Forman-Kay, J. D. and Kay, L. E. (1994). Backbone dynamics of a free and a phosphopeptide-complexed src homology 2 domain studied by <sup>15</sup>N NMR relaxation. *Biochemistry* **33**, 5984-6003

- Fischer, M. W. F., Majumdar, A. and Zuiderweg, E. R. P. (1998). Protein NMR relaxation: theory, applications and outlook. *Progress in Nuclear Magnetic Resonance Spectroscopy* **33**, 207-272
- Fletcher, R. (1980). *Practical methods of optimization, Vol. 1, Unconstrained Optimization*, John Wiley and Sons, New York
- Folli, C., Calderone, V., Ottonello, S., Bolchi, A., Zanotti, G., Stoppini, M. and Berni, R. (2001). Identification, retinoid binding, and x-ray analysis of a human retinol-binding protein. *Proc. Natl. Acad. Sci. USA* **98**, 3710-3715
- García de la Torre, J. and Bloomfield, V. (1981). Hydrodynamic properties of complex rigid, biological macromolecules: Theory and applications. *Quart. Rev. Biophys.* **14**, 81-139
- Glatz, J. F. and Veerkamp, J. H. (1983). Removal of fatty acids from serum albumin by Lipidex 1000 chromatography. *J. Biochem. Biophys. Methods* **8**, 57-61
- Glatz, J. and Van der Vusse, G. (1996). Cellular fatty acid binding proteins: Their function and physiological significance. *Prog. Lip. Res.* **35**, 243-282
- Güntert, P. (1993). Neue Rechenverfahren für die Proteinstrukturbestimmung mit Hilfe der Magnetischen Kernspinresonanz, Doktorarbeit, ETH, Zürich
- Güntert, P., Braun, W. and Wüthrich, K.. (1991). Efficient computation of three-dimensional protein structures in solution from nuclear magnetic resonance data using the program DIANA and the supporting programs CALIBA, HABAS and GLOMSA. *J. Mol. Biol.* **217**, 517-530
- Güntert, P., Mumenthaler, C. and Wüthrich, K. (1997). Torsion angle dynamics for NMR structure calculation with the new program DYANA. *J. Mol. Biol.* **273**, 283-298
- Hagens, G., Masouyé, I., Augsburger, E., Hotz, R., Saurat J.-H. and Siegenthaler, G. (1999). Calcium-binding protein S100A7 and epidermal-type fatty acid-binding protein are associated in the cytosol of human keratinocytes. *Biochem. J.* **339**, 419-427
- Hayasaka, K., Nanao, K., Tahara, M., Sato, W., Takada, G., Miura, M. and Uyemura, K. (1991). Isolation and sequence determination of cDNA encoding P2 protein of human peripheral myelin. *Biochem. Biophys. Res. Commun.* **181**, 204-207
- Helledie, T., Antonius, M., Sørensen, R. V., Hertzfel, A. V., Bernlohr, D. A., Kølvrå, S., Kristiansen, K. and Mandrup, S. (2000). Lipid-binding proteins modulate ligand-dependent trans-activation by peroxisome proliferator-activated receptors and localize to the nucleus as well as the cytoplasm. *J. Lipid Res.* **41**, 1740-1751

- 
- Herr, F. M., Aronson, J. and Storch, J. (1996). Role of portal region lysine residues in electrostatic interactions between heart fatty acid binding protein and phospholipid membranes. *Biochemistry* **35**, 1296-1303
- Hertzel A. V. and Bernlohr, D. A. (1998). Cloning and chromosomal location of the murine keratinocyte lipid-binding protein gene. *Gene* **221**, 235-243
- Hiyama, Y., Niu, C., Silverton, J. V., Bavoso, A. and Torchia, D. A. (1988). Determination of  $^{15}\text{N}$  chemical shift tensor via  $^{15}\text{N}$  -  $^2\text{H}$  dipolar coupling in boc-glycylglycyl[ $^{15}\text{N}$ ]glycine benzyl ester *J. Am. Chem. Soc.* **110**, 2378
- Hodsdon M. E., Ponder J. W. and Cistola D. P. (1996). The NMR solution structure of intestinal fatty acid-binding protein complexed with palmitate: application of a novel distance geometry algorithm. *J. Mol. Biol.* **264**, 585-602
- Hodsdon, M. E. and Cistola, D. P. (1997). Ligand binding alters the backbone mobility of intestinal fatty acid-binding protein as monitored by  $^{15}\text{N}$  NMR relaxation and  $^1\text{H}$  exchange. *Biochemistry* **36**, 2278-2290
- Hohoff, C., Borchers, T., Rüstow, B., Spener, F. and van Tilbeurgh, H. (1999). Expression, purification, and crystal structure of recombinant human epidermal-type fatty acid binding protein. *Biochemistry* **38**, 12229-12239
- Jain, A., Vaidehi, N. and Rodríguez, G. (1993). Fast recursive algorithm for molecular dynamics simulation. *J. Comput. Phys.* **106**, 258-268
- Jaworski, C. and Wistow, G. (1996). LP2, a differentiation-associated lipid-binding protein expressed in bovine lens. *Biochem. J.* **320**, 49-54
- Jeener, J., Meier, B. H., Bachmann, P. and Ernst, R. R. (1979). Investigation of exchange progress by two-dimensional NMR spectroscopy. *J. Chem. Phys.* **71**, 4546-4553
- Johnson, C. E. and Bovey, F. A. (1958). Calculation of nuclear magnetic resonance spectra of aromatic hydrocarbons. *J. Chem. Phys.* **29**, 1012
- Kay, L. E., Torchia, D. A. and Bax, A. (1989). Backbone dynamics of proteins as studied by  $^{15}\text{N}$  inverse detected heteronuclear NMR spectroscopy: application to staphylococcal nuclease. *Biochemistry* **28**, 8972-8979
- Kay, L. E., Keifer, P. and Saarinen, T. (1992). Pure absorption gradient enhanced heteronuclear single quantum correlation spectroscopy with improved sensitivity. *J. Am. Chem. Soc.* **114**, 10663-10665
- Kingma, P. B., Bok, D. and Ong, D. E. (1998). Bovine epidermal fatty acid-binding protein: determination of ligand specificity and cellular localization in retina and testis. *Biochemistry* **37**, 3250-3257



- 
- Kitamura, K., Suzuki, M., Suzuki, A. and Uyemura, K. (1980). The complete amino acid sequence of the P2 protein in bovine peripheral nerve myelin. *FEBS Lett.* **115**, 27-30
- Kraulis, P. J. (1991). MOLSCRIPT: A program to produce both detailed and schematic plots of protein structures. *J. Appl. Crystallogr.* **24**, 946-950
- Krieg, P., Feil, S., Fürstenberger, G. and Bowden, G. T. (1993). Tumor specific over-expression of a novel keratinocyte lipid-binding protein. Identification and characterization of a cloned sequence activated during multistage carcinogenesis in mouse skin. *J. Biol. Chem.* **268**, 17362-17369
- Krishnan, V.V., Sukumar, M., Gierasch, L. M. and Cosman, M. (2000). Dynamics of cellular retinoic acid binding protein I on multiple time scales with implications for ligand binding. *Biochemistry* **39**, 9119-9129
- Laskowski, R. A., MacArthur, M. W., Moss, D. S. and Thornton, J. M. (1993). AQUA and PROCHECK-NMR: Programs for checking the quality of protein structures solved by NMR. *J. Appl. Crystallogr.* **26**, 283-291
- Lassen, D., Lücke, C., Kveder, M., Mesgarzadeh, A., Schmidt, J. M., Specht, B., Lezius, A., Spener, F. and Rüterjans, H. (1995). Three-dimensional structure of bovine heart fatty-acid-binding protein with bound palmitic acid, determined by multidimensional NMR spectroscopy. *Eur. J. Biochem.* **230**, 266-280
- Lipari, G. and Szabo, A. (1982a). Model-free approach to the interpretation of nuclear magnetic resonance relaxation in macromolecules. 1. Theory and range of validity. *J. Am. Chem. Soc.* **104**, 4546-4559
- Lipari, G. and Szabo, A. (1982b). Model-free approach to the interpretation of nuclear magnetic resonance relaxation in macromolecules. 2. Analysis of experimental results. *J. Am. Chem. Soc.* **104**, 4559-4570
- Londrville, R. L. and Sidell, B. D. (1995). Purification and characterization of fatty acid-binding protein from aerobic muscle of the antarctic icefish *Chaenocephalus aceratus*. *J. Exp. Zool.* **273**, 190-203
- Londrville, R. L. and Sidell, B. D. (1996). Cold acclimation increases fatty acid-binding protein concentration in aerobic muscle of striped bass, *Morone saxatilis*. *J. Exp. Zool.* **275**, 36-44
- Lowe, J. B., Boguski, M. S., Sweetser, D. A., Elshourbagy, N. A., Taylor, J. M. and Gordon, J. I. (1985). Human liver fatty acid binding protein. *J. Biol. Chem.* **260**, 3413-3417

- 
- Lu, J., Lin, C.-L., Tang, C., Ponder, J. W., Kao, J. L. F., Cistola, D. P. and Li, E. (1999). The structure and dynamics of rat apo-cellular retinol-binding protein II in solution: comparison with the X-ray structure. *J. Mol. Biol.* **286**, 1179-1195
- Lu, J., Lin, C.-L., Tang, C., Ponder, J. W., Kao, J. L. F., Cistola, D. P. and Li, E. (2000). Binding of retinol induces changes in rat cellular retinol-binding protein II conformation and backbone dynamics. *J. Mol. Biol.* **300**, 619-632
- Lücke, C., Lassen, D., Kreienkamp, H.-J., Spener, F. and Rüterjans, H. (1992). Sequence-specific <sup>1</sup>H-NMR assignment and determination of the secondary structure of bovine heart fatty-acid-binding protein. *Eur. J. Biochem.* **210**, 901-910
- Lücke, C., Zhang, F., Rüterjans, H., Hamilton, J. A. and Sacchettini, J. C. (1996). Flexibility is a likely determinant of binding in the case of ileal lipid binding protein. *Structure* **4**, 785-800
- Lücke, C., Fushman, D., Ludwig, C., Hamilton, J. A., Sacchettini, J. C. and Rüterjans, H. (1999). A comparative study of the backbone dynamics of two closely related lipid binding proteins: Bovine heart fatty acid binding protein and porcine ileal lipid binding protein. *Mol. Cell. Biochem.* **192**, 109-121
- Lücke, C., Rademacher, M., Zimmerman, A. W., van Moerkerk, H. T. B., Veerkamp, J. H. and Rüterjans, H. (2001). Spin-system heterogeneities indicate a selected-fit mechanism in fatty acid binding to heart-type fatty acid-binding protein (H-FABP). *Biochem. J.* **354**, 259-266
- Madsen, P., Rasmussen, H. H., Leffers, H., Honoré, B. and Celis, J.E. (1992). Molecular cloning and expression of a novel keratinocyte protein (psoriasis-associated fatty acid binding protein [PA-FABP]) that is highly upregulated in psoriatic skin and that shares similarity to fatty acid binding proteins. *J. Invest. Dermatol.* **99**, 299-305
- Mandel, A. M., Akke, M. and Palmer, A. G. (1995). Backbone dynamics of *Escherichia coli* ribonuclease HI: Correlations with structure and function in an active enzyme. *J. Mol. Biol.* **246**, 144-163
- Matarese, V., Stone, R. L., Waggoner, D. W. and Bernlohr, D. A. (1989). Intracellular fatty acid trafficking and the role of cytosolic lipid binding proteins. *Prog. Lip. Res.* **28**, 245-272
- Mathiowetz, A., Jain, A., Karasawa, N. and Goddard, W. I. (1994). Protein simulations using techniques suitable for large systems: The cell multipole method for nonbond interactions and the Newton-Euler inverse mass operator for internal coordinate dynamics. *Proteins: Struct. Funct. Genet.* **20**, 227-247

- Medzihradzky, K. F., Gibson, B. W., Kaur, S., Yu, Z. H., Medzihradzky, D., Burlingame, A. L. and Bass, N. M. (1992). The primary structure of fatty acid-binding protein from nurse shark liver. Structural and evolutionary relationship to the mammalian fatty acid-binding protein family. *Eur. J. Biochem.* **203**, 327-339
- Merrit, E. A. and Bacon, D. J. (1997). Raster3D: Photorealistic molecular graphics. *Methods Enzymol.* **277**, 505-524
- Morris, G. A. and Freeman, R. (1979). Enhancement of nuclear magnetic resonance signals by polarisation transfer. *J. Am. Chem. Soc.* **101**, 760-762
- Moser, D., Tendler, M., Griffiths, G. and Klinkert, M. Q. (1991). A 14-kDa *Schistosoma mansoni* polypeptide is homologous to a gene family of fatty acid binding proteins. *J. Biol. Chem.* **266**, 8447-8454
- Neuhaus, D. and Williamson, M. (1989). *The Nuclear Overhauser Effect in Structural and Conformational Analysis*, VCH Publishers, New York
- Nicholls, A., Sharp, K. A. and Honig, B. (1991). Protein folding and association: Insights from the interfacial and thermodynamic properties of hydrocarbons. *Proteins* **11**, 281-296
- Nilsson M. H., Spurr, N. K., Lundvall, J., Rask, L. and Peterson, P. A. (1988). Human cellular retinol-binding protein gene organization and chromosomal location. *Eur. J. Biochem.* **173**, 35-44
- Palmer, A. G., Rance, M. and Wright, P. E. (1991). Intramolecular motions of a zinc finger DNA-binding domain from Xfin characterized by proton-detected natural abundance <sup>13</sup>C heteronuclear NMR spectroscopy. *J. Am. Chem. Soc.* **113**, 4371-4380
- Peeters, R. A., Veerkamp, J. H., van Kessel, G. A., Kanda, T. and Ono, T. (1991). Cloning of the cDNA encoding human skeletal-muscle fatty acid-binding protein, its peptide sequence and chromosomal localisation. *Biochem. J.* **276**, 203-206
- Rademacher, M., Lücke, C. Zimmerman, A. W., Veerkamp, J. H. and Rüterjans, H. (in preparation). Solution structure of fatty acid binding protein from human brain.
- Rasmussen, H. H., van Damme, J., Puype, M., Gesser, B., Celis, J. E. and Vandekerckhove, J. (1992). Microsequences of 145 proteins recorded in the two-dimensional gel protein database of normal human epidermal keratinocytes. *Electrophoresis* **13**, 960-969
- Ross, A. C. (1993). Cellular metabolism and activation of retinoids: roles of cellular retinoid-binding proteins. *FASEB J.* **7**, 317-327
- Sacchettini, J. C., Gordon, J. I. and Banaszak, L. J. (1989). Crystal structure of rat intestinal fatty-acid-binding protein. Refinement and analysis of the *Escherichia coli*-derived protein with bound palmitate. *J. Mol. Biol.* **208**, 327-339

- Sacchettini, J. C. and Gordon, J. I. (1993). Rat intestinal fatty acid binding protein. *J. Biol. Chem.* **268**, 18399-18402
- Scapin, G., Young, A. C., Kromminga, A., Veerkamp, J. H., Gordon, J. I. and Sacchettini, J. C. (1993). High resolution X-ray studies of mammalian intestinal and muscle fatty acid-binding proteins provide an opportunity for defining the chemical nature of fatty acid: protein interactions. *Mol. Cell. Biochem.* **123**, 3-13
- Schaefer, W. H., Kakkad, B., Crow, J. A., Blair, I. A. and Ong, D. E. (1989). Purification, primary structure characterization, and cellular distribution of two forms of cellular retinol-binding protein type II from adult rat small intestine. *J. Biol. Chem.* **264**, 4212-4221
- Schleicher, C. H., Córdoba, O. L., Santomé J. A. and Dell'Angelica, E. C. (1995). Molecular evolution of the multigene family of intracellular lipid binding proteins. *Biochem. Mol. Biol. Int.*, **36**, 1117-1125
- Schleucher, J., Sattler, M. and Griesinger, C. (1993). Coherence selection by gradients without signal attenuation: application to the three-dimensional-HNCO experiment. *Angew. Chem. Int. Ed. Eng.* **32**, 1489-1491
- Schmidt, J. and Rüterjans, H. (1990). Proton detected 2D heteronuclear shift correlation via multiple-quantum coherences of the type I<sub>2</sub>S. *J. Am. Chem. Soc.* **112**, 1279-1280
- Shimizu, F., Watanabe, T. K., Shinomiya, H., Nakamura, Y. and Fujiwara, T. (1997). Isolation and expression of a cDNA for human brain fatty acid-binding protein (B-FABP). *Biochim. Biophys. Acta* **1354**, 24-28
- Siegenthaler, G., Hotz, R., Chatellard-Gruaz, L., Jaconi, S. and Saurat, J.-H. (1993). Characterization and expression of a novel human fatty acid-binding protein: the epidermal type (E-FABP). *Biochem Biophys. Res. Commun.* **190**, 482-487
- Siegenthaler, G., Hotz, R., Chatellard-Gruaz, L., Didierjan, L. and Hellmann, U. (1994). Purification and characterization of the human epidermal fatty acid-binding protein: localization during epidermal cell differentiation *in vivo* and *in vitro*. *Biochem. J.* **302**, 363-371
- Slichter, C. P. (1978). *Principles of magnetic resonance*. Springer-Verlag, Berlin.
- Stone, M. J., Fairbrother, W. J., Palmer, A. G., Reizer, J., Saier, M. H. Jr. and Wright, P. E. (1992). The backbone dynamics of the *Bacillus subtilis* glucose permease IIA domain determined from <sup>15</sup>N NMR relaxation measurements. *Biochemistry* **31**, 4394-4406
- Storch, J. and Thumser, A. E. A. (2000). The fatty acid transport function of fatty acid-binding proteins. *Biochim. Biophys. Acta* **1486**, 28-44

- Studier, F. W., Rosenberg, A. H., Dunn, J. J. and Dubendorff, J. W. (1990). Use of T7 RNA polymerase to direct expression of cloned genes. *Methods Enzymol.* **185**, 60-89
- Sweetser, D. A., Birkenmeier, E. H., Klisak, I. J., Zollman, S., Sparkes, R. S., Mohandas, T., Lusic, A. J. and Gordon, J. I. (1987). The human and rodent intestinal fatty acid binding protein genes. *J. Biol. Chem.* **262**, 16060-16071
- Thompson, J., Winter, N., Terwey, D., Bratt, J. and Banaszak, L. (1997). The crystal structure of the liver fatty acid-binding protein. *J. Biol. Chem.* **272**, 7140-7150
- Tjandra, N., Feler, S. E., Pastor, R. W. and Bax, A. (1995). Rotational diffusion anisotropy of human ubiquitin from  $^{15}\text{N}$  NMR relaxation. *J. Am. Chem. Soc.* **117**, 12562-12566
- Veerkamp, J. H. and Maatman, R. G. H. J. (1995). Cytoplasmic fatty acid-binding proteins: their structure and genes. *Prog. Lip. Res.* **34**, 17-52
- Veerkamp, J. H. and Zimmerman, A. W. (2001). Fatty acid-binding proteins of nervous tissue. *J. Mol. Neurosci.* **16**, 133-142
- Wallach, D. J. (1967). Effect of internal rotation on angular correlation functions. *J. Chem. Phys.* **47**, 5258-5268
- Walz, D. A., Wider, M. D., Snow, J. W., Dass, C. and Desiderio, D. M. (1988). The complete amino acid sequence of porcine gastrotropin, an ileal protein which stimulates gastric acid and pepsinogen. *J. Biol. Chem.* **263**, 14189-14195
- Wang, L., Li, Y., Abildgaard, F., Markley, J. L. and Yan, H. (1998). NMR solution structure of type II human cellular retinoic acid binding protein: implications for ligand binding. *Biochemistry* **37**, 12727-12736
- Watanabe, R., Fujii, H., Odani, S., Sakakibara, J., Yamamoto, A., Ito, M. and Ono, T. (1994). Molecular cloning of a cDNA encoding a novel fatty acid-binding protein from rat skin. *Biochem. Biophys. Res. Commun.* **200**, 253-259
- Watson, P. H., Leygue, E. R. and Murphy, L. C. (1998). Psoriasin (S100A7). *Int. J. Biochem. Cell Biol.*, **30**, 567-571
- Wen, Y., Li, G. W., Chen, P., Wong, E. and Bekhor, I. (1995). Lens epithelial cell mRNA, II. Expression of a mRNA encoding a lipid-binding protein in rat lens epithelial cells. *Gene* **158**, 269-274
- Wittebort, R. J. and Szabo, A. J. (1978). Theory of NMR relaxation in macromolecules: restricted diffusion and jump models for multiple internal rotations in amino acid side chains. *J. Chem. Phys.* **69**, 1722-1736

- 
- Wolfrum, C., Ellinghaus, P., Fobker, M., Seedorf, U., Assmann, G., Borchers, T. and Spener, F. (1999). Phytanic acid is ligand and transcriptional activator of murine liver fatty acid binding protein. *J. Lipid Res.* **40**, 704-714
- Wolfrum, C., Borchers, T., Sacchettini, J. C. and Spener, F. (2000). Binding of fatty acids and peroxisome proliferators to orthologous fatty acid binding proteins from human, murine, and bovine liver. *Biochemistry* **39**, 1469-1474
- Wolfrum, C., Borrmann, C. M., Borchers, T. and Spener, F. (2001). Fatty acids and hypolipidemic drugs regulate peroxisome proliferator-activated receptors  $\alpha$ - and  $\gamma$ -mediated gene expression via liver fatty acid binding protein: A signaling path to the nucleus. *Proc Natl Acad Sci U S A* **98**, 2323-2328
- Wüthrich, K., Billeter, M. and Braun, W. (1983). Pseudo structures for the 20 common amino acids for use in studies of protein conformations by measurements of intramolecular proton-proton distance constraints with nuclear magnetic resonance. *J. Mol. Biol.* **169**, 949-961
- Wüthrich, K. (1986). *NMR of Proteins and Nucleic Acids*, Wiley, New York
- Xu, Z., Bernlohr, D. A. and Banaszak, L. J. (1993). The adipocyte lipid-binding protein at 1.6-Å resolution. *J. Biol. Chem.* **268**, 7874-7884
- Yang, Y., Spitzer, E., Kenney, N., Zschiesche, W., Li, M., Kromminga, A., Müller, T., Spener, F., Lezius, A., Veerkamp, J. H. and Smith, G. H. (1994). Members of the fatty acid binding protein family are differentiation factors for the mammary gland. *J. Cell. Biol.* **127**, 1097-1109
- Zhang F., Lücke C., Baier L. J., Sacchettini J. C. and Hamilton J. A. (1997). Solution structure of human intestinal fatty acid binding protein: implications for ligand entry and exit. *J. Biomol. NMR* **9**, 213-228
- Zimmerman, A. W., van Moerkerk, H. T. B. and Veerkamp, J. H. (2001). Ligand specificity and conformational stability of human fatty acid-binding proteins. *Int. J. Biochem. Cell Biol.* **33**, 865-876

**Appendix A.1 Distance constraints in Å used for the structure calculations of human E-FABP complexed with stearic acid at pH 5.6 and 298 K. The pseudoatoms are used as described in Table 3.2.**

**Upper limit list**

					6 GLN	HE21	6 GLN	HE22	2.5	9 GLY	HA1	10 ARG+	HN	3.0
					6 GLN	HE21	6 GLN	HG1	4.5	9 GLY	HA1	45 ILE	HN	6.0
3 THR	HA	3 THR	HB	3.0	6 GLN	HE21	6 GLN	HG2	4.5	9 GLY	HA2	9 GLY	HA1	2.5
3 THR	HA	4 VAL	HN	4.0	6 GLN	HE22	6 GLN	HB1	4.5	9 GLY	HA2	10 ARG+	HN	3.0
3 THR	HA	89 PHE	HZ	4.0	6 GLN	HE22	6 GLN	HB2	6.0	9 GLY	HA2	133 LYS+	HE1	5.0
3 THR	HB	3 THR	QG2	3.6	6 GLN	HE22	6 GLN	HG1	4.5	9 GLY	HA2	133 LYS+	HE2	5.0
3 THR	HB	4 VAL	HN	3.0	6 GLN	HE22	6 GLN	HG2	4.5	9 GLY	HN	9 GLY	HA1	3.0
3 THR	HB	5 GLN	HN	4.5	6 GLN	HG1	6 GLN	HB2	3.5	9 GLY	HN	9 GLY	HA2	3.5
3 THR	HB	89 PHE	HZ	4.5	6 GLN	HG2	6 GLN	HB1	3.5	9 GLY	HN	10 ARG+	HN	5.0
3 THR	HB	89 PHE	QE	6.7	6 GLN	HG2	6 GLN	HB2	3.5	9 GLY	HN	44 ILE	HA	6.0
3 THR	HN	3 THR	HA	3.0	6 GLN	HG2	6 GLN	HG1	3.5	9 GLY	HN	44 ILE	QG2	5.6
3 THR	HN	3 THR	QG2	5.6	6 GLN	HN	6 GLN	HA	3.0	9 GLY	HN	45 ILE	HB	3.5
3 THR	QG2	4 VAL	HN	6.1	6 GLN	HN	6 GLN	HB1	4.0	9 GLY	HN	45 ILE	HG12	6.0
3 THR	QG2	89 PHE	HZ	7.1	6 GLN	HN	6 GLN	HB2	4.0	9 GLY	HN	45 ILE	HN	3.5
3 THR	QG2	89 PHE	QD	8.3	6 GLN	HN	6 GLN	HG1	4.5	9 GLY	HN	45 ILE	HN	4.5
3 THR	QG2	89 PHE	QE	7.8	6 GLN	HN	6 GLN	HG2	4.5	9 GLY	HN	45 ILE	QG2	5.6
4 VAL	HA	4 VAL	HB	3.0	6 GLN	HN	7 LEU	HN	3.5	9 GLY	HN	46 THR	QG2	7.1
4 VAL	HA	4 VAL	QG1	5.6	6 GLN	HN	8 GLU-	HN	6.0	10 ARG+	HA	11 TRP	HN	2.5
4 VAL	HA	4 VAL	QG2	4.1	7 LEU	HA	7 LEU	HB2	3.5	10 ARG+	HA	45 ILE	HN	4.5
4 VAL	HA	5 GLN	HN	4.5	7 LEU	HA	7 LEU	HG	3.5	10 ARG+	HB1	10 ARG+	HB2	3.5
4 VAL	HA	6 GLN	HN	5.0	7 LEU	HA	7 LEU	QD2	4.1	10 ARG+	HB1	10 ARG+	HG1	3.5
4 VAL	HA	7 LEU	HB1	5.0	7 LEU	HA	8 GLU-	HN	4.0	10 ARG+	HB1	10 ARG+	HG2	3.5
4 VAL	HA	7 LEU	HN	4.5	7 LEU	HA	11 TRP	HE1	4.5	10 ARG+	HD1	10 ARG+	HB1	4.5
4 VAL	HA	7 LEU	QD1	5.1	7 LEU	HA	11 TRP	HH2	4.5	10 ARG+	HD1	10 ARG+	HD2	3.5
4 VAL	HA	7 LEU	QD2	7.1	7 LEU	HA	11 TRP	HZ2	3.0	10 ARG+	HD1	10 ARG+	HG1	4.5
4 VAL	HA	89 PHE	HZ	4.5	7 LEU	HA	111 LEU	QD2	5.1	10 ARG+	HD1	10 ARG+	HG2	3.5
4 VAL	HA	89 PHE	QD	6.2	7 LEU	HB1	7 LEU	QD1	4.1	10 ARG+	HD1	134 VAL	QG1	4.6
4 VAL	HA	89 PHE	QE	5.7	7 LEU	HB1	7 LEU	QD2	5.1	10 ARG+	HD1	134 VAL	QG2	5.6
4 VAL	HB	4 VAL	QG1	4.1	7 LEU	HB1	8 GLU-	HN	4.5	10 ARG+	HD2	10 ARG+	HB1	4.5
4 VAL	HB	4 VAL	QG2	4.1	7 LEU	HB1	45 ILE	QG2	7.1	10 ARG+	HD2	10 ARG+	HG1	4.5
4 VAL	HB	89 PHE	HB1	4.5	7 LEU	HB1	116 LEU	QD1	7.1	10 ARG+	HD2	10 ARG+	HG2	3.5
4 VAL	HB	89 PHE	HB2	5.0	7 LEU	HB2	7 LEU	HB1	3.5	10 ARG+	HD2	134 VAL	HB	5.0
4 VAL	HB	89 PHE	QD	5.7	7 LEU	HB2	7 LEU	QD2	5.1	10 ARG+	HD2	134 VAL	QG2	5.6
4 VAL	HN	4 VAL	HA	3.5	7 LEU	HB2	45 ILE	QD1	5.1	10 ARG+	HE	10 ARG+	HB1	4.5
4 VAL	HN	4 VAL	HB	3.5	7 LEU	HB2	116 LEU	QD1	7.1	10 ARG+	HE	10 ARG+	HD1	4.5
4 VAL	HN	4 VAL	QG1	4.6	7 LEU	HG	7 LEU	QD1	4.1	10 ARG+	HE	10 ARG+	HD2	3.5
4 VAL	HN	4 VAL	QG2	6.1	7 LEU	HG	7 LEU	QD2	4.1	10 ARG+	HE	10 ARG+	HG1	4.5
4 VAL	HN	89 PHE	HZ	6.0	7 LEU	HG	45 ILE	QG2	7.1	10 ARG+	HE	10 ARG+	HG2	4.5
4 VAL	HN	89 PHE	QD	7.2	7 LEU	HN	7 LEU	HA	4.5	10 ARG+	HE	44 ILE	QD1	5.6
4 VAL	HN	89 PHE	QE	6.7	7 LEU	HN	7 LEU	HB1	4.0	10 ARG+	HE	44 ILE	QG2	6.1
4 VAL	QG1	5 GLN	HN	5.1	7 LEU	HN	7 LEU	HB2	4.0	10 ARG+	HG1	10 ARG+	HG2	2.5
4 VAL	QG1	89 PHE	HB1	7.1	7 LEU	HN	7 LEU	HG	4.5	10 ARG+	HG1	11 TRP	HN	4.5
4 VAL	QG1	89 PHE	HB2	7.1	7 LEU	HN	7 LEU	QD1	5.6	10 ARG+	HG1	134 VAL	HB	4.5
4 VAL	QG2	4 VAL	QG1	5.2	7 LEU	HN	7 LEU	QD2	5.6	10 ARG+	HG2	11 TRP	HN	4.5
4 VAL	QG2	5 GLN	HN	6.1	7 LEU	HN	8 GLU-	HN	3.0	10 ARG+	HG2	42 ASP-	HA	5.0
4 VAL	QG2	7 LEU	HG	5.6	7 LEU	QD1	7 LEU	QD2	4.7	10 ARG+	HG2	134 VAL	HB	4.5
4 VAL	QG2	7 LEU	QD1	5.7	7 LEU	QD1	45 ILE	QG2	6.7	10 ARG+	HG2	134 VAL	QG2	5.6
4 VAL	QG2	52 LEU	QDQ	6.9	7 LEU	QD1	89 PHE	QE	6.3	10 ARG+	HN	10 ARG+	HA	3.0
4 VAL	QG2	89 PHE	HB1	5.6	7 LEU	QD1	93 ALA	HA	5.6	10 ARG+	HN	10 ARG+	HG1	6.0
4 VAL	QG2	89 PHE	HB2	7.1	7 LEU	QD1	94 LEU	HA	6.1	10 ARG+	HN	11 TRP	HN	6.0
4 VAL	QG2	89 PHE	QD	7.8	7 LEU	QD1	94 LEU	HB1	4.6	11 TRP	N	43 CYS	O	3.2
4 VAL	QG2	89 PHE	QE	8.3	7 LEU	QD1	94 LEU	HN	4.6	11 TRP	HA	11 TRP	HB1	4.5
4 VAL	QG2	94 LEU	QD1	6.7	7 LEU	QD1	109 ARG+	HB2	5.1	11 TRP	HA	11 TRP	HB2	4.5
5 GLN	HA	5 GLN	HB1	3.5	7 LEU	QD1	109 ARG+	HD2	6.1	11 TRP	HA	12 ARG+	HN	2.5
5 GLN	HA	5 GLN	HB2	3.5	7 LEU	QD1	116 LEU	QD1	6.2	11 TRP	HA	131 TYR	HB1	6.0
5 GLN	HA	5 GLN	HG1	3.5	7 LEU	QD2	11 TRP	HZ2	7.1	11 TRP	HA	131 TYR	QD	6.7
5 GLN	HA	5 GLN	HG2	3.5	7 LEU	QD2	89 PHE	HZ	7.1	11 TRP	HA	133 LYS+	HA	3.5
5 GLN	HA	6 GLN	HN	4.5	7 LEU	QD2	89 PHE	QE	7.3	11 TRP	HA	134 VAL	HN	3.5
5 GLN	HA	7 LEU	HN	6.0	7 LEU	QD2	94 LEU	HN	6.1	11 TRP	HB1	11 TRP	HB2	3.5
5 GLN	HA	8 GLU-	HG1	5.0	7 LEU	QD2	109 ARG+	HB1	7.1	11 TRP	HB1	12 ARG+	HN	4.5
5 GLN	HA	8 GLU-	HG2	4.5	7 LEU	QD2	111 LEU	HA	6.6	11 TRP	HB1	43 CYS	HB2	6.0
5 GLN	HB1	6 GLN	HN	5.0	7 LEU	QD2	111 LEU	HB1	6.1	11 TRP	HB2	12 ARG+	HN	6.0
5 GLN	HE21	5 GLN	HB2	3.5	7 LEU	QD2	111 LEU	HG	5.1	11 TRP	HB2	43 CYS	HN	6.0
5 GLN	HE21	5 GLN	HE22	2.5	7 LEU	QD2	111 LEU	HN	4.6	11 TRP	HB2	116 LEU	QD2	5.6
5 GLN	HE21	5 GLN	HG1	4.0	7 LEU	QD2	111 LEU	QD2	5.2	11 TRP	HB2	131 TYR	QD	6.2
5 GLN	HE21	5 GLN	HG2	4.0	7 LEU	QD2	116 LEU	HG	7.1	11 TRP	HB2	131 TYR	QE	6.7
5 GLN	HE22	5 GLN	HG1	5.0	7 LEU	QD2	116 LEU	QD1	5.2	11 TRP	HD1	11 TRP	HB1	4.5
5 GLN	HE22	5 GLN	HG2	4.5	8 GLU-	HA	8 GLU-	HB1	3.5	11 TRP	HD1	11 TRP	HB2	4.0
5 GLN	HG1	5 GLN	HB1	3.5	8 GLU-	HA	8 GLU-	HB2	3.5	11 TRP	HD1	43 CYS	HB2	6.0
5 GLN	HG1	5 GLN	HB2	3.5	8 GLU-	HA	8 GLU-	HG1	4.5	11 TRP	HD1	43 CYS	HN	6.0
5 GLN	HG1	5 GLN	HG2	2.5	8 GLU-	HA	8 GLU-	HG2	4.5	11 TRP	HD1	44 ILE	HA	4.0
5 GLN	HG2	5 GLN	HB2	3.5	8 GLU-	HA	9 GLY	HN	2.5	11 TRP	HD1	45 ILE	HB	4.5
5 GLN	HG2	6 GLN	HN	6.0	8 GLU-	HA	45 ILE	HN	6.0	11 TRP	HD1	45 ILE	HG12	4.5
5 GLN	HN	5 GLN	HA	3.5	8 GLU-	HA	45 ILE	QD1	7.1	11 TRP	HD1	45 ILE	HN	3.5
5 GLN	HN	5 GLN	HB1	3.5	8 GLU-	HA	45 ILE	QG2	5.1	11 TRP	HD1	45 ILE	QD1	4.6
5 GLN	HN	5 GLN	HB2	3.5	8 GLU-	HB1	8 GLU-	HB2	2.5	11 TRP	HE1	11 TRP	HB2	6.0
5 GLN	HN	5 GLN	HE21	5.0	8 GLU-	HB1	8 GLU-	HG1	3.5	11 TRP	HE1	11 TRP	HD1	3.0
5 GLN	HN	5 GLN	HE22	5.0	8 GLU-	HG1	9 GLY	HN	5.0	11 TRP	HE1	11 TRP	HH2	5.0
5 GLN	HN	5 GLN	HG1	5.0	8 GLU-	HG1	47 CYS	HN	4.5	11 TRP	HE1	11 TRP	HN	5.5
5 GLN	HN	5 GLN	HG2	5.0	8 GLU-	HG2	8 GLU-	HB1	3.5	11 TRP	HE1	11 TRP	HZ2	3.0
6 GLN	HA	6 GLN	HN	3.5	8 GLU-	HG2	8 GLU-	HB2	3.5	11 TRP	HE1	45 ILE	HB	3.5
6 GLN	HA	6 GLN	HB1	4.0	8 GLU-	HG2	8 GLU-	HG1	2.5	11 TRP	HE1	45 ILE	HN	4.5
6 GLN	HA	6 GLN	HB2	3.5	8 GLU-	HG2	9 GLY	HN	6.0	11 TRP	HE1	45 ILE	HN	6.0
6 GLN	HA	6 GLN	HG1	3.5	8 GLU-	HG2	47 CYS	HN	6.0	11 TRP	HE1	45 ILE	QD1	4.6
6 GLN	HA	6 GLN	HG2	3.5	8 GLU-	HN	8 GLU-	HA	3.5	11 TRP	HE1	45 ILE	QG2	6.1
6 GLN	HA	7 LEU	HN	4.0	8 GLU-	HN	8 GLU-	HB1	4.0	11 TRP	HE1	116 LEU	QD2	5.6
6 GLN	HA	8 GLU-	HN	4.5	8 GLU-	HN	8 GLU-	HB2	4.5	11 TRP	HE3	11 TRP	HA	4.5
6 GLN	HB1	6 GLN	HB2	3.0	8 GLU-	HN	8 GLU-	HG1	6.0	11 TRP	HE3	11 TRP	HB1	4.5
6 GLN	HB1	7 LEU	HN	5.0	8 GLU-	HN	8 GLU-	HG2	4.5	11 TRP	HE3	11 TRP	HB2	4.5
6 GLN	HB2	7 LEU	HN	5.0	8 GLU-	HN	9 GLY	HN	5.0	11 TRP	HE3	11 TRP	HH2	4.5
6 GLN	HE21	6 GLN	HB1	6.0	8 GLU-	HN	45 ILE	QG2	7.1	11 TRP	HE3	12 ARG+	HN	4.5

11 TRP	HE3	116 LEU	HB1	4.5	13 LEU	HB2	13 LEU	QD1	4.6	17 LYS+	HG2	18 GLY	HN	6.0
11 TRP	HE3	116 LEU	HB2	6.0	13 LEU	HB2	14 VAL	HN	6.0	17 LYS+	HN	17 LYS+	HA	4.5
11 TRP	HE3	116 LEU	HN	4.5	13 LEU	HB2	131 TYR	QE	8.2	17 LYS+	HN	17 LYS+	HB1	4.0
11 TRP	HE3	116 LEU	QD1	7.1	13 LEU	HG	13 LEU	QD1	3.6	17 LYS+	HN	17 LYS+	HB2	4.5
11 TRP	HE3	116 LEU	QD2	5.6	13 LEU	HG	13 LEU	QD2	3.6	17 LYS+	HN	17 LYS+	HG1	5.0
11 TRP	HE3	131 TYR	HN	6.0	13 LEU	HG	14 VAL	HN	3.5	17 LYS+	HN	17 LYS+	HG2	6.0
11 TRP	HE3	132 GLU-	HN	6.0	13 LEU	HN	13 LEU	HA	4.5	17 LYS+	HN	19 PHE	HN	6.0
11 TRP	HE3	133 LYS+	HA	3.5	13 LEU	HN	13 LEU	HB1	4.5	17 LYS+	HN	127 CYSS	HA	6.0
11 TRP	HE3	133 LYS+	HN	3.5	13 LEU	HN	13 LEU	HB2	4.5	17 LYS+	HN	128 THR	HB	4.5
11 TRP	HE3	134 VAL	HN	6.0	13 LEU	HN	13 LEU	HG	6.0	17 LYS+	HN	130 ILE	HN	6.0
11 TRP	HH2	111 LEU	QD1	3.6	13 LEU	HN	13 LEU	QD1	7.1	17 LYS+	QE	17 LYS+	HD2	3.4
11 TRP	HH2	111 LEU	QD2	3.6	13 LEU	HN	13 LEU	QD2	6.1	17 LYS+	QE	17 LYS+	HG1	4.9
11 TRP	HH2	116 LEU	HN	6.0	13 LEU	HN	14 VAL	HN	6.0	17 LYS+	QE	17 LYS+	HG2	3.9
11 TRP	HH2	133 LYS+	HD1	4.5	13 LEU	HN	42 ASP-	HA	6.0	17 LYS+	QE	128 THR	HB	6.9
11 TRP	HH2	133 LYS+	HE2	5.0	13 LEU	HN	131 TYR	QD	6.7	18 GLY	HA1	127 CYSS	HA	5.0
11 TRP	HN	11 TRP	HA	3.0	13 LEU	HN	131 TYR	QE	8.2	18 GLY	HA2	18 GLY	HA1	2.5
11 TRP	HN	11 TRP	HB1	6.0	13 LEU	QD1	14 VAL	HN	4.6	18 GLY	HA2	19 PHE	HN	6.0
11 TRP	HN	11 TRP	HB2	4.5	13 LEU	QD1	16 SER	HB2	5.6	18 GLY	HA2	127 CYSS	HA	4.0
11 TRP	HN	11 TRP	HD1	3.5	13 LEU	QD1	16 SER	HN	7.1	18 GLY	HN	18 GLY	HA1	3.0
11 TRP	HN	12 ARG+	HN	6.0	13 LEU	QD1	41 PRO	HG1	7.1	18 GLY	HN	18 GLY	HA2	3.5
11 TRP	HN	43 CYS	HB1	6.0	13 LEU	QD1	129 ARG+	HB1	5.6	18 GLY	HN	19 PHE	HN	4.0
11 TRP	HN	43 CYS	HN	4.5	13 LEU	QD1	129 ARG+	HB2	5.6	19 PHE	HA	19 PHE	HB1	3.5
11 TRP	HN	43 CYS	O	2.2	13 LEU	QD1	130 ILE	HN	4.6	19 PHE	HA	19 PHE	HB2	4.5
11 TRP	HN	44 ILE	QG2	7.1	13 LEU	QD1	131 TYR	QD	6.8	19 PHE	HA	20 ASP-	HN	4.5
11 TRP	HN	45 ILE	HN	6.0	13 LEU	QD1	131 TYR	QE	6.8	19 PHE	HA	22 TYR	HB2	3.5
11 TRP	HN	134 VAL	QG2	7.1	13 LEU	QD2	13 LEU	QD1	4.7	19 PHE	HA	22 TYR	HN	4.5
11 TRP	HZ2	11 TRP	HH2	2.5	13 LEU	QD2	16 SER	HB2	5.6	19 PHE	HA	22 TYR	QD	6.7
11 TRP	HZ2	45 ILE	QD1	7.1	13 LEU	QD2	41 PRO	HD2	7.1	19 PHE	HA	127 CYSS	HA	4.5
11 TRP	HZ2	111 LEU	HG	4.5	13 LEU	QD2	131 TYR	QE	8.3	19 PHE	HA	127 CYSS	HB1	6.0
11 TRP	HZ2	111 LEU	QD1	5.6	14 VAL	N	130 ILE	O	3.2	19 PHE	HB1	20 ASP-	HN	6.0
11 TRP	HZ2	111 LEU	QD2	4.1	14 VAL	HA	14 VAL	HB	2.5	19 PHE	HB1	127 CYSS	HB1	6.0
11 TRP	HZ2	116 LEU	HB1	6.0	14 VAL	HA	14 VAL	QG1	3.6	19 PHE	HB2	19 PHE	HB1	3.5
11 TRP	HZ2	116 LEU	QD1	5.6	14 VAL	HA	14 VAL	QG2	4.1	19 PHE	HB2	20 ASP-	HN	4.5
11 TRP	HZ2	116 LEU	QD2	6.1	14 VAL	HA	15 ASP-	HN	4.0	19 PHE	HN	19 PHE	HA	4.5
11 TRP	HZ2	133 LYS+	HB1	6.0	14 VAL	HA	131 TYR	HA	6.0	19 PHE	HN	19 PHE	HB1	4.5
11 TRP	HZ3	116 LEU	HN	6.0	14 VAL	HB	14 VAL	QG1	3.6	19 PHE	HN	19 PHE	HB2	4.0
11 TRP	HZ3	133 LYS+	HA	6.0	14 VAL	HB	14 VAL	QG2	3.6	19 PHE	HN	19 PHE	QD	6.7
12 ARG+	N	132 GLU-	O	3.2	14 VAL	HB	15 ASP-	HN	4.5	19 PHE	HN	20 ASP-	HN	3.5
12 ARG+	HA	12 ARG+	HB1	3.5	14 VAL	HN	14 VAL	HA	3.5	19 PHE	HZ	22 TYR	QD	7.2
12 ARG+	HA	12 ARG+	HB2	4.5	14 VAL	HN	14 VAL	HB	4.5	19 PHE	HZ	22 TYR	QE	7.7
12 ARG+	HA	12 ARG+	QG	5.4	14 VAL	HN	14 VAL	QG1	5.1	19 PHE	HZ	36 GLY	HA2	6.0
12 ARG+	HA	13 LEU	HN	3.0	14 VAL	HN	14 VAL	QG2	3.6	19 PHE	QD	19 PHE	HA	4.7
12 ARG+	HA	42 ASP-	HA	4.5	14 VAL	HN	15 ASP-	HN	2.5	19 PHE	QD	19 PHE	HB1	5.2
12 ARG+	HA	42 ASP-	HN	6.0	14 VAL	HN	130 ILE	HB	4.5	19 PHE	QD	19 PHE	HB2	5.7
12 ARG+	HA	43 CYS	HN	4.0	14 VAL	HN	130 ILE	HN	4.5	19 PHE	QD	19 PHE	HZ	6.7
12 ARG+	HA	134 VAL	QG2	6.1	14 VAL	HN	130 ILE	HN	6.0	19 PHE	QD	20 ASP-	HN	8.2
12 ARG+	HB1	13 LEU	HN	4.5	14 VAL	HN	130 ILE	O	2.2	19 PHE	QD	22 TYR	HB2	6.7
12 ARG+	HB1	42 ASP-	HA	4.5	14 VAL	HN	131 TYR	HA	3.5	19 PHE	QD	22 TYR	HN	8.2
12 ARG+	HB1	132 GLU-	HG2	6.0	14 VAL	HN	131 TYR	QD	8.2	19 PHE	QD	22 TYR	QD	7.9
12 ARG+	HB1	132 GLU-	HN	6.0	14 VAL	HN	132 GLU-	HN	6.0	19 PHE	QD	22 TYR	QE1	0.4
12 ARG+	HB2	132 GLU-	HN	6.0	14 VAL	QG1	14 VAL	QG2	4.7	19 PHE	QD	23 MET	HN	8.2
12 ARG+	HD1	12 ARG+	HB1	3.5	14 VAL	QG1	131 TYR	HA	5.6	19 PHE	QD	37 ALA	HA	5.7
12 ARG+	HD1	12 ARG+	HB2	3.5	14 VAL	QG1	132 GLU-	HA	7.1	19 PHE	QD	37 ALA	HN	8.2
12 ARG+	HD1	13 LEU	HN	5.5	14 VAL	QG1	132 GLU-	HG1	5.1	19 PHE	QD	127 CYSS	HB1	6.7
12 ARG+	HD1	14 VAL	QG1	5.1	14 VAL	QG1	132 GLU-	HG2	7.1	19 PHE	QD	127 CYSS	HB2	6.7
12 ARG+	HD2	12 ARG+	HB1	4.5	14 VAL	QG1	132 GLU-	HN	4.6	19 PHE	QE	22 TYR	QD1	0.4
12 ARG+	HD2	12 ARG+	HB2	4.5	14 VAL	QG1	132 GLU-	QB	5.5	19 PHE	QE	23 MET	HG2	8.2
12 ARG+	HD2	12 ARG+	HD1	2.5	14 VAL	QG2	15 ASP-	HN	4.1	20 ASP-	HA	20 ASP-	HB1	3.5
12 ARG+	HD2	12 ARG+	QD	4.4	14 VAL	QG2	115 LYS+	HD2	5.6	20 ASP-	HA	20 ASP-	HB2	3.0
12 ARG+	HD2	14 VAL	QG1	5.6	14 VAL	QG2	130 ILE	HN	5.6	20 ASP-	HA	21 GLU-	HN	4.0
12 ARG+	HE	12 ARG+	HB1	4.5	14 VAL	QG2	131 TYR	HA	4.1	20 ASP-	HA	23 MET	HB1	5.0
12 ARG+	HE	12 ARG+	HB2	4.5	14 VAL	QG2	132 GLU-	HA	7.1	20 ASP-	HA	23 MET	HB2	5.0
12 ARG+	HE	12 ARG+	HD1	4.5	15 ASP-	HA	15 ASP-	HB1	3.0	20 ASP-	HA	23 MET	HN	4.0
12 ARG+	HE	12 ARG+	HD2	3.5	15 ASP-	HA	15 ASP-	HB2	3.5	20 ASP-	HA	23 MET	QE	4.6
12 ARG+	HE	12 ARG+	QG	4.4	15 ASP-	HA	16 SER	HN	2.5	20 ASP-	HA	33 ARG+	HE	6.0
12 ARG+	HE	134 VAL	QG2	5.6	15 ASP-	HB1	16 SER	HN	4.5	20 ASP-	HB1	20 ASP-	HB2	2.5
12 ARG+	HN	12 ARG+	HA	3.5	15 ASP-	HB1	130 ILE	HB	4.5	20 ASP-	HB1	21 GLU-	HN	3.5
12 ARG+	HN	12 ARG+	HB1	4.5	15 ASP-	HB1	130 ILE	HG11	6.0	20 ASP-	HB2	21 GLU-	HN	4.5
12 ARG+	HN	12 ARG+	HB2	6.0	15 ASP-	HB2	15 ASP-	HB1	2.5	20 ASP-	HB2	23 MET	QE	7.1
12 ARG+	HN	12 ARG+	HD1	6.0	15 ASP-	HB2	16 SER	HN	4.5	20 ASP-	HN	20 ASP-	HA	3.5
12 ARG+	HN	12 ARG+	HD2	6.0	15 ASP-	HB2	130 ILE	HN	4.5	20 ASP-	HN	20 ASP-	HB1	3.5
12 ARG+	HN	12 ARG+	QG	5.4	15 ASP-	HN	15 ASP-	HA	3.5	20 ASP-	HN	20 ASP-	HB2	3.5
12 ARG+	HN	131 TYR	HA	6.0	15 ASP-	HN	15 ASP-	HB1	4.0	20 ASP-	HN	21 GLU-	HN	3.5
12 ARG+	HN	131 TYR	HB1	6.0	15 ASP-	HN	15 ASP-	HB2	4.0	21 GLU-	HA	21 GLU-	HB1	3.5
12 ARG+	HN	131 TYR	QD	6.7	15 ASP-	HN	16 SER	HN	5.0	21 GLU-	HA	21 GLU-	HB2	3.0
12 ARG+	HN	132 GLU-	HN	3.5	15 ASP-	HN	129 ARG+	HA	5.0	21 GLU-	HA	21 GLU-	HG1	4.0
12 ARG+	HN	132 GLU-	HN	3.5	15 ASP-	HN	130 ILE	HA	6.0	21 GLU-	HA	21 GLU-	HG2	4.5
12 ARG+	HN	132 GLU-	O	2.2	15 ASP-	HN	130 ILE	HB	3.5	21 GLU-	HA	22 TYR	HN	4.5
12 ARG+	HN	132 GLU-	QB	6.9	15 ASP-	HN	130 ILE	HN	3.5	21 GLU-	HA	24 LYS+	HB1	5.0
12 ARG+	HN	133 LYS+	HA	4.5	15 ASP-	HN	130 ILE	HN	3.5	21 GLU-	HA	24 LYS+	HB2	5.0
12 ARG+	HN	134 VAL	HN	5.0	15 ASP-	HN	131 TYR	HA	5.0	21 GLU-	HA	24 LYS+	QD	4.0
12 ARG+	HN	134 VAL	HN	6.0	16 SER	HA	16 SER	HB1	3.5	21 GLU-	HA	24 LYS+	HN	5.4
12 ARG+	HN	134 VAL	QG2	4.6	16 SER	HA	16 SER	HB2	4.5	21 GLU-	HA	24 LYS+	QE	5.4
12 ARG+	QG	12 ARG+	HB2	4.4	16 SER	HA	17 LYS+	HN	2.5	21 GLU-	HA	24 LYS+	QG	4.9
12 ARG+	QG	132 GLU-	HG1	6.9	16 SER	HB1	16 SER	HB2	3.5	21 GLU-	HB1	21 GLU-	HG2	3.0
12 ARG+	QG	132 GLU-	HG2	5.4	16 SER	HB1	17 LYS+	HN	4.5	21 GLU-	HB1	22 TYR	HN	5.0
12 ARG+	QG	132 GLU-	HN	5.4	16 SER	HB2	19 PHE	HB2	6.0	21 GLU-	HB2	21 GLU-	HB1	4.5
12 ARG+	QG	134 VAL	QG2	5.6	16 SER	HN	16 SER	HA	3.5	21 GLU-	HB2	21 GLU-	HG2	3.5
13 LEU	HA	13 LEU	HB1	6.0	16 SER	HN	16 SER	HB1	4.5	21 GLU-	HB2	22 TYR	HN	6.0
13 LEU	HA	13 LEU	HB2	4.5	16 SER	HN	16 SER	HB2	4.0	21 GLU-	HB2	24 LYS+	QD	6.9
13 LEU	HA	13 LEU	HG	4.5	16 SER	HN	17 LYS+	HN	6.0	21 GLU-	HG1	21 GLU-	HB2	3.0
13 LEU	HA	14 VAL	HN	2.5	17 LYS+	HA	17 LYS+	HB1	3.5	21 GLU-	HG1	21 GLU-	HG2	2.5
13 LEU	HA	130 ILE	HN	6.0	17 LYS+	HA	17 LYS+	HB2	3.5	21 GLU-	HG1	22 TYR	HN	6.0
13 LEU	HA	131 TYR	HA	4.5	17 LYS+	HA	17 LYS+	HG1	4.5	21 GLU-	HG2	22 TYR	HN	6.0
13 LEU	HA	131 TYR	HB1	6.0	17 LYS+	HA	17 LYS+	HG2	4.0	21 GLU-	HN	21 GLU-	HA	3.5
13 LEU	HA	131 TYR	QE	6.7	17 LYS+	HA	18 GLY	HN	2.5	21 GLU-	HN	21 GLU-	HB1	4.0
13 LEU	HA	132 GLU-	HN	4.5	17 LYS+	HA	19 PHE	HN	4.5	21 GLU-	HN	21 GLU-	HB2	4.5
13 LEU	HB1	13 LEU	HB2	2.5	17 LYS+	HB1	17 LYS+	HD2	3.5	21 GLU-	HN	21 GLU-	HG2	3.5
13 LEU	HB1	13 LEU	HG	3.5	17 LYS+	HB1	128 THR	HN	6.0	21 GLU-	HN	22 TYR	HN	4.5
13 LEU	HB1	13 LEU	QD1	5.6	17 LYS+	HB2	17 LYS+	HG1	3.0	21 GLU-	HN	23 MET	HN	6.0
13 LEU	HB1	13 LEU	QD2	3.6	17 LYS+	HB2	128 THR	HB	6.0	22 TYR	HA	22 TYR	HB2	3.5
13 LEU	HB1	14 VAL	HN	4.5	17 LYS+	HD2	17 LYS+	HG1						



22 TYR	HA	125 VAL	QG1	4.1	26 LEU	HA	26 LEU	HG	3.5	30 ILE	QG2	31 ALA	HN	7.1
22 TYR	HB1	23 MET	HN	4.5	26 LEU	HA	26 LEU	QD1	5.6	30 ILE	QG2	33 ARG+	HB1	5.6
22 TYR	HB2	23 MET	HN	3.5	26 LEU	HA	26 LEU	QD2	3.6	31 ALA	HA	31 ALA	QB	3.6
22 TYR	HN	22 TYR	HA	3.0	26 LEU	HA	27 GLY	HN	4.5	31 ALA	HA	32 LEU	HN	4.0
22 TYR	HN	22 TYR	HB1	3.5	26 LEU	HA	100 TRP	HZ2	4.0	31 ALA	HA	34 LYS+	HB1	4.5
22 TYR	HN	22 TYR	HB2	3.5	26 LEU	HA	122 MET	QE	4.6	31 ALA	HA	34 LYS+	HB2	3.5
22 TYR	HN	22 TYR	QD	7.2	26 LEU	HB1	28 VAL	HN	4.5	31 ALA	HA	34 LYS+	HN	4.5
22 TYR	HN	23 MET	HN	3.5	26 LEU	HB2	27 GLY	HN	3.5	31 ALA	HN	31 ALA	HA	3.0
22 TYR	QD	22 TYR	HA	4.7	26 LEU	HG	26 LEU	QD1	4.1	31 ALA	HN	31 ALA	QB	3.6
22 TYR	QD	22 TYR	QE	6.9	26 LEU	HG	26 LEU	QD2	4.1	31 ALA	HN	32 LEU	HN	3.0
22 TYR	QD	23 MET	HN	6.7	26 LEU	HG	27 GLY	HN	6.0	31 ALA	HN	33 ARG+	HN	4.5
22 TYR	QD	25 GLU-	HB2	7.2	26 LEU	HN	26 LEU	HA	3.5	31 ALA	HN	33 ARG+	HN	4.5
22 TYR	QD	105 SER	HG	8.2	26 LEU	HN	26 LEU	HB2	4.5	31 ALA	HN	34 LYS+	HN	6.0
22 TYR	QD	122 MET	HB1	6.7	26 LEU	HN	26 LEU	HG	3.5	31 ALA	QB	32 LEU	HN	3.6
22 TYR	QD	122 MET	HN	5.7	26 LEU	HN	26 LEU	QD1	5.6	31 ALA	QB	33 ARG+	HN	6.1
22 TYR	QD	125 VAL	HB	6.7	26 LEU	HN	26 LEU	QD2	5.1	32 LEU	HA	32 LEU	HB1	3.0
22 TYR	QD	125 VAL	QG1	6.8	26 LEU	HN	27 GLY	HN	3.0	32 LEU	HA	32 LEU	HG	3.5
22 TYR	QD	126 THR	HA	8.2	26 LEU	HN	28 VAL	QG2	6.1	32 LEU	HA	32 LEU	QD1	5.6
22 TYR	QE	22 TYR	HA	8.2	26 LEU	QD1	27 GLY	HN	7.1	32 LEU	HA	32 LEU	QD2	3.6
22 TYR	QE	22 TYR	HB2	8.2	26 LEU	QD1	28 VAL	HN	7.1	32 LEU	HA	33 ARG+	HN	4.0
22 TYR	QE	105 SER	HA	6.7	26 LEU	QD1	28 VAL	QG2	5.7	32 LEU	HA	35 MET	HB1	4.5
22 TYR	QE	105 SER	HB1	6.7	26 LEU	QD1	81 ARG+	HE	5.1	32 LEU	HA	35 MET	HG1	6.0
22 TYR	QE	105 SER	HB2	6.7	26 LEU	QD1	100 TRP	HH2	7.1	32 LEU	HA	35 MET	QE	4.6
22 TYR	QE	105 SER	HG	5.7	26 LEU	QD1	105 SER	HG	7.1	32 LEU	HB1	32 LEU	QD1	4.1
22 TYR	QE	106 THR	HN	8.2	26 LEU	QD2	26 LEU	QD1	4.7	32 LEU	HB1	32 LEU	QD2	4.1
22 TYR	QE	107 ILE	QD1	8.3	26 LEU	QD2	27 GLY	HN	7.1	32 LEU	HB1	33 ARG+	HN	4.0
22 TYR	QE	120 CYSS	HB1	5.7	26 LEU	QD2	81 ARG+	HD1	7.1	32 LEU	HB1	34 LYS+	HN	6.0
22 TYR	QE	121 VAL	HN	6.7	26 LEU	QD2	81 ARG+	HD2	5.6	32 LEU	HG	32 LEU	QD2	3.6
22 TYR	QE	121 VAL	QG1	9.3	26 LEU	QD2	81 ARG+	HE	5.6	32 LEU	HN	32 LEU	HA	3.5
22 TYR	QE	121 VAL	QG2	9.3	26 LEU	QD2	100 TRP	HE1	7.1	32 LEU	HN	32 LEU	HB1	4.0
22 TYR	QE	122 MET	HB1	5.7	26 LEU	QD2	100 TRP	HH2	4.1	32 LEU	HN	32 LEU	HG	4.5
22 TYR	QE	122 MET	HG1	7.2	26 LEU	QD2	100 TRP	HZ2	4.6	32 LEU	HN	32 LEU	QD2	5.6
22 TYR	QE	122 MET	HN	6.7	26 LEU	QD2	105 SER	HB1	5.1	32 LEU	HN	33 ARG+	HN	3.0
23 MET	HA	23 MET	HB1	3.5	26 LEU	QD2	105 SER	HB2	5.6	32 LEU	HN	33 ARG+	HN	3.5
23 MET	HA	23 MET	HB2	4.5	26 LEU	QD2	105 SER	HG	7.1	32 LEU	HN	34 LYS+	HN	4.5
23 MET	HA	23 MET	HG1	4.0	26 LEU	QD2	122 MET	HB1	5.6	32 LEU	QD1	32 LEU	QD2	4.7
23 MET	HA	24 LYS+	HN	4.5	26 LEU	QD2	122 MET	QE	5.7	32 LEU	QD1	35 MET	QE	8.2
23 MET	HA	27 GLY	HN	6.0	27 GLY	HA1	27 GLY	HA2	2.5	32 LEU	QD1	79 ASP-	HA	3.6
23 MET	HA	28 VAL	QG2	7.1	27 GLY	HA1	28 VAL	HN	3.5	32 LEU	QD2	35 MET	HB1	6.1
23 MET	HA	33 ARG+	QG	6.9	27 GLY	HA2	28 VAL	HN	3.5	32 LEU	QD2	35 MET	QE	5.2
23 MET	HB1	23 MET	HB2	2.5	27 GLY	HN	27 GLY	HA1	3.0	32 LEU	QD2	79 ASP-	HA	4.6
23 MET	HB1	28 VAL	QG1	5.1	27 GLY	HN	27 GLY	HA2	3.0	33 ARG+	HA	36 GLY	HN	4.5
23 MET	HB1	28 VAL	QG2	4.6	27 GLY	HN	28 VAL	HN	2.5	33 ARG+	HA	37 ALA	HN	4.5
23 MET	HB1	33 ARG+	QG	3.9	28 VAL	HA	28 VAL	QG1	4.1	33 ARG+	HB1	34 LYS+	HN	3.5
23 MET	HG1	23 MET	HB1	6.0	28 VAL	HA	28 VAL	QG2	4.1	33 ARG+	HB2	33 ARG+	HB1	2.5
23 MET	HG1	23 MET	HG2	2.5	28 VAL	HA	29 GLY	HN	2.5	33 ARG+	HD1	33 ARG+	HB1	4.5
23 MET	HG1	23 MET	QE	6.1	28 VAL	HA	32 LEU	QD1	5.6	33 ARG+	HD1	33 ARG+	HD2	2.5
23 MET	HG1	28 VAL	QG2	7.1	28 VAL	HB	28 VAL	QG1	3.6	33 ARG+	HD1	33 ARG+	QG	4.4
23 MET	HG1	33 ARG+	HA	6.0	28 VAL	HB	29 GLY	HN	4.5	33 ARG+	HD2	33 ARG+	HB1	6.0
23 MET	HG2	23 MET	HB1	3.0	28 VAL	HB	33 ARG+	HA	6.0	33 ARG+	HD2	33 ARG+	HB2	6.0
23 MET	HN	23 MET	HA	3.5	28 VAL	HB	33 ARG+	QG	3.9	33 ARG+	HE	33 ARG+	HB1	4.5
23 MET	HN	23 MET	HB1	4.0	28 VAL	HN	28 VAL	HA	3.0	33 ARG+	HE	33 ARG+	HD1	6.0
23 MET	HN	23 MET	HG1	4.0	28 VAL	HN	28 VAL	HB	3.5	33 ARG+	HE	33 ARG+	HD2	6.0
23 MET	HN	23 MET	HG2	3.5	28 VAL	HN	28 VAL	QG1	5.6	33 ARG+	HE	33 ARG+	QG	4.9
23 MET	HN	23 MET	QE	5.6	28 VAL	HN	28 VAL	QG2	3.6	33 ARG+	HN	33 ARG+	HA	3.5
23 MET	HN	24 LYS+	HN	3.0	28 VAL	HN	29 GLY	HN	6.0	33 ARG+	HN	33 ARG+	HB1	4.0
23 MET	QE	23 MET	HB1	4.6	28 VAL	HN	33 ARG+	QG	6.9	33 ARG+	HN	33 ARG+	QG	6.9
23 MET	QE	33 ARG+	HA	4.6	28 VAL	QG1	28 VAL	QG2	4.7	33 ARG+	HN	34 LYS+	HN	3.5
23 MET	QE	33 ARG+	HB1	7.1	28 VAL	QG1	29 GLY	HN	4.6	33 ARG+	HN	34 LYS+	HN	3.5
23 MET	QE	33 ARG+	QG	6.0	28 VAL	QG1	33 ARG+	HD1	7.1	33 ARG+	HN	35 MET	HN	6.0
23 MET	QE	36 GLY	HA1	7.1	28 VAL	QG1	33 ARG+	HN	5.6	34 LYS+	HA	34 LYS+	HB1	3.0
23 MET	QE	36 GLY	HN	5.6	28 VAL	QG1	33 ARG+	QG	5.5	34 LYS+	HA	34 LYS+	HB2	3.0
23 MET	QE	37 ALA	HN	5.6	28 VAL	QG2	29 GLY	HN	5.6	34 LYS+	HA	34 LYS+	QD	4.4
23 MET	QE	37 ALA	QB	5.7	28 VAL	QG2	33 ARG+	QG	6.5	34 LYS+	HA	35 MET	HN	4.5
24 LYS+	HA	24 LYS+	HB1	3.5	29 GLY	HA1	29 GLY	HA2	2.5	34 LYS+	HA	37 ALA	HN	4.5
24 LYS+	HA	24 LYS+	HB2	3.5	29 GLY	HA1	30 ILE	HG12	6.0	34 LYS+	HA	37 ALA	QB	4.1
24 LYS+	HA	24 LYS+	QG	4.4	29 GLY	HA1	30 ILE	HN	3.0	34 LYS+	HB1	34 LYS+	QD	4.9
24 LYS+	HA	27 GLY	HA1	6.0	29 GLY	HA1	31 ALA	HN	6.0	34 LYS+	HB1	37 ALA	QB	7.1
24 LYS+	HA	27 GLY	HN	4.0	29 GLY	HA2	30 ILE	HN	3.5	34 LYS+	HB2	34 LYS+	HG2	3.5
24 LYS+	HA	33 ARG+	HD1	4.5	29 GLY	HA2	31 ALA	HN	4.5	34 LYS+	HB2	35 MET	HN	3.5
24 LYS+	HA	33 ARG+	HD2	4.5	29 GLY	HN	29 GLY	HA1	3.0	34 LYS+	HG1	35 MET	HN	6.0
24 LYS+	HA	33 ARG+	QG	6.9	29 GLY	HN	29 GLY	HA2	3.0	34 LYS+	HG1	38 MET	QE	5.6
24 LYS+	HB1	24 LYS+	QG	3.4	29 GLY	HN	30 ILE	HN	5.0	34 LYS+	HN	34 LYS+	HA	3.5
24 LYS+	HB1	25 GLU-	HN	4.5	30 ILE	HA	30 ILE	HB	3.0	34 LYS+	HN	34 LYS+	HB1	4.0
24 LYS+	HB2	24 LYS+	HB1	3.5	30 ILE	HA	30 ILE	HG12	4.5	34 LYS+	HN	34 LYS+	HB2	3.5
24 LYS+	HN	24 LYS+	HA	3.0	30 ILE	HA	30 ILE	QD1	5.1	34 LYS+	HN	34 LYS+	HG1	4.5
24 LYS+	HN	24 LYS+	HB1	4.5	30 ILE	HA	30 ILE	QG2	4.1	34 LYS+	HN	34 LYS+	HG2	4.5
24 LYS+	HN	24 LYS+	HB2	4.5	30 ILE	HA	31 ALA	HN	4.0	34 LYS+	HN	34 LYS+	QD	5.4
24 LYS+	HN	24 LYS+	QG	6.9	30 ILE	HA	32 LEU	HN	6.0	34 LYS+	HN	35 MET	HN	4.5
24 LYS+	HN	25 GLU-	HN	3.5	30 ILE	HA	33 ARG+	HB1	4.0	34 LYS+	QD	34 LYS+	HG2	3.4
24 LYS+	HN	26 LEU	HN	4.5	30 ILE	HA	33 ARG+	HD2	6.0	35 MET	HA	35 MET	HB1	3.5
24 LYS+	QE	24 LYS+	HB2	5.9	30 ILE	HA	33 ARG+	HE	6.0	35 MET	HA	35 MET	HB2	4.5
24 LYS+	QG	25 GLU-	HN	6.9	30 ILE	HA	33 ARG+	HN	4.0	35 MET	HA	35 MET	HG1	4.5
24 LYS+	QG	33 ARG+	HE	4.4	30 ILE	HA	33 ARG+	QG	4.4	35 MET	HA	35 MET	HG2	4.5
25 GLU-	HA	25 GLU-	HB1	3.5	30 ILE	HA	34 LYS+	HN	4.5	35 MET	HA	38 MET	HG2	4.5
25 GLU-	HA	25 GLU-	HB2	3.5	30 ILE	HB	30 ILE	HG11	3.0	35 MET	HA	38 MET	HN	4.5
25 GLU-	HA	25 GLU-	HG1	4.0	30 ILE	HB	30 ILE	HG12	3.5	35 MET	HA	39 ALA	HN	6.0
25 GLU-	HA	26 LEU	HN	4.0	30 ILE	HB	30 ILE	QD1	3.6	35 MET	HA	39 ALA	QB	6.1
25 GLU-	HA	27 GLY	HN	6.0	30 ILE	HB	30 ILE	QG2	4.1	35 MET	HA	60 LEU	QD2	4.6
25 GLU-	HB1	125 VAL	HB	4.0	30 ILE	HB	31 ALA	HN	3.5	35 MET	HB1	36 GLY	HN	4.5
25 GLU-	HB2	26 LEU	HN	4.0	30 ILE	HG11	30 ILE	QD1	3.6	35 MET	HB1	60 LEU	QB	5.4
25 GLU-	HB2	125 VAL	HB	4.0	30 ILE	HG11	30 ILE	QG2	4.1	35 MET	HB1	60 LEU	QD1	7.1
25 GLU-	HB2	125 VAL	QG1	5.1	30 ILE	HG12	30 ILE	HG11	2.5	35 MET	HB2	60 LEU	QD2	7.1
25 GLU-	HB2	125 VAL	QG2	5.6	30 ILE	HG12	30 ILE	QD1	3.6	35 MET	HB2	35 MET	HB1	2.5
25 GLU-	HG1	25 GLU-	HB1	3.5	30 ILE	HG12	30 ILE	QG2	4.6	35 MET	HB2	36 GLY	HN	4.5
25 GLU-	HG1	25 GLU-	HB2	3.5	30 ILE	HG12	31 ALA	HN	6.0	35 MET	HG1	35 MET	HB1	3.5
25 GLU-	HG1	26 LEU	HN	5.0	30 ILE	HN	30 ILE	HA	3.0	35 MET	HG1	35 MET	HB2	4.5
25 GLU-	HG1	122 MET	HB2	4.5	30 ILE	HN	30 ILE	HB	4.0	35 MET	HG1	35 MET	HG2	2.5
25 GLU-	HG2	25 GLU-	HB1	3.5	30 ILE	HN	30 ILE	HG11	3.5	35 MET	HG1	61 LYS+	HB1	6.0
25 GLU-	HG2	25 GLU-	HB2	3.5	30 ILE	HN	30 ILE	HG12	3.0	35 MET	HG1	61 LYS+	HN	6.0
25 GLU-	HN	25 GLU-	HA	3.0	30 ILE	HN	30 ILE	QD1	5.6	35 MET	HG2	60 LEU	QB	5.4
25 GLU-	HN	25 GLU-	HB2	3.0	30 ILE	HN	30 ILE	QG2	5.1	35 MET	HG2	60 LEU	QD1	7.1

35 MET	HN	35 MET	HB2	4.5	43 CYS	HA	56 THR	QG2	5.6	46 THR	HN	54 ILE	QG1	6.9
35 MET	HN	35 MET	HG1	6.0	43 CYS	HA	57 GLU-	HN	4.5	46 THR	HN	55 LYS+	HN	6.0
35 MET	HN	36 GLY	HN	6.0	43 CYS	HB1	43 CYS	HB2	2.5	46 THR	QG2	47 CYS	HN	5.6
35 MET	QE	61 LYS+	HA	7.1	43 CYS	HB1	43 CYS	HB2	4.5	46 THR	QG2	53 THR	HB	6.1
35 MET	QE	61 LYS+	QG	5.5	43 CYS	HB1	44 ILE	HN	4.5	47 CYS	HA	47 CYS	HB1	4.5
35 MET	QE	78 ALA	QB	6.7	43 CYS	HB1	54 ILE	QG2	7.1	47 CYS	HA	47 CYS	HB2	4.5
35 MET	QE	79 ASP-	HA	7.1	43 CYS	HB1	116 LEU	QD2	5.6	47 CYS	HA	48 ASP-	HN	2.5
36 GLY	HA1	37 ALA	HN	6.0	43 CYS	HB1	131 TYR	QD	6.7	47 CYS	HA	52 LEU	HB1	6.0
36 GLY	HA1	39 ALA	QB	5.1	43 CYS	HB1	131 TYR	QE	5.7	47 CYS	HA	52 LEU	QDQ	5.8
36 GLY	HA2	36 GLY	HA1	2.5	43 CYS	HB2	43 CYS	HG	4.5	47 CYS	HB1	47 CYS	HB2	4.5
36 GLY	HA2	37 ALA	HN	4.5	43 CYS	HB2	44 ILE	HN	4.5	47 CYS	HB1	52 LEU	HA	6.0
36 GLY	HN	36 GLY	HA1	6.0	43 CYS	HB2	131 TYR	QE	6.7	47 CYS	HB1	52 LEU	QDQ	5.8
36 GLY	HN	36 GLY	HA2	3.5	43 CYS	HG	44 ILE	HN	6.0	47 CYS	HB2	48 ASP-	HN	6.0
36 GLY	HN	37 ALA	HN	4.5	43 CYS	HG	45 ILE	HG11	4.0	47 CYS	HN	47 CYS	HA	5.5
37 ALA	HA	37 ALA	QB	3.6	43 CYS	HG	54 ILE	QG1	6.9	47 CYS	HN	47 CYS	HB1	6.0
37 ALA	HA	38 MET	HN	4.5	43 CYS	HG	54 ILE	QG2	4.6	47 CYS	HN	47 CYS	HB2	6.0
37 ALA	HN	37 ALA	HA	3.0	43 CYS	HN	43 CYS	HA	6.0	48 ASP-	HB2	48 ASP-	HB1	2.5
37 ALA	HN	37 ALA	QB	3.6	43 CYS	HN	43 CYS	HB1	3.5	48 ASP-	HN	48 ASP-	HA	4.5
37 ALA	HN	38 MET	HN	3.5	43 CYS	HN	43 CYS	HB2	3.5	48 ASP-	HN	48 ASP-	HB1	3.5
37 ALA	HN	38 MET	HN	3.5	43 CYS	HN	131 TYR	QD	6.7	48 ASP-	HN	48 ASP-	HB2	4.5
37 ALA	HN	39 ALA	HN	4.5	43 CYS	HN	131 TYR	QE	6.7	48 ASP-	HN	49 GLY	HN	4.0
37 ALA	QB	38 MET	HN	4.1	43 CYS	HN	11 TRP	O	3.2	48 ASP-	HN	50 LYS+	HN	6.0
38 MET	HA	38 MET	HG1	4.0	43 CYS	HN	11 TRP	O	2.2	48 ASP-	HN	51 ASN	HN	4.5
38 MET	HA	38 MET	HG2	4.0	44 ILE	N	55 LYS+	O	3.2	49 GLY	HA1	49 GLY	HA2	2.5
38 MET	HA	38 MET	QB	3.4	44 ILE	HA	44 ILE	HB	4.5	49 GLY	HA1	50 LYS+	HN	3.5
38 MET	HA	39 ALA	HN	3.5	44 ILE	HA	44 ILE	HG11	3.5	49 GLY	HA2	50 LYS+	HN	3.5
38 MET	HG1	38 MET	QB	4.4	44 ILE	HA	44 ILE	HG12	6.0	49 GLY	HN	49 GLY	HA1	3.0
38 MET	HG2	38 MET	QB	4.4	44 ILE	HA	44 ILE	QD1	5.6	49 GLY	HN	49 GLY	HA2	3.0
38 MET	HG2	39 ALA	HN	4.5	44 ILE	HA	44 ILE	QG2	3.6	49 GLY	HN	50 LYS+	HN	4.5
38 MET	HG2	60 LEU	QD1	4.1	44 ILE	HA	45 ILE	HB	6.0	50 LYS+	HA	50 LYS+	HG1	4.0
38 MET	HN	38 MET	HA	3.5	44 ILE	HA	45 ILE	HG12	6.0	50 LYS+	HA	50 LYS+	HG2	4.0
38 MET	HN	38 MET	HG1	6.0	44 ILE	HA	45 ILE	HN	2.5	50 LYS+	HA	50 LYS+	QB	4.4
38 MET	HN	38 MET	HG2	4.5	44 ILE	HA	45 ILE	QD1	7.1	50 LYS+	HA	50 LYS+	QD	6.9
38 MET	HN	38 MET	QB	5.4	44 ILE	HB	44 ILE	QG2	3.6	50 LYS+	HA	51 ASN	HN	3.5
38 MET	HN	39 ALA	HN	3.0	44 ILE	HB	53 THR	QG2	7.1	50 LYS+	HA	69 LEU	HB1	4.5
38 MET	QB	38 MET	QE	4.5	44 ILE	HB	55 LYS+	HN	6.0	50 LYS+	HA	69 LEU	QD2	4.6
38 MET	QB	60 LEU	QD1	6.5	44 ILE	HB	55 LYS+	QD	4.4	50 LYS+	HG1	50 LYS+	HG2	2.5
39 ALA	HA	39 ALA	QB	3.6	44 ILE	HG11	44 ILE	HG12	2.5	50 LYS+	HG1	51 ASN	HN	6.0
39 ALA	HA	40 LYS+	HN	3.5	44 ILE	HG11	44 ILE	QD1	3.6	50 LYS+	HG1	69 LEU	QD2	5.1
39 ALA	HA	41 PRO	HD2	5.0	44 ILE	HG11	44 ILE	QG2	4.6	50 LYS+	HG2	51 ASN	HN	6.0
39 ALA	HA	60 LEU	HG	4.5	44 ILE	HG11	45 ILE	HN	6.0	50 LYS+	HN	50 LYS+	HA	3.5
39 ALA	HA	60 LEU	HN	6.0	44 ILE	HG12	44 ILE	QD1	3.6	50 LYS+	HN	50 LYS+	QB	4.4
39 ALA	HN	39 ALA	HA	3.5	44 ILE	HG12	44 ILE	QG2	4.6	50 LYS+	HN	51 ASN	HN	2.5
39 ALA	HN	39 ALA	QB	3.6	44 ILE	HN	44 ILE	HA	4.5	50 LYS+	QB	50 LYS+	HG1	3.9
39 ALA	HN	40 LYS+	HN	6.0	44 ILE	HN	44 ILE	HB	4.5	50 LYS+	QB	50 LYS+	HG2	3.9
39 ALA	QB	40 LYS+	HN	4.6	44 ILE	HN	44 ILE	HG12	4.5	50 LYS+	QB	51 ASN	HN	4.9
39 ALA	QB	41 PRO	HD2	5.6	44 ILE	HN	44 ILE	QD1	4.6	50 LYS+	QB	68 THR	HA	6.9
39 ALA	QB	60 LEU	HA	7.1	44 ILE	HN	44 ILE	QG2	5.6	50 LYS+	QB	68 THR	QG2	4.5
39 ALA	QB	60 LEU	QD1	4.7	44 ILE	HN	45 ILE	HN	4.5	50 LYS+	QB	69 LEU	QD2	6.5
39 ALA	QB	61 LYS+	HN	5.6	44 ILE	HN	54 ILE	QG2	7.1	50 LYS+	QD	50 LYS+	HG1	3.4
40 LYS+	HN	40 LYS+	HA	6.0	44 ILE	HN	55 LYS+	HB2	6.0	50 LYS+	QD	50 LYS+	HG2	3.4
40 LYS+	HN	40 LYS+	HG2	4.5	44 ILE	HN	55 LYS+	HN	4.5	50 LYS+	QD	68 THR	QG2	8.0
40 LYS+	HN	40 LYS+	QB	4.4	44 ILE	HN	55 LYS+	O	2.2	50 LYS+	QE	50 LYS+	HG1	4.4
40 LYS+	HN	40 LYS+	QD	6.9	44 ILE	HN	57 GLU-	HN	6.0	50 LYS+	QE	50 LYS+	HG2	4.9
40 LYS+	HN	58 SER	HB2	6.0	44 ILE	QD1	55 LYS+	HN	7.1	50 LYS+	QE	50 LYS+	QD	4.3
40 LYS+	QB	40 LYS+	HG1	3.9	44 ILE	QD1	55 LYS+	QG	4.5	50 LYS+	QE	68 THR	HA	5.4
40 LYS+	QB	41 PRO	HD1	5.9	44 ILE	QD1	57 GLU-	HB2	7.1	50 LYS+	QE	68 THR	QG2	4.5
40 LYS+	QD	40 LYS+	HG1	3.9	44 ILE	QG2	45 ILE	HN	5.6	51 ASN	HA	51 ASN	HB1	3.5
40 LYS+	QE	40 LYS+	HG2	4.9	44 ILE	QG2	55 LYS+	HN	7.1	51 ASN	HA	51 ASN	HB2	3.5
40 LYS+	QE	40 LYS+	QB	6.3	44 ILE	QG2	55 LYS+	QD	6.5	51 ASN	HA	52 LEU	HN	2.5
40 LYS+	QE	40 LYS+	QD	4.3	45 ILE	HA	46 THR	HN	3.5	51 ASN	HA	68 THR	HA	2.5
41 PRO	HA	42 ASP-	HN	3.0	45 ILE	HA	53 THR	HN	6.0	51 ASN	HA	68 THR	QG2	5.6
41 PRO	HD2	42 ASP-	HN	6.0	45 ILE	HB	45 ILE	HG12	3.5	51 ASN	HA	69 LEU	HN	4.5
41 PRO	HD2	58 SER	HB1	6.0	45 ILE	HB	45 ILE	QD1	4.1	51 ASN	HB1	51 ASN	HB2	3.5
41 PRO	HG1	56 THR	QG2	7.1	45 ILE	HB	45 ILE	QG2	3.6	51 ASN	HB1	52 LEU	HN	5.0
41 PRO	HG1	131 TYR	QE	5.7	45 ILE	HB	46 THR	HN	4.5	51 ASN	HB1	68 THR	HA	6.0
41 PRO	HG2	41 PRO	HG1	2.5	45 ILE	HG11	45 ILE	QD1	4.1	51 ASN	HB2	52 LEU	HN	4.5
41 PRO	HG2	42 ASP-	HN	6.0	45 ILE	HG11	45 ILE	QG2	4.1	51 ASN	HB2	68 THR	HA	6.0
41 PRO	QB	41 PRO	HG1	3.4	45 ILE	HG11	52 LEU	QDQ	8.3	51 ASN	HD21	51 ASN	HB1	4.0
41 PRO	QB	41 PRO	HG2	3.4	45 ILE	HG11	54 ILE	QD1	4.6	51 ASN	HD21	51 ASN	HB2	4.5
41 PRO	QB	42 ASP-	HN	3.4	45 ILE	HG11	54 ILE	QG2	4.6	51 ASN	HD21	51 ASN	HD22	2.5
41 PRO	QB	57 GLU-	HN	5.4	45 ILE	HG11	109 ARG+	HD1	6.0	51 ASN	HD22	51 ASN	HA	6.0
41 PRO	QB	58 SER	HB1	5.4	45 ILE	HG11	109 ARG+	HD2	6.0	51 ASN	HD22	51 ASN	HB1	4.5
41 PRO	QB	131 TYR	QE	7.6	45 ILE	HG11	116 LEU	QD2	7.1	51 ASN	HD22	51 ASN	HB2	4.5
42 ASP-	HA	42 ASP-	HB1	4.5	45 ILE	HG12	45 ILE	HG11	2.5	51 ASN	HD22	51 ASN	HD21	2.5
42 ASP-	HA	43 CYS	HN	2.5	45 ILE	HG12	45 ILE	QG2	5.1	51 ASN	HD22	51 ASN	HN	6.0
42 ASP-	HA	134 VAL	QG2	7.1	45 ILE	HG12	46 THR	HN	6.0	51 ASN	HN	51 ASN	HA	3.5
42 ASP-	HB1	44 ILE	HG12	6.0	45 ILE	HG12	54 ILE	HA	6.0	51 ASN	HN	51 ASN	HB1	4.0
42 ASP-	HB1	44 ILE	QD1	5.1	45 ILE	HG12	54 ILE	QG1	5.4	51 ASN	HN	51 ASN	HB2	4.0
42 ASP-	HB1	57 GLU-	HB2	6.0	45 ILE	HG12	54 ILE	QG2	5.4	51 ASN	HN	51 ASN	HD21	5.0
42 ASP-	HB1	57 GLU-	HN	4.5	45 ILE	HN	45 ILE	HB	3.5	51 ASN	HN	51 ASN	HD22	5.0
42 ASP-	HB2	44 ILE	HG12	4.5	45 ILE	HN	45 ILE	HG12	4.5	51 ASN	HN	52 LEU	HN	6.0
42 ASP-	HB2	57 GLU-	HB1	5.5	45 ILE	HN	45 ILE	QD1	5.6	51 ASN	HN	68 THR	QG2	7.1
42 ASP-	HB2	57 GLU-	HG2	6.0	45 ILE	HN	45 ILE	QG2	5.6	52 LEU	N	67 CYS	O	3.2
42 ASP-	HB2	57 GLU-	HN	4.5	45 ILE	HN	46 THR	HN	4.5	52 LEU	HA	52 LEU	HB1	3.5
42 ASP-	HN	42 ASP-	HA	4.5	45 ILE	QD1	94 LEU	QD2	6.7	52 LEU	HA	52 LEU	HB2	3.5
42 ASP-	HN	42 ASP-	HB1	6.0	45 ILE	QD1	109 ARG+	HB1	7.1	52 LEU	HA	52 LEU	HG	3.0
42 ASP-	HN	42 ASP-	HB2	6.0	45 ILE	QD1	109 ARG+	HD1	5.6	52 LEU	HA	52 LEU	QDQ	5.3
42 ASP-	HN	43 CYS	HN	4.5	45 ILE	QD1	116 LEU	HB1	7.1	52 LEU	HA	53 THR	HN	2.5
42 ASP-	HN	43 CYS	HN	6.0	45 ILE	QD1	116 LEU	HG	7.1	52 LEU	HB1	52 LEU	QDQ	4.8
42 ASP-	HN	56 THR	QG2	5.6	45 ILE	QD1	116 LEU	QD2	4.7	52 LEU	HB1	53 THR	HN	4.5
42 ASP-	HN	57 GLU-	HA	5.0	45 ILE	QG2	46 THR	HN	4.6	52 LEU	HB1	67 CYS	HN	6.0
42 ASP-	HN	57 GLU-	HB1	4.5	45 ILE	QG2	46 THR	HN	5.6	52 LEU	HB2	52 LEU	HG	3.5
42 ASP-	HN	57 GLU-	HB2	4.5	45 ILE	QG2	47 CYS	HB1	7.1	52 LEU	HB2	52 LEU	QDQ	4.8
42 ASP-	HN	57 GLU-	HN	4.5	45 ILE	QG2	52 LEU	QDQ	6.9	52 LEU	HB2	53 THR	HN	4.5
42 ASP-	HN	57 GLU-	HN	4.5	45 ILE	QG2	53 THR	HN	7.1	52 LEU	HB2	69 LEU	QD1	5.6
42 ASP-	HN	58 SER	HA	6.0	45 ILE	QG2	54 ILE	HA	7.1	52 LEU	HG	52 LEU	HB1	3.5
42 ASP-	HN	58 SER	HB1	6.0	45 ILE	QG2	54 ILE	QG2	7.2	52 LEU	HG	52 LEU	QDQ	4.8
42 ASP-	HN	58 SER	HN	5.0	46 THR	HB	46 THR	QG2	3.6	52 LEU	HG	53 THR	HN	3.5
43 CYS	HA	43 CYS	HB1	4.5	46 THR	HN	46 THR	HB	4.5	52 LEU	HG	54 ILE	QG1	4.4
43 CYS	HA	43 CYS	HG	4.5	46 THR	HN	46 THR	QG2	5.6	52 LEU	HG	94 LEU	QD2	7.1
43 CYS	HA	44 ILE	HN	2.5	46 THR	HN	52 LEU	QDQ	8.3	52 LEU				

52 LEU	HN	52 LEU	QQD	7.8	55 LYS+	QG	57 GLU-	HB1	6.9	63 THR	QG2	78 ALA	HN	5.6
52 LEU	HN	53 THR	HN	4.5	55 LYS+	QG	57 GLU-	HG1	4.4	64 GLN	HA	64 GLN	HB1	3.5
52 LEU	HN	67 CYS	HN	3.5	55 LYS+	QG	64 GLN	HA	5.4	64 GLN	HA	64 GLN	HB2	4.0
52 LEU	HN	67 CYS	O	2.2	55 LYS+	QG	64 GLN	HB1	5.4	64 GLN	HA	64 GLN	HG1	4.5
52 LEU	HN	68 THR	HA	4.0	55 LYS+	QG	64 GLN	HB2	5.4	64 GLN	HA	64 GLN	HG2	4.5
52 LEU	QQD	53 THR	HN	4.8	56 THR	HA	56 THR	HB	6.0	64 GLN	HA	65 PHE	HN	3.0
52 LEU	QQD	54 ILE	QG1	6.2	56 THR	HB	56 THR	QG2	3.6	64 GLN	HB1	65 PHE	HN	4.5
52 LEU	QQD	65 PHE	QE	9.0	56 THR	HB	57 GLU-	HN	6.0	64 GLN	HB2	65 PHE	HN	4.5
52 LEU	QQD	65 PHE	QR	9.8	56 THR	HB	63 THR	QG2	7.1	64 GLN	HE21	64 GLN	HB2	5.0
52 LEU	QQD	67 CYS	HN	6.8	56 THR	HN	56 THR	HB	3.5	64 GLN	HE21	64 GLN	HE22	2.5
52 LEU	QQD	69 LEU	HG	6.8	56 THR	HN	57 GLU-	HN	4.5	64 GLN	HE22	64 GLN	HG1	4.5
52 LEU	QQD	69 LEU	QD1	6.9	56 THR	HN	62 THR	QG2	7.1	64 GLN	HE22	64 GLN	HG2	4.5
52 LEU	QQD	87 CYS	HB2	6.8	56 THR	HN	63 THR	HN	4.5	64 GLN	HG1	64 GLN	HB1	3.5
52 LEU	QQD	94 LEU	QD2	5.9	56 THR	HN	64 GLN	HA	3.5	64 GLN	HG1	64 GLN	HB2	3.5
53 THR	N	46 THR	O	3.2	56 THR	QG2	57 GLU-	HN	4.6	64 GLN	HG1	65 PHE	HN	6.0
53 THR	HA	53 THR	HB	4.0	56 THR	QG2	61 LYS+	HB2	7.1	64 GLN	HG2	64 GLN	HB2	3.5
53 THR	HA	53 THR	QG2	3.6	56 THR	QG2	131 TYR	QE	9.3	64 GLN	HG2	65 PHE	HN	5.0
53 THR	HA	54 ILE	HN	2.5	57 GLU-	N	42 ASP-	O	3.2	64 GLN	HN	64 GLN	HA	4.5
53 THR	HA	65 PHE	HN	6.0	57 GLU-	HA	57 GLU-	HB1	3.5	64 GLN	HN	64 GLN	HA	6.0
53 THR	HA	66 SER	HA	3.5	57 GLU-	HA	57 GLU-	HB2	4.5	64 GLN	HN	64 GLN	HB1	5.0
53 THR	HA	66 SER	HB2	4.5	57 GLU-	HA	57 GLU-	HG2	6.0	64 GLN	HN	64 GLN	HB2	5.0
53 THR	HA	67 CYS	HN	4.0	57 GLU-	HA	58 SER	HN	2.5	64 GLN	HN	64 GLN	HG1	6.0
53 THR	HB	53 THR	QG2	4.1	57 GLU-	HA	62 THR	HB	5.0	65 PHE	HA	66 SER	HN	2.5
53 THR	HB	54 ILE	HN	4.5	57 GLU-	HA	62 THR	QG2	4.1	65 PHE	HA	73 PHE	QE	8.2
53 THR	HN	46 THR	O	2.2	57 GLU-	HB1	58 SER	HN	4.5	65 PHE	HB1	66 SER	HN	4.5
53 THR	HN	53 THR	HA	3.0	57 GLU-	HB2	58 SER	HN	4.5	65 PHE	HB1	73 PHE	HZ	6.0
53 THR	HN	53 THR	HB	3.5	57 GLU-	HB2	62 THR	QG2	5.6	65 PHE	HB1	73 PHE	QE	6.2
53 THR	HN	53 THR	QG2	5.6	57 GLU-	HG1	62 THR	QG2	4.6	65 PHE	HB1	75 GLU-	HA	6.0
53 THR	HN	54 ILE	HN	4.5	57 GLU-	HG2	57 GLU-	HB1	3.0	65 PHE	HB1	75 GLU-	QB	6.9
53 THR	HN	54 ILE	HN	6.0	57 GLU-	HG2	57 GLU-	HB2	3.5	65 PHE	HB2	65 PHE	HB1	4.5
53 THR	QG2	54 ILE	HN	4.6	57 GLU-	HG2	57 GLU-	HG1	2.5	65 PHE	HB2	66 SER	HN	4.5
53 THR	QG2	55 LYS+	QD	8.0	57 GLU-	HG2	62 THR	QG2	5.6	65 PHE	HB2	75 GLU-	HA	6.0
53 THR	QG2	64 GLN	HE21	5.6	57 GLU-	HN	42 ASP-	O	2.2	65 PHE	HN	65 PHE	HA	3.5
53 THR	QG2	64 GLN	HE22	5.6	57 GLU-	HN	57 GLU-	HA	3.0	65 PHE	HN	65 PHE	HB2	6.0
53 THR	QG2	65 PHE	HN	5.6	57 GLU-	HN	57 GLU-	HB1	4.5	65 PHE	HN	65 PHE	QE	7.2
53 THR	QG2	66 SER	HA	4.6	57 GLU-	HN	57 GLU-	HG1	6.0	65 PHE	HN	66 SER	HN	4.5
53 THR	QG2	66 SER	HB1	7.1	57 GLU-	HN	57 GLU-	HG2	4.5	65 PHE	QE	65 PHE	HB1	6.7
53 THR	QG2	66 SER	HB2	4.6	58 SER	HA	59 THR	HN	4.5	65 PHE	QE	65 PHE	QB	6.7
53 THR	QG2	66 SER	HN	7.1	58 SER	HA	59 THR	QG2	5.6	65 PHE	QE	65 PHE	QR	7.2
54 ILE	N	65 PHE	O	3.2	58 SER	HA	60 LEU	HN	4.5	65 PHE	QE	73 PHE	HZ	6.7
54 ILE	HA	54 ILE	QD1	5.6	58 SER	HA	61 LYS+	HN	5.0	65 PHE	QE	87 CYS	HG	6.2
54 ILE	HA	54 ILE	QG1	5.4	58 SER	HB1	59 THR	HN	4.5	65 PHE	QE	96 GLN	HE21	7.2
54 ILE	HA	54 ILE	QG2	4.6	58 SER	HB1	60 LEU	HN	6.0	65 PHE	QE	109 ARG+	QH1	9.1
54 ILE	HA	55 LYS+	HN	3.5	58 SER	HB2	59 THR	HN	6.0	65 PHE	QR	65 PHE	HA	7.0
54 ILE	HB	54 ILE	QD1	4.6	58 SER	HB2	60 LEU	QD1	7.1	65 PHE	QR	65 PHE	HB1	6.0
54 ILE	HB	54 ILE	QG2	4.1	58 SER	HN	62 THR	HA	6.0	65 PHE	QR	65 PHE	HB2	5.0
54 ILE	HB	55 LYS+	HN	4.5	58 SER	HN	62 THR	QG2	7.1	65 PHE	QR	66 SER	HN	6.0
54 ILE	HB	65 PHE	QE	6.7	59 THR	HA	59 THR	QG2	4.1	65 PHE	QR	67 CYS	HN	7.0
54 ILE	HB	65 PHE	QR	7.0	59 THR	HA	60 LEU	HN	4.5	65 PHE	QR	73 PHE	HZ	6.0
54 ILE	HN	54 ILE	HA	3.5	59 THR	HB	59 THR	HA	3.0	65 PHE	QR	73 PHE	QD1	0.7
54 ILE	HN	54 ILE	HB	6.0	59 THR	HB	59 THR	QG2	3.6	65 PHE	QR	75 GLU-	HG2	8.5
54 ILE	HN	54 ILE	QD1	7.1	59 THR	HB	60 LEU	HC	5.0	65 PHE	QR	87 CYS	HC	8.0
54 ILE	HN	54 ILE	QG2	5.6	59 THR	HB	60 LEU	HN	6.0	65 PHE	QR	96 GLN	HG2	8.5
54 ILE	HN	55 LYS+	HN	6.0	59 THR	HN	59 THR	HA	4.5	66 SER	HA	66 SER	HB1	3.5
54 ILE	HN	65 PHE	HN	6.0	59 THR	HN	59 THR	HB	4.5	66 SER	HA	66 SER	HB2	3.5
54 ILE	HN	65 PHE	O	2.2	59 THR	HN	59 THR	QG2	5.6	66 SER	HA	67 CYS	HN	2.5
54 ILE	HN	65 PHE	QR	8.5	59 THR	HN	60 LEU	HN	6.0	66 SER	HB1	67 CYS	HN	4.5
54 ILE	HN	66 SER	HA	4.5	59 THR	QG2	60 LEU	HN	7.1	66 SER	HB2	66 SER	HB1	2.5
54 ILE	HN	67 CYS	HN	6.0	60 LEU	HA	60 LEU	QB	3.4	66 SER	HB2	67 CYS	HN	4.5
54 ILE	HN	67 CYS	HN	6.0	60 LEU	HA	60 LEU	QD1	5.6	66 SER	HN	66 SER	HA	3.5
54 ILE	QD1	54 ILE	QG2	4.7	60 LEU	HA	60 LEU	QD2	3.6	66 SER	HN	66 SER	HB1	4.0
54 ILE	QD1	65 PHE	QR	6.6	60 LEU	HN	60 LEU	HA	3.5	66 SER	HN	66 SER	HB2	4.5
54 ILE	QD1	96 GLN	QB	8.0	60 LEU	HN	60 LEU	QB	3.4	66 SER	HN	67 CYS	HN	4.5
54 ILE	QG1	54 ILE	QD1	4.5	60 LEU	HN	60 LEU	QD2	5.6	66 SER	HN	67 CYS	HN	6.0
54 ILE	QG1	54 ILE	QG2	5.5	60 LEU	HN	61 LYS+	HN	4.5	67 CYS	HA	67 CYS	HB1	6.0
54 ILE	QG1	55 LYS+	HN	6.9	60 LEU	QB	60 LEU	QD1	4.5	67 CYS	HA	67 CYS	HB2	3.5
54 ILE	QG1	65 PHE	QE	9.1	60 LEU	QB	60 LEU	QD2	4.5	67 CYS	HA	68 THR	HN	3.5
54 ILE	QG1	65 PHE	QR	7.9	60 LEU	QB	61 LYS+	HB2	6.9	67 CYS	HB1	68 THR	HN	4.0
54 ILE	QG2	55 LYS+	HN	4.6	60 LEU	QB	61 LYS+	HN	4.4	67 CYS	HB2	67 CYS	HB1	6.0
54 ILE	QG2	65 PHE	QE	7.3	60 LEU	QB	61 LYS+	HN	4.9	67 CYS	HB2	68 THR	HN	4.5
54 ILE	QG2	65 PHE	QR	7.6	60 LEU	QD2	61 LYS+	HN	7.1	67 CYS	HG	69 LEU	QD1	7.1
54 ILE	QG2	109 ARG+	HD1	7.1	61 LYS+	HA	61 LYS+	HB1	3.0	67 CYS	HN	67 CYS	HA	3.5
55 LYS+	N	44 ILE	O	3.2	61 LYS+	HA	61 LYS+	HB2	3.5	67 CYS	HN	67 CYS	HB1	4.5
55 LYS+	HA	55 LYS+	HB1	3.5	61 LYS+	HA	61 LYS+	QD	4.4	67 CYS	HN	67 CYS	HB2	6.0
55 LYS+	HA	55 LYS+	HB2	3.5	61 LYS+	HA	61 LYS+	QE	5.4	67 CYS	HN	68 THR	HN	6.0
55 LYS+	HA	55 LYS+	QG	4.4	61 LYS+	HA	62 THR	HN	2.5	68 THR	HA	68 THR	HN	3.5
55 LYS+	HA	56 THR	HN	2.5	61 LYS+	HB1	61 LYS+	QD	3.9	68 THR	HA	68 THR	QG2	4.1
55 LYS+	HA	64 GLN	HA	2.5	61 LYS+	HB1	62 THR	HN	4.5	68 THR	HA	69 LEU	HN	2.5
55 LYS+	HA	64 GLN	HB1	4.5	61 LYS+	HB2	61 LYS+	QG	3.4	68 THR	HB	68 THR	QG2	3.6
55 LYS+	HA	64 GLN	HB2	4.5	61 LYS+	HB2	62 THR	HN	4.5	68 THR	HB	69 LEU	HN	4.5
55 LYS+	HA	64 GLN	HG1	6.0	61 LYS+	HB2	78 ALA	QB	7.1	68 THR	HB	71 GLU-	HN	6.0
55 LYS+	HB1	55 LYS+	HB2	2.5	61 LYS+	HN	61 LYS+	HA	4.5	68 THR	HN	68 THR	HA	3.0
55 LYS+	HB1	55 LYS+	QG	5.4	61 LYS+	HN	61 LYS+	HB1	4.5	68 THR	HN	68 THR	HB	3.5
55 LYS+	HB1	56 THR	HN	4.5	61 LYS+	HN	61 LYS+	QB	3.5	68 THR	HN	68 THR	QG2	5.6
55 LYS+	HB2	55 LYS+	QD	3.4	61 LYS+	HN	61 LYS+	HD	6.9	68 THR	HN	69 LEU	HN	4.5
55 LYS+	HB2	56 THR	HN	4.5	61 LYS+	HN	61 LYS+	QG	6.9	68 THR	HN	73 PHE	QD	6.7
55 LYS+	HN	44 ILE	O	2.2	61 LYS+	HN	62 THR	HN	6.0	68 THR	HN	73 PHE	QE	8.2
55 LYS+	HN	55 LYS+	HA	6.0	61 LYS+	HN	62 THR	HN	6.0	68 THR	QG2	69 LEU	HN	4.6
55 LYS+	HN	55 LYS+	HB1	3.5	61 LYS+	QD	62 THR	HN	4.4	68 THR	QG2	71 GLU-	HN	5.6
55 LYS+	HN	55 LYS+	HB2	3.5	61 LYS+	QE	61 LYS+	HB1	6.9	69 LEU	HA	69 LEU	HB1	3.5
55 LYS+	HN	56 THR	HN	6.0	61 LYS+	QG	61 LYS+	QD	6.3	69 LEU	HB1	69 LEU	QD1	5.1
55 LYS+	HN	56 THR	HN	6.0	61 LYS+	QE	61 LYS+	QD	4.3	69 LEU	HB1	69 LEU	QD2	4.1
55 LYS+	QD	55 LYS+	QG	4.8	62 THR	HA	62 THR	HB	4.5	69 LEU	HB1	70 GLY	HN	4.5
55 LYS+	QD	56 THR	HN	6.4	62 THR	HA	62 THR	QG2	4.6	69 LEU	HB2	70 GLY	HN	4.5
55 LYS+	QD	57 GLU-	HG2	5.4	62 THR	HB	62 THR	QG2	3.6	69 LEU	HG	69 LEU	QD2	3.6
55 LYS+	QD	64 GLN	HB1	6.9	62 THR	HN	62 THR	HA	3.5	69 LEU	HN	69 LEU	HA	3.0
55 LYS+	QE	55 LYS+	HB1	6.9	62 THR	HN	62 THR	HB	3.5	69 LEU	HN	69 LEU	HB1	3.5
55 LYS+	QE	55 LYS+	QD	5.3	62 THR	HN	62 THR	QG2	5.6	69 LEU	HN	69 LEU	HB2	4.0
55 LYS+	QE	55 LYS+	QG	6.3	62 THR	QG2	63 THR	HN	5.1	69 LEU	HN	69 LEU	HG	4.5
55 LYS+	QE	57 GLU-	HA	6.9	63 THR	HA	64 GLN	HN	3.5	69 LEU	HN	69 LEU	QD1	5.1
55 LYS+	QE	57 GLU-	HB1	5.9	63 THR	HB	63 THR	QG2	3.6	69 LEU	HN	69 LEU	QD2	5.6
55 LYS+	QE	57 GLU-	HG2	4.4	63 THR	HB	64 GLN	HN	4.0	69 LEU	HN	70 GLY	HN	5.0
55 LYS+	QE	62 THR	QG2	5.5	63 THR	HN	63 THR							

69 LEU	QD1	87 CYS	HN	7.1	74 GLU-	HA	83 THR	HN	4.5	78 ALA	HN	78 ALA	QB	3.6
69 LEU	QD1	88 ASN	HA	7.1	74 GLU-	HA	83 THR	HN	6.0	78 ALA	HN	79 ASP-	HN	4.5
69 LEU	QD1	89 PHE	HB1	6.1	74 GLU-	HA	84 GLN	HE21	4.0	78 ALA	HN	80 GLY	HN	6.0
69 LEU	QD1	89 PHE	HN	6.1	74 GLU-	HA	85 THR	HB	6.0	78 ALA	QB	79 ASP-	HN	4.1
69 LEU	QD1	94 LEU	QD1	6.2	74 GLU-	HN	74 GLU-	HA	3.0	78 ALA	QB	80 GLY	HN	7.1
69 LEU	QD2	69 LEU	QD1	4.7	74 GLU-	HN	74 GLU-	QB	3.4	79 ASP-	HA	79 ASP-	HB2	3.5
69 LEU	QD2	88 ASN	HA	5.6	74 GLU-	HN	74 GLU-	QG	5.4	79 ASP-	HA	80 GLY	HA2	6.0
69 LEU	QD2	89 PHE	HB1	4.6	74 GLU-	HN	75 GLU-	HN	4.5	79 ASP-	HA	80 GLY	HN	3.5
69 LEU	QD2	89 PHE	HN	4.6	74 GLU-	HN	75 GLU-	HN	6.0	79 ASP-	HB2	80 GLY	HN	6.0
70 GLY	HN	71 GLU-	HN	3.5	74 GLU-	QB	74 GLU-	QG	4.3	79 ASP-	HN	79 ASP-	HA	3.5
70 GLY	HN	71 GLU-	HN	4.5	74 GLU-	QB	75 GLU-	HN	5.4	79 ASP-	HN	79 ASP-	HB2	4.5
70 GLY	HN	86 VAL	QGG	6.3	74 GLU-	QB	84 GLN	HE21	5.4	79 ASP-	HN	80 GLY	HN	3.5
70 GLY	HN	88 ASN	HA	3.5	74 GLU-	QB	84 GLN	HE22	4.4	79 ASP-	HN	80 GLY	HN	3.5
70 GLY	HN	88 ASN	HB1	6.0	74 GLU-	QG	75 GLU-	HN	4.4	79 ASP-	HN	81 ARG+	HN	4.5
71 GLU-	HA	72 LYS+	HN	2.5	74 GLU-	QG	82 LYS+	HA	6.9	80 GLY	HA1	81 ARG+	HN	4.5
71 GLU-	HB1	71 GLU-	HB2	2.5	74 GLU-	QG	82 LYS+	HB1	5.9	80 GLY	HA2	80 GLY	HA1	2.5
71 GLU-	HG1	71 GLU-	HB1	3.5	74 GLU-	QG	82 LYS+	HB2	4.4	80 GLY	HA2	81 ARG+	HN	4.5
71 GLU-	HG1	71 GLU-	HB2	3.0	74 GLU-	QG	83 THR	HN	6.9	80 GLY	HN	80 GLY	HA1	3.5
71 GLU-	HG1	71 GLU-	HG2	2.5	74 GLU-	QG	84 GLN	HE22	4.4	80 GLY	HN	80 GLY	HA2	3.0
71 GLU-	HG1	72 LYS+	HN	4.5	75 GLU-	N	83 THR	O	3.2	80 GLY	HN	81 ARG+	HN	3.5
71 GLU-	HN	71 GLU-	HA	3.5	75 GLU-	HA	83 THR	HG1	4.5	80 GLY	HN	81 ARG+	HN	3.5
71 GLU-	HN	71 GLU-	HG1	5.0	75 GLU-	HA	75 GLU-	HG2	4.5	81 ARG+	HA	81 ARG+	HB2	3.5
71 GLU-	HN	72 LYS+	HN	4.5	75 GLU-	HA	75 GLU-	QB	4.4	81 ARG+	HA	81 ARG+	HG1	3.5
71 GLU-	HN	72 LYS+	HN	6.0	75 GLU-	HA	76 THR	HN	2.5	81 ARG+	HA	82 LYS+	HA	6.0
71 GLU-	HN	86 VAL	QGG	6.8	75 GLU-	HA	85 THR	HB	6.0	81 ARG+	HA	82 LYS+	HN	2.5
72 LYS+	HA	72 LYS+	QB	3.4	75 GLU-	HG2	76 THR	HN	4.5	81 ARG+	HB1	83 THR	QG2	4.6
72 LYS+	HA	72 LYS+	QE	6.9	75 GLU-	HG2	77 THR	QG2	5.6	81 ARG+	HB2	81 ARG+	HD1	4.5
72 LYS+	HA	72 LYS+	QG	3.9	75 GLU-	HN	75 GLU-	HA	3.5	81 ARG+	HB2	82 LYS+	HN	4.5
72 LYS+	HA	73 PHE	HN	2.5	75 GLU-	HN	75 GLU-	HG1	4.5	81 ARG+	HD1	100 TRP	HE1	4.0
72 LYS+	HA	73 PHE	QD	6.2	75 GLU-	HN	75 GLU-	HG2	6.0	81 ARG+	HE	81 ARG+	HB2	4.5
72 LYS+	HA	85 THR	HN	6.0	75 GLU-	HN	75 GLU-	QB	3.4	81 ARG+	HE	81 ARG+	HD2	6.0
72 LYS+	HA	86 VAL	HA	4.5	75 GLU-	HN	76 THR	HN	4.5	81 ARG+	HG1	81 ARG+	HB2	6.0
72 LYS+	HA	86 VAL	QGG	4.8	75 GLU-	HN	76 THR	HN	6.0	81 ARG+	HG1	81 ARG+	HD1	4.5
72 LYS+	HA	87 CYS	HN	6.0	75 GLU-	HN	82 LYS+	HA	6.0	81 ARG+	HG1	82 LYS+	HN	5.5
72 LYS+	HN	72 LYS+	HA	3.5	75 GLU-	HN	83 THR	HN	3.5	81 ARG+	HG1	83 THR	QG2	7.1
72 LYS+	HN	72 LYS+	QB	3.9	75 GLU-	HN	83 THR	HN	3.5	81 ARG+	HG1	100 TRP	HE1	6.0
72 LYS+	HN	72 LYS+	QG	5.4	75 GLU-	HN	83 THR	O	2.2	81 ARG+	HG2	81 ARG+	HB2	4.5
72 LYS+	HN	73 PHE	HN	5.0	75 GLU-	HN	84 GLN	HE22	6.0	81 ARG+	HG2	81 ARG+	HD1	4.5
72 LYS+	HN	86 VAL	QGG	6.8	75 GLU-	QB	75 GLU-	HG1	4.4	81 ARG+	HG2	81 ARG+	HG1	2.5
72 LYS+	QB	72 LYS+	QG	4.8	75 GLU-	QB	75 GLU-	HG2	3.4	81 ARG+	HG2	82 LYS+	HN	5.5
72 LYS+	QB	73 PHE	HN	4.9	75 GLU-	QB	76 THR	HN	5.4	81 ARG+	HN	81 ARG+	HA	3.5
72 LYS+	QB	86 VAL	QGG	6.2	75 GLU-	QB	77 THR	QG2	6.5	81 ARG+	HN	81 ARG+	HB1	3.5
72 LYS+	QD	72 LYS+	QG	4.8	75 GLU-	QB	83 THR	HN	4.4	81 ARG+	HN	81 ARG+	HG1	4.5
72 LYS+	QD	84 GLN	HB1	4.9	75 GLU-	QB	83 THR	QG2	7.0	81 ARG+	HN	81 ARG+	HG2	3.5
72 LYS+	QD	84 GLN	HB2	4.9	75 GLU-	QB	85 THR	HB	3.9	81 ARG+	HN	82 LYS+	HN	6.0
72 LYS+	QD	84 GLN	HG2	4.9	76 THR	HA	76 THR	HB	3.5	81 ARG+	QH1	81 ARG+	HD1	6.9
72 LYS+	QE	72 LYS+	QB	5.3	76 THR	HA	76 THR	QG2	3.6	81 ARG+	QH1	81 ARG+	HE	6.9
72 LYS+	QE	72 LYS+	QD	4.3	76 THR	HA	77 THR	HN	2.5	82 LYS+	HA	82 LYS+	HB1	3.5
72 LYS+	QE	72 LYS+	QG	5.3	76 THR	HA	82 LYS+	HA	3.5	82 LYS+	HA	82 LYS+	HB2	3.5
72 LYS+	QE	84 GLN	HB1	5.4	76 THR	HA	82 LYS+	HG1	6.0	82 LYS+	HA	82 LYS+	HG1	4.0
72 LYS+	QE	84 GLN	HB2	4.9	76 THR	HA	82 LYS+	HN	6.0	82 LYS+	HA	82 LYS+	HG2	4.5
72 LYS+	QE	84 GLN	HG2	5.4	76 THR	HA	82 LYS+	QD	5.4	82 LYS+	HA	83 THR	HN	2.5
72 LYS+	QE	86 VAL	QGG	6.7	76 THR	HB	76 THR	QG2	3.6	82 LYS+	HB1	82 LYS+	HB2	2.5
72 LYS+	QG	73 PHE	HN	4.4	76 THR	HB	77 THR	HN	4.5	82 LYS+	HB1	82 LYS+	HG2	3.5
72 LYS+	QG	84 GLN	HB2	5.4	76 THR	HB	82 LYS+	QD	5.9	82 LYS+	HB1	83 THR	HN	4.5
72 LYS+	QG	86 VAL	HA	6.9	76 THR	HN	76 THR	HA	3.5	82 LYS+	HB2	82 LYS+	HG1	3.5
73 PHE	N	85 THR	O	3.2	76 THR	HN	76 THR	HB	3.5	82 LYS+	HB2	82 LYS+	HG2	3.5
73 PHE	HA	73 PHE	HB1	2.5	76 THR	HN	76 THR	QG2	5.6	82 LYS+	HB2	83 THR	HN	4.5
73 PHE	HA	73 PHE	HB2	2.5	76 THR	HN	77 THR	HN	4.5	82 LYS+	HG1	83 THR	HN	6.0
73 PHE	HA	74 GLU-	HN	2.5	76 THR	HN	77 THR	HN	6.0	82 LYS+	HG2	83 THR	HN	6.0
73 PHE	HB1	73 PHE	HB2	2.5	76 THR	HN	82 LYS+	HA	6.0	82 LYS+	HN	82 LYS+	HA	3.5
73 PHE	HB1	74 GLU-	HN	4.0	76 THR	QG2	77 THR	HN	4.6	82 LYS+	HN	82 LYS+	HB1	4.5
73 PHE	HB2	74 GLU-	HN	4.5	76 THR	QG2	80 GLY	HA1	4.6	82 LYS+	HN	82 LYS+	HG1	6.0
73 PHE	HN	73 PHE	HA	3.5	76 THR	QG2	80 GLY	HN	5.6	82 LYS+	HN	82 LYS+	HG2	4.5
73 PHE	HN	73 PHE	HB1	4.5	76 THR	QG2	82 LYS+	HA	5.1	82 LYS+	HN	83 THR	HN	4.5
73 PHE	HN	73 PHE	HB2	4.5	76 THR	QG2	82 LYS+	QE	5.5	82 LYS+	HN	100 TRP	HD1	6.0
73 PHE	HN	73 PHE	QD	5.7	77 THR	HA	77 THR	HB	3.0	82 LYS+	QD	82 LYS+	HG2	3.4
73 PHE	HN	73 PHE	QE	8.2	77 THR	HA	77 THR	QG2	3.6	82 LYS+	QE	82 LYS+	HB1	5.9
73 PHE	HN	74 GLU-	HN	6.0	77 THR	HA	78 ALA	HA	5.0	82 LYS+	QE	82 LYS+	HG2	3.9
73 PHE	HN	85 THR	HB	4.5	77 THR	HA	78 ALA	HN	3.5	82 LYS+	QE	82 LYS+	QD	4.3
73 PHE	HN	85 THR	HN	3.5	77 THR	HA	78 ALA	QB	7.1	83 THR	N	75 GLU-	O	3.2
73 PHE	HN	85 THR	O	2.2	77 THR	HA	79 ASP-	HN	6.0	83 THR	HA	83 THR	HB	4.5
73 PHE	HN	86 VAL	HA	6.0	77 THR	HB	77 THR	QG2	3.6	83 THR	HA	83 THR	QG2	4.1
73 PHE	HN	86 VAL	QGG	6.8	77 THR	HB	78 ALA	HN	3.5	83 THR	HA	84 GLN	HN	2.5
73 PHE	HZ	75 GLU-	QB	6.9	77 THR	HB	79 ASP-	HN	3.5	83 THR	HA	100 TRP	HB1	3.5
73 PHE	HZ	85 THR	HB	6.0	77 THR	HB	80 GLY	HN	4.5	83 THR	HA	100 TRP	HB2	3.5
73 PHE	HZ	85 THR	QG2	4.6	77 THR	HB	81 ARG+	HB1	4.5	83 THR	HA	100 TRP	HE3	6.0
73 PHE	HZ	87 CYS	HG	4.5	77 THR	HB	81 ARG+	HN	4.5	83 THR	HB	83 THR	QG2	3.6
73 PHE	QD	73 PHE	HA	6.7	77 THR	HG1	77 THR	HA	6.0	83 THR	HB	84 GLN	HN	3.5
73 PHE	QD	73 PHE	HB1	4.7	77 THR	HG1	77 THR	HB	4.5	83 THR	HB	98 GLN	HA	4.5
73 PHE	QD	73 PHE	HB2	4.7	77 THR	HG1	77 THR	QG2	5.6	83 THR	HB	99 GLU-	HN	3.5
73 PHE	QD	73 PHE	HZ	6.7	77 THR	HG1	80 GLY	HN	4.5	83 THR	HB	100 TRP	HB1	6.0
73 PHE	QD	73 PHE	QE	6.9	77 THR	HG1	81 ARG+	HE	6.0	83 THR	HB	100 TRP	HB2	4.0
73 PHE	QD	74 GLU-	HA	6.7	77 THR	HG1	81 ARG+	HN	3.5	83 THR	HB	100 TRP	HE3	4.5
73 PHE	QD	74 GLU-	HN	5.7	77 THR	HG1	81 ARG+	QH1	6.9	83 THR	HN	75 GLU-	O	2.2
73 PHE	QD	75 GLU-	HN	8.2	77 THR	HN	77 THR	HA	3.5	83 THR	HN	83 THR	HA	3.5
73 PHE	QD	75 GLU-	QB	7.6	77 THR	HN	77 THR	HB	4.5	83 THR	HN	83 THR	HB	4.0
73 PHE	QD	85 THR	HB	8.2	77 THR	HN	77 THR	QG2	3.6	83 THR	HN	83 THR	QG2	4.6
73 PHE	QD	85 THR	QG2	9.3	77 THR	HN	78 ALA	HN	6.0	83 THR	QH2	84 GLN	HN	5.6
73 PHE	QD	86 VAL	HA	6.7	77 THR	HN	80 GLY	HN	6.0	83 THR	QG2	98 GLN	HA	7.1
73 PHE	QE	73 PHE	HB2	7.2	77 THR	HN	81 ARG+	HA	6.0	83 THR	QG2	98 GLN	HB1	5.6
73 PHE	QE	73 PHE	HZ	4.7	77 THR	HN	81 ARG+	HN	4.5	83 THR	QG2	98 GLN	HB2	5.6
73 PHE	QE	75 GLU-	HA	8.2	77 THR	HN	83 THR	HN	4.5	83 THR	QG2	98 GLN	HE21	7.1
73 PHE	QE	75 GLU-	HG2	5.7	77 THR	HN	83 THR	QG2	7.1	83 THR	QG2	98 GLN	HG1	7.1
73 PHE	QE	75 GLU-	HN	8.2	77 THR	QG2	78 ALA	HN	5.6	83 THR	QG2	99 GLU-	HN	5.6
73 PHE	QE	75 GLU-	QB	6.6	77 THR	QG2	81 ARG+	HE	5.6	83 THR	QG2	100 TRP	HB1	4.6
73 PHE	QE	76 THR	HN	8.2	77 THR	QG2	81 ARG+	HN	7.1	83 THR	QG2	100 TRP	HB2	4.6
73 PHE	QE	85 THR	HB	6.7	77 THR	QG2	81 ARG+	QH1	8.0	83 THR	QG2	100 TRP	HD1	6.1
73 PHE	QE	85 THR	QG2	6.8	77 THR	QG2	83 THR	HN	5.1	83 THR	QG2	100 TRP	HE1	7.1
73 PHE	QE	86 VAL	HA	8.2	77 THR	QG2	83 THR	QG2	5.7	83 THR	QG2	100 TRP	HE3	4.1
73 PHE	QE	87 CYS	HG	5.7	77 THR	QG2	83 THR	HE21	7.1	83 THR	QG2	100 TRP	HN	6.1
73 PHE	QE	87 CYS	HN	8.2	78 ALA	HA	79 ASP-	HA	6.0	83 THR	QG2	100 TRP	HZ3	5.6
74 GLU-	HA	74 GLU-	QB	3.9	78 ALA	HA	79 ASP-	HN	4.5	84 GLN	HA	85 THR	HN	3.5
74 GLU-	HA	7												

84 GLN	HB2	85 THR	HN	4.5	89 PHE	HB2	89 PHE	HB1	2.5	95 VAL	HA	96 GLN	HN	3.5
84 GLN	HE21	84 GLN	HB2	4.5	89 PHE	HB2	90 THR	HN	5.0	95 VAL	HA	108 THR	HA	3.5
84 GLN	HE21	84 GLN	HG2	6.0	89 PHE	HN	89 PHE	HA	3.5	95 VAL	HA	108 THR	QG2	5.1
84 GLN	HE22	84 GLN	HG2	4.5	89 PHE	HN	89 PHE	HB2	3.5	95 VAL	HA	109 ARG+	HN	4.5
84 GLN	HG2	84 GLN	HB1	3.5	89 PHE	HN	89 PHE	QD	6.7	95 VAL	HB	95 VAL	QG1	3.6
84 GLN	HG2	84 GLN	HB2	3.5	89 PHE	HN	90 THR	HN	6.0	95 VAL	HB	95 VAL	QG2	3.6
84 GLN	HG2	84 GLN	HG1	2.5	89 PHE	HZ	92 GLY	HA1	3.5	95 VAL	HB	96 GLN	HN	4.5
84 GLN	HG2	99 GLU-	HB2	6.0	89 PHE	HZ	92 GLY	HA2	5.0	95 VAL	HN	88 ASN	O	2.2
84 GLN	HN	84 GLN	HB1	4.0	89 PHE	HZ	92 GLY	HN	6.0	95 VAL	HN	95 VAL	HA	4.5
84 GLN	HN	84 GLN	HB2	4.5	89 PHE	QD	89 PHE	HA	4.7	95 VAL	HN	95 VAL	HB	3.5
84 GLN	HN	84 GLN	HG1	4.5	89 PHE	QD	89 PHE	HB1	4.7	95 VAL	HN	95 VAL	QG1	6.1
84 GLN	HN	84 GLN	HG2	4.5	89 PHE	QD	89 PHE	HB2	4.7	95 VAL	HN	95 VAL	QG2	4.6
84 GLN	HN	85 THR	HN	4.5	89 PHE	QD	89 PHE	HZ	6.7	95 VAL	HN	96 GLN	HN	4.5
84 GLN	HN	99 GLU-	HN	3.5	89 PHE	QD	90 THR	HN	6.7	95 VAL	QG1	96 GLN	HN	4.6
85 THR	N	73 PHE	O	3.2	89 PHE	QD	93 ALA	HN	8.2	95 VAL	QG1	97 HIS+	HB1	6.1
85 THR	HA	85 THR	HB	4.5	89 PHE	QD	94 LEU	HA	5.2	95 VAL	QG2	96 GLN	HN	6.1
85 THR	HA	85 THR	QG2	4.6	89 PHE	QD	94 LEU	HG	7.2	95 VAL	QG2	108 THR	HA	5.6
85 THR	HA	86 VAL	HB	6.0	89 PHE	QD	94 LEU	HN	6.7	95 VAL	QG2	108 THR	HB	7.1
85 THR	HA	86 VAL	HN	2.5	89 PHE	QD	94 LEU	QD1	6.8	95 VAL	QG2	108 THR	QG2	5.7
85 THR	HA	98 GLN	HA	2.5	89 PHE	QD	94 LEU	QD1	6.8	96 GLN	HA	96 GLN	HG1	4.5
85 THR	HA	98 GLN	HG2	6.0	89 PHE	QD	94 LEU	QD2	8.8	96 GLN	HA	96 GLN	HG2	4.5
85 THR	HA	99 GLU-	HN	4.5	89 PHE	QD	95 VAL	HN	6.7	96 GLN	HA	96 GLN	QB	6.9
85 THR	HB	85 THR	QG2	3.6	89 PHE	QE	89 PHE	HA	6.7	96 GLN	HA	97 HIS+	HN	2.5
85 THR	HB	86 VAL	HN	4.5	89 PHE	QE	89 PHE	HB1	8.2	96 GLN	HE21	96 GLN	HG1	4.0
85 THR	HB	98 GLN	HA	6.0	89 PHE	QE	89 PHE	HZ	4.7	96 GLN	HG1	96 GLN	HG2	4.5
85 THR	HN	73 PHE	O	2.2	89 PHE	QE	89 PHE	QD	6.9	96 GLN	HG1	98 GLN	HG1	6.0
85 THR	HN	85 THR	HA	4.5	89 PHE	QE	92 GLY	HA1	5.2	96 GLN	HG1	107 ILE	HB	4.5
85 THR	HN	86 VAL	HN	6.0	89 PHE	QE	92 GLY	HA2	7.2	96 GLN	HG1	107 ILE	QG1	4.9
85 THR	QN2	86 VAL	HN	4.6	89 PHE	QE	94 LEU	HA	6.7	96 GLN	HG2	97 HIS+	HN	4.5
85 THR	QN2	96 GLN	HE21	4.6	89 PHE	QE	94 LEU	HB1	6.7	96 GLN	HG2	98 GLN	HG1	6.0
85 THR	QN2	98 GLN	HA	5.1	89 PHE	QE	94 LEU	HN	6.7	96 GLN	HN	96 GLN	HA	3.0
86 VAL	N	97 HIS+	O	3.2	89 PHE	QE	94 LEU	QD1	8.3	96 GLN	HN	96 GLN	QB	4.4
86 VAL	HA	86 VAL	HB	3.5	90 THR	HA	90 THR	HB	2.5	96 GLN	HN	107 ILE	HB	4.5
86 VAL	HA	86 VAL	QOG	4.8	90 THR	HA	90 THR	QG2	5.1	96 GLN	HN	107 ILE	HN	4.5
86 VAL	HA	87 CYS	HN	2.5	90 THR	HA	91 ASP-	HN	2.5	96 GLN	QB	96 GLN	HG2	5.4
86 VAL	HB	86 VAL	QOG	4.8	90 THR	HA	92 GLY	HN	5.0	96 GLN	QB	97 HIS+	HN	6.9
86 VAL	HB	87 CYS	HN	4.5	90 THR	HB	90 THR	QG2	3.6	96 GLN	QB	107 ILE	HB	5.4
86 VAL	HB	97 HIS+	HB2	4.5	90 THR	HB	91 ASP-	HN	6.0	96 GLN	QB	107 ILE	HN	5.4
86 VAL	HN	86 VAL	HA	3.5	90 THR	HN	90 THR	HA	3.0	97 HIS+	N	86 VAL	O	3.2
86 VAL	HN	86 VAL	HB	3.5	90 THR	HN	90 THR	HB	3.5	97 HIS+	HA	97 HIS+	HB1	3.5
86 VAL	HN	86 VAL	QOG	5.3	90 THR	HN	90 THR	QG2	3.6	97 HIS+	HA	97 HIS+	HB2	4.5
86 VAL	HN	87 CYS	HN	6.0	90 THR	HN	91 ASP-	HN	6.0	97 HIS+	HA	98 GLN	HN	2.5
86 VAL	HN	97 HIS+	HB1	6.0	90 THR	HN	93 ALA	HN	3.5	97 HIS+	HA	106 THR	HA	3.5
86 VAL	HN	97 HIS+	HB2	6.0	90 THR	HN	93 ALA	HN	3.5	97 HIS+	HA	106 THR	HB	4.5
86 VAL	HN	97 HIS+	HN	4.0	90 THR	HN	95 VAL	HN	4.5	97 HIS+	HA	106 THR	QG2	4.6
86 VAL	HN	97 HIS+	O	2.2	90 THR	HN	95 VAL	HN	5.0	97 HIS+	HA	107 ILE	HN	4.5
86 VAL	HN	98 GLN	HA	6.0	90 THR	QG2	91 ASP-	HN	5.6	97 HIS+	HB1	98 GLN	HN	4.5
86 VAL	QOG	87 CYS	HA	6.8	90 THR	QG2	93 ALA	HN	6.1	97 HIS+	HB1	106 THR	QG2	5.6
86 VAL	QOG	87 CYS	HN	5.3	90 THR	QG2	95 VAL	HN	5.6	97 HIS+	HB2	97 HIS+	HB1	2.5
86 VAL	QOG	88 ASN	HD21	5.8	90 THR	QG2	95 VAL	QG2	5.2	97 HIS+	HB2	98 GLN	HN	4.5
86 VAL	QOG	88 ASN	HD22	5.3	91 ASP-	HA	91 ASP-	HB1	3.5	97 HIS+	HD2	97 HIS+	HA	3.5
86 VAL	QOG	97 HIS+	HB2	6.8	91 ASP-	HA	91 ASP-	HB2	4.0	97 HIS+	HD2	97 HIS+	HB1	4.5
87 CYS	HA	87 CYS	HB1	4.5	91 ASP-	HA	92 GLY	HA1	5.0	97 HIS+	HD2	97 HIS+	HB2	4.0
87 CYS	HA	87 CYS	HB2	3.5	91 ASP-	HA	92 GLY	HN	4.5	97 HIS+	HD2	98 GLN	HN	4.5
87 CYS	HA	87 CYS	HG	4.5	91 ASP-	HA	93 ALA	HN	6.0	97 HIS+	HD2	106 THR	HA	4.5
87 CYS	HA	88 ASN	HN	2.5	91 ASP-	HB1	91 ASP-	HB2	2.5	97 HIS+	HD2	106 THR	QG2	3.6
87 CYS	HA	94 LEU	QD1	6.1	91 ASP-	HB1	92 GLY	HN	6.0	97 HIS+	HE1	97 HIS+	HD2	6.0
87 CYS	HA	96 GLN	HA	3.5	91 ASP-	HB2	92 GLY	HN	5.0	97 HIS+	HE1	99 GLU-	HG1	3.5
87 CYS	HA	96 GLN	QB	5.4	91 ASP-	HN	91 ASP-	HA	2.5	97 HIS+	HE1	104 GLU-	HB1	4.0
87 CYS	HA	97 HIS+	HN	4.5	91 ASP-	HN	91 ASP-	HB1	4.5	97 HIS+	HE1	104 GLU-	HB2	4.0
87 CYS	HB1	88 ASN	HN	4.5	91 ASP-	HN	91 ASP-	HB2	4.5	97 HIS+	HN	86 VAL	O	2.2
87 CYS	HB2	87 CYS	HG	3.5	91 ASP-	HN	92 GLY	HN	4.5	97 HIS+	HN	97 HIS+	HA	3.5
87 CYS	HB2	88 ASN	HN	4.5	91 ASP-	HN	93 ALA	HN	5.0	97 HIS+	HN	97 HIS+	HB1	3.5
87 CYS	HB2	94 LEU	QD1	5.6	92 GLY	HA1	93 ALA	HN	4.0	97 HIS+	HN	97 HIS+	HB2	3.5
87 CYS	HG	88 ASN	HN	6.0	92 GLY	HA2	92 GLY	HA1	2.5	97 HIS+	HN	98 GLN	HN	4.5
87 CYS	HG	96 GLN	HA	3.5	92 GLY	HA2	93 ALA	HN	4.5	98 GLN	HA	98 GLN	HB1	3.5
87 CYS	HG	96 GLN	HG2	3.0	92 GLY	HN	92 GLY	HA1	3.0	98 GLN	HA	98 GLN	HB2	4.5
87 CYS	HN	87 CYS	HA	4.5	92 GLY	HN	92 GLY	HA2	3.5	98 GLN	HA	98 GLN	HG1	4.5
87 CYS	HN	87 CYS	HB1	4.0	92 GLY	HN	93 ALA	HN	3.0	98 GLN	HA	98 GLN	HG2	4.5
87 CYS	HN	87 CYS	HB2	4.5	93 ALA	HA	93 ALA	QB	3.6	98 GLN	HA	99 GLU-	HN	2.5
87 CYS	HN	87 CYS	HG	4.5	93 ALA	HA	94 LEU	HN	2.5	98 GLN	HB1	100 TRP	HE3	4.5
87 CYS	HN	88 ASN	HN	4.5	93 ALA	HN	93 ALA	HA	3.0	98 GLN	HB1	100 TRP	HZ3	4.5
87 CYS	N	71 GLU-	O	3.2	93 ALA	HN	93 ALA	QB	4.1	98 GLN	HB1	105 SER	HN	5.0
87 CYS	HN	71 GLU-	O	2.2	93 ALA	HN	94 LEU	HN	4.5	98 GLN	HB2	98 GLN	HB1	2.5
88 ASN	N	95 VAL	O	3.2	93 ALA	HN	94 LEU	HN	6.0	98 GLN	HB2	99 GLU-	HN	4.5
88 ASN	HA	88 ASN	HB1	3.5	93 ALA	HN	110 LYS+	HB2	6.0	98 GLN	HE21	98 GLN	HB2	5.0
88 ASN	HA	88 ASN	HB2	3.5	93 ALA	QB	94 LEU	HN	4.1	98 GLN	HE21	98 GLN	HE22	3.5
88 ASN	HA	89 PHE	HN	2.5	94 LEU	N	109 ARG+	O	3.2	98 GLN	HE21	98 GLN	HG2	6.0
88 ASN	HB1	89 PHE	HN	5.0	94 LEU	HA	94 LEU	QD1	3.6	98 GLN	HE22	98 GLN	HB2	6.0
88 ASN	HB1	90 THR	HB	6.0	94 LEU	HA	95 VAL	HN	2.5	98 GLN	HE22	98 GLN	HE21	3.5
88 ASN	HD21	88 ASN	HA	5.0	94 LEU	HB1	94 LEU	HG	3.5	98 GLN	HE22	98 GLN	HG2	4.5
88 ASN	HD21	88 ASN	HB1	4.5	94 LEU	HB1	94 LEU	QD2	4.1	98 GLN	HG1	98 GLN	HB1	4.5
88 ASN	HD21	88 ASN	HB2	5.0	94 LEU	HB1	95 VAL	HN	5.0	98 GLN	HG1	99 GLU-	HN	6.0
88 ASN	HD21	88 ASN	HD22	2.5	94 LEU	HB2	94 LEU	HB1	2.5	98 GLN	HG1	107 ILE	QG1	6.9
88 ASN	HD22	88 ASN	HA	6.0	94 LEU	HB2	94 LEU	HG	3.5	98 GLN	HG2	98 GLN	HB2	6.0
88 ASN	HD22	88 ASN	HB1	4.5	94 LEU	HB2	94 LEU	QD2	5.6	98 GLN	HN	98 GLN	HA	3.5
88 ASN	HD22	88 ASN	HB2	5.0	94 LEU	HG	94 LEU	QD1	4.1	98 GLN	HN	98 GLN	HB1	4.5
88 ASN	HN	88 ASN	HA	3.5	94 LEU	HG	94 LEU	QD2	4.1	98 GLN	HN	98 GLN	HB2	4.5
88 ASN	HN	88 ASN	HB1	4.5	94 LEU	HN	94 LEU	HA	3.5	98 GLN	HN	98 GLN	HG1	3.5
88 ASN	HN	88 ASN	HD21	6.0	94 LEU	HN	94 LEU	HB1	3.5	98 GLN	HN	98 GLN	HG2	4.5
88 ASN	HN	88 ASN	HD22	6.0	94 LEU	HN	94 LEU	QD1	7.1	98 GLN	HN	99 GLU-	HN	5.0
88 ASN	HN	89 PHE	HN	4.5	94 LEU	HN	95 VAL	HN	4.5	98 GLN	HN	100 TRP	HZ3	6.0
88 ASN	HN	94 LEU	QD1	5.1	94 LEU	HN	95 VAL	HN	6.0	98 GLN	HN	105 SER	HN	4.5
88 ASN	HN	95 VAL	HN	3.5	94 LEU	HN	109 ARG+	HB2	4.5	98 GLN	HN	106 THR	HA	3.5
88 ASN	HN	95 VAL	HN	4.5	94 LEU	HN	109 ARG+	HN	6.0	98 GLN	HN	106 THR	QG2	5.6
88 ASN	HN	95 VAL	O	2.2	94 LEU	HN	109 ARG+	O	2.2	99 GLU-	N	84 GLN	O	3.2
88 ASN	HN	95 VAL	QG2	7.1	94 LEU	HN	110 LYS+	HA	4.5	99 GLU-	HA	99 GLU-	HB1	3.5
89 PHE	HA	89 PHE	HB1	3.5	94 LEU	QN1	94 LEU	QD2	4.7	99 GLU-	HA	99 GLU-	HB2	4.0
89 PHE	HA	89 PHE	HB2	3.5	94 LEU	QN1	95 VAL	HN	4.6					

99	GLU-	HG2	99	GLU-	HB1	3.5	103	LYS+	HN	103	LYS+	HA	3.0	108	THR	HB	119	GLU-	HN	4.5
99	GLU-	HN	84	GLN	O	2.2	103	LYS+	HN	103	LYS+	HD1	6.0	108	THR	HN	108	THR	HA	3.5
99	GLU-	HN	99	GLU-	HA	4.5	103	LYS+	HN	103	LYS+	HD2	5.0	108	THR	HN	108	THR	HB	3.5
99	GLU-	HN	99	GLU-	HB1	4.5	103	LYS+	HN	103	LYS+	HE1	6.0	108	THR	HN	108	THR	QG2	5.6
99	GLU-	HN	99	GLU-	HG1	4.5	103	LYS+	HN	103	LYS+	HE2	6.0	108	THR	HN	109	ARG+	HN	6.0
99	GLU-	HN	100	TRP	HN	6.0	103	LYS+	HN	103	LYS+	HG1	4.5	108	THR	HN	119	GLU-	HB1	6.0
99	GLU-	QG	104	GLU-	HA	5.9	103	LYS+	HN	103	LYS+	HG2	3.0	108	THR	HN	119	GLU-	HN	4.5
100	TRP	HA	100	TRP	HB1	3.5	103	LYS+	HN	103	LYS+	QB	3.9	108	THR	HN	119	GLU-	O	2.2
100	TRP	HA	100	TRP	HB2	3.5	103	LYS+	HN	104	GLU-	HN	5.0	108	THR	HN	120	CYSS	HA	3.5
100	TRP	HA	101	ASP-	HN	2.5	103	LYS+	QB	104	GLU-	HN	4.4	108	THR	HN	121	VAL	HN	6.0
100	TRP	HA	102	GLY	HN	4.5	103	LYS+	QB	122	MET	QE	4.5	108	THR	QG2	109	ARG+	HN	4.6
100	TRP	HB1	100	TRP	HB2	3.5	104	GLU-	HA	104	GLU-	HB1	3.5	108	THR	QG2	110	LYS+	HB1	7.1
100	TRP	HB1	101	ASP-	HN	4.5	104	GLU-	HA	104	GLU-	HB2	3.0	108	THR	QG2	119	GLU-	HB1	5.6
100	TRP	HB2	101	ASP-	HN	4.5	104	GLU-	HA	104	GLU-	HG1	4.5	108	THR	QG2	119	GLU-	HN	5.6
100	TRP	HD1	100	TRP	HA	4.5	104	GLU-	HA	104	GLU-	HG2	4.5	109	ARG+	N	94	LEU	O	3.2
100	TRP	HD1	100	TRP	HB1	4.0	104	GLU-	HA	105	SER	HN	2.5	109	ARG+	HA	109	ARG+	HB1	4.5
100	TRP	HD1	100	TRP	HB2	4.0	104	GLU-	HB1	105	SER	HN	4.5	109	ARG+	HA	109	ARG+	HB2	4.5
100	TRP	HD1	101	ASP-	HN	4.5	104	GLU-	HB2	104	GLU-	HB1	2.5	109	ARG+	HA	109	ARG+	HD1	6.0
100	TRP	HD1	103	LYS+	QB	6.9	104	GLU-	HB2	105	SER	HN	4.5	109	ARG+	HA	109	ARG+	HG2	4.5
100	TRP	HE1	100	TRP	HB1	6.0	104	GLU-	HG1	104	GLU-	HB1	3.5	109	ARG+	HA	110	LYS+	HN	2.5
100	TRP	HE1	100	TRP	HB2	6.0	104	GLU-	HG1	105	SER	HA	5.0	109	ARG+	HA	110	LYS+	QG	6.9
100	TRP	HE1	100	TRP	HD1	2.5	104	GLU-	HG1	105	SER	HN	5.0	109	ARG+	HA	116	LEU	QD1	5.6
100	TRP	HE1	100	TRP	HD2	6.0	104	GLU-	HG2	105	SER	HN	5.0	109	ARG+	HA	117	VAL	HB	6.0
100	TRP	HE1	100	TRP	HZ2	3.0	104	GLU-	HN	104	GLU-	HA	3.5	109	ARG+	HA	118	VAL	HA	3.5
100	TRP	HE1	103	LYS+	QB	6.9	104	GLU-	HN	104	GLU-	HB1	5.0	109	ARG+	HA	118	VAL	HG1	5.6
100	TRP	HE1	122	MET	QE	6.1	104	GLU-	HN	104	GLU-	HG1	3.5	109	ARG+	HA	118	VAL	QG2	5.6
100	TRP	HE3	100	TRP	HA	4.5	104	GLU-	HN	104	GLU-	HG2	4.5	109	ARG+	HB1	110	LYS+	HN	4.5
100	TRP	HE3	100	TRP	HB1	4.5	104	GLU-	HN	105	SER	HN	4.5	109	ARG+	HB1	116	LEU	QD1	5.6
100	TRP	HE3	100	TRP	HB2	4.5	104	GLU-	HN	122	MET	QE	4.6	109	ARG+	HB1	118	VAL	QG1	7.1
100	TRP	HE3	100	TRP	HZ3	2.5	105	SER	N	98	GLN	O	3.2	109	ARG+	HB2	110	LYS+	HN	4.5
100	TRP	HE3	103	LYS+	HN	6.0	105	SER	HA	105	SER	HB1	3.5	109	ARG+	HB2	116	LEU	QD1	4.1
100	TRP	HE3	105	SER	HB2	6.0	105	SER	HA	105	SER	HB2	4.5	109	ARG+	HB2	116	LEU	QD2	5.6
100	TRP	HE3	105	SER	HN	5.0	105	SER	HA	106	THR	HN	2.5	109	ARG+	HB2	118	VAL	HA	6.0
100	TRP	HH2	100	TRP	HZ3	2.5	105	SER	HB1	105	SER	HB2	3.5	109	ARG+	HD1	109	ARG+	HB1	4.5
100	TRP	HH2	105	SER	HA	5.0	105	SER	HB1	106	THR	HN	6.0	109	ARG+	HD1	109	ARG+	HB2	4.0
100	TRP	HH2	105	SER	HB1	4.5	105	SER	HB1	122	MET	QE	6.1	109	ARG+	HD1	109	ARG+	HG1	4.5
100	TRP	HH2	105	SER	HB2	4.5	105	SER	HB2	106	THR	HN	6.0	109	ARG+	HD1	116	LEU	QD1	7.1
100	TRP	HH2	105	SER	HG	6.0	105	SER	HG	105	SER	HA	4.5	109	ARG+	HD2	109	ARG+	HB2	3.0
100	TRP	HH2	105	SER	HN	5.0	105	SER	HG	105	SER	HB1	4.5	109	ARG+	HD2	109	ARG+	HG1	4.5
100	TRP	HH2	122	MET	QE	4.6	105	SER	HG	105	SER	HB2	4.5	109	ARG+	HD2	116	LEU	QD1	7.1
100	TRP	HN	100	TRP	HA	3.5	105	SER	HG	106	THR	HN	4.0	109	ARG+	HD2	118	VAL	HG1	7.1
100	TRP	HN	100	TRP	HB1	4.5	105	SER	HG	122	MET	HA	6.0	109	ARG+	HD2	118	VAL	QG2	5.6
100	TRP	HN	100	TRP	HB2	4.5	105	SER	HN	98	GLN	O	2.2	109	ARG+	HE	109	ARG+	HB2	6.0
100	TRP	HN	100	TRP	HB3	3.5	105	SER	HN	105	SER	HA	3.5	109	ARG+	HE	109	ARG+	HD1	6.0
100	TRP	HN	100	TRP	HZ3	5.0	105	SER	HN	105	SER	HB1	4.5	109	ARG+	HE	118	VAL	QG1	7.1
100	TRP	HN	101	ASP-	HN	6.0	105	SER	HN	105	SER	HB2	4.0	109	ARG+	HG1	116	LEU	QD1	6.1
100	TRP	HN	103	LYS+	QB	6.9	105	SER	HN	105	SER	HG	5.0	109	ARG+	HG1	116	LEU	QD2	7.1
100	TRP	HN	104	GLU-	HA	4.5	105	SER	HN	106	THR	HN	4.5	109	ARG+	HG1	118	VAL	HA	6.0
100	TRP	HN	105	SER	HN	6.0	105	SER	HN	106	THR	HN	4.5	109	ARG+	HG1	118	VAL	QG1	5.6
100	TRP	HZ2	100	TRP	HH2	2.5	106	THR	HA	106	THR	HB	4.5	109	ARG+	HG1	118	VAL	QG2	4.6
100	TRP	HZ2	100	TRP	HZ3	4.5	106	THR	HA	106	THR	QG2	4.6	109	ARG+	HG2	118	VAL	HA	6.0
100	TRP	HZ2	103	LYS+	QB	5.4	106	THR	HA	107	ILE	HB	6.0	109	ARG+	HG2	118	VAL	QG2	5.6
100	TRP	HZ2	122	MET	QE	4.1	106	THR	HA	107	ILE	HN	2.5	109	ARG+	HN	94	LEU	O	2.2
100	TRP	HZ3	104	GLU-	HN	6.0	106	THR	HA	107	ILE	QG1	6.9	109	ARG+	HN	109	ARG+	HB1	4.5
100	TRP	HZ3	105	SER	HA	5.0	106	THR	HB	106	THR	QG2	3.6	109	ARG+	HN	109	ARG+	HG1	6.0
100	TRP	HZ3	105	SER	HB1	4.0	106	THR	HB	107	ILE	HN	6.0	109	ARG+	HN	109	ARG+	HG2	6.0
100	TRP	HZ3	105	SER	HB2	4.0	106	THR	HB	121	VAL	QG1	7.1	109	ARG+	QH1	109	ARG+	HE	6.9
100	TRP	HZ3	105	SER	HN	3.5	106	THR	HN	106	THR	HA	4.5	109	ARG+	QH1	118	VAL	QG1	8.0
100	TRP	HZ3	122	MET	QE	7.1	106	THR	HN	106	THR	HB	4.0	109	ARG+	QH1	118	VAL	QG2	8.0
101	ASP-	HA	101	ASP-	HB1	3.0	106	THR	HN	106	THR	QG2	4.6	110	LYS+	N	117	VAL	O	3.2
101	ASP-	HA	101	ASP-	HB2	3.5	106	THR	HN	107	ILE	HN	6.0	110	LYS+	HA	111	LEU	HN	2.5
101	ASP-	HA	102	GLY	HA2	6.0	106	THR	HN	121	VAL	HB	6.0	110	LYS+	HB1	117	VAL	HB	6.0
101	ASP-	HA	102	GLY	HN	3.0	106	THR	HN	121	VAL	HN	4.5	110	LYS+	HB2	110	LYS+	HB1	2.5
101	ASP-	HB1	102	GLY	HN	6.0	106	THR	HN	121	VAL	QG1	5.6	110	LYS+	HB2	110	LYS+	QD	4.4
101	ASP-	HB1	103	LYS+	HN	6.0	106	THR	HN	121	VAL	QG2	7.1	110	LYS+	HB2	111	LEU	HN	4.5
101	ASP-	HB2	101	ASP-	HB1	2.5	106	THR	QG2	107	ILE	HN	7.1	110	LYS+	HN	110	LYS+	HA	3.5
101	ASP-	HB2	102	GLY	HN	4.5	106	THR	QG2	121	VAL	HN	7.1	110	LYS+	HN	110	LYS+	HB1	4.5
101	ASP-	HB2	103	LYS+	HG2	6.0	107	ILE	N	96	GLN	O	3.2	110	LYS+	HN	110	LYS+	HB2	4.0
101	ASP-	HN	101	ASP-	HA	2.5	107	ILE	HA	107	ILE	HB	3.5	110	LYS+	HN	110	LYS+	QG	4.4
101	ASP-	HN	101	ASP-	HB1	4.0	107	ILE	HA	107	ILE	QD1	4.6	110	LYS+	HN	116	LEU	QD1	5.1
101	ASP-	HN	101	ASP-	HB2	4.5	107	ILE	HA	107	ILE	QG2	4.1	110	LYS+	HN	117	VAL	HB	4.0
101	ASP-	HN	102	GLY	HN	3.5	107	ILE	HA	108	THR	HN	2.5	110	LYS+	HN	117	VAL	HN	3.5
101	ASP-	HN	103	LYS+	HN	6.0	107	ILE	HA	120	CYSS	HB1	4.5	110	LYS+	HN	117	VAL	O	2.2
102	GLY	HA1	102	GLY	HA2	2.5	107	ILE	HA	121	VAL	HN	4.5	110	LYS+	HN	118	VAL	HA	4.5
102	GLY	HA1	103	LYS+	HN	3.5	107	ILE	HB	107	ILE	QD1	5.1	110	LYS+	QD	112	LYS+	QE	7.8
102	GLY	HA2	103	LYS+	HN	3.5	107	ILE	HB	107	ILE	QG2	3.6	110	LYS+	QD	117	VAL	HB	5.9
102	GLY	HN	102	GLY	HA1	3.5	107	ILE	HB	109	ARG+	HG1	6.0	110	LYS+	QE	112	LYS+	HG1	6.9
102	GLY	HN	102	GLY	HA2	3.0	107	ILE	HN	96	GLN	O	2.2	110	LYS+	QE	112	LYS+	HG2	6.9
102	GLY	HN	103	LYS+	HN	3.0	107	ILE	HN	107	ILE	HB	3.5	110	LYS+	QE	112	LYS+	QE	5.3
103	LYS+	N	100	TRP	O	3.2	107	ILE	HN	107	ILE	QD								

111 LEU	HN	112 LYS+	HN	4.5	116 LEU	HB1	131 TYR	HB2	6.0	119 GLU-	HB2	128 THR	QG2	6.1
111 LEU	HN	116 LEU	QD1	7.1	116 LEU	HB1	131 TYR	HN	6.0	119 GLU-	HG1	119 GLU-	HB1	3.5
111 LEU	QD1	111 LEU	QD2	4.7	116 LEU	HB1	131 TYR	QD	8.2	119 GLU-	HG1	119 GLU-	HB2	3.0
111 LEU	QD1	112 LYS+	HN	4.1	116 LEU	HB2	116 LEU	HB1	3.5	119 GLU-	HG1	128 THR	HA	4.5
111 LEU	QD1	114 GLY	HA1	5.6	116 LEU	HB2	116 LEU	HG	3.5	119 GLU-	HG1	128 THR	QG2	4.6
111 LEU	QD1	115 LYS+	HN	5.6	116 LEU	HB2	116 LEU	QD1	5.1	119 GLU-	HG2	119 GLU-	HB1	3.0
111 LEU	QD1	116 LEU	HB1	7.1	116 LEU	HB2	116 LEU	QD2	4.1	119 GLU-	HG2	128 THR	QG2	4.6
111 LEU	QD1	116 LEU	HN	7.1	116 LEU	HB2	117 VAL	HN	4.5	119 GLU-	HN	108 THR	O	2.2
111 LEU	QD2	112 LYS+	HN	5.1	116 LEU	HB2	131 TYR	HN	6.0	119 GLU-	HN	119 GLU-	HA	3.5
111 LEU	QD2	115 LYS+	HN	7.1	116 LEU	HB2	131 TYR	QD	6.2	119 GLU-	HN	119 GLU-	HB1	4.0
111 LEU	QD2	116 LEU	HA	4.6	116 LEU	HG	116 LEU	HB1	3.5	119 GLU-	HN	119 GLU-	HB2	4.5
111 LEU	QD2	116 LEU	HB1	4.6	116 LEU	HG	116 LEU	QD1	3.6	119 GLU-	HN	119 GLU-	HG1	4.0
111 LEU	QD2	116 LEU	HN	7.1	116 LEU	HG	116 LEU	QD2	3.6	119 GLU-	HN	119 GLU-	HG2	4.0
111 LEU	QD2	116 LEU	QD1	5.7	116 LEU	HG	117 VAL	HN	4.0	119 GLU-	QG	120 CYSS	HN	6.9
112 LYS+	HA	112 LYS+	HB1	3.5	116 LEU	HG	131 TYR	QD	6.7	120 CYSS	N	127 CYSS	O	3.2
112 LYS+	HA	112 LYS+	HB2	3.5	116 LEU	HN	116 LEU	HA	3.5	120 CYSS	CB	127 CYSS	SG	3.5
112 LYS+	HA	112 LYS+	HD2	6.0	116 LEU	HN	116 LEU	HB1	4.5	120 CYSS	HA	120 CYSS	HB1	3.5
112 LYS+	HA	112 LYS+	HG1	3.5	116 LEU	HN	116 LEU	HB2	4.5	120 CYSS	HA	120 CYSS	HB2	3.0
112 LYS+	HA	112 LYS+	HG2	3.5	116 LEU	HN	116 LEU	HG	5.0	120 CYSS	HA	121 VAL	HN	2.5
112 LYS+	HA	112 LYS+	QE	6.9	116 LEU	HN	116 LEU	QD1	6.1	120 CYSS	HB1	121 VAL	HN	4.5
112 LYS+	HA	113 ASP-	HN	3.0	116 LEU	HN	116 LEU	QD2	6.1	120 CYSS	HB2	121 VAL	HN	4.5
112 LYS+	HA	114 GLY	HN	4.5	116 LEU	HN	117 VAL	HN	6.0	120 CYSS	HB2	127 CYSS	HN	6.0
112 LYS+	HA	115 LYS+	HN	6.0	116 LEU	HN	130 ILE	QG2	5.6	120 CYSS	HN	120 CYSS	HA	3.5
112 LYS+	HB1	112 LYS+	HG1	3.5	116 LEU	HN	131 TYR	HB2	4.5	120 CYSS	HN	120 CYSS	HB1	4.5
112 LYS+	HB1	112 LYS+	HG2	3.5	116 LEU	HN	131 TYR	HN	4.5	120 CYSS	HN	120 CYSS	HB2	4.5
112 LYS+	HB1	113 ASP-	HN	5.0	116 LEU	HN	131 TYR	O	2.2	120 CYSS	HN	127 CYSS	HN	5.0
112 LYS+	HB1	117 VAL	QG2	4.1	116 LEU	HN	132 GLU-	HA	4.5	120 CYSS	HN	127 CYSS	O	2.2
112 LYS+	HB2	112 LYS+	HB1	2.5	116 LEU	QD1	116 LEU	HB1	4.1	120 CYSS	HN	128 THR	HA	4.5
112 LYS+	HB2	117 VAL	QG2	5.1	116 LEU	QD1	116 LEU	QD2	5.2	120 CYSS	SG	127 CYSS	CB	3.5
112 LYS+	HD2	117 VAL	HB	3.5	116 LEU	QD1	117 VAL	HN	4.6	120 CYSS	SG	127 CYSS	SG	2.5
112 LYS+	HG1	112 LYS+	HG2	2.5	116 LEU	QD1	118 VAL	QG2	6.2	121 VAL	N	106 THR	O	3.2
112 LYS+	HG1	113 ASP-	HN	6.0	116 LEU	QD2	116 LEU	HB1	4.1	121 VAL	HA	121 VAL	QG1	5.6
112 LYS+	HG2	117 VAL	QG2	5.6	116 LEU	QD2	118 VAL	QG2	6.2	121 VAL	HA	121 VAL	QG2	4.1
112 LYS+	HN	112 LYS+	HA	3.5	116 LEU	QD2	131 TYR	HA	7.1	121 VAL	HA	122 MET	HN	2.5
112 LYS+	HN	112 LYS+	HB1	3.5	116 LEU	QD2	131 TYR	HB1	5.6	121 VAL	HA	126 THR	HA	3.5
112 LYS+	HN	112 LYS+	HB2	4.5	116 LEU	QD2	131 TYR	HB2	4.6	121 VAL	HA	126 THR	HB	6.0
112 LYS+	HN	112 LYS+	HG1	6.0	116 LEU	QD2	131 TYR	HN	6.1	121 VAL	HA	126 THR	QG2	4.6
112 LYS+	HN	112 LYS+	HG2	6.0	116 LEU	QD2	131 TYR	QD	6.8	121 VAL	HA	127 CYSS	HN	4.5
112 LYS+	HN	113 ASP-	HN	4.5	116 LEU	QD2	131 TYR	QE	7.8	121 VAL	HA	127 CYSS	HN	6.0
112 LYS+	HN	114 GLY	HN	6.0	117 VAL	N	110 LYS+	O	3.2	121 VAL	HB	121 VAL	QG1	3.6
112 LYS+	HN	115 LYS+	HN	3.5	117 VAL	HA	117 VAL	HB	4.5	121 VAL	HB	121 VAL	QG2	3.6
112 LYS+	HN	116 LEU	HA	4.0	117 VAL	HA	117 VAL	QG2	3.6	121 VAL	HB	122 MET	HN	4.5
112 LYS+	HN	117 VAL	QG2	5.1	117 VAL	HA	118 VAL	HN	2.5	121 VAL	HB	126 THR	HA	4.5
112 LYS+	QE	112 LYS+	HB1	5.4	117 VAL	HA	130 ILE	HA	6.0	121 VAL	HB	126 THR	QG2	3.6
112 LYS+	QE	112 LYS+	HD1	3.4	117 VAL	HA	130 ILE	QG2	5.1	121 VAL	HB	127 CYSS	HN	5.0
112 LYS+	QE	112 LYS+	HD2	3.4	117 VAL	HB	117 VAL	QG2	3.6	121 VAL	HN	106 THR	O	2.2
112 LYS+	QE	112 LYS+	HG2	4.4	117 VAL	HB	118 VAL	HN	4.5	121 VAL	HN	121 VAL	HA	3.0
112 LYS+	QE	117 VAL	QG2	5.5	117 VAL	HN	110 LYS+	O	2.2	121 VAL	HN	121 VAL	HB	3.5
113 ASP-	HA	113 ASP-	HB1	4.0	117 VAL	HN	117 VAL	HA	4.5	121 VAL	HN	121 VAL	QG1	4.6
113 ASP-	HA	113 ASP-	HB2	3.5	117 VAL	HN	117 VAL	HB	3.0	121 VAL	HN	121 VAL	QG2	6.1
113 ASP-	HA	114 GLY	HN	3.5	117 VAL	HN	117 VAL	QG1	5.6	121 VAL	HN	122 MET	HN	4.5
113 ASP-	HA	115 LYS+	HN	4.5	117 VAL	HN	117 VAL	QG2	4.1	121 VAL	QG1	122 MET	HN	5.6
113 ASP-	HB1	113 ASP-	HB2	2.5	117 VAL	HN	118 VAL	HN	6.0	121 VAL	QG2	122 MET	HN	5.1
113 ASP-	HB1	114 GLY	HN	5.0	117 VAL	QG1	118 VAL	HN	5.1	121 VAL	QG2	124 ASN	HA	6.1
113 ASP-	HB2	114 GLY	HN	5.5	117 VAL	QG1	128 THR	QG2	5.7	121 VAL	QG2	124 ASN	HN	5.1
113 ASP-	HN	113 ASP-	HA	3.0	117 VAL	QG1	130 ILE	HA	5.6	121 VAL	QG2	125 VAL	HN	5.1
113 ASP-	HN	113 ASP-	HB1	4.0	117 VAL	QG2	117 VAL	QG1	4.7	121 VAL	QG2	126 THR	HA	5.6
113 ASP-	HN	113 ASP-	HB2	4.5	117 VAL	QG2	118 VAL	HN	6.1	121 VAL	QG2	126 THR	HB	6.1
113 ASP-	HN	114 GLY	HN	6.0	117 VAL	QG2	130 ILE	QD1	4.7	121 VAL	QG2	126 THR	HN	7.1
114 GLY	HA1	114 GLY	HA2	2.5	118 VAL	N	129 ARG+	O	3.2	121 VAL	QG2	126 THR	QG2	4.7
114 GLY	HA1	115 LYS+	HN	4.0	118 VAL	HA	118 VAL	HB	4.5	122 MET	HA	122 MET	HB1	3.5
114 GLY	HA2	115 LYS+	HN	4.0	118 VAL	HA	119 GLU-	HN	2.5	122 MET	HA	122 MET	HG1	4.5
114 GLY	HN	114 GLY	HA1	3.0	118 VAL	HB	118 VAL	QG1	3.6	122 MET	HA	123 ASN	HN	3.5
114 GLY	HN	114 GLY	HA2	3.0	118 VAL	HB	118 VAL	QG2	3.6	122 MET	HB1	123 ASN	HN	5.0
114 GLY	HN	115 LYS+	HN	3.0	118 VAL	HB	129 ARG+	HG1	6.0	122 MET	HG1	122 MET	HB1	3.5
115 LYS+	HA	115 LYS+	HB1	3.5	118 VAL	HB	129 ARG+	HG2	5.0	122 MET	HG1	122 MET	QE	4.1
115 LYS+	HA	115 LYS+	HB2	3.5	118 VAL	HB	129 ARG+	HN	3.5	122 MET	HG1	123 ASN	HD21	4.0
115 LYS+	HA	115 LYS+	HD1	4.5	118 VAL	HB	131 TYR	QE	6.7	122 MET	HG1	123 ASN	HD22	4.0
115 LYS+	HA	115 LYS+	QG	4.4	118 VAL	HN	118 VAL	HA	4.5	122 MET	HG1	123 ASN	HN	4.5
115 LYS+	HA	116 LEU	HN	2.5	118 VAL	HN	118 VAL	HB	3.5	122 MET	HG2	122 MET	HB1	3.5
115 LYS+	HA	132 GLU-	HA	4.0	118 VAL	HN	118 VAL	QG1	6.1	122 MET	HG2	122 MET	HG1	2.5
115 LYS+	HB1	115 LYS+	QG	3.4	118 VAL	HN	118 VAL	QG2	4.6	122 MET	HG2	122 MET	QE	4.1
115 LYS+	HB1	116 LEU	HN	4.5	118 VAL	HN	119 GLU-	HN	6.0	122 MET	HG2	123 ASN	HD21	5.0
115 LYS+	HB1	130 ILE	QG2	5.1	118 VAL	HN	128 THR	QG2	6.1	122 MET	HG2	123 ASN	HD22	5.0
115 LYS+	HB2	115 LYS+	HB1	2.5	118 VAL	HN	129 ARG+	HN	3.5	122 MET	HG2	123 ASN	HN	4.5
115 LYS+	HB2	115 LYS+	HD1	4.5	118 VAL	HN	129 ARG+	O	4.5	122 MET	HN	122 MET	HA	4.5
115 LYS+	HB2	115 LYS+	HD2	4.5	118 VAL	HN	129 ARG+	O	2.2	122 MET	HN	122 MET	HB1	4.5
115 LYS+	HB2	116 LEU	HN	4.5	118 VAL	HN	130 ILE	HA	4.5	122 MET	HN	123 ASN	HN	6.0
115 LYS+	HB2	117 VAL	QG2	7.1	118 VAL	HN	130 ILE	QD1	5.6	122 MET	HN	125 VAL	HB	4.5
115 LYS+	HB2	130 ILE	QG2	4.1	118 VAL	HN	131 TYR	HN	5.0	122 MET	HN	125 VAL	HN	4.0
115 LYS+	HD1	115 LYS+	QG	3.4	118 VAL	HN	131 TYR	QD	8.2	122 MET	HN	125 VAL	QG1	6.6
115 LYS+	HD1	132 GLU-	QB	5.4	118 VAL	HN	131 TYR	QE	7.2	122 MET	HN	125 VAL	QG2	7.1
115 LYS+	HD2	116 LEU	HN	4.5	118 VAL	QG1	119 GLU-	HN	5.6	122 MET	HN	126 THR	HA	4.5
115 LYS+	HD2	130 ILE	QG2	5.6	118 VAL	QG1	129 ARG+	HG2	5.6	122 MET	HN	126 THR	QG2	5.6
115 LYS+	HD2	132 GLU-	QB	5.4	118 VAL	QG1	129 ARG+	HN	7.1	122 MET	QE	122 MET	HB1	6.1
115 LYS+	HN	115 LYS+	HA	3.5	118 VAL	QG1	131 TYR	QE	7.8	122 MET	QE	123 ASN	HD21	5.6
115 LYS+	HN	115 LYS+	HB1	3.5	118 VAL	QG2	118 VAL	QG1	4.7	122 MET	QE	123 ASN	HD22	5.6
115 LYS+	HN	115 LYS+	HB2	4.0	118 VAL	QG2	119 GLU-	HN	6.1	123 ASN	HA	123 ASN	HB1	3.5
115 LYS+	HN	115 LYS+	HD1	6.0	118 VAL	QG2	129 ARG+	HE	7.1	123 ASN	HA	123 ASN	HB2	3.0
115 LYS+	HN	115 LYS+	QG	5.4	118 VAL	QG2	129 ARG+	HG2	7.1	123 ASN	HA	124 ASN	HN	3.5
115 LYS+	HN	116 LEU	HN	5.0	118 VAL	QG2	129 ARG+	HN	7.1	123 ASN	HA	125 VAL	HN	6.0
115 LYS+	QE	115 LYS+	HD2	4.4	118 VAL	QG2	131 TYR	QD	6.3	123 ASN	HB1	123 ASN	HB2	2.5
115 LYS+	QE	115 LYS+	QG	5.3	118 VAL	QG2	131 TYR	QE	5.8	123 ASN	HB1	124 ASN	HN	5.0
115 LYS+	QE	132 GLU-	HA	5.4	119 GLU-	N	108 THR	O	3.2	123 ASN	HB2	124 ASN	HN	5.0
115 LYS+	QE	132 GLU-	QB	7.8	119 GLU-	HA	119 GLU-	HB2	3.5	123 ASN	HD21	123 ASN	HA	5.0
115 LYS+	QG	116 LEU	HN	6.4	119 GLU-	HA	119 GLU-	HG1	3.5	123 ASN	HD21	123 ASN	HB1	4.0
115 LYS+	QG	130 ILE	QG2	5.5	119 GLU-	HA	119 GLU-	HG2	3.5	123 ASN	HD21	123 ASN	HB2	4.0
116 LEU	N	131 TYR	O	3.2	119 GLU-	HA	120 CYSS	HN	2.5	123 ASN	HD21	123 ASN	HD22	2.5

124 ASN	HA	124 ASN	HB2	3.5	130 ILE	HN	130 ILE	HG11	4.5	<b>Lower limit list</b>				
124 ASN	HA	125 VAL	HN	4.0	130 ILE	HN	130 ILE	HG12	4.5					
124 ASN	HB1	125 VAL	QG2	6.1	130 ILE	HN	130 ILE	QD1	5.1					
124 ASN	HB2	124 ASN	HB1	2.5	130 ILE	HN	130 ILE	QG2	5.6					
124 ASN	HD21	124 ASN	HA	6.0	130 ILE	HN	131 TYR	HN	6.0					
124 ASN	HD21	124 ASN	HB1	4.0	130 ILE	QD1	131 TYR	HN	5.6					
124 ASN	HD21	124 ASN	HB2	4.5	130 ILE	QG2	131 TYR	HN	4.1					
124 ASN	HD21	124 ASN	HD22	2.5	131 TYR	N	116 LEU	O	3.2					
124 ASN	HD22	124 ASN	HB1	4.5	131 TYR	HA	131 TYR	HB1	4.5					
124 ASN	HD22	124 ASN	HB2	5.0	131 TYR	HA	131 TYR	HB2	5.0					
124 ASN	HD22	124 ASN	HD21	2.5	131 TYR	HA	132 GLU-	HN	2.5					
124 ASN	HN	124 ASN	HA	3.5	131 TYR	HB1	132 GLU-	HN	5.0					
124 ASN	HN	124 ASN	HB1	4.5	131 TYR	HB2	132 GLU-	HN	4.5					
124 ASN	HN	124 ASN	HB2	4.5	131 TYR	HN	116 LEU	O	2.2					
124 ASN	HN	124 ASN	HD21	6.0	131 TYR	HN	131 TYR	HA	4.5					
124 ASN	HN	124 ASN	HD22	6.0	131 TYR	HN	131 TYR	HB1	4.5					
124 ASN	HN	125 VAL	HN	3.5	131 TYR	HN	131 TYR	HB2	6.0					
125 VAL	HA	125 VAL	HB	3.5	131 TYR	HN	131 TYR	QD	5.7					
125 VAL	HA	125 VAL	QG1	4.1	131 TYR	HN	132 GLU-	HN	6.0					
125 VAL	HA	125 VAL	QG2	3.6	131 TYR	QD	131 TYR	HA	5.7					
125 VAL	HA	126 THR	HN	2.5	131 TYR	QD	131 TYR	HB1	5.7					
125 VAL	HB	125 VAL	QG1	3.6	131 TYR	QD	131 TYR	HB2	4.7					
125 VAL	HB	125 VAL	QG2	3.6	131 TYR	QD	131 TYR	QE	6.9					
125 VAL	HB	126 THR	HN	4.5	131 TYR	QD	132 GLU-	HN	6.7					
125 VAL	HN	125 VAL	HA	3.5	131 TYR	QE	131 TYR	HB1	8.2					
125 VAL	HN	125 VAL	HB	2.5	131 TYR	QE	131 TYR	HB2	8.2					
125 VAL	HN	125 VAL	QG1	5.6	132 GLU-	N	12 ARG+	O	3.2					
125 VAL	HN	125 VAL	QG2	4.1	132 GLU-	HA	132 GLU-	HG1	4.5					
125 VAL	HN	126 THR	HN	4.5	132 GLU-	HA	132 GLU-	HG2	4.5					
125 VAL	HN	126 THR	HN	4.5	132 GLU-	HA	132 GLU-	QB	3.4					
125 VAL	QG1	126 THR	HN	4.6	132 GLU-	HA	133 LYS+	HN	3.0					
125 VAL	QG2	126 THR	HN	6.1	132 GLU-	HG1	132 GLU-	QB	3.9					
126 THR	HA	126 THR	HB	2.5	132 GLU-	HG2	132 GLU-	HG1	2.5					
126 THR	HA	126 THR	QG2	3.6	132 GLU-	HG2	132 GLU-	QB	3.4					
126 THR	HA	127 CYSS	HN	2.5	132 GLU-	HG2	133 LYS+	HN	6.0					
126 THR	HA	127 CYSS	HN	2.5	132 GLU-	HN	12 ARG+	O	2.2					
126 THR	HB	126 THR	QG2	3.6	132 GLU-	HN	132 GLU-	HA	3.0					
126 THR	HB	127 CYSS	HN	3.5	132 GLU-	HN	132 GLU-	HG1	3.5					
126 THR	HN	126 THR	HA	3.0	132 GLU-	HN	132 GLU-	HG2	4.5					
126 THR	HN	126 THR	HB	4.0	132 GLU-	HN	132 GLU-	QB	4.4					
126 THR	HN	126 THR	QG2	4.1	132 GLU-	QB	133 LYS+	HN	4.4					
126 THR	HN	127 CYSS	HN	6.0	133 LYS+	HA	133 LYS+	HB1	3.0					
126 THR	HN	127 CYSS	HN	6.0	133 LYS+	HA	133 LYS+	HB2	3.5					
126 THR	QG2	127 CYSS	HN	5.6	133 LYS+	HA	133 LYS+	HD1	6.0					
126 THR	QG2	127 CYSS	HN	5.6	133 LYS+	HA	133 LYS+	HG1	4.0					
127 CYSS	HA	127 CYSS	HB1	3.5	133 LYS+	HA	133 LYS+	HG2	4.0					
127 CYSS	HA	127 CYSS	HB2	3.5	133 LYS+	HA	134 VAL	HN	2.5					
127 CYSS	HA	128 THR	HN	2.5	133 LYS+	HA	134 VAL	QG2	5.1					
127 CYSS	HB1	127 CYSS	HB2	3.5	133 LYS+	HB1	133 LYS+	HG1	3.5					
127 CYSS	HB1	128 THR	HN	4.5	133 LYS+	HB1	133 LYS+	HG2	3.5					
127 CYSS	HB2	128 THR	HN	5.0	133 LYS+	HB2	133 LYS+	HB1	2.5					
127 CYSS	HN	127 CYSS	HB1	6.0	133 LYS+	HB2	133 LYS+	HD1	4.5					
127 CYSS	HN	127 CYSS	HB2	4.5	133 LYS+	HB2	133 LYS+	HD2	3.5					
127 CYSS	HN	128 THR	HN	6.0	133 LYS+	HB2	133 LYS+	HG1	3.5					
128 THR	HA	128 THR	HB	4.5	133 LYS+	HB2	133 LYS+	HG2	3.5					
128 THR	HA	128 THR	QG2	3.6	133 LYS+	HB2	134 VAL	HN	4.5					
128 THR	HA	129 ARG+	HN	2.5	133 LYS+	HD1	133 LYS+	HG2	3.5					
128 THR	HB	128 THR	QG2	3.6	133 LYS+	HD1	134 VAL	HN	6.0					
128 THR	HB	129 ARG+	HN	4.5	133 LYS+	HD2	133 LYS+	HG2	3.5					
128 THR	HB	130 ILE	QD1	5.6	133 LYS+	HD2	134 VAL	HN	6.0					
128 THR	HN	128 THR	HA	3.0	133 LYS+	HD2	135 GLU-	QG	5.4					
128 THR	HN	128 THR	HB	3.5	133 LYS+	HE1	133 LYS+	HD1	6.0					
128 THR	HN	128 THR	QG2	5.6	133 LYS+	HE1	133 LYS+	HD2	3.5					
128 THR	HN	129 ARG+	HN	4.5	133 LYS+	HE1	133 LYS+	HG2	4.5					
128 THR	HN	129 ARG+	HN	4.5	133 LYS+	HE2	133 LYS+	HD1	4.5					
128 THR	QG2	129 ARG+	HN	4.6	133 LYS+	HE2	133 LYS+	HD2	4.5					
128 THR	QG2	130 ILE	HG11	7.1	133 LYS+	HE2	133 LYS+	HG1	4.0					
128 THR	QG2	130 ILE	QD1	4.7	133 LYS+	HE2	133 LYS+	HG2	4.5					
129 ARG+	N	118 VAL	O	3.2	133 LYS+	HG1	133 LYS+	HG2	2.5					
129 ARG+	HA	129 ARG+	HB1	3.5	133 LYS+	HG1	134 VAL	HN	3.5					
129 ARG+	HA	129 ARG+	HB2	3.5	133 LYS+	HG1	135 GLU-	QG	3.4					
129 ARG+	HA	129 ARG+	HD2	5.0	133 LYS+	HG2	134 VAL	HN	4.5					
129 ARG+	HA	130 ILE	HN	2.5	133 LYS+	HG2	135 GLU-	QG	6.9					
129 ARG+	HA	131 TYR	QE	8.2	133 LYS+	HN	133 LYS+	HA	3.5					
129 ARG+	HB1	129 ARG+	HB2	2.5	133 LYS+	HN	133 LYS+	HB1	3.5					
129 ARG+	HB1	130 ILE	HN	6.0	133 LYS+	HN	133 LYS+	HB2	3.5					
129 ARG+	HB2	130 ILE	HN	4.5	133 LYS+	HN	133 LYS+	HG1	5.0					
129 ARG+	HD2	129 ARG+	HB2	4.5	133 LYS+	HN	133 LYS+	HG2	5.5					
129 ARG+	HE	129 ARG+	HB1	3.5	133 LYS+	HN	134 VAL	HN	5.0					
129 ARG+	HE	129 ARG+	HB2	4.5	134 VAL	HA	134 VAL	HB	3.5					
129 ARG+	HE	129 ARG+	HG1	4.5	134 VAL	HA	134 VAL	QG1	4.1					
129 ARG+	HG2	129 ARG+	HB1	3.5	134 VAL	HA	134 VAL	QG2	4.1					
129 ARG+	HG2	129 ARG+	HB2	3.5	134 VAL	HA	135 GLU-	HN	2.5					
129 ARG+	HN	118 VAL	O	2.2	134 VAL	HB	134 VAL	QG1	3.6					
129 ARG+	HN	129 ARG+	HA	4.5	134 VAL	HB	134 VAL	QG2	3.6					
129 ARG+	HN	129 ARG+	HB1	6.0	134 VAL	HB	135 GLU-	HN	4.5					
129 ARG+	HN	129 ARG+	HB2	6.0	134 VAL	HN	134 VAL	HA	3.5					
129 ARG+	HN	130 ILE	HN	6.0	134 VAL	HN	134 VAL	HB	3.0					
129 ARG+	HN	130 ILE	HN	6.0	134 VAL	HN	134 VAL	QG1	5.6					
130 ILE	N	15 ASP-	O	3.2	134 VAL	HN	134 VAL	QG2	4.1					
130 ILE	HA	130 ILE	HB	3.5	134 VAL	HN	135 GLU-	HN	4.5					
130 ILE	HA	130 ILE	HG11	4.5	134 VAL	HN	135 GLU-	QG	6.9					
130 ILE	HA	130 ILE	QD1	3.6	134 VAL	QG1	135 GLU-	HN	5.1					
130 ILE	HA	130 ILE	QG2	3.6	134 VAL	QG2	135 GLU-	HN	6.1					
130 ILE	HA	131 TYR	HN	2.5	135 GLU-	HA	135 GLU-	HB1	3.0					
130 ILE	HB	130 ILE	HG11	3.0	135 GLU-	HA	135 GLU-	HB2	3.5					
130 ILE	HB	130 ILE	HG12	3.5	135 GLU-	HA	135 GLU-	QG	3.9					
130 ILE	HB	131 TYR	HN	6.0	135 GLU-	HB1	135 GLU-	HB2	2.5					
130 ILE	HG11	130 ILE	HG12	2.5	135 GLU-	HN	135 GLU-	HA	3.0					
130 ILE	HG11	130 ILE	QD1	3.6	135 GLU-	HN	135 GLU-	HB1	4.0					
130 ILE	HG11	131 TYR	HN	5.5	135 GLU-	HN	135 GLU-	HB2	4.0					
130 ILE	HG12	130 ILE	QD1	3.6	135 GLU-	HN	135 GLU-	QG	4.9					
130 ILE	HG12	130 ILE	QG2	4.6	135 GLU-	QG	135 GLU-	HB1	3.9					
130 ILE	HN	15 ASP-	O	2.2	135 GLU-	QG	135 GLU-	HB2	3.9					
130 ILE	HN	130 ILE	HB	3.0										







```

=====
% Dataset: (1H, 15N)-HSQC of EFABP in H2O at 298K at 600MHz T1-Measurements
=====

NOISE=0.100
T_MIX=[16      32      48      96     128     192     384     512     768]*1e-3

%-----
% acquisition parameters as shown by "dpa" in "uxnmr"
%-----

BF= [ 60.81                600.13      ];   % in [MHz]
OF= [ 7814.3              2821        ];   % in [Hz]
SW= [ 2131.29            3591.954     ];   % in [Hz]
TD= [ 512/2              2048/2      ];   % complex points

%-----
% processing parameters as shown by "dpp" in "uxnmr"
%-----

SI= [ 1024                1024        ];   % real points
SR= [ 530.32             -21.52-3591.954/2 ];   % in [Hz]
%SR= [ 549.19           -2075.6      ];   % in [Hz]
SSB= [ 2                  2          ];   % sinebell phase shift

=====
% Dataset: (1H, 15N)-HSQC of EFABP in H2O at 298K at 600MHz T2-Measurements
=====

NOISE=0.100
T_MIX=[25.64     51.28     76.92     128.21     153.85     179.49     205.13
256.42     282.06]*1e-3

%-----
% acquisition parameters as shown by "dpa" in "uxnmr"
%-----

BF= [ 60.81                600.13      ];   % in [MHz]
OF= [ 7814.3              2821        ];   % in [Hz]
SW= [ 2131.29            3591.954     ];   % in [Hz]
TD= [ 512/2              2048/2      ];   % complex points

%-----
% processing parameters as shown by "dpp" in "uxnmr"
%-----

SI= [ 1024                1024        ];   % real points
SR= [ 530.32             -21.52-3591.954/2 ];   % in [Hz]
%SR= [ 549.19           -2075.6      ];   % in [Hz]
SSB= [ 2                  2          ];   % sinebell phase shift

```

```

=====
% Dataset: (1H, 15N)-HSQC of EFABP in H2O at 298K at 800MHz NOE-Measurements
=====

```

```

NOISE=0.100
T_MIX=[1 5]

```

```

%-----
% acquisition parameters as shown by "dpa" in "uxnmr"
%-----

```

```

BF= [ 81.08           800.13      ]; % in [MHz]
OF= [ 9540.0         3751.0       ]; % in [Hz]
SW= [ 2840.91        4882.81      ]; % in [Hz]
TD= [ 512/2          2048/2       ]; % complex points

```

```

%-----
% processing parameters as shown by "dpp" in "uxnmr"
%-----

```

```

SI= [ 1024           1024         ]; % real points
SR= [ -178.34        -42.72-4882.81/2 ]; % in [Hz]
%SR= [ 549.19         -2075.6       ]; % in [Hz]
SSB= [ 2              2           ]; % sinebell phase shift

```

```

=====
% Dataset: (1H, 15N)-HSQC of EFABP in H2O at 298K at 800MHz T1-Measurements
=====

```

```

NOISE=0.100
T_MIX=[20 40 60 80 100 120 160 240 320 480 640
960]*1e-3

```

```

%-----
% acquisition parameters as shown by "dpa" in "uxnmr"
%-----

```

```

BF= [ 81.08           800.13      ]; % in [MHz]
OF= [ 9540.0         3751.0       ]; % in [Hz]
SW= [ 2840.91        4882.81      ]; % in [Hz]
TD= [ 512/2          2048/2       ]; % complex points

```

```

%-----
% processing parameters as shown by "dpp" in "uxnmr"
%-----

```

```

SI= [ 1024           1024         ]; % real points
SR= [ -178.34        -42.72-4882.81/2 ]; % in [Hz]
%SR= [ 549.19         -2075.6       ]; % in [Hz]
SSB= [ 2              2           ]; % sinebell phase shift

```



---

**Appendix A.3 Stereospecific assignments used in the DYANA calculations. Residues with reversed stereospecific assignments are marked with “r”.**

```

atoms stereo HA1 9 18 29 36 80 92 102 114
9r18r 80r92r
atoms stereo HB1 5 7 8 11 15 16 19 21 22 23 24 25 26 33 34 35 48
5r7r 15r 19r21r22r 24r 26r 35r48r
atoms stereo HB1 51 52 55 57 61 64 65 66 67 69 79 82 84 87 88 89
52r 57r61r64r65r66r67r69r79r 84r87r 89r
atoms stereo HB1 91 94 97 98 99 100 101 104 105 109 110 111 112
91r94r97r98r99r 101r104r 109r110r111r112r
atoms stereo HB1 113 115 116 119 120 122 123 124 127 131 133 135
115r116r119r120r122r 124r 131r133r
atoms stereo HG1 5 6 8 17 21 23 25 38 41 57 71 75 81 82 84 96 98
6r8r 38r41r57r 75r81r82r84r 98r
atoms stereo HG1 99 103 109 112 119 122 129 132 133
119r122r129r132r
atoms stereo HD1 10 12 41 81 109 112 133
12r 81r109r112r133r
atoms stereo HD21 51 88 123 124
atoms stereo HE1
atoms stereo HE21 5 6 98
atoms stereo HG11 30 44 45
30r 45r
atoms stereo QG1 4 14 28 95 117 118 125 134
4r 95r117r118r125r
atoms stereo QD1 7 13 26 32 60 69 94 111 116
13r26r 69r

```

**Appendix A.4**  $^{15}\text{N}$  relaxation data of human E-FABP at 3 different fields. s.d. represents the standard deviation. The NOE error was set to a constant value (0.03) for all residues.

499.870 MHz

AA	R1 [1/s]	s.d. [1/s]	R2 [1/s]	s.d. [1/s]	NOE	error
M1						
A2						
T3	1,587	0,084	3,734	0,295	0,468	0,030
V4	1,724	0,024	10,325	0,456	0,834	0,030
Q5	1,788	0,046	10,748	0,214	0,774	0,030
Q6	1,708	0,036	9,878	0,239	0,767	0,030
L7	1,781	0,046	10,218	0,157	0,837	0,030
E8	1,642	0,022	10,425	0,144	0,777	0,030
G9	1,681	0,053	9,494	0,232	0,800	0,030
R10	1,734	0,027	10,834	0,127	0,784	0,030
W11	1,692	0,074	9,275	0,835	0,846	0,030
R12	1,678	0,030	9,864	0,373	0,769	0,030
L13	1,776	0,127	10,109	0,944		
V14						
D15	1,661	0,038	10,085	0,296	0,716	0,030
S16	1,569	0,024	9,491	0,123	0,739	0,030
K17	1,636	0,019	10,172	0,332	0,833	0,030
G18	1,700	0,073	10,555	0,134	0,770	0,030
F19	1,775	0,065	11,152	0,390	0,807	0,030
D20	1,868	0,079	10,760	0,289	0,771	0,030
E21	1,758	0,045	10,243	0,370	0,840	0,030
Y22	1,663	0,177			0,922	0,030
M23						
K24	1,982	0,121	10,342	0,386	0,724	0,030
E25	1,811	0,037	10,418	0,139	0,763	0,030
L26	1,681	0,023	10,478	0,327	0,801	0,030
G27	1,673	0,023	9,806	0,193	0,831	0,030
V28	1,649	0,066	11,009	0,530	0,854	0,030
G29	1,687	0,036	9,910	0,144	0,726	0,030
I30	1,694	0,045	9,550	0,224	0,675	0,030
A31	1,822	0,016	10,682	0,157	0,722	0,030
L32	1,576	0,038	9,933	0,206	0,728	0,030
R33	1,658	0,030	8,771	0,487	0,719	0,030
K34						
M35	1,598	0,045	10,083	0,129	0,770	0,030
G36	1,614	0,061	10,295	0,477	0,762	0,030
A37	1,729	0,076	10,498	0,822	0,804	0,030
M38	1,638	0,068	9,079	0,395	0,702	0,030
A39	1,666	0,082	10,106	0,446	0,635	0,030
K40	1,761	0,229	8,333	0,636	0,677	0,030
P41						
D42	1,740	0,023	9,942	0,270	0,747	0,030
C43	1,849	0,115	10,011	0,339	0,766	0,030
I44	1,693	0,055	10,159	0,329	0,755	0,030
I45	1,688	0,035	10,104	0,214	0,831	0,030
T46	1,690	0,044	10,481	0,342	0,839	0,030
C47	1,733	0,034	9,621	0,138	0,783	0,030
D48						
G49	1,688	0,050	10,135	0,202	0,790	0,030
K50	1,718	0,085	9,409	0,561	0,730	0,030
N51	1,644	0,037	9,861	0,253	0,783	0,030

AA	R1 [1/s]	s.d. [1/s]	R2 [1/s]	s.d [1/s]	NOE	error
L52	1,691	0,058	9,649	0,315	0,788	0,030
T53	1,727	0,048	10,531	0,278	0,767	0,030
I54	1,836	0,103	10,774	0,255	0,737	0,030
K55	1,778	0,061	11,049	0,928	0,746	0,030
T56	1,658	0,060	9,321	0,410	0,903	0,030
E57	1,734	0,123	10,528	0,799	0,701	0,030
S58	1,672	0,088	8,371	0,607	0,647	0,030
T59						
L60						
K61	1,695	0,066	8,190	0,480	0,690	0,030
T62	1,858	0,089	9,815	0,662	0,683	0,030
T63	1,553	0,145	9,251	0,814	0,629	0,030
Q64	1,879	0,146	10,787	0,497	0,660	0,030
F65	1,829	0,062	10,502	0,377	0,820	0,030
S66						
C67	1,682	0,064	10,413	0,201	0,727	0,030
T68	1,702	0,033	10,159	0,301	0,803	0,030
L69	1,668	0,044	10,232	0,400	0,773	0,030
G70	1,660	0,061	10,158	0,226	0,734	0,030
E71	1,759	0,026	10,177	0,201	0,822	0,030
K72						
F73	1,790	0,059	10,205	0,312	0,760	0,030
E74	1,621	0,026	9,579	0,144	0,744	0,030
E75	1,745	0,049	9,828	0,339	0,753	0,030
T76	1,841	0,106	9,555	0,423	0,738	0,030
T77	1,650	0,058	10,548	0,253	0,875	0,030
A78	1,778	0,089	10,131	0,455	0,827	0,030
D79	1,768	0,076	10,417	0,658	0,764	0,030
G80	1,555	0,046	10,115	0,445	0,815	0,030
R81	1,651	0,037	9,795	0,357	0,744	0,030
K82	1,660	0,049	9,909	0,210	0,828	0,030
T83	1,630	0,029	9,818	0,139	0,766	0,030
Q84	1,633	0,036	10,360	0,225	0,798	0,030
T85	1,740	0,107	9,728	0,384	0,702	0,030
V86	1,588	0,059	11,298	0,373	0,737	0,030
C87	1,718	0,074	9,385	0,316	0,734	0,030
N88	1,702	0,038	9,982	0,284	0,745	0,030
F89	1,571	0,026	9,297	0,127	0,755	0,030
T90	1,609	0,054	9,915	0,151	0,804	0,030
D91	1,829	0,133	9,414	0,742	0,804	0,030
G92	1,599	0,027	9,310	0,219	0,744	0,030
A93	1,725	0,029	10,016	0,287	0,786	0,030
L94	1,761	0,051	10,273	0,366	0,852	0,030
V95	1,753	0,050	11,677	0,352	0,815	0,030
Q96						
H97	1,791	0,078	10,914	0,395	0,741	0,030
Q98	1,661	0,052	9,698	0,279	0,772	0,030
E99	1,558	0,043	10,208	0,320	0,771	0,030
W100	1,670	0,039	10,622	0,189	0,766	0,030
D101	1,706	0,026	9,650	0,271	0,788	0,030
G102	1,623	0,029	9,959	0,192	0,742	0,030
K103						
E104	1,543	0,024	9,093	0,143	0,728	0,030
S105	1,768	0,059	9,892	0,231	0,839	0,030
T106						
I107	1,832	0,073	9,560	0,515	0,645	0,030
T108	1,722	0,033	10,861	0,282	0,791	0,030
R109	1,691	0,090	10,355	0,362	0,764	0,030
K110	1,728	0,020	10,368	0,214	0,746	0,030



---

AA	R1 [1/s]	s.d. [1/s]	R2 [1/s]	s.d [1/s]	NOE	error
L111	1,565	0,032	10,062	0,107	0,682	0,030
K112	1,695	0,030	9,586	0,183	0,729	0,030
D113	1,741	0,116	10,429	0,441	0,761	0,030
G114	1,619	0,026	9,923	0,177	0,743	0,030
K115						
L116	1,728	0,049	10,173	0,257	0,821	0,030
V117	1,658	0,034	10,164	0,294	0,753	0,030
V118	1,783	0,042	10,181	0,352	0,742	0,030
E119	1,643	0,042	10,150	0,238	0,830	0,030
C120	1,714	0,071	10,007	0,337	0,726	0,030
V121	1,645	0,078	10,583	0,469	0,714	0,030
M122	1,746	0,024	10,193	0,351	0,813	0,030
N123	1,661	0,015	10,237	0,118	0,715	0,030
N124	1,618	0,119			0,787	0,030
V125						
T126	1,811	0,103	11,654	0,545	0,886	0,030
C127	1,696	0,055	10,266	0,435	0,854	0,030
T128	1,635	0,045	10,778	0,218	0,817	0,030
R129	1,840	0,048	10,382	0,360	0,730	0,030
I130	1,614	0,038	10,674	0,348	0,804	0,030
Y131	1,651	0,065	9,496	0,353	0,777	0,030
E132	1,692	0,024	10,367	0,171	0,770	0,030
K133	1,790	0,054	9,702	0,289	0,722	0,030
V134	1,683	0,022	9,498	0,162	0,738	0,030
E135	1,508	0,026	8,008	0,221	0,466	0,030

**(Cont.)**

600.130 MHz

AA	R1 [1/s]	s.d. [1/s]	R2 [1/s]	s.d. [1/s]	NOE	error
M1						
A2						
T3	1,312	0,149	7,687	0,809	0,797	0,030
V4	1,375	0,027	12,039	0,484	0,820	0,030
Q5	1,405	0,031	12,856	0,175	0,818	0,030
Q6	1,422	0,033	11,939	0,314	0,823	0,030
L7	1,383	0,022	11,812	0,337	0,806	0,030
E8	1,356	0,025	11,767	0,327	0,797	0,030
G9	1,283	0,042	10,988	0,466	0,819	0,030
R10	1,281	0,056	12,091	0,242	0,800	0,030
W11	1,371	0,095	11,454	0,502	0,796	0,030
R12	1,313	0,035	10,857	0,973	0,769	0,030
L13	1,432	0,093	10,586	0,509	0,829	0,030
V14						
D15	1,331	0,015	11,445	0,174	0,783	0,030
S16	1,231	0,028	10,611	0,150	0,791	0,030
K17	1,291	0,046	11,776	0,647	0,778	0,030
G18	1,422	0,066	11,167	0,467	0,807	0,030
F19	1,407	0,036	12,353	0,437	0,787	0,030
D20	1,529	0,102	11,431	0,791	0,906	0,030
E21	1,345	0,035	11,215	0,603	0,844	0,030
Y22	1,486	0,067	11,588	0,709	0,975	0,030
M23						
K24	1,319	0,061	11,742	0,779	0,863	0,030
E25	1,391	0,053	11,781	0,985	0,839	0,030
L26	1,333	0,037	11,535	0,564	0,850	0,030
G27	1,383	0,032	11,476	0,553	0,815	0,030
V28	1,296	0,091	12,132	0,606	0,941	0,030
G29	1,303	0,032	11,525	0,602	0,813	0,030
I30	1,294	0,036	10,284	0,424	0,819	0,030
A31	1,488	0,017	11,438	0,179	0,812	0,030
L32	1,308	0,039	11,391	0,417	0,754	0,030
R33	1,374	0,043	12,537	1,223	0,739	0,030
K34						
M35	1,265	0,055	11,522	0,459	0,811	0,030
G36	1,469	0,069	12,198	0,854	0,820	0,030
A37	1,313	0,040	12,158	0,355	0,821	0,030
M38	1,289	0,071	10,091	0,428	0,692	0,030
A39	1,301	0,067	11,312	0,214	0,772	0,030
K40	1,327	0,170	11,895	0,775	0,722	0,030
P41						
D42	1,361	0,044	11,697	0,189	0,867	0,030
C43	1,250	0,066	11,039	0,655	0,799	0,030
I44	1,437	0,091	10,857	0,654	0,734	0,030
I45	1,405	0,058	11,618	0,897	0,827	0,030
T46	1,375	0,045	12,073	0,609	0,773	0,030
C47	1,289	0,022	10,436	0,195	0,784	0,030
D48	1,516	0,044	12,595	0,648	0,842	0,030
G49	1,369	0,044	10,995	0,341	0,823	0,030
K50	1,388	0,043	10,667	0,317	0,803	0,030
N51	1,284	0,047	11,011	0,439	0,752	0,030

AA	R1 [1/s]	s.d. [1/s]	R2 [1/s]	s.d [1/s]	NOE	error
L52	1,304	0,037	11,168	0,482	0,788	0,030
T53	1,342	0,033	11,704	0,301	0,802	0,030
I54	1,268	0,040	11,424	0,469	0,814	0,030
K55	1,475	0,107	10,776	1,086	0,789	0,030
T56	1,337	0,087	11,509	0,665	0,808	0,030
E57	1,356	0,132	10,515	0,791	0,836	0,030
S58	1,443	0,111	10,097	1,077	0,783	0,030
T59						
L60						
K61	1,333	0,064	9,699	0,850	0,717	0,030
T62	1,535	0,073	10,957	0,598	0,831	0,030
T63	1,246	0,082	11,964	0,936	0,844	0,030
Q64	1,502	0,070	12,565	0,788	0,747	0,030
F65	1,370	0,036	11,927	0,330	0,824	0,030
S66						
C67	1,361	0,045	11,821	0,507	0,831	0,030
T68	1,267	0,053	11,575	0,480	0,779	0,030
L69	1,395	0,042	11,458	0,503	0,877	0,030
G70	1,328	0,061	10,610	0,562	0,840	0,030
E71	1,353	0,023	11,113	0,266	0,793	0,030
K72						
F73	1,428	0,043	10,915	0,424	0,768	0,030
E74	1,324	0,024	11,015	0,221	0,798	0,030
E75	1,410	0,048	12,718	0,776	0,795	0,030
T76	1,281	0,073	11,095	0,461	0,825	0,030
T77	1,354	0,052	12,079	0,503	0,806	0,030
A78	1,388	0,046	10,710	0,958	0,805	0,030
D79	1,406	0,123	12,575	0,778	0,788	0,030
G80	1,297	0,051	11,632	0,636	0,803	0,030
R81	1,259	0,049	11,581	0,494	0,762	0,030
K82	1,195	0,042	11,320	0,495	0,836	0,030
T83	1,280	0,033	11,137	0,422	0,791	0,030
Q84	1,324	0,046	11,602	0,383	0,819	0,030
T85	1,404	0,041	10,746	0,426	0,796	0,030
V86	1,455	0,070	10,489	0,500	0,811	0,030
C87	1,292	0,068	10,135	0,595	0,813	0,030
N88	1,310	0,027	11,391	0,344	0,835	0,030
F89	1,283	0,029	10,617	0,118	0,789	0,030
T90	1,299	0,028	11,032	0,269	0,809	0,030
D91	1,397	0,089	11,124	0,705	0,798	0,030
G92	1,324	0,037	10,945	0,518	0,811	0,030
A93	1,360	0,024	11,401	0,194	0,796	0,030
L94	1,320	0,063	11,604	0,181	0,856	0,030
V95	1,294	0,028	13,704	0,520	0,835	0,030
Q96						
H97	1,392	0,074	11,302	0,345	0,830	0,030
Q98	1,356	0,051	10,702	0,568	0,821	0,030
E99	1,304	0,043	10,914	0,256	0,765	0,030
W100	1,422	0,033	10,208	0,342	0,898	0,030
D101	1,351	0,022	11,246	0,244	0,811	0,030
G102	1,328	0,029	11,699	0,132	0,807	0,030
K103						
E104	1,275	0,021	10,439	0,397	0,773	0,030
S105	1,324	0,023	11,429	0,363	0,803	0,030
T106						
I107	1,313	0,071	11,026	0,952	0,855	0,030
T108	1,337	0,044	12,272	0,536	0,840	0,030
R109	1,350	0,064	11,452	0,584	0,752	0,030
K110	1,304	0,030	12,250	0,590	0,833	0,030

---

AA	R1 [1/s]	s.d. [1/s]	R2 [1/s]	s.d [1/s]	NOE	error
L111	1,301	0,024	11,109	0,232	0,760	0,030
K112	1,325	0,025	10,770	0,162	0,796	0,030
D113	1,362	0,092	11,125	0,614	0,816	0,030
G114	1,332	0,054	11,006	0,250	0,790	0,030
K115						
L116	1,372	0,076	11,610	0,302	0,799	0,030
V117	1,307	0,044	12,177	0,339	0,823	0,030
V118	1,336	0,062	10,854	0,587	0,792	0,030
E119	1,300	0,040	10,464	0,339	0,828	0,030
C120	1,319	0,069	11,811	0,726	0,806	0,030
V121	1,308	0,058	12,193	0,475	0,793	0,030
M122	1,413	0,024	11,670	0,297	0,832	0,030
N123	1,361	0,042	11,486	0,271	0,787	0,030
N124	1,420	0,130	11,896	0,205	0,682	0,030
V125						
T126	1,279	0,063	11,888	0,584	0,813	0,030
C127	1,362	0,072	11,971	1,036	0,924	0,030
T128	1,271	0,025	11,669	0,289	0,857	0,030
R129	1,328	0,032	12,563	0,473	0,791	0,030
I130	1,251	0,039	12,310	0,251	0,799	0,030
Y131	1,332	0,087	11,353	0,545	0,807	0,030
E132	1,348	0,047	11,582	0,279	0,838	0,030
K133	1,333	0,039	10,965	0,313	0,777	0,030
V134	1,403	0,023	10,730	0,167	0,779	0,030
E135	1,297	0,025	9,428	0,263	0,614	0,030

**(Cont.)**

800.130 MHz

AA	R1 [1/s]	s.d. [1/s]	R2 [1/s]	s.d [1/s]	NOE	error
M1						
A2						
T3	1,062	0,076	8,169	0,776	0,716	0,030
V4	0,998	0,010	14,972	0,286	0,815	0,030
Q5	1,001	0,014	15,969	0,316	0,834	0,030
Q6	1,015	0,009	14,580	0,202	0,850	0,030
L7	0,972	0,007	14,485	0,151	0,836	0,030
E8	0,952	0,009	14,535	0,174	0,849	0,030
G9	0,951	0,012	14,115	0,187	0,832	0,030
R10	0,915	0,012	15,055	0,324	0,825	0,030
W11	0,966	0,022	14,311	0,468	0,878	0,030
R12	0,927	0,023	14,187	0,370	0,829	0,030
L13	1,049	0,038	14,819	0,879	0,949	0,030
V14						
D15	0,962	0,007	13,815	0,178	0,825	0,030
S16	0,884	0,005	12,691	0,157	0,857	0,030
K17	0,931	0,009	14,987	0,352	0,838	0,030
G18	0,994	0,033	13,784	0,258	0,831	0,030
F19	0,949	0,013	14,500	0,227	0,870	0,030
D20	1,105	0,024	14,781	0,249	0,859	0,030
E21	0,935	0,015	14,040	0,234	0,886	0,030
Y22	1,017	0,026	17,449	0,897	0,942	0,030
M23						
K24	1,017	0,025	13,925	0,282	0,857	0,030
E25	0,981	0,008	15,687	0,224	0,866	0,030
L26	0,949	0,011	14,244	0,149	0,864	0,030
G27	0,952	0,014	14,112	0,219	0,837	0,030
V28	0,987	0,017	17,002	0,204	0,826	0,030
G29	0,976	0,010	14,577	0,270	0,780	0,030
I30	0,960	0,024	15,294	0,805	0,850	0,030
A31	1,076	0,009	14,464	0,179	0,823	0,030
L32	0,893	0,017	13,767	0,229	0,806	0,030
R33	0,984	0,026	15,008	0,428	0,800	0,030
K34						
M35	0,925	0,015	14,157	0,218	0,791	0,030
G36	1,002	0,034	15,160	0,323	0,815	0,030
A37	0,996	0,008	15,221	0,266	0,839	0,030
M38	0,940	0,013	12,953	0,375	0,744	0,030
A39	0,923	0,016	13,923	0,202	0,794	0,030
K40	0,950	0,051	12,115	0,338	0,759	0,030
P41						
D42	0,922	0,009	14,125	0,199	0,835	0,030
C43	0,915	0,016	13,724	0,135	0,831	0,030
I44	0,940	0,035	14,468	0,515	0,877	0,030
I45	0,907	0,009	14,422	0,154	0,847	0,030
T46	0,915	0,013	14,718	0,356	0,839	0,030
C47	0,906	0,008	13,595	0,261	0,825	0,030
D48	0,984	0,014	14,353	0,363	0,860	0,030
G49	0,957	0,013	14,521	0,238	0,848	0,030
K50	1,007	0,009	13,206	0,215	0,813	0,030
N51	0,899	0,009	13,788	0,178	0,809	0,030

AA	R1 [1/s]	s.d. [1/s]	R2 [1/s]	s.d [1/s]	NOE	error
L52	0,929	0,018	13,909	0,170	0,861	0,030
T53	0,919	0,011	14,266	0,188	0,883	0,030
I54	0,926	0,010	14,433	0,195	0,852	0,030
K55	1,011	0,028	14,114	0,682	0,864	0,030
T56	0,937	0,021	14,187	0,554	0,865	0,030
E57	0,946	0,047	13,960	0,401	0,762	0,030
S58	0,981	0,025	13,078	0,503	0,767	0,030
T59						
L60						
K61	1,007	0,012	12,456	0,186	0,758	0,030
T62	1,095	0,037	13,715	0,547	0,768	0,030
T63	1,009	0,031	13,733	0,257	0,807	0,030
Q64	1,016	0,063	14,382	0,282	0,836	0,030
F65	0,989	0,017	14,913	0,376	0,888	0,030
S66						
C67	0,957	0,011	14,643	0,243	0,851	0,030
T68	0,895	0,012	14,518	0,300	0,860	0,030
L69	0,966	0,016	15,176	0,338	0,863	0,030
G70	0,938	0,022	14,723	0,267	0,840	0,030
E71	0,987	0,011	14,146	0,108	0,862	0,030
K72						
F73	1,023	0,011	14,162	0,213	0,851	0,030
E74	0,921	0,009	13,238	0,087	0,841	0,030
E75	0,998	0,018	14,080	0,691	0,831	0,030
T76	0,878	0,010	13,919	0,276	0,824	0,030
T77	0,967	0,015	14,859	0,336	0,862	0,030
A78	0,976	0,041	14,471	0,605	0,892	0,030
D79	1,000	0,068	15,503	0,733	0,842	0,030
G80	0,924	0,021	15,813	0,166	0,849	0,030
R81	0,950	0,011	14,822	0,149	0,868	0,030
K82	0,835	0,005	14,564	0,476	0,847	0,030
T83	0,903	0,006	13,558	0,198	0,849	0,030
Q84	0,937	0,011	14,227	0,341	0,850	0,030
T85	0,963	0,014	13,811	0,277	0,874	0,030
V86	1,024	0,023	15,237	0,687	0,858	0,030
C87	0,928	0,014	13,586	0,235	0,863	0,030
N88	0,881	0,005	14,083	0,129	0,843	0,030
F89	0,929	0,010	13,356	0,195	0,832	0,030
T90	0,902	0,010	13,475	0,146	0,834	0,030
D91	0,998	0,047	13,825	0,355	0,803	0,030
G92	0,953	0,025	14,219	0,384	0,817	0,030
A93	0,998	0,006	14,482	0,151	0,798	0,030
L94	0,934	0,009	14,287	0,113	0,861	0,030
V95	0,924	0,015	18,454	0,307	0,900	0,030
Q96						
H97	0,957	0,010	15,344	0,341	0,873	0,030
Q98	0,937	0,018	13,698	0,246	0,877	0,030
E99	0,905	0,018	13,430	0,211	0,833	0,030
W100	0,961	0,012	13,873	0,229	0,883	0,030
D101	0,955	0,008	13,521	0,129	0,831	0,030
G102	0,943	0,011	13,821	0,131	0,825	0,030
K103						
E104	0,897	0,004	12,394	0,330	0,809	0,030
S105	0,929	0,011	13,637	0,224	0,867	0,030
T106						
I107	0,935	0,035	14,227	0,380	0,840	0,030
T108	0,925	0,013	16,747	0,236	0,865	0,030
R109	0,888	0,019	14,636	0,401	0,841	0,030
K110	0,905	0,012	15,124	0,217	0,853	0,030

---

AA	R1 [1/s]	s.d. [1/s]	R2 [1/s]	s.d [1/s]	NOE	error
L111	0,933	0,006	11,717	0,405	0,745	0,030
K112	0,934	0,016	13,098	0,457	0,823	0,030
D113	0,981	0,039	14,557	0,381	0,822	0,030
G114	0,951	0,016	13,520	0,118	0,824	0,030
K115						
L116	0,929	0,018	13,877	0,097	0,867	0,030
V117	0,909	0,014	15,108	0,226	0,865	0,030
V118	0,935	0,015	14,417	0,167	0,854	0,030
E119	0,893	0,015	14,076	0,132	0,859	0,030
C120	0,942	0,015	13,674	0,533	0,901	0,030
V121	0,953	0,024	14,877	0,217	0,886	0,030
M122	0,972	0,009	14,655	0,242	0,860	0,030
N123	0,959	0,014	14,748	0,185	0,830	0,030
N124	1,107	0,101			0,914	0,030
V125						
T126	0,952	0,014	16,546	0,989	0,896	0,030
C127	0,992	0,024	14,958	0,739	0,810	0,030
T128	0,870	0,008	14,866	0,122	0,865	0,030
R129	0,910	0,026	15,573	0,348	0,847	0,030
I130	0,823	0,017	14,639	0,323	0,863	0,030
Y131	0,931	0,024	14,644	0,616	0,883	0,030
E132	0,895	0,013	14,532	0,219	0,847	0,030
K133	0,950	0,024	13,831	0,238	0,833	0,030
V134	0,972	0,016	13,829	0,177	0,809	0,030
E135	0,938	0,009	11,307	0,078	0,605	0,030

## **Untersuchungen von Struktur und Dynamik des humanen epidermalen Fettsäurebindungsproteins mittels hochaufgelöster NMR-Spektroskopie.**

Das humane epidermale Fettsäurebindungsprotein (E-FABP) gehört zur Familie der intrazellulären Lipidbindungsproteine (LBP), die Fettsäuren, Gallensäuren oder Retinoide spezifisch binden und transportieren. Gallensäure-bindendes Protein (ILBP), zelluläre Retinoidbindungsproteine und mehrere Typen von Fettsäurebindungsproteinen (FABPs) sind Mitglieder dieser Proteinfamilie. Ihre Funktionen sind mit Fettsäure-Signalgebung sowie Zellwachstum, -regulation und -differenzierung in Verbindung gebracht worden. FABPs werden gewebespezifisch exprimiert und spielen eine wichtige Rolle im Metabolismus von langkettigen, nicht-gesättigten Fettsäuren.

Mindestens dreizehn verschiedene Typen von LBPs sind bis jetzt identifiziert worden. Sie enthalten 127-135 Aminosäurereste und werden nach dem Gewebe ihrer ersten Isolierung oder Identifizierung benannt. Die Sequenzübereinstimmung verschiedener LBPs rangiert zwischen 38 und 70 %. Die Übereinstimmung ist in Proteinen aus gleichen Geweben und unterschiedlichen Organismen höher als in Proteinen aus gleichen Organismen und unterschiedlichem Gewebe.

Rekombinantes humanes E-FABP enthält 135 Aminosäurereste (15.2 kDa) und zeigt eine starke Affinität zu Stearinsäure. Die Röntgenstruktur von humanem E-FABP zeigt die Existenz einer Disulfidbrücke zwischen Cysteinresten 120 und 127, was einzigartig in der ganzen LBP-Familie ist. Außerdem bildet E-FABP einen Komplex mit Psoriasin (auch bekannt als S100A7), einem Protein der S100-Genfamilie, das mit psoriasisähnlicher Hyperplasie oder mit Brustkrebs in Verbindung gebracht worden ist. Die Untersuchung des E-FABP:Psoriasin-Komplexes könnte eventuell zu einem besseren Verständnis der Wechselwirkung von E-FABP und S100A7 bei einer Psoriasis-erkrankung führen.

Um die Beziehung zwischen Struktur und Funktion dieses Proteins besser zu verstehen, wurde seine Lösungsstruktur mittels NMR-Spektroskopie bestimmt. Sowohl unmarkierte als auch  $^{15}\text{N}$ -markierte Proben von rekombinantem humanem E-FABP wurden im bakteriellen System *Escherichia coli* exprimiert, mit dem Isotop  $^{15}\text{N}$  angereichert und zur Aufnahme von multidimensionalen NMR-Spektren verwendet. Mit Hilfe von heteronuklearen HTQC-, HSQC-, TOCSY-HSQC- und NOESY-HMQC-Spektren wurde die Zuordnung der  $^1\text{H}$ - und  $^{15}\text{N}$ -Resonanzen des Peptidrückgrats erfolgreich durchgeführt. Außerdem war es mit



Hilfe homonuklearer COSY- und TOCSY-Spektren möglich, die Zuordnung der  $^1\text{H}$ -Resonanzen der Seitenketten zu vervollständigen. Hierbei ergaben sich Strukturhomologien zu anderen Fettsäurebindungsproteinen, die die Richtigkeit der Zuordnung unterstützten. Die vollständige Zuordnung der  $^1\text{H}$ - und  $^{15}\text{N}$ -Resonanzen des Peptidrückgrats sowie der Seitenketten erfolgte in der vorliegenden Arbeit, und die Daten wurden in der BioMagResBank unter BMRB-5083 abgelegt.

Das Vorkommen von sechs Cysteinresten in der Aminosäuresequenz von humanem E-FABP ist äußerst ungewöhnlich für LBPs. Vier dieser sechs Cysteinreste sind einzigartig in E-FABPs: C43, C47, C67 und C87. In der dreidimensionalen Struktur von humanem E-FABP wurden mittels Röntgenbeugungsanalyse zwei Cysteinpaare (C67/C87 and C120/C127) identifiziert, die ausreichend nahe beieinander eingeordnet sind, um eine Disulfidbrücke bilden zu können. Eine solche S-S-Bindung konnte jedoch nur zwischen C120 and C127 eindeutig nachgewiesen werden [Hohoff *et al.*, 1999]. Da der Ausschluss einer Disulfidbrücke zwischen C67 and C87 den  $R_{\text{free}}$ -Faktor der Röntgenstruktur verbesserte, wurde die Existenz einer kovalenten Bindung zwischen diesen zwei Seitenketten als eher unwahrscheinlich angesehen. Dies stimmt mit den hier präsentierten NMR-Daten überein, in denen  $\text{S}^{\gamma}\text{H}$ -Resonanzen für die Cysteinreste C43, C67 (vorläufige Zuordnung) und C87 beobachtet worden sind, wodurch die Möglichkeit einer zweiten Disulfidbrücke in Lösung definitiv ausgeschlossen wird.

Die Auswertung der NOESY-Spektren wurde mittels einer semi-automatischen Zuordnungsroutine im Programm MATLAB 5.0 durchgeführt. Weitere Verfeinerungen mußten manuell im direkten Vergleich mit den Spektren vorgenommen werden, wobei die NOE-Intensitäten in Abstände zwischen den Wasserstoffatomen des Proteins übersetzt wurden. Die maximalen Abstände bei gegebener Intensität wurden durch Kalibrierung auf die Intensitäten von sequentiellen und ‘medium-range’ NOE-Werten aus Aminosäureresten in bekannten Sekundärstrukturelementen bestimmt. Die Intensitäten der Kreuzsignale wurden in vier verschiedene Abstandskategorien eingestuft: 2.5, 3.5, 4.5 und 6.0 Å. Informationen über Wasserstoffbrücken wurden aus Wasserstoff-Deuterium-Austauschexperimente mit deuteriertem Puffer erhalten.

Auf den NOE- und Wasserstoffaustauschdaten basierend wurde ein Ensemble von 20 energieminierten Konformeren errechnet, das die Lösungsstruktur von humanem E-FABP im Komplex mit Stearinsäure darstellt. Die Analyse von homonuklearen 2D NOESY- und

<sup>15</sup>N-editierten 3D NOESY-Spektren führte zu einer Gesamtzahl von 2926 NOE-abgeleiteten Abstandsbeschränkungen. Außerdem wurden 37 langsam-austauschende Amidprotonen des Peptidrückgrats identifiziert, die Teil des Wasserstoffbindungsnetzwerks zwischen den  $\beta$ -Faltblattsträngen darstellen und in 74 zusätzliche Abstandsbeschränkungen umgesetzt wurden. Zusätzlich wurde die Disulfidbrücke zwischen C120 und C127 durch 3 maximale und 3 minimale Abstandsbeschränkungen definiert. Das Strukturrechnungsprogramm DYANA stufte 998 von diesen Abstandsbeschränkungen als überflüssig ein. Von den restlichen 2008 nicht-trivialen Abstandsbeschränkungen, waren 371 intraresiduell ( $i = j$ ), 508 sequentiell ( $|i - j| = 1$ ), 233 ‘medium-range’ ( $1 < |i - j| \leq 4$ ), und 896 ‘long-range’ ( $|i - j| > 4$ ). 300 Konformere, jedes nach 8000 ‘annealing’ Schritten, wurden *ab initio* errechnet. Eine Gesamtzahl von 126 stereospezifischen Zuordnungen der prochiralen Methyl- und Isopropylgruppen wurde mit dem Programm GLOMSA erzielt [Güntert *et al.*, 1991]. Wie von Wüthrich *et al.* [1983] vorgeschlagen wurden Pseudoatome für die nicht zugeordneten Stereopaare und für magnetisch gleichwertige Protonen verwendet. Die Energieminimierung der Struktur wurde für die 20 besten Konformeren aus DYANA mit dem Programm DISCOVER (INSIGHT 97, Molecular Simulations Inc., San Diego, USA) durchgeführt.

Das Protein besteht hauptsächlich aus 10 antiparallelen  $\beta$ -Faltblattsträngen, die eine  $\beta$ -Fasstruktur mit einer großen, inneren Bindungstasche bilden, und zwei kurze  $\alpha$ -Helices, die ein Helix-Turn-Helix-Motif bilden. Die N-terminalen Reste V4-L7 bilden eine helicale Schlaufe (wahrscheinlich mit einer  $3_{10}$  Konformation), die zum  $\beta$ -Strang  $\beta$ A (G9-K17) führt. Aminosäurereste V14 und D15 bilden ein “ $\beta$ -Bulge” im  $\beta$ -Strang  $\beta$ A. G18 verbindet den ersten  $\beta$ -Strang  $\beta$ A mit der  $\alpha$ -Helix I, die aus den Aminosäureresten F19-L26 besteht. Die Aminosäurereste G27-G29 bilden einen “Turn”, der zur  $\alpha$ -Helix II führt. Diese Helix enthält die Aminosäurereste I30-M38. Die Aminosäurereste A39-P41 verbinden  $\alpha$ -Helix II und  $\beta$ -Strang  $\beta$ B (D42-C47). Die restliche Struktur besteht aus einer Serie von  $\beta$ -Strängen:  $\beta$ C (L52-E57),  $\beta$ D (T62-T68),  $\beta$ E (K72-T77),  $\beta$ F (R81-F89),  $\beta$ G (L94-E99),  $\beta$ H (E104-L111),  $\beta$ I (L116-V121), und  $\beta$ J (T126-K133), die hauptsächlich durch Hairpinturns verbunden sind.

Ohne die terminalen Reste zu berücksichtigen, wurde für die dreidimensionale Lösungsstruktur des humanen E-FABP eine mittlere quadratische Abweichung von  $0,92 \pm 0,11$  Å bzw.  $1,46 \pm 0,10$  Å für die Peptidrückgrat- und die Schweratome bestimmt. Ohne die Portalregion (*d.h.*, für Aminosäurereste 4-26, 40-56, 63-75 und 83-134; die Portalregion stellt anscheinend die einzige Öffnung in der Proteinoberfläche dar, durch die der Fettsäureligand ein- oder austreten kann) wurde eine mittlere quadratische Abweichung des Peptidrückgrats

von  $0,85 \pm 0,10 \text{ \AA}$  errechnet, was die höhere konformationelle Dispersion in der Portalregion widerspiegelt. Die Überlagerung mit der Röntgenstruktur des humanen E-FABP (die terminalen Aminosäurereste ausgeschlossen) lieferte eine mittlere quadratische Abweichung des Peptidrückgrats von  $1,00 \pm 0,07 \text{ \AA}$  für die ganze Aminosäuresequenz bzw. von  $0,98 \pm 0,06 \text{ \AA}$  ohne die Portalregion. Diese Ergebnisse deuten auf eine starke Ähnlichkeit zwischen den Röntgen- und Lösungsstrukturen hin. Die Strukturkoordinaten wurden in der RCSB Datenbank unter PDB ID 1JJJ abgelegt.

$^{15}\text{N}$ -Relaxationsexperimente ( $T_1$ ,  $T_2$  und heteronukleare NOE) mit humanem E-FABP bei drei verschiedenen Feldstärken (500, 600 und 800 MHz) lieferten Informationen über die innere Dynamik des Peptidrückgrats. Die longitudinalen und transversalen ( $R_1$  und  $R_2$ ) Relaxationsraten wurden durch nicht-lineare Fehlerquadratanpassung der Peakintensitäten bestimmt (was unter Verwendung der durch das RMX-Programm erzeugten monoexponentiellen Funktionen erzielt wurde). Stationäre heteronukleare  $^{15}\text{N}\{^1\text{H}\}$  NOE-Werte wurden durch das Verhältnis der Peakintensitäten mit und ohne  $^1\text{H}$ -Sättigung gemessen. Die mikrodynamischen Parameter der HN-Peptidrückgratvektoren (der verallgemeinerte Ordnungsparameter  $S^2$  und die effektive interne Korrelationszeit  $\tau_e$ ) sowie der Beitrag von konformationellem Austausch zu der transversalen Relaxationsrate (der Austauschparameter  $R_{ex}$ ) wurden mit dem Programm Modelfree4 errechnet und angepasst [Mandel *et al.*, 1995; Palmer *et al.*, 1991]. Es wurden drei verschiedene Modelle für die spektrale Dichtefunktion verwendet. Das erste Modell basiert auf dem von Lipari und Szabo [1982] vorgeschlagenen model-free Formalismus. Es werden  $S^2$  und  $\tau_e$  bestimmt. Das zweite Modell berücksichtigt außerdem einen Austausch-Term  $R_{ex}$ ; es werden  $S^2$  und  $R_{ex}$  bestimmt. Schließlich wurde die erweiterte Variante des model-free Formalismus [Clore *et al.*, 1990] als drittes Modell für die spektrale Dichtefunktion verwendet, wobei die Parameter  $S_s^2$ ,  $S_f^2$  und  $\tau_e$  angepasst wurden.

Die Ordnungsparameter ( $S^2$ ) der Amidprotonen des Peptidrückgrats wurden für alle drei Feldstärken bestimmt, wobei eine Korrelationszeit  $\tau_c = 8.6 \text{ ns}$  für die Umorientierung des Gesamtproteins errechnet wurde. Nahezu alle nicht-terminalen Peptidrückgratgruppen zeigten Ordnungsparameterwerte  $S^2 > 0,8$  (durchschnittlicher Wert von  $0,88 \pm 0,04$ ), was eine gleichmäßig niedrige Beweglichkeit des Peptidrückgrats im ns-ps-Zeitbereich über die ganze Aminosäuresequenz nahelegt. Die N-terminale helikale Schlaufe und die  $\alpha$ -Helix I zeigen überdurchschnittliche  $S^2$ -Werte, was auf eine niedrigere Beweglichkeit des Peptidrückgrats hindeutet, während die  $\alpha$ -Helix II, die Teil der Portalregion ist, eine höhere Flexibilität aufweist. Austauschparameter ( $R_{ex}$ ) wurden hauptsächlich im mittleren Teil der  $\beta$ -Stränge

beobachtet, in dem sich auch die langsam-austauschenden Amidprotonen befinden, *d.h.*, Wasserstoff-Deuterium-Austauschexperimente deuteten eine direkte Korrelation zwischen der Stabilität des Wasserstoffbrückennetzwerks in der  $\beta$ -Faltblattstruktur und dem konformationellen Austausch ( $R_{ex}$ ) im ms- $\mu$ s-Zeitbereich an.

Die Eigenschaften der hier ausgearbeiteten Peptidrückgratdynamik des humanen E-FABP unterscheiden sich von denen des phylogenetisch eng verwandten Herztyp-FABP und des etwas entfernter verwandten Gallensäure-bindenden ILBP. Die in dieser Arbeit erzielten Resultate der Proteindynamik führen zu dem Schluss, dass verschiedene Mitglieder der LBP-Familie wie E-FABP, H-FABP und ILBP durch eine unterschiedliche Dynamik in den Peptidrückgratstrukturen charakterisiert sind. Wasserstoff-Deuterium-Austauschexperimente zeigten deutliche Unterschiede im chemischen Austausch mit dem Lösungsmittel für die Peptidrückgratprotonen des Wasserstoffbindungsnetzwerks zwischen den  $\beta$ -Faltblattsträngen. Die  $\beta$ -Fasstruktur des H-FABP ist anscheinend nur wenig beweglich, mit Austauschvorgängen, die vermutlich oberhalb des ms- $\mu$ s-Zeitbereichs einzuordnen sind. Diese Divergenzen könnten dadurch zustandekommen, dass das hydrophobe Cluster in der Bindungstasche teilweise von unterschiedlichen Aminosäureresten gebildet wird. So kommt es zum Beispiel zu einer Substitution von F4 in H-FABP zu L7 in E-FABP. Außerdem könnte die höhere konformationelle Stabilität von H-FABP mit der stärkeren Bindung der Fettsäureliganden zu H-FABP im Vergleich zu E-FABP zusammenhängen [Zimmerman *et al.*, 2001]. ILBP zeigt andererseits den schnellsten Wasserstoffaustausch und eine erhebliche Anzahl von Austauschparametern ( $R_{ex}$ ), was auf eine reduzierte Stabilität in der  $\beta$ -Faltblattstruktur im ms- $\mu$ s-Zeitbereich hindeutet. Schließlich rangiert E-FABP aufgrund des Wasserstoff-Deuterium-Austausches zwischen diesen zwei Proteinen, mit  $R_{ex}$ -Termen in den  $\beta$ -Faltblattsträngen, die auf Austauschvorgänge im ms- $\mu$ s-Zeitbereich wie in ILBP hinweisen. Es gibt möglicherweise eine Korrelation zwischen der Proteinstabilität und der Bindungsaffinität der Liganden, wenn eine flexiblere Struktur dem gebundenen Liganden erlaubt, die Bindungstasche leichter auszutreten. Andererseits könnte das Fehlen des hochkonservierten Phenylalanin (F57 in H-FABP) der Portalklappe in E-FABP ein wichtiger Faktor für die niedrigere Fettsäurebindungsaffinität von E-FABP sein. Untersuchungen von Punktmutanten des humanen E-FABP könnten eine Antwort auf diese Fragen geben.

## Lebenslauf

Luis Horacio Gutiérrez González

geboren am 6. Oktober 1963 in Saltillo, Mexiko.

### Schulbildung:

- 1970 - 1976 „Primaria“ in Mexiko-Stadt (Grundschule und Gymnasium Grundstufe)
- 1976 - 1979 „Secundaria“ in Mexiko-Stadt (Gymnasium Sekundärstufe)
- 1979 - 1982 „Preparatoria“ in Mexiko-Stadt (Gymnasium Oberstufe)
- 1982 Abschluss (Hochschulzugangsberechtigung) „Bachillerato“

### Hochschulbildung:

- 1983 - 1990 Physikstudium an der Universidad Nacional Autónoma de México in Mexiko-Stadt
- 1991 „Licenciatura“ in Physik (entspricht Diplom) mit der Arbeit:  
„Physikalische Vorgänge in Polarlichtern.“
- 1993 - 1995 Chemiestudium an der Universidad Autónoma Metropolitana in Mexiko-Stadt
- 1996 „Maestría“ in Chemie (entspricht Magister) mit der Arbeit:  
„Untersuchung der chemischen Stabilität von Chymopapain: Auswirkung des pH-Werts auf die Aktivierungsparameter.“
- 1997 - 2001 Anfertigung der vorliegenden Dissertation unter der Leitung von Herrn Prof. Dr. Heinz Rüterjans am Institut für Biophysikalische Chemie der Johann Wolfgang Goethe-Universität in Frankfurt am Main.